



# Design, Synthesis and Biological Evaluation of Tool Compounds for the Cellular Investigation of Deubiquitinases

## Dissertation

zur Erlangung des akademischen Grades  
des Doktors der Naturwissenschaften  
(Dr. rer. nat.)

der Fakultät der Chemie und Chemischen Biologie  
der Technischen Universität Dortmund

vorgelegt von

**Mirko Schmidt, M.Sc.**

geboren am 09.11.1992 in Essen

Dortmund, den 26.09.2023



The work presented in this thesis was executed in the period from February 2019 to August 2023 under the supervision of Dr. Malte Gersch at the Chemical Genomics Centre, the Max Planck Institute for Molecular Physiology, Dortmund, and the Faculty of Chemistry and Chemical Biology at the TU Dortmund.

1<sup>st</sup> Examiner: Dr. Malte Gersch

2<sup>nd</sup> Examiner: Prof. Dr. Dr. h.c. Herbert Waldmann



Results displayed in this thesis contributed to the following publication:

C. Grethe\*, **M. Schmidt\***, G. M. Kipka, R. O’Dea, K. Gallant, P. Janning & M. Gersch, “*Structural basis for specific inhibition of the deubiquitinase UCHL1*” *Nat. Commun.*, **13**, 5920 (2022),

**M. Schmidt\***, C. Grethe\*, J. M. Pérez, J. Seier, S. Recknagel, G. M. Kipka, A. Paschen, E. Sanchez-García & M. Gersch, „*N-Cyanopiperazines as Specific Covalent Inhibitors of the Deubiquitinating Enzyme UCHL1*” (Unpublished)

\*Authors contributed equally

## Disclaimer

The results in this thesis were developed in collaboration with Dr. Christian Grethe. This thesis discusses and illustrates data from Dr. Christian Grethe to understand the process of tool development as a whole. Experimental data produced and evaluated by Dr. Christian Grethe might be published and discussed in his doctoral thesis in more detail.

Dr. Christian Grethe synthesized the probes **CG017**, **CG041**, **CG173**, **CG050R**, as well as **GK13S** and corresponding analogs (with the help of MSc. Marvin Gian Kipka). Furthermore, he chemically improved the structure of **GK13S**, resulting in various 5-membered cyanopyrrolidine and 6-membered cyanopiperazine compounds (including **CG341** and **CG306**) targeting UCHL1. He biochemically characterized all UCHL1 probes via intact protein mass spectrometry and performed all kinetic measurements, Rh-cleavage- and TSA assays. In addition, he solved and analyzed the crystal structure of UCHL1 in co-complex with **GK13S**.

The probes **MS023** and **MS037** as well as all PROTAC molecules were synthesized by myself. The initial profiling to identify DUBs that are covalently modified by the synthesized probes, as well as the proteomics-based target identification, was carried out by myself. I also performed and optimized all cellular assays of all molecules described in this thesis. I carried out experiments that used the characterized probes as tool compounds for the phenotypic characterization and investigation of the target spectrum of UCHL1. In addition, I optimized the CuAAC conditions, resulting in the full conversion of **GK13S** to the “clicked” species.

Dr. Rachel O’Dea performed cell viability assays shown in the supplementary data.

MSc. Kai Gallant helped with performing and analyzing experiments detecting changes in the mono Ub-pool after inhibition of cellular UCHL1.



## Acknowledgment

Almost five years have passed during my stay at the Chemical Genomics Center and the execution of this thesis. Ups and downs marked my time as a doctoral candidate, and yet the time flew by. This is not least due to the outstanding working atmosphere at the CGC and the Max Planck Institute, for which I would like to thank all the people who have accompanied me over the last four and a half years.

Special thanks go to my supervisor, Dr. Malte Gersch, for not only giving me the opportunity to work in the exciting DUB field but for always welcoming me, whether I needed a scientific advice or wanted to have an excited discussion about the latest results. Thank you for sharing your experience and knowledge over the past years, which were invaluable for the success of my research.

I am deeply grateful to Prof. Herbert Waldmann for not only agreeing to be the second examiner of this thesis, but also for initiating the third funding period of the chemical genomics center. Without this, I would not have had the chance to work on this highly interesting project. In the same breath, I would like to thank the responsible of Merck, AstraZeneca and Pfizer for funding the chemical genomics center.

I would like to thank all members of the Gersch working group, who helped me to grow both my scientific skills and interpersonally. Thank you for all the helpful advice and countless discussions. Thanks for the encouraging coffee breaks and the get-togethers outside the lab that made the bad mood about failed experiments go away quickly.

I would like to express special thanks to Christian Grethe, a true friend I met at the beginning of my studies and with whom I had the honor of working on the same doctoral project. Without your dedication and expertise, the DUB probe project would not be where it is right now. I am grateful for the exciting collaboration but also for the fact that you always had an open ear for me whether it was a scientific discussion or something of personal nature.

I thank Nikolas Klink, for the dedication and excitement during your master thesis. You made the supervision very easy for me. I also thank you for sharing all the great insights into the PROTAC field and the many fruitful discussions we had.

## Acknowledgement

I thank Dr. Rachel O'Dea and Kai Gallant for their valuable contributions to the project and the many points you raised during various meetings, which contributed not insignificantly to the success of the project.

I would like to thank Kim Wendrich for providing a number of Ub probes and purified proteins. Furthermore, I would like to thank you for your numerous assistance at the ÄKTA, when my protein eluted into the waste again.

I thank all collaboration partners for their contributions. I would especially like to thank Dr. Petra Janning and the proteomics facility for the high quality and extremely fast measurements of all proteomics samples.

I am incredibly grateful to Sven Brandherm and Christian Grethe for their friendship and cohesion during what was sometimes a very stressful time. Our hangouts have helped me to keep a clear head.

Finally, I would like to thank my partner Carina Seitz. Thank you for always being by my side and motivating me to keep going, no matter how long the road may be. I thank you from the bottom of my heart that I can always rely on you.

Cheers to the HS42 gang and to many more evenings in Düsseldorf!



# Table of Contents

<b>Acknowledgment</b> .....	<b>I</b>
<b>Table of Contents</b> .....	<b>III</b>
<b>Abstract</b> .....	<b>VI</b>
<b>Kurzzusammenfassung</b> .....	<b>VII</b>
<b>1. Introduction</b> .....	<b>1</b>
1.1 The ubiquitin-proteasome system.....	1
1.2 The ubiquitin code and Ubls .....	3
1.5 Deubiquitinases - The erasers of the code.....	6
1.6 UCHL1 – much studied, but far from understood.....	11
1.7 Deubiquitinases in a therapeutic context .....	14
1.8 Tools to study deubiquitinases.....	17
1.8.1 Ubiquitin-based probes .....	20
1.8.2 Small molecules-based probes .....	21
1.8.3 Bifunctional molecules.....	22
<b>2. Motivation and Aims</b> .....	<b>26</b>
<b>3. Results</b> .....	<b>28</b>
3.1 Synthesis of a focused deubiquitinase probe library .....	28
3.1.1 Finding suitable molecular scaffolds for probe design .....	28
3.1.2 Synthesis of an aliphatic nitrile probe .....	30
3.1.3 Synthesis of aryl nitrile probes.....	34
3.1.4 Synthesis of cyanopyrrolidine probes .....	37
3.2 Biological characterization of tool compounds to study deubiquitinases .....	38
3.2.1 Evaluation of activity-based probe library identifies GK13S as a specific DUB binder .....	38
3.2.2 Cellular characterization yields a pair of chemogenomic probes for UCHL1.....	45
3.2.3 GK13S shows exquisite binding parameters for UCHL1.....	51
3.2.4 Crystal structure reveals hybrid conformation of UCHL1 after modification with GK13S .....	56
3.2.5 GK13S and GK16S as tools to unravel UCHL1 substrates.....	61
3.2.6 Utilizing an inactive UCHL1 mutant for substrate trapping.....	68
3.3 Structural improvement of GK13S towards selective UCHL1 probes .....	70

## Table of Contents

3.3.1 <i>N</i> -cyanopyrrolidines with more complex decorations.....	70
3.3.2 Warhead optimization led to <i>N</i> -cyanopiperazine probes with enhanced specificity....	73
3.3.3 Copper-catalyzed cycloaddition reverses covalent modification with CG341 and CG306 .....	76
3.3.4 <i>N</i> -cyanopiperazine probes usable for the specific investigation of UCHL1 .....	80
3.4 PROTAC tool compounds for the degradation of DUBs.....	83
3.4.1 Identification and synthesis of suitable USP7 binder for PROTAC generation.....	83
3.4.2 Design and synthesis of PROTACs targeting USP7 .....	89
3.4.3 Biochemical evaluation of synthesized PROTACs reveals potent binding and degradation of USP7 in HEK293 cells.....	91
3.4.4 Transformation of GK13S into bifunctional molecule to degrade UCHL1.....	94
<b>4. Discussion and Conclusion .....</b>	<b>98</b>
<b>5. Methods .....</b>	<b>106</b>
5.1 Biology .....	106
5.1.1 Biochemical assays.....	106
5.1.2 Cellular assays.....	109
5.2 Chemical synthesis.....	118
5.2.1 Preparation of probe molecules MS037 and MS023 .....	119
5.2.2 Preparation of UCHL1 PROTACs .....	126
5.2.3 Preparation of USP7 PROTACs.....	129
<b>6. Supplementary Data .....</b>	<b>139</b>
<b>7. References.....</b>	<b>161</b>
<b>8. List of Abbreviations .....</b>	<b>170</b>

## Abstract

Modern medicine made great leaps in curing many diseases with tailor-made molecules over the past decades. However, many diseases are incurable because there are no effective drugs available or resistance against known therapeutic agents occurred. Therefore, alternative signaling pathways must be investigated for medicinal purposes. One of those pathways is the ubiquitin proteasomal system, which is mainly involved in protein homeostasis through the ubiquitination of substrates and coordinates various other functions throughout the cell. Significantly the deubiquitinases (DUBs) are essential regulators within this system. They are a specialized class of proteases that can cleave ubiquitin from its substrates. This enzymatic activity has a significant influence on the signal transduction within the cell, and dysregulation triggers many diseases. However, the understanding regarding their substrates, cellular localization, their involvement in cellular signaling and structural features remains limited for most of the DUBs. Despite the importance of the DUBs in disease development, only a handful of inhibitors are known, whereas most are not biologically characterized or show a poor specificity profile. This highlights the need for tools to enhance the understanding of DUBs and the ubiquitin proteasomal system in general to pave the path for future drug development.

This thesis describes the discovery, chemical synthesis and biological evaluation of such tool compounds for investigating DUBs in a living environment. To accomplish this, literature-known compounds were resynthesized to introduce alkyne tags to utilize their use as activity-based probes in cell-based systems. Chemical synthesis led to the small molecule probes **MS023** and **MS037**.

The biological evaluation of a broader in-house synthesized chemical probe library for DUBs yielded the chemogenomic pair of probes **GK13S** and **GK16S** as tool compounds for the investigation of DUBs. To use the probes for cellular activity-based protein profiling (ABPP), optimal conditions for the copper-catalyzed azide-alkyne cycloaddition (CuAAC) were screened and established. These “click” conditions were applied to proteomics-based target validation experiments to identify UCHL1 as the DUB, bound by **GK13S**. UCHL1, associated with various cancers and neurological disorders, is one of the most studied DUBs in the literature, yet only few of its substrates are known. **GK13S** displayed exquisite inhibition parameters towards endogenous UCHL1 *in vitro* and in different cellular settings. Mutations of UCHL1 confirmed the covalent modification by the probe at the catalytic cysteine. **GK13S** was further used to show that the inhibition of UCHL1 in human glioblastoma cells reduced mono ubiquitin availability. Digestion

of the proteome and subsequent mass spectrometry-assisted analysis of the same cell line after treatment with **GK13S** revealed reduced protein levels of Rac1 and HtrA2, among others.

The biological evaluation of **CG306** and **CG341**, improved versions of **GK13S**, demonstrated in-family specificity for UCHL1 and discriminated major off-targets, bound by **GK13S**. In-Gel fluorescence and target validation experiments confirmed the complete and specific modification of the DUB *in vitro* and in cellular systems. Furthermore, also the treatment with **CG306** confirmed the reduction of mono-Ub after the inhibition of endogenous UCHL1 in glioblastoma cells.

To investigate DUBs beyond inhibition of their catalytic activity, proteolysis targeting chimeras (PROTACs) against USP7 were synthesized and characterized in a cellular setting. **XL188**, a literature-known inhibitor, was used to target USP7. Others can use those tool compounds to assess the behavior of an organism, not only following the inhibition of a DUB but also after its degradation. That might lead to hints about relevant non-catalytic functions of DUBs that would be otherwise overshadowed by only inhibiting the enzyme. The IC<sub>50</sub> value for the inhibition of USP7 by the PROTACs, was in a similar range to that of the parent inhibitor **XL188**. Treatment with the molecules resulted in reduced levels of USP7 in HEK293 cells.

The small molecule tools described, evaluated and characterized within this thesis should bolster the work of other researchers to enhance the understanding of DUBs in living systems.

## Kurzzusammenfassung

Die moderne Medizin hat in den letzten Jahrzehnten große Fortschritte bei der Heilung vieler Krankheiten mit speziell entwickelten Medikamenten, basierend auf kleinen Molekülen, gemacht. Viele andere Krankheiten sind jedoch weiterhin nicht behandelbar, da die Verfügbarkeit von wirksamen Medikamenten fehlt, oder Resistenzen gegen bekannte Therapeutika aufgetreten sind. Daher müssen stets alternative Signalwege für therapeutische Zwecke aufgefunden und untersucht werden. Einer dieser Signalwege ist das Ubiquitin-Proteasom-System, welches hauptsächlich an der Qualitätssicherung von Proteinen durch die Ubiquitinierung und den Abbau dieser beteiligt ist. Darüber hinaus koordiniert es aber auch verschiedenste andere Funktionen innerhalb der Zelle. Insbesondere die Deubiquitinasen (DUBs) sind wichtige regulatorische Enzyme innerhalb dieses Systems. Sie stellen eine spezialisierte Klasse von Proteasen dar, die in der Lage sind Ubiquitin von ihren Substraten abzuspalten. Die enzymatische Aktivität hat einen großen Einfluss auf die Signaltransduktion innerhalb der Zelle, und eine Dysregulation ist der

Auslöser für eine Vielzahl von Krankheiten. Die meisten DUBs sind jedoch hinsichtlich ihrer Substrate, ihrer zellulären Lokalisierung, ihrer genauen Beteiligung an der zellulären Signalübertragung und ihrer strukturellen Merkmale noch nicht ausreichend untersucht. Trotz der Bedeutung der DUBs bei der Entstehung von Krankheiten sind nur eine Handvoll Inhibitoren bekannt, während die meisten von ihnen nicht biologisch charakterisiert sind oder ein schlechtes Spezifitätsprofil aufweisen. Deshalb ist es von äußerster Wichtigkeit, molekulare Werkzeuge zu etablieren, um das Verständnis von DUBs und Ubiquitin-Proteasom-System insgesamt zu fördern, um so den Weg für die zukünftige Entwicklung von Medikamenten zu ebnen.

Die vorliegende Arbeit beschreibt die Entdeckung, die chemische Synthese und die biologische Testung solcher molekularen Werkzeuge zur Untersuchung von DUBs in einer lebenden Umgebung. Zu diesem Zweck wurden literaturbekannte Verbindungen resynthetisiert und mit Alkin-Tags versehen, um ihre Verwendung als aktivitätsbasierte Sonden in zellbasierten Systemen zu ermöglichen. Die chemische Synthese führte zu den kleinen Molekülsonden **MS023** und **MS037**.

Die biologische Auswertung einer breiteren, intern synthetisierten chemischen Sondenbibliothek für DUBs resultierte in dem chemogenomische Sondenpaar **GK13S** und **GK16S** als Modelverbindungen für die Untersuchung von DUBs. Um die Sonden für das zelluläre aktivitätsbasierte Proteinprofiling (ABPP) zu verwenden, wurden optimale Bedingungen für die kupferkatalysierte Azid-Alkin-Cycloaddition (CuAAC) untersucht und erarbeitet. Diese "Klick"-Bedingungen wurden für Massenspektrometrisch gestützte Validierungsexperimente genutzt, um UCHL1 als DUB zu identifizieren, die von GK13S gebunden wird. UCHL1, ein Protein das mit verschiedenen Krebsarten und neurologischen Erkrankungen in Verbindung gebracht wird, ist eine der am meisten untersuchtesten DUBs in der Literatur. Dennoch sind nur wenige Substrate von UCHL1 bekannt. **GK13S** weist sowohl *in vitro* als auch in verschiedenen Zelllinien eine vollständige kovalente Inhibition von endogenem UCHL1 auf. Mutationen von UCHL1 bestätigten die kovalente Modifikation durch die Sonde am katalytischen Cystein. Mit **GK13S** konnte bewiesen werden, dass die Hemmung von UCHL1 in menschlichen Glioblastomazellen zu einer verringerten Verfügbarkeit von Monoubiquitin innerhalb der Zellen führt. Die Verdauung des Proteoms und die anschließende massenspektrometrische Analyse derselben Zelllinie nach Behandlung mit der Sonde, resultierte in einem verringerten Gehalt der Proteine Rac1 und HtrA2.

Die biologische Auswertung der kleinen Molekül Sonden **CG306** und **CG341**, welche eine verbesserte Version von **GK13S** darstellen, zeigten eine Spezifität für UCHL1 innerhalb der DUB Familie und binden nicht an „Off-Targets“, die von **GK13S** gebunden werden. In-Gel-Fluoreszenz-

## Abstract/Kurzzusammenfassung

und Verdrängungsexperimente mit Ub-Sonden, bestätigten die vollständige und spezifische Modifikation des DUB *in vitro* und in zellulären Systemen. Darüber hinaus bewies auch die Behandlung mit **CG306** die Verringerung von Mono-Ub nach der Hemmung von endogenem UCHL1 in Glioblastomzellen.

Um DUBs über die Hemmung ihrer katalytischen Aktivität hinaus zu untersuchen, wurden Proteolysis-Targeting-Chimeras (PROTACs) gegen die DUB USP7 auf der Grundlage des in der Literatur beschriebenen Deubiquitinase Inhibitors **XL188** synthetisiert und in einer zellulären Umgebung charakterisiert. Diese Verbindungen können als Werkzeuge verwendet werden, um das Verhalten eines Organismus nicht nur nach der Hemmung einer DUB, sondern auch nach deren Abbau zu untersuchen. Dies kann Hinweise auf relevante und nicht-katalytische Funktionen von DUBs liefern. Diese Interaktionen könnten andernfalls durch die alleinige Hemmung des Enzyms unentdeckt bleiben. Der  $IC_{50}$ -Wert für die Hemmung von USP7 durch die PROTACs lag in einem ähnlichen Bereich wie der des Vorläufer Inhibitors **XL188**. Die Behandlung mit den Molekülen führte zu einer Verringerung der USP7-Konzentration in HEK293-Zellen.

Die in dieser Arbeit beschriebenen, evaluierten und charakterisierten kleinen Moleküle sollten die Arbeit anderer Forscher unterstützen, um das Verständnis von DUBs in lebenden Systemen zu verbessern.

# 1. Introduction

## 1.1 The ubiquitin-proteasome system

Cells are constantly pressured to react to altered extra- and intracellular circumstances to sustain protein homeostasis.<sup>[1]</sup> To respond to such changes, cellular proteins are in a dynamic state of turnover.<sup>[2]</sup> The degradation of a protein is dependent on various factors such as dysfunctions, external stimuli, or the half-life.<sup>[3]</sup> The underlying mechanisms for protein turnover must be highly selective since a wide variety of cellular signaling pathways is regulated via protein degradation.<sup>[4]</sup> In eukaryotic cells, this regulatory challenge is broadly achieved by two major processes: the ubiquitin-proteasome system (UPS) (Fig. 1 A) and autophagy. Autophagy describes a degradative mechanism in which the lysosome digests cellular components.<sup>[5]</sup> Among other, the UPS accounts for the cleavage of proteins that contain biosynthetic errors or are misfolded.<sup>[6]</sup> Impairments within the UPS are connected to critical diseases such as cancer, cardiovascular diseases and neurodegenerative disorders among others.<sup>[7]</sup> The significant similarity of both systems is the use of ubiquitination as a linkage-specific degron signal.<sup>[8]</sup>

The highly conserved small protein and post-translational modifier (PTM) ubiquitin (Ub) comprises 76 amino acids and a mass of 8.5 kDa. It was the pioneering work of Avram Herschok, Irwin A. Rose, Aaron Ciechanover (all awarded the Nobel Prize for the discovery of ubiquitin-mediated protein degradation) and coworkers who postulated that the consumption of adenosine triphosphate (ATP) is needed for the modification of a proteolytic substrate with ubiquitin.<sup>[9]</sup> The ubiquitin is covalently bound to a substrate protein through an isopeptide bond, linking its C-terminal carboxylic acid to a lysine's amino group.<sup>[10]</sup> The transfer of ubiquitin to its intracellular substrate is a stepwise process which utilizes three different enzyme classes (Fig. 1B). First, an activating enzyme (E1) attaches to the ubiquitin under the consumption of ATP, and the release of adenosine monophosphate (AMP). An E2 enzyme binds to the activated ubiquitin~E1, which is then transferred to the E2's active cysteine through a transacylation reaction, forming a thioester linkage. Next, the E2 enzyme enters a complex with a ubiquitin-ligase (E3). Depending on the subfamily of the E3, the Ub is either transferred directly-(RING/RING-like E3s), or temporarily to the ligase (HECT E3s) and finally to the amino group of the substrate's lysine residue.<sup>[11]</sup>

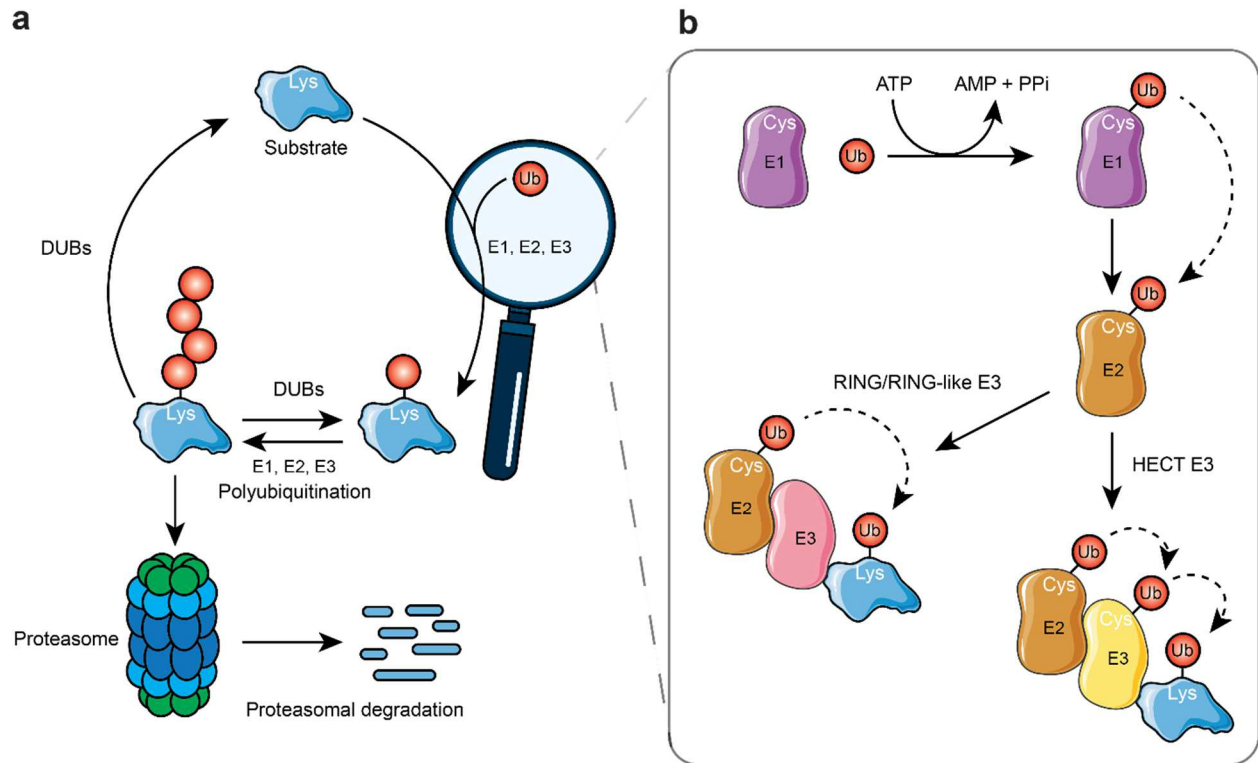


**Fig. 1 | The ubiquitin-proteasome system and the ubiquitin-conjugation machinery. a)** Schematic illustration of the ubiquitin-proteasome system. A substrate gets ubiquitinated via E1, E2 and E3 enzymes. As more ubiquitins are added, they form chains known as polyubiquitin. Those chains are recognized by the proteasome, leading to proteolytic digestion of the substrate. DUBs tightly regulate the system through deubiquitination. These enzymes are able to cleave off mono Ub, whole chains or trim those to a desired number of ubiquitin moieties. **b)** Schematic illustration of the ubiquitin conjugation machinery. The E1 enzyme activates Ub in an ATP-dependent manner. Ub is transferred to the E2 enzyme. Based on the E3, the Ub is transferred directly (RING/RING-like E3) or in a two-step process (HECT E3) to the substrate.<sup>[6a, 11]</sup>

Mono ubiquitination can work as a signal for the ubiquitination machinery to add additional Ubs to the substrate. Polyubiquitin chains are formed as a result of this process. This macromolecular sequence is an important recognition feature for proteasomal degradation.<sup>[12]</sup> Recent studies show that ubiquitination is also involved in various non-degradative signaling pathways, such as cell cycle regulation, differentiation and development, modulation of the cell surface, DNA damage repair and many more.<sup>[13]</sup>

Polyubiquitinated substrates are channeled through Ub-binding proteins to the (26S-) proteasome. This complex is an ATP-dependent barrel-shaped protease with a total mass of 2.5 MDa. It comprises the catalytic 20S core (700 kDa) and up to two 19S regulatory particles (900 kDa) mounted at each end of the core particle.<sup>[14]</sup> Since its three active sites are buried within the core, only unfolded substrates can enter the proteasome to get proteolyzed. In this way, a layer



## Introduction

of specificity is added to the complex. Once a protein enters the proteasome, its fate is dedicated to degradation and the process cannot be reversed. This ensures that no partially unfolded proteins interfere with normal cellular processes.<sup>[15]</sup> The Ub is recycled in its functional form and the originated amino acids or peptides are spliced into other biological proceedings.<sup>[16]</sup>

Even though Ub is covalently fused to its substrates, which get rapidly proteolyzed once polyubiquitinated, the Ub itself is a long-lasting protein *in vivo*. The reason for this is the occurrence of different ubiquitination states since the ubiquitylation of substrates can be reversed.<sup>[17]</sup> The enzymes that can cleave the isopeptide bond between Ub and another Ub or the substrate protein are called deubiquitinases (DUBs). They are the counterparts of the E3 ligases and play essential roles in removing mono- and polyubiquitin chains to maintain the available Ub pool and regulate the UPS.<sup>[18]</sup> DUBs are specialized hydrolases, whereas most carry a catalytic cysteine in their enzymatic center. Several DUBs are located at the proteasome and contribute significantly to ubiquitin recycling during the degradation process. Others have been associated with different biological processes, including transcriptional regulation via histone deubiquitination, cell growth and differentiation among them.<sup>[19]</sup>

### 1.2 The ubiquitin code and Ubls

Ubiquitination is a specialized way for cells to encode information about a substrate's process or development. Substrates are modified with a single Ub at a defined site, such as the histone H2B at lysine120. This monoubiquitylation has a massive influence on the histone's role in chromatin accessibility, which is important for transcriptional elongation, the DNA damage response and cellular proliferation.<sup>[20]</sup> Other substrates get multimonomubiquitylated at various lysine residues present at the substrates surface, as in the case of the epidermal growth factor receptor (EGFR).<sup>[21]</sup> (Multi-)Monoubiquitylation can already contain various informations important for different biological pathways. However, because Ub itself can be further modified with other ubiquitin or ubiquitin-like entities, this system creates myriad distinct signals and possible cellular responses. It is therefore termed "the ubiquitin code" (Fig. 2). This code is not fully deciphered up to today.

The amino acid sequence of ubiquitin features eight modification sites to build up chains (Fig 2A, C). These are seven lysines (Lys6, Lys11, Lys27, Lys29, Lys33, Lys48, Lys63) and the N-terminal methionine (Met1).<sup>[22]</sup> Chains formed at these residues can have a length ranging from two to more than ten ubiquitin moieties. Furthermore, ubiquitin chains can have different topologies,

## Introduction

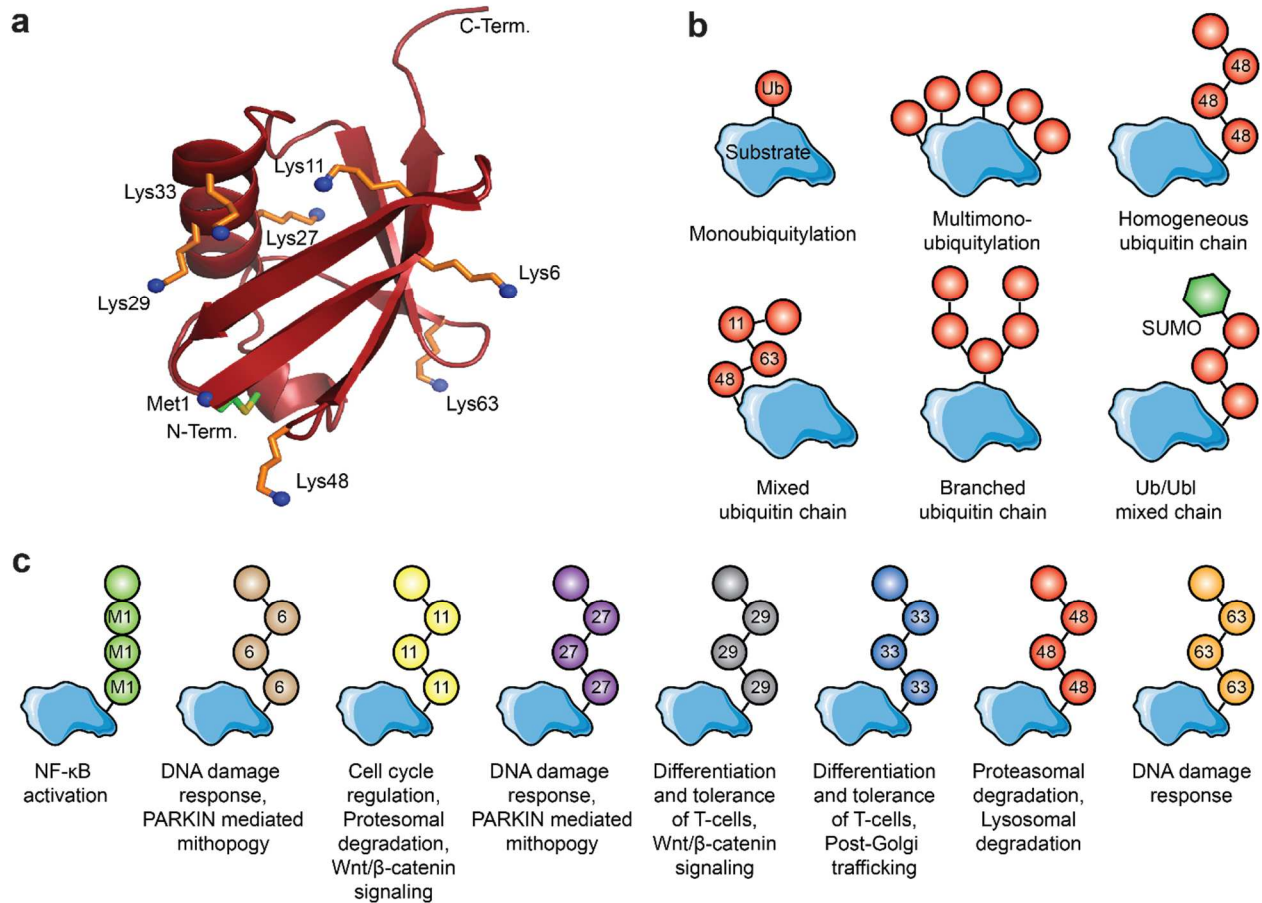


**Fig. 2 | The ubiquitin code. a)** Crystal structure of ubiquitin (red) with the seven lysines (orange) and one methionine (green) for chain elongation highlighted (PDB: 1ubq). The blue sphere represents the atom where the isopeptide bonds with the next Ub form. **b)** Schematic illustration of ubiquitylation topologies. **c)** Schematic illustration of the eight different polyubiquitin linkage types. Below are listed examples of signaling pathways in those chains play important roles.<sup>[24]</sup>

which can control their substrates' stability, activity, interaction properties or localization of their substrates (Fig. 2B).<sup>[23]</sup> In homotypic chains, all ubiquitins are fused via the same lysine-, or as in linear chains via the same methionine residue during elongation. This topology is well studied for Lys11-, Lys48- and Lys63 chains (Fig. 2B, C). Whereas homogenic Lys11 chains play essential roles in the cell cycle regulation and Lys48 chains are unavoidable for proteasomal and lysosomal degradation.<sup>[25]</sup> Lys63 conjugates promote DNA damage repair and regulate protein localization.<sup>[20]</sup> J. R. Morris and coworkers could prove that the BRAC1/BARD1 complex is vital for elongating homotypic lysine 6 Ub chains, which also transduce essential information for the DNA damage response pathway.<sup>[26]</sup> Whereas Lys27 chains are important for that pathway too.<sup>[27]</sup> Later publications suggest that both chain types also play a significant role in PARKIN-mediated mitophagy.<sup>[28]</sup> Both Lys29 and Lys33 chains are signals for immunogenic pathways, while the

## Introduction

former chain type also mediates Wnt/ $\beta$ -catenin signaling.<sup>[29]</sup> Furthermore, Lys 33 chains are also used for Post-Golgi trafficking.<sup>[30]</sup>

Heterotypic chains consist of Ubs linked through different residues and are further divided into mixed and branched chains. Mixed chains are produced if the ubiquitins are modified at alternating residues, but each Ub is only modified with one other Ub. This feature is essential for protein trafficking among others.<sup>[31]</sup> Branched chains are another topology that occurs when a single Ub is modified by two other Ubs at different residues (Fig. 2B). Although less is known about this topology than about its homotypic orthologues, recent studies unveiled that branched chains represent a significant fraction among all Ub chain. Ranging from 5-20 % depending on cell type and measurement used for the investigation.<sup>[32]</sup> The physiological roles of chains containing Lys11/Lys48, Lys29/Lys48 or Lys48/Lys63 linkages are deciphered. Some of these functions are cell cycle and protein quality control functions and are used as an enhanced signal for degradation.<sup>[33]</sup> Other branches have been verified *in vitro* or in cells, but their functions remain to be investigated. However, others are unknown to exist in a cellular setting.

Polyubiquitin chains can be further decorated with non-Ub post-translational modifications, adding another layer of complexity to the ubiquitin code. The two most common post-translational modifications (PTMs) are phosphorylation and acetylation. With the increasing precision of mass spectrometry techniques and the growing availability of datasets, it is now possible to identify up to nine potential phosphorylation sites on each ubiquitin (Ub). Revision of available datasets highlights that six out of seven lysine residues can be acetylated.<sup>[34]</sup> Another class of modifications closely related to Ub, are the Ubiquitin like modifiers (Ubl). Those small proteins are similar to ubiquitin regarding their substrate proteins, structure and biochemical behavior. They are covalently bound to a lysine residue through their own dedicated ligase cascade. In total eight Ubl families are known: small ubiquitin like modifier (SUMO), neural precursor cell-expressed developmentally down-regulated protein 8 (NEDD8), interferon-stimulated gene 15 (ISG15), autophagy-related protein (ATG12), human leukocyte antigen F-associated transcript 10 (FAT10), ubiquitin-fold modifier 1 (UFM1), *fau* and its ubiquitin-like domain (FUBI) and ubiquitin-related modifier 1 (URM1). The better understood are SUMO, NEDD8 and ISG15. Those three can occur directly linked to a substrate or within a heterotypic polyubiquitin chain, altering the informational output a homotypic ubiquitin chain would have.<sup>[35]</sup>

Effector proteins (readers) consisting of ubiquitin-binding domains (UBD) can attach to all those modifications and translate the ubiquitin code into specific actions. Whereas some bind

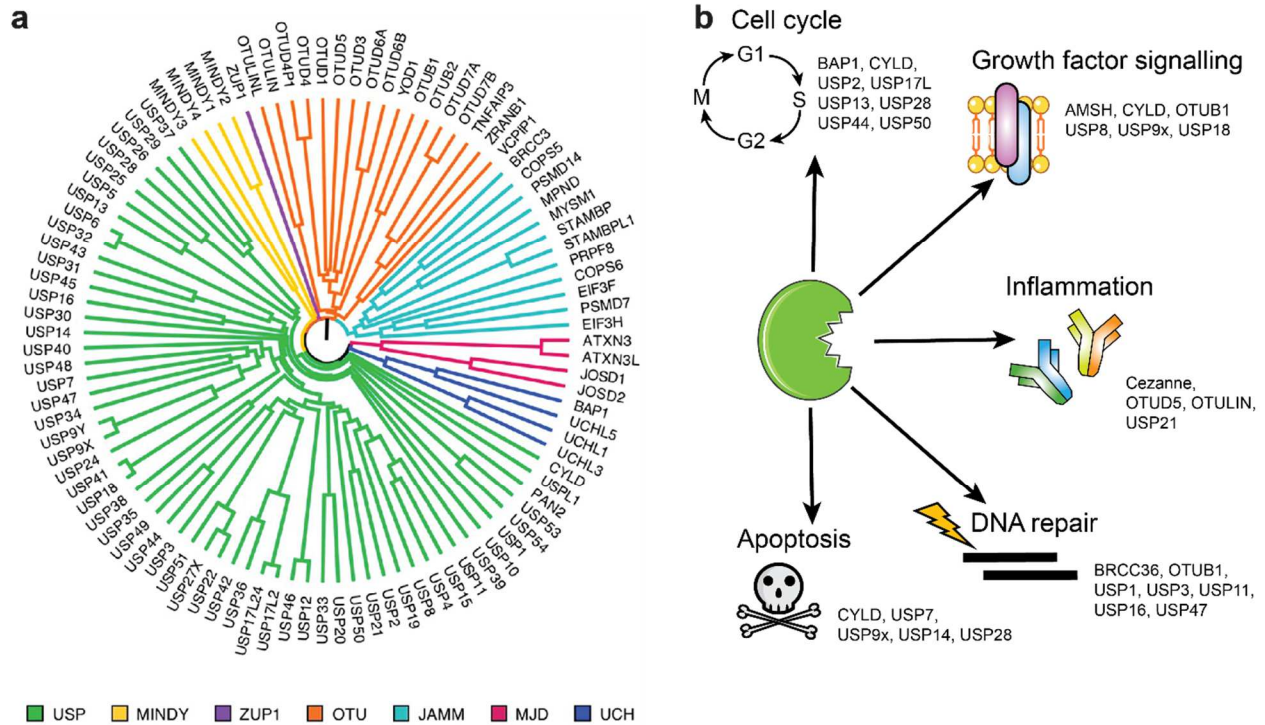
unspecifically, there are also several mechanisms for binding to a specific chain sequence. Some readers contain several UBDs to exploit the distance between Ub molecules depending on the linkage type.<sup>[36]</sup> Others are using the chain's flexibility to distinguish between different chains, because some linkage types are more compact and therefore, some UBD-containing proteins can slot between two Ubs to interact with different patches of the Ubs surface.<sup>[37]</sup>

### **1.5 Deubiquitinases - The erasers of the code**

Deubiquitinase activity is another important regulator of protein homeostasis and the UPS. DUBs, which possess a specialized hydrolase activity, can cleave the peptide- or isopeptide bond at the C-terminal glycine of Ubs. In eukaryotes, the central role of DUB activity is the maintenance of the ubiquitin pool, from which the writer enzymes can draw to target other proteins for degradation or signaling.<sup>[38]</sup> Three fundamental processes achieve this. First, Ub is encoded by four genes (UBA52, RPS27A, UBB, UBC), as a linear chain of multiple ubiquitin or as a ribosomal fusion protein.<sup>[39]</sup> DUBs cleave these precursor proteins and convert Ub into its mature form. The most active DUBs acting on Ub precursors are UCHL3, USP9x, USP5 and USP7.<sup>[40]</sup> Secondly, DUBs can remove whole ubiquitin chains from substrate proteins to stabilize them and therefore rescue them from proteasomal or lysosomal degradation. Even though proteins were not rescued and classified for degradation, some DUBs are associated with the proteasome to recycle the Ub shortly before the digestion of the substrate. DUBs directly interact with the proteasome are RNP11, USP14 and UCHL5.<sup>[41]</sup> Thirdly, DUB activity plays a crucial role in trimming ubiquitin modifications. Thereby, they regulate several critical cellular processes, including the cell cycle, growth factor signaling, inflammation, DNA damage repair and apoptosis, among others (Fig. 3B). All of these processes need rapid and dynamic adaptations due to shifts in the surrounding environment, handled through the fast editing of Ub chains by DUBs.<sup>[42]</sup>

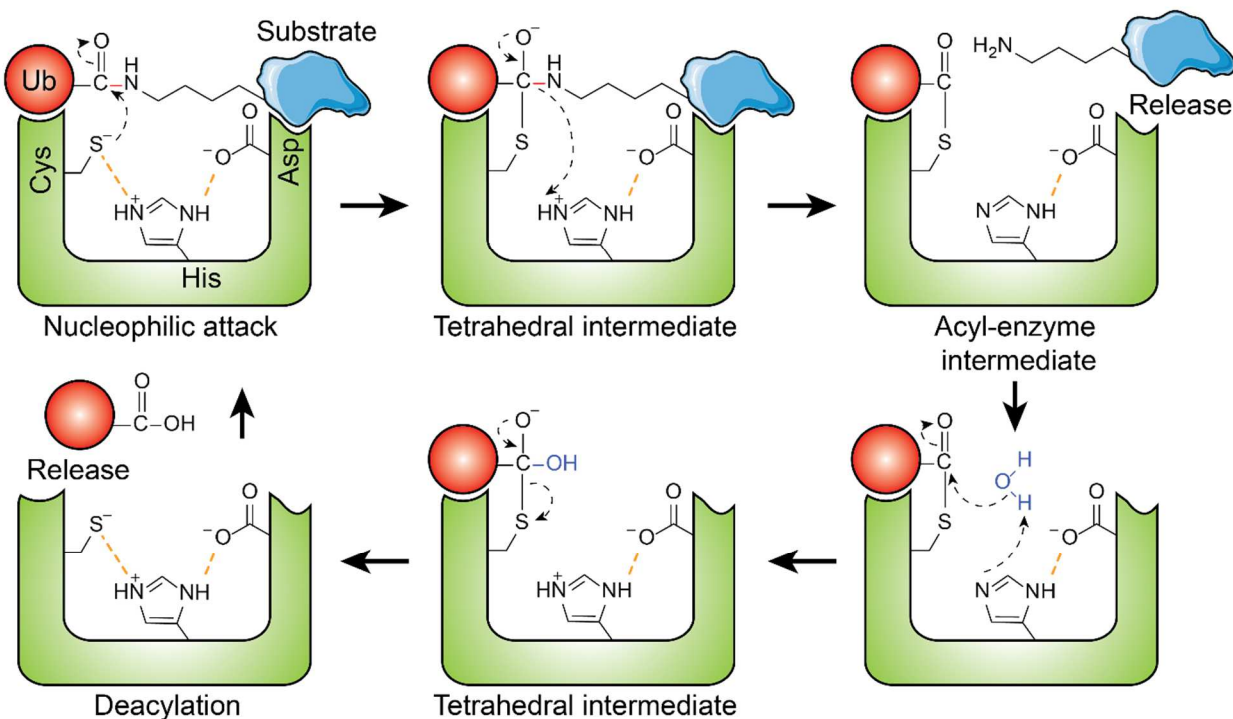
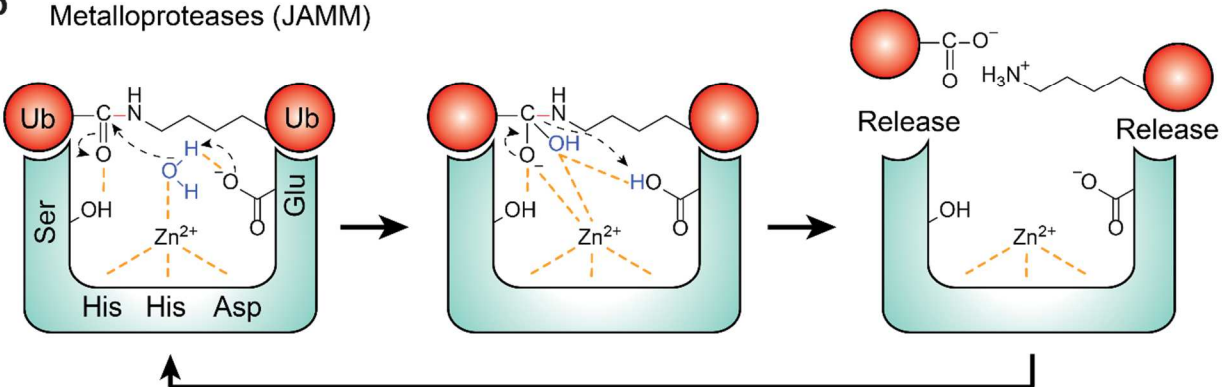
In humans, around 100 of these specialized enzymes are identified, which can be divided into seven structurally distinct families based on the architecture of their catalytic pockets.<sup>[43]</sup> Those are the ubiquitin C-terminal hydrolases (UCHs), ubiquitin specific proteases (USPs), Machado-Josephin domain proteases (MJDs), ovarian tumor proteases (OTUs), motif interacting with Ub-containing novel DUB family (MINDY), zinc-finger-containing Ub peptidase (ZUP1) and the Jab1/Mov34/MPN+ protease (JAMM) (Fig. 3A).<sup>[44]</sup> With over 50 members, the USPs present the largest superfamily.

## Introduction



**Fig. 3 | DUB families and their cellular functions.** **a)** DUB phylogenetic tree. Based on the sequence similarity of their catalytic centers, DUBs are divided into seven distinct families: USPs, MINDYs, ZUP1, OTUs, JAMMs, MJDs and UCHs. Phylogenetic tree was adapted from N. J. Schauer *et al.*<sup>[44]</sup> **b)** schematic illustration of the interplay of DUBs in various important cellular pathways.<sup>[46]</sup>

Most of the DUBs are cysteine proteases determined by their characteristic catalytic triad.<sup>[45]</sup> The cascade is located in the catalytic center of the protein. Most commonly it consists of three amino acids, cysteine (Cys), histidine (His) and aspartic acid (Asp), that are responsible for the catalytic activity (Fig 4A). In this covalent catalysis, the thiol of the cysteine works as a nucleophile. Both the aspartic acid and the histidine's functional groups increase the thiol's reactivity. The histidine acts as a base to polarize and stabilize the cysteine. The aspartic acid stabilizes the base. The activated thiol attacks the carbonyl carbon of the isopeptide bond between Ub and the substrate. This results in a tetrahedral intermediate and a negatively charged carbonyl oxygen.<sup>[47]</sup> The oxyanion hole compromises this charge. The oxyanion hole is a cavity found within the active site of the DUB and stabilizes transition state negative charges on deprotonated oxygens or alkoxides. It typically consists of backbone amides or positively charged residues. Stabilizing the intermediate lowers the activation energy and therefore favors the catalysis.<sup>[48]</sup> The free lysine residue of the substrate is released and an acyl-enzyme intermediate is formed. In a hydrolysis reaction, the thioester forms an additional tetrahedral intermediate, which resolves by releasing the distal Ub with its free C-terminus and the thiol of the DUB, ready for another catalytic cycle.<sup>[47b]</sup> The only non-cysteine protease DUB family discovered so far are the

**a** Cysteine proteases (USP, MINDY, ZUP1, OTU, MJD, UCH)**b** Metalloproteases (JAMM)

**Fig. 4 | The catalytic mechanisms of DUBs. a)** Schematic representation of the catalytic mechanism of cysteine DUBs. The active site with the amino acid residues belonging to the catalytic triad is illustrated in green. Water molecules are blue and non-covalent interactions are indicated by yellow dashed lines. The deprotonated thiol group acts as a nucleophile, attacking the carbonyl carbon at the isopeptide bond. A negatively charged tetrahedral intermediate is formed. Collapse of the intermediate releases the substrate, leaving the Ub in an acyl-enzyme intermediate. The Ub is released by the attack of a water molecule, also recovering the triad's original state. **b)** Schematic illustration of the catalytic mechanism of metallo DUBs. The active site with amino acid residues important for catalysis and coordination of the zinc ion is depicted in cyan. The hydroxyl group of the water molecule coordinating

## Introduction

the zinc ion acts as a nucleophile attacking the carbonyl carbon of the isopeptide bond. A tetrahedral intermediate is formed, which upon collapsing, releases the Ub and the substrate (here, the distal Ub from an Ub dimer).<sup>[47a]</sup>

JAMMs. They belong to the metalloproteases. A zinc ion is coordinated by water, two His and one Asp in the catalytic center (Fig. 4B). Upon binding to a substrate, a nearby glutamine (Glu) abstracts a proton from the coordinating water molecule. The hydroxy ion attacks the substrate's carbonyl carbon. The resulting tetrahedral intermediate collapses and leaves the free lysine residue of the substrate. The hydroxy group replaces the COOH group at the distal Ub.<sup>[47a]</sup>

Most of the DUBs are active enzymes, but eleven are considered to be inactive. These DUBs are classified as pseudoenzymes. They are particularly abundant among the JAMMs, with five out of 12 members identified as pseudoenzymes.<sup>[49]</sup> Nevertheless, do they interfere in signaling pathways via protein-protein interactions. Many DUBs throughout all families are conserved from yeast to humans. One exception is the MJD family.<sup>[43]</sup> The molecular weight of DUBs drastically differs. This is because DUBs possess various structural elements besides the catalytic center to present binding sites for protein-protein interactions, recognize substrates or ubiquitin moieties, and regulate enzyme kinetics.<sup>[44]</sup>

The specific selection of their substrates and the type of ubiquitin(chain) is regulated by various mechanisms. Homogenic Ubiquitin- and Ub/Ubl mixed chains are distinguished via different surface properties. Each modifier is recognized through a primary binding site. It is called the S1 site. Crystallization efforts revealed two surface patches of ubiquitin, with which the DUB interacts in its S1-binding site. Those regions are the Isoleucin(Ile)44 and Ile36 patches. Except NEDD8, Ubl's share little sequence similarity with Ub in this regions and thus discriminated by Ub-DUBs.<sup>[50]</sup> Deubiquitination can either occur by binding of the DUB directly to the substrate or to the Ub-chain. The latter is made possible by additional protein interaction domains, inside or outside the catalytic pocket.<sup>[47a]</sup> These domains recruit single protein substrates to the enzyme, enabling a DUB to regulate a specific signaling pathway. The DUBs following this binding mechanism cleave Ub chains regardless of their linkage type.<sup>[51]</sup> Conversely, DUBs that target their substrates via the Ub-chain are often linkage specific. A prominent example is OTULIN, which exclusively cleaves Met1 chains.<sup>[52]</sup> A unique feature of those DUBs is the arrangement of their ubiquitin-interacting motifs (UIM), which determines if a chain is cleaved from within (endo-cleavage) or from the distal- or proximal site (exo-cleavage). Endo-cleavage provides an efficient method to remove a chain (partly) from a substrate, but the chain needs to be further processed by other DUBs to regenerate the monoUb pool. Exo-cleavage results directly in monoUb, but the same DUB must work multiple times on the substrate. Another type of substrate specificity lies in the

## Introduction

Ub chain length since some DUBs prefer longer chains.<sup>[53]</sup> The kind of cleavage processed highly depends on the DUB family and the linkage type.<sup>[54]</sup>

As various cellular processes depend on specific and individual DUBs, they also rely on the intrinsic regulation of their activity.<sup>[45]</sup> In general, DUBs antagonize Ub writer enzymes and their relative abundance and activity can be understood as a switch, keeping each other in balance.<sup>[51]</sup> Nevertheless, like most proteins, DUBs can be regulated by fundamental mechanisms: PTMs, allosteric interactions, regulation of the individual abundance by altered gene expression and subcellular localization. In response to environmental stress factors or metabolic needs, PTMs on DUBs can act as a switch to shut them down rapidly or to bolster their activity. Covalent modifications such as phosphorylation, ubiquitylation or SUMOylation can appear on DUBs.<sup>[55]</sup> Those modifications do not only act as a degradation signal. Ubiquitylation of ATXN3 activates its catalytic activity, whereas SUMOylation of USP25 prevents the interaction with its substrates thereby inhibiting its activity.<sup>[56]</sup> Most of the DUBs possess an autodeubiquitinase activity to remove the regulation.<sup>[57]</sup> Many DUBs need to interact with other proteins to access additional ubiquitin-binding domains for efficient hydrolase activity. Therefore, these UIMs containing interactors might directly regulate DUBs.<sup>[58]</sup> AMSH gets activated by the interaction with the UIM-containing signal transducing adaptor molecule 2 (STAM2).<sup>[59]</sup> The allosteric binding of Ub to the N-terminal ZnF-domain of USP5 results in a conformational change leading to increased catalytic activity of the DUB.<sup>[60]</sup> Protein-DUB interactions can also inhibit activity, which is the case for UCHL5 by association with the INO80 chromatin-remodeling complex.<sup>[61]</sup> Subcellular localization is another crucial pillar of DUB regulation since it determines the array of available substrates for a given DUB. A prominent example is USP30, one of the few DUBs with a transmembrane domain to localize to mitochondria.<sup>[62]</sup> S. Urbé *et al.* used GFP-tagged DUBs to determine the distribution of cytosolic deubiquitinases and the ones that co-localize at cell organelles.<sup>[63]</sup> Several DUBs accumulate to the nucleus to regulate its functions and structure (Fig. 5). Others are associated with microtubules and the plasma membrane. A unique role is attributed to USP19, which can be localized to the ER or cytosol, depending on its splicing variant.<sup>[64]</sup>

To understand the impact of a specific DUB on an essential signaling pathway, it is important to consider its individual abundance. With mass spectrometry measurements becoming more accurate regarding resolution, the global copy number of single proteins is estimated more precisely.<sup>[65]</sup> Linkage-specific DUBs like OTULIN (Met1), Cezanne (Lys11) and OTUB1 (Lys48) show higher copy numbers per cell than others. It is hypothesized that these DUBs have



## Introduction

housekeeping functions and are intended to prevent the accumulation of a particular chain type, while some rarer forms play more specialist role.<sup>[43]</sup>

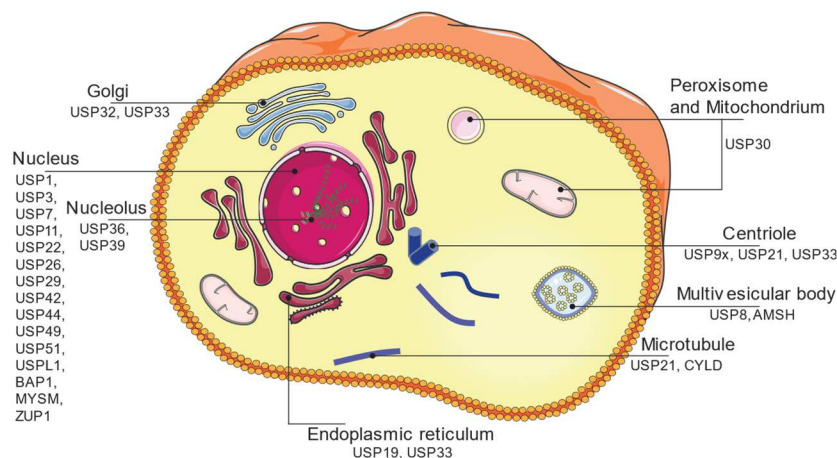


**Fig. 5 | Cellular localization of DUBs.** Schematic depiction of the subcellular localization of exemplary DUBs in a eukaryotic cell.<sup>[43]</sup>

### 1.6 UCHL1 – much studied, but far from understood

The UCH family consists of four members: BAP1, UCHL5, UCHL3, and UCHL1, ranked by their molecular weight (MW). With a MW of ~25 kilodalton (kDa) and a length of 223 amino acids, UCHL1, also known as neuron-specific protein PGP9.5, is the smallest member of the family.<sup>[66]</sup> Although the UCHs and the USPs have a similar 3D structure and their catalytic center, both feature a catalytic triad, they differ in the amino acid sequence of their catalytic pocket. The catalytic Cys of the UCHs is embedded into a narrow cleft on the protein's surface, restricting the substrate availability and increasing specificity.<sup>[17]</sup> Another structural feature that all members of the family share is the so-called crossover loop. This loop covers the catalytic cleft and further restricts the access of substrates. Also, this structural element varies in size depending on the family member. UCHL1 has the smallest crossover loop, which results in the lowest accessibility to the catalytic pocket.<sup>[67]</sup> Furthermore, the catalytic center's polypeptide backbone of UCHL1, comprising five crossings forming a "Gordian" knot, the most complicated eukaryotic protein structure discovered.<sup>[68]</sup> The basic 3D structure of UCHL1 is composed of two  $\alpha$ -helices, covering a conserved and densely packed hydrophobic core of multiple  $\beta$ -strands.<sup>[69]</sup> The catalytic triad comprises Cys90, His161 and Asp176 (Fig. 6). Mutation of any of these residues abolishes catalytic activity.<sup>[70]</sup>

## Introduction

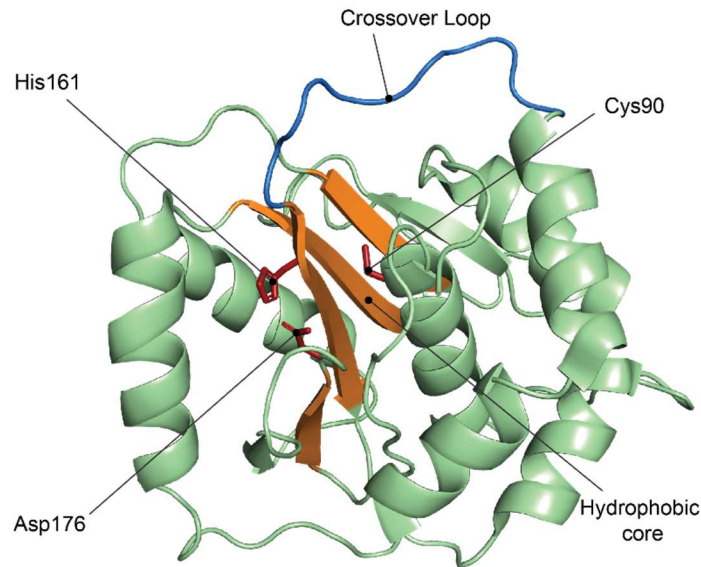


**Fig. 6 | Structural characteristics of the DUB UCHL1.** Overview of the structural elements of UCHL1 (PDB: 2ETL). The catalytic triad is composed of Cys90, His161 and Asp176 (red sticks). The hydrophobic core consists of several  $\beta$ -strands (orange), covered by  $\alpha$ -helices (light green). The crossover loop (blue) restricts the accessibility to the catalytic pocket and therefore generates substrate specificity.

Even though UCHL1 is one of the most studied DUBs, its full substrate spectrum remains far from understood.<sup>[71]</sup> It is a single-domain protein, which can hydrolyse small Ub derivatives *in vitro* but fails to process diUb or longer Ub chains. It has been structurally rationalized that the activity of UCHL1 is limited to small Ub conjugates because of its crossover loop.<sup>[72]</sup> Early works suggest the cleavage of short ubiquitylated peptides as the preferred substrates of UCHL1 to maintain the free Ub-pool.<sup>[73]</sup> In contrast, Y. Liu and coworkers found that homodimeric UCHL1 is not only capable of hydrolysing Ub-derivatives but also exhibits an E3-ligase activity by catalyzing the formation of Lys48 linked poly Ub chains on  $\alpha$ -synuclein.<sup>[70]</sup> Later, another group used the same approach but failed to reproduce the suggested ligase activity. Their results show that UCHL1 has no ligase activity, and did not ubiquitylate  $\alpha$ -synuclein.<sup>[74]</sup> Further investigations are needed to clarify UCHL1's function.

The DUB is highly abundant in brain tissues, making up to 5 % of the soluble neuronal proteins. It is also expressed at much lower levels in the testis, gonads and other clonal cell culture models.<sup>[75]</sup> Surprisingly, UCHL1 is detectable in tumor cells derived from tissue samples that do not express UCHL1 in their healthy population. Those include pancreatic, colorectal and invasive breast cancer.<sup>[76]</sup> The role of UCHL1 in cancer is multifaceted and highly dependent on the cancer entity. There are studies that show an oncogenic role.<sup>[77]</sup> Others are proposing a tumor suppressor activity.<sup>[78]</sup> In colorectal cancer, UCHL1 is associated with the  $\beta$ -catenin/TCF signaling pathway

## Introduction

and the promotion of tumor malignancy by removing Ub from  $\beta$ -catenin.<sup>[79]</sup> Recent studies suggest emerging evidence for the participation of UCHL1 in the most aggressive forms of breast cancer (estrogen receptor (ER)- or triple-negative breast cancers (TNBC)), through the regulation of the ER and the interplay in the transforming growth factor  $\beta$  (TGF- $\beta$ ) pathway.<sup>[80]</sup> Furthermore, hypoxia-inducible factor 1 (HIF-1) is a significant driver for breast and lung cancer tumor metastases. UCHL1 was identified as an essential upstream activator of HIF-1 by deubiquitinating its  $\alpha$ -subunit and therefore promotes tumor metastases.<sup>[81]</sup>

Besides the link to cancer, UCHL1 dysregulation is associated with neurodegenerative diseases, such as Parkinson's disease (PD), Alzheimer's disease (AD) and brain injury among them.<sup>[82]</sup> One of the main reasons for the development of AD is the aggregation of  $\beta$ -amyloid peptides. This 39-43 amino acid long fragment is produced from larger precursors by the protease BACE1.<sup>[83]</sup> Zhang and coworkers report that the inhibition of UCHL1 significantly increased BACE1 expression and therefore increased the total concentration of  $\beta$ -amyloid aggregates. On the other hand, overexpression of UCHL1 resulted in decreased aggregates and delayed AD progression.<sup>[84]</sup> There are two UCHL1 polymorphisms identified, which are linked to the progression of PD. The I93M mutation increases PD risk, whereas the S18Y polymorphism reduces the susceptibility to PD and other neurodegenerative diseases.<sup>[70]</sup> *In vitro* analysis of the I93M variant revealed decreased catalytic activity and a lower stability than the wild type.<sup>[85]</sup> The overexpression of I93M UCHL1 in mice led to common physiological phenotypes of PD and the degeneration of dopaminergic neurons.<sup>[86]</sup> Another polymorphism in the UCHL1 gene leads to an E7A mutation, which decreases the DUBs catalytic activity and manifests in progressive early-onset neurodegeneration.<sup>[74]</sup>

Furthermore, the disfunction of UCHL1 is linked to various other phenotypes in brain tissue. The central nervous system of gracile axonal dystrophy (*gad*) mice exhibits impaired ubiquitination of dystrophic axons and a reduced free monoubiquitin pool. The *gad* mutation resulted from an in-frame deletion, including exons 7 and 8 of the UCHL1 gene, and as a consequence, the loss of 42 amino acids along with the catalytic His161.<sup>[87]</sup> Furthermore, the S-nitrosylation on Cys152 results in the structural instability of UCHL1 and promotes the co-aggregation with  $\alpha$ -synuclein in Lewy bodies.<sup>[85]</sup> Another PTM of UCHL1 is the farnesylation of Cys220, which is reported to enhance the binding of UCHL1 to the endoplasmic reticulum and increases  $\alpha$ -synuclein neurotoxicity. Other studies prove that the farnesylation at Cys220 is unnecessary to recruit UCHL1 to membranes in general, as a C220S mutant did not reduce the total amount of UCHL1 in the membrane fraction.<sup>[88]</sup>

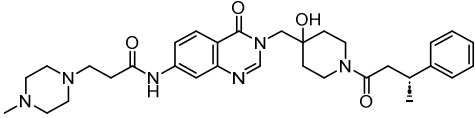
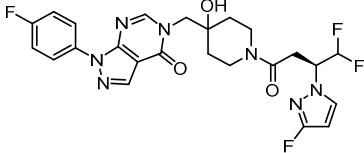
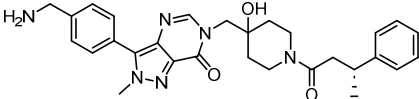
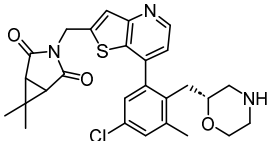
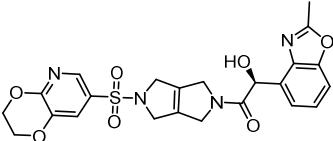
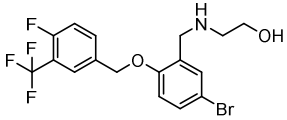
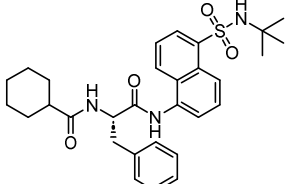
In addition, UCHL1 is connected to various other functions with metabolism, oxidative stress and autophagy among others.<sup>[75, 89]</sup> The connection of UCHL1 to a myriad of diseases and many different functions makes it an attractive therapeutic target, but after years of studies, its exact function or direct substrates remain to be disentangled.

### **1.7 Deubiquitinases in a therapeutic context**

Since many DUBs regulate various important signaling pathways, UCHL1 is not the only one studied in a disease-related context. Besides UCHL1, many other DUBs emerged as therapeutically targets of neurological disorders. Among those are USP15, USP30, USP33, USP35 and USP8.<sup>[90]</sup> Most of them inhibit parkin-dependent mitophagy by deubiquitinating mitochondrial-relevant proteins. This leads to mitochondrial dysfunction and finally neurodegeneration.<sup>[91]</sup> With 17.8 million deaths in 2017, cardiovascular diseases remain one of the most common cause of death worldwide.<sup>[92]</sup> It was demonstrated, that DUBs significantly impact vascular diseases, such as atherosclerosis, aortic aneurysm, angiogenesis and hypertension.<sup>[93]</sup> Since the success of the broadly acting proteasome inhibitor bortezomib in clinical trials, used to treat myeloid cell leukemia and refractory multiple myelomas, the UPS and DUBs have become attractive targets in the search for novel cancer therapies.<sup>[94]</sup> Several DUBs have been associated with tumorigenesis, highlighting their role as oncogenes and tumor suppressors. Genetically altered versions of USP4, USP7, USP6, USP15, USP16, USP28 and USP46 were identified as oncogenes, whereas CYLD, A20 and BAP1 were reported to act as tumor suppressors.<sup>[18, 95]</sup> In addition, the altered activity of DUBs was identified in commonly mutated cancer pathways such as p53, NF- $\kappa$ B, RTKs, Wnt and TGF- $\beta$  signaling.<sup>[96]</sup>

Especially the tumor suppressor p53 is of great interest in the context of the influence of DUBs on cancer. To date, eleven DUBs have been associated with its regulation.<sup>[97]</sup> Next-generation sequencing (NGS) revealed that p53 mutations are the most frequent genetic alteration in cancer. The unique mode of p53 inactivation in cancer makes it an attractive target and the reactivation by stabilizing its folding with small molecules appears feasible. However, the fact that p53 is a transcriptional factor and has been classified as “undruggable” calls for alternative treatment strategies.<sup>[98]</sup> In this context, the p53/MDM2/USP7 axis is of special interest. MDM2 is an E3-ligase directly acting on p53 and marking it for degradation. USP7, on the other hand, deubiquitinates MDM2 and stabilizes it. With the inhibition of USP7, MDM2 is no longer

## Introduction

Name	Structure	Target	IC <sub>50</sub> [μM]
XL188 <sup>[103]</sup>		USP7	0.09
FT671 <sup>[104]</sup>		USP7	0.052
Compound 4 <sup>[105]</sup>		USP7	0.006
Compound 41 <sup>[106]</sup>		USP7	0.00044
FT709 <sup>[107]</sup>		USP9x	0.46
AZ1 <sup>[108]</sup>		USP25/USP28	0.7/0.6
MF-094 <sup>[109b]</sup>		USP30	0.12

**Table 1 | Potent and selective DUB inhibitors.** The literature known compounds show excellent inhibition and selectivity against the deubiquitinases USP7, USP9x, USP25, USP28 and USP30.

deubiquitinated and destabilized, USP7 therefore indirectly stabilizing p53 in a cancer-relevant setting. This makes the inhibition of USP7 a novel strategy in cancer treatment.<sup>[99]</sup>

Beginning in late 2019, the COVID-19 pandemic caused devastating damage to the world-wide health system. By the middle of 2020, 12 million infections and over half a million deaths were

## Introduction

confirmed.<sup>[100]</sup> The novel SARS-CoV-2 coronavirus causes severe acute respiratory syndrome and the options for antiviral treatments remain scarce. The early sequencing of the SARS-CoV-2 genome and the comparisons to other coronaviruses (MERS-CoV and SARS-CoV-1) allowed the identification of the cysteine protease PLpro.<sup>[101]</sup> Its proteolytic activity is essential for the virus replication cycle. In addition, its protease activity can further remove Ub and ISG15 from its host targets to circumvent antiviral immunity. Inhibition of this viral deubiquitinase represents another promising strategy for the clinical intervention of SARS-CoV-2 infections.<sup>[102]</sup> Although there is evidence that the dysregulation of many DUBs is significantly involved in the onset of humanity's deadliest diseases, only a few selective and potent inhibitors exist to date (Table 1). Those include USP7, USP9x, USP25, USP28 and USP30.<sup>[107-109]</sup>

Due to its indirect stabilization of p53, the inhibition of USP7 is of special interest. Some of the earliest molecules targeting USP7 are the compounds **HBX41108** and **P22077**. Both were optimized from hits found in screening campaigns.<sup>[110]</sup> Later studies revealed that the compounds were not USP7 specific, but rather bound various additional other proteins including different DUBs.<sup>[111]</sup> In 2017 and 2018, screening efforts resulted in three potent and selective inhibitors against USP7 (Table 1).<sup>[103-105]</sup> All compounds bind non-covalently near the catalytic center of USP7 and abolish its deubiquitinating activity. The molecules share a hydroxy-piperidine binding element and show potencies in the low nanomolar range. The treatment of different cancer related cell lines with the compounds resulted in increased p53 protein levels, correlating with the decrease of MDM2. Furthermore, treatment with **FT671** led to degradation of N-myc in neuroblastoma cells. In addition, the compound was used to prove that USP7 is a stabilizing part of a demethylase complex. USP7 inhibition by **FT671** resulted in the degradation of E3 ligase UHRF1 and the DNA methylase DNMT1. Both proteins are involved in the same methylase complex as USP7.<sup>[104]</sup> In 2020 P. R. Leger *et al.* published a highly and extremely selective USP7 inhibitor based on a novel thienopyridine scaffold, which demonstrated the suppression of tumor growth in xenograft studies.<sup>[106]</sup>

A. Clancy *et al.* report a potent and selective inhibitor for USP9x based on a pyrrolopyrrol scaffold (Table 1). **FT709** was hit optimized from a high-throughput screen of a diverse collection of 140000 compounds. The compounds show specificity for USP9X among all DUBs, with an IC<sub>50</sub> of 0.5 μM and approx. 5 μM in MCF7 cell lysates and intact MCF7 cells, respectively. By the use of **FT709** the authors were able to prove that the E3-ligases Makorin 2 and ZNF598 belong to the substrate spectrum of USP9x. Inhibition of the DUB resulted in reduced levels of the ligases and ribosomal stalling.<sup>[107]</sup>

## Introduction

The compound **AZ1** exhibits a dual inhibition towards the evolutionarily closely related DUBs USP25 and USP28 (Table 1). The compound has an IC<sub>50</sub> value of 0.7 μM and 0.6 μM against USP25 and USP28 respectively. USP28 stabilizes c-Myc, yet another oncogene. Consequently, treatment of several colon cancer cell lines with the compound led to the inhibition of USP28 and to reduced levels of the c-Myc oncoprotein. The authors were able to prove that the inhibitor AZ1 could be used to induce concentration and time dependent cell cycle perturbations and cell death, having an antiproliferative effect on cancer cells.<sup>[108]</sup>

A. F. Kluge *et al.* reported a selective and potent USP30 inhibitor based on a naphthalene-sulfonamide scaffold. A HTS campaign identified compounds with a racemic phenylalanine core scaffold as USP30 inhibitors. A dedicated SAR study revealed, that the three hydrogens at the nitrogens are essential, since methylation of any of these nitrogens led to drastic drop in USP30 inhibition. Furthermore, the sulfonamide region seemed restrictive regarding tolerated substations. Introducing an additional methylene between the sulfonamide and the phenyl ring resulted in complete loss of inhibition. Electron withdrawing groups at the phenyl ring are preferred over electron donating groups. Chemical optimizations yielded the highly selective USP30 inhibitor **MF-094** with an IC<sub>50</sub> value of 0.12 μM. The compound increases and accelerates mitophagy and ubiquitination of mitochondrial-associated proteins.<sup>[109b]</sup>

### 1.8 Tools to study deubiquitinases

The dysregulation of DUBs is implicated in several human diseases, with cancer, neurological disorders and autoimmune disorders among them.<sup>[112]</sup> This highlights the importance of DUBs as promising drug targets. However, there are no approved drugs based on DUB inhibitors so far. This is due to the poor selectivity profile of a wide range of small molecule DUB inhibitors and the poor understanding of basic DUB biology regarding substrates, interaction partners and the cellular mechanism in which these enzymes are involved. In order to overcome these hurdles, tool molecules that function in a complex cellular environment are needed.<sup>[113]</sup> Recently, several of those tool molecules have been developed to accelerate the understanding of DUB biology. These chemical biology tools can generally be divided into three categories: Ub-based probes, small molecule-based probes and bifunctional molecules (Fig 7 A-C).

The Ub- and small molecule-based probes can be further summarized as activity-based probes (ABP). These chemical tools are frequently used to profile the enzymatic activity of a given protein

## Introduction

*in vivo* and *in vitro* by mimicking the substrate. Instead of being processed, the ABP covalently attaches to the catalytic center via an enzyme-catalyzed reaction.<sup>[114]</sup>

There are a lot of well-established methods to measure protein abundance. However, some proteins are expressed in an inactive state and therefore, protein abundance does not necessarily correlate with activity. Since ABPs do not react with inactive enzymes, the probe labeling indirectly measures catalytic activity.<sup>[115]</sup> In order to react with their targets, the probes require a nucleophilic amino acid residue in the catalytic center. ABPs are particularly suitable for studying enzymes with a catalytic cysteine, threonine or serine in their active site. Classic activity-based probes consist of three components:

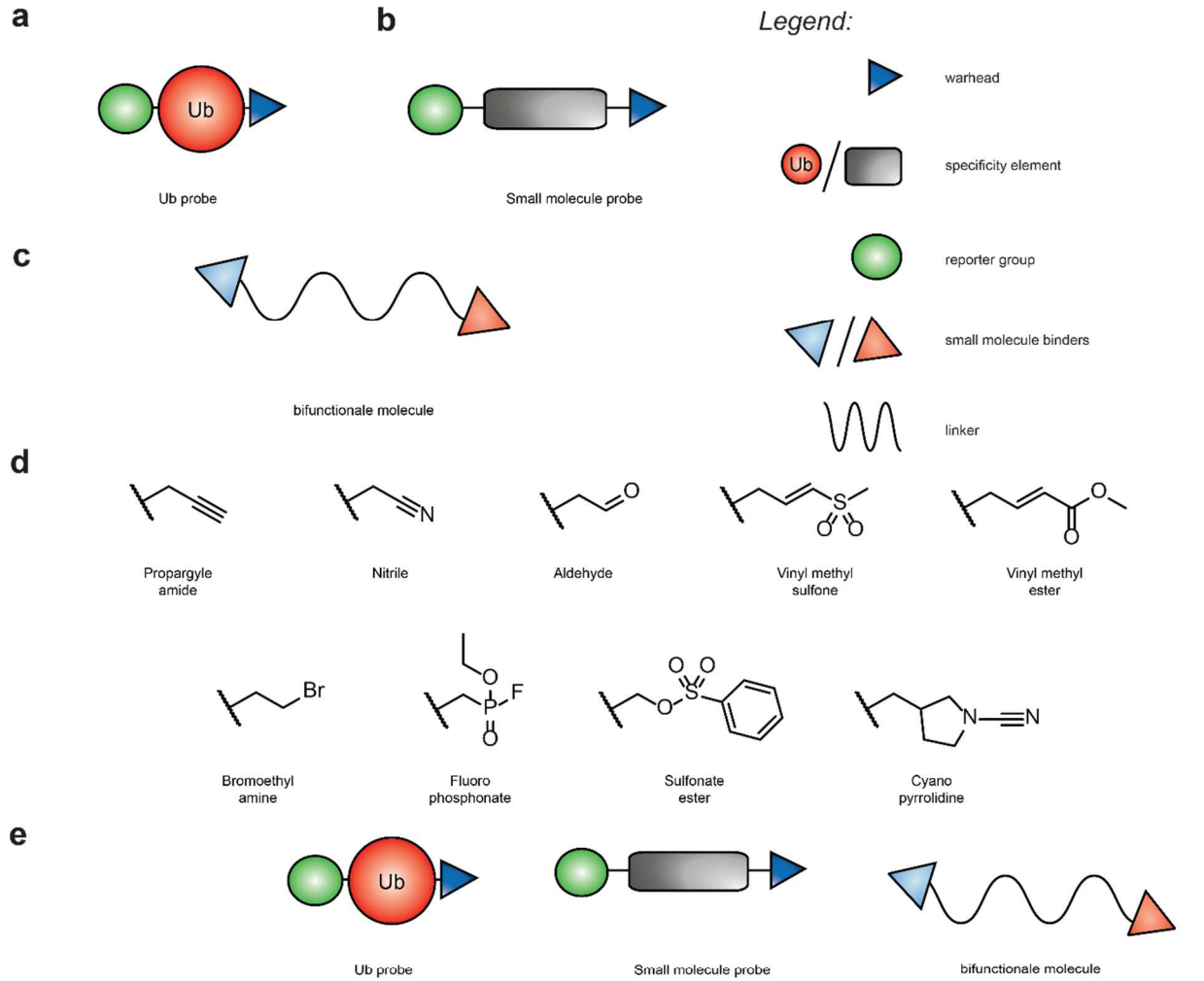
**I)** A reactive group also, called the warhead. In the case of enzymes with active site nucleophiles, an electrophilic moiety is used.<sup>[116]</sup> Other probes can target metalloproteases and utilize polydentate ligands as their reactive group.<sup>[117]</sup> The choice of the warhead structure heavily influences both the reactivity and the selectivity of the probe.<sup>[114]</sup> Depending on the warhead, the probe can mechanistically react with a nucleophilic residue via a direct addition (1,2-addition), a conjugate addition (1,4-addition) or a nucleophilic substitution.<sup>[118]</sup>

**II)** The recognition element is the ABP's core structure and is highly important for the specific targeting of probe towards the protein of interest (POI). This may be a small molecule inhibitor (as used for the small-molecule based probes), a short peptide or a full-length protein.

**III)** A reporter tag for detection and isolation of the bound protein is the third component of the ABP. Whereas a fluorophore as a reporter tag can be used for sensitive visualization, affinity labels such as biotin or a peptide epitope are utilized to enrich the probe from complex protein mixtures. In addition, a small biorthogonal group, such as an alkyne or azide, can be used to incorporate the reporter after the initial binding of the probe. This process, often called "two-step" labeling, can be advantageous when larger reporter groups might interfere with the probe's physiochemical properties, reactivity or selectivity.<sup>[119]</sup> Since most of the DUBs are cysteine proteases, activity-based probes equipped with a Cys-modifying electrophile have been proven successfully to be powerful tools to shed light on the activity and selectivity of DUB inhibitors and to determine the enzymatic activity and physiological roles of these specialized hydrolases.<sup>[114]</sup>



# Introduction



Total DUB specificity	✓	✗	✗
Probe Discoverability	✓	✗	✗
Membrane permeability	✗	✓	~
Individual DUBs targetable	✗	✓	✓
Applicable to inactive targets	✗	✗	✓

**Fig. 7 | Tools to study deubiquitinases. a-c)** Schematic overview of the different chemical biology tools. **a)** Ub-based probes, **b)** small molecule-based probes, **c)** bifunctional molecules. **d)** Structural depiction of commonly used electrophilic moieties for activity-based probes. **e)** Advantages and disadvantages of the individual tools.

### 1.8.1 Ubiquitin-based probes

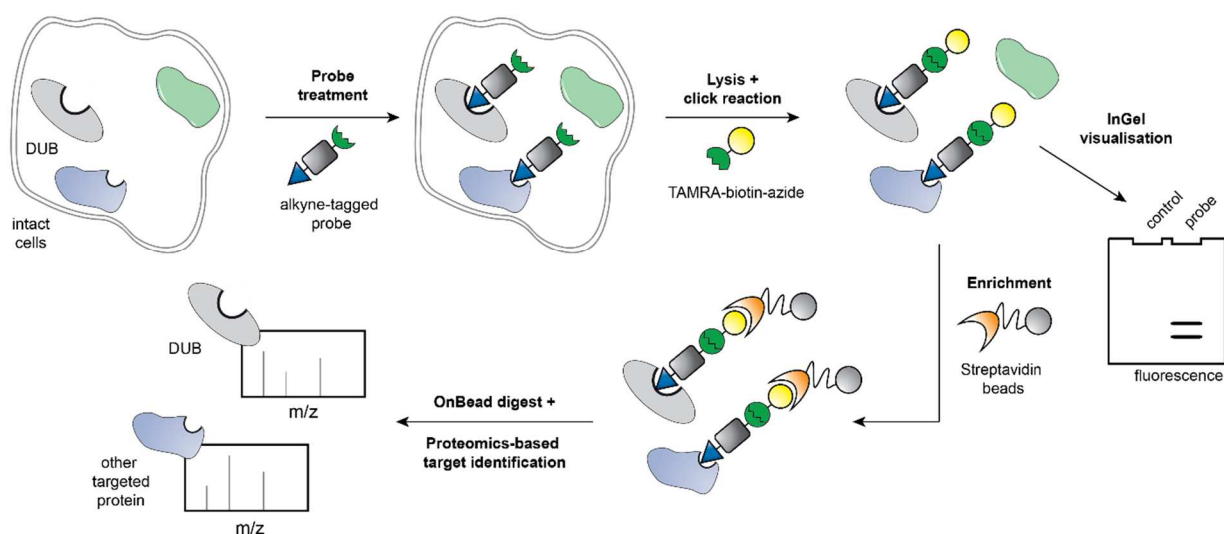
Ubiquitin-based probes represent a unique form of ABPs that specifically target deubiquitinases since ubiquitin is used as the recognition element. The first covalent probes used for DUB targeting used full-length Ub with the C-terminal glycine (Gly76) replaced for an electrophile.<sup>[120]</sup> Ub-aldehyde (Ub-Al) and Ub-nitrile (Ub-CN) were critical early tools for the mechanistic investigation of deubiquitinases.<sup>[121]</sup> The Ub-Al probe was used to solve the first crystal structure of a DUB in co-complex with Ub. The structure revealed significant conformational changes of the DUB upon Ub binding.<sup>[122]</sup> However, the covalent bond of both probes are reversible under certain conditions.<sup>[123]</sup> This restriction was overcome by using a C-terminal vinyl methyl sulfone as the warhead. The resulting Ub-vinyl methyl sulfone (Ub-VS) probe covalently modified UCH and USP DUBs under reducing conditions and was used to detect those enzymes in cell lysates due to an HA-tag on the probe.<sup>[124]</sup> Since then, various C-terminal electrophiles have been exploited for the use as Ub probes (Fig. 7 D), with Ub-VS, Ub-vinyl methyl ester (Ub-VME) and Ub-propargyl amides (Ub-PA) being the most common ones. Later, the recognition element was extended to di-ubiquitin to improve the understanding of the linkage specificity of DUBs and their interaction with substrates.<sup>[125]</sup>

One way to generate Ub probes is the expression of an Ub precursor, which reacts with 2-mercaptoethane sulfonate sodium (Mesna) in a transthioesterification to an Ub-Mesna species. This molecule contains a highly reactive thioester bond. Ub-Mesna reacts with the free amine of the warhead molecule in a nucleophilic addition to form the final probe. Because Ub-Mesna is easy to express in high amounts and the subsequent reaction is optimized for most warheads, the Ub-probes are available to investigate a variety of DUBs.<sup>[126]</sup> Using ubiquitin as a recognition element for probes allows the exquisite covalent modification and detection of DUBs in complex mixtures. However, it is not easy to address individual DUBs with Ub probes, as ubiquitin is the preferred substrate of these hydrolases. In addition, the scope of application is limited to cell lysates as the size of the Ub recognition element precludes membrane permeability.<sup>[114]</sup> Consequently, the cell lysis leads to a dilution of cytoplasmic and nuclear proteins and a dissolution of the cellular organization and localization. This ultimately results in the dissociation of protein-protein interactions, which might be necessary for DUB activity and the dysregulation

of the ubiquitin plexus.<sup>[127]</sup> To address those vulnerabilities, small molecule-based probes are used and investigated.

### 1.8.2 Small molecules-based probes

**a**



**b**

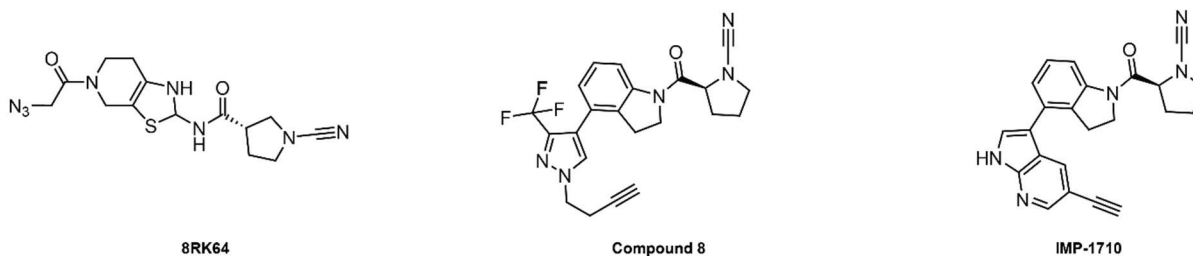


**Fig. 8 | Activity-based protein profiling. a)** Schematic workflow of the two-step labeling activity-based protein profiling. Intact cells are treated with a probe, followed by lysis. In a labeling reaction, the reporter is installed. In case a fluorophore is used, modified targets can be visualized. In the case of biotin as a reporter, covalent-bound proteins can be enriched, digested and analyzed via mass spectrometry-based techniques. **b)** Overview of recently published small-molecule based probes for investigating UCHL1.<sup>[129]</sup> All three structures share a cyanopyrrolidine moiety as their warhead (blue) and an alkyne or azide handle (green) to further install a reporter group.

Small molecule-based probes present another form of ABPs, utilizing warheads similar to those used for Ub-probes. They differ in their recognition element, based on known DUB inhibitors. Therefore, small molecule-based probes have a much smaller MW, leading to increased membrane permeability compared to their Ub counterpart.<sup>[128]</sup> Small molecule probes bearing a reporter group such as biotin, a fluorophore or an alkyne moiety can be employed to activity-based protein profiling (ABPP) methods. ABPP describes a powerful strategy to study enzymes

in complex proteomes. Those experiments include the monitoring of a specific enzymatic activity, the characterization of protein functions, the identification of up- and down-regulated proteins in disease states and the evaluation of newly synthesized inhibitors in cell cultures and living organisms.<sup>[130]</sup> First, a given proteome is treated with the APB, whereas the probe covalently modifies the protein of interest. In a direct approach, the POI can be visualized by using fluorophors as a reporter group after lysis or homogenization of the cells or tissue. In a two-step approach, the reporter is installed via a labeling reaction. Several bioorthogonal reactions have been established. The most commonly used is the copper-catalyzed 1,3-cyclo-addition.<sup>[131]</sup> Furthermore, using a biotin entity allows the isolation of modified targets on a streptavidin matrix for subsequent mass spectrometry analysis. This sheds light on the entire target spectrum a small molecule inhibitor might bind to (Fig. 8 A).<sup>[132]</sup>

The first small molecule-based probe designed to target DUBs was found in 2016 by *J. Ward* and coworkers. The underlying inhibitor used as a recognition element was found in a high-throughput screening (HTS) campaign. The probe is based on a chloroacetylpyrrole scaffold and shows potent activity against 12 DUBs in living U2OS cells.<sup>[133]</sup> Recently, the Buhrlage lab utilized a DUB-focused covalent library for activity-based protein profiling to identify selective hits against 23 endogenous DUBs spanning four subfamilies. Followed by hit optimization, the authors presented a small molecule-based probe for the understudied DUB VCPIP1 with nanomolar potency and in-family selectivity.<sup>[113]</sup> In the last years, tremendous progress in small-molecule based probe discovery for UCHL1 was achieved, with several groups publishing potent molecules for cellular investigation of this DUB in live cells and zebrafish embryos (Fig. 8 B).<sup>[129]</sup>

### 1.8.3 Bifunctional molecules

A small molecule is often thought to be an inhibitor. However, beyond inhibition, some compounds can enhance the activity of their target, dictate novel functions or induce non-endogenous protein-protein interactions.<sup>[134]</sup> If a molecule promotes the formation of new multiprotein complexes by binding at the protein-protein interface, it is called a “molecular glue”.<sup>[135]</sup> Traditional small molecule inhibitors bind to well-defined active- or allosteric pockets, where they are in direct competition with substrates, ligands or other allosteric modulators. In contrast, molecular glues do not require a well-defined binding pocket or catalytic activity of their target as they serve as an interface between two proteins.<sup>[136]</sup> A specialized version of molecular glues are bifunctional

## Introduction

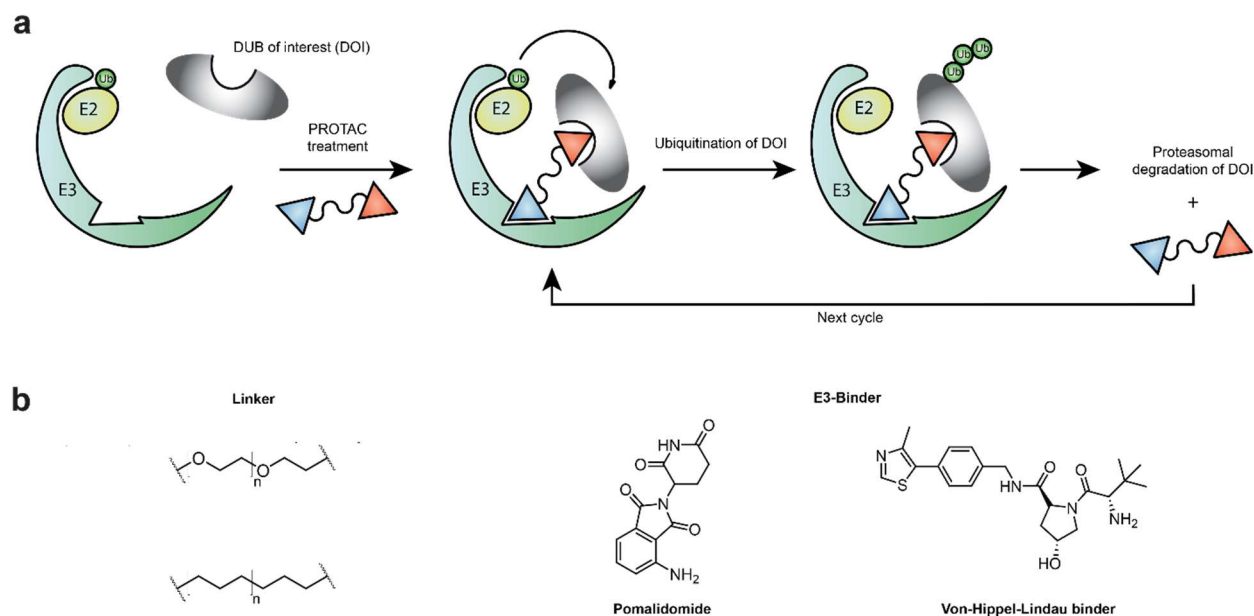


**Fig. 9 | Proteolysis targeting chimeras (PROTACs).** **a** Schematic overview of the PROTAC strategy. The PROTAC molecule aligns the POI in close proximity to an E3-ligase. As a result, the protein of interest gets ubiquitinated and marked for degradation. The ubiquitinated protein gets channeled to the proteasome, where it gets digested. Since the PROTAC molecule is not affected by the proteasome, it is available for another labeling cycle. **b** Molecular structures of common PROTAC features. The right linker length is essential for successful degradation. Linkers most commonly consists of alkyl chains or repeating polyethylene glycol (PEG) units (top). The most established E3-ligands are binders for the E3-ligases cereblon (CRBN) (bottom left) and the Von-Hippel-Lindau (VHL) ligase (bottom right).

molecules. A famous example of such molecules is the proteolysis-targeting chimeras (PROTACs). Heterobifunctional PROTACs consist of two small molecules connected via a chemical linker, independently binding to a POI and an E3 ligase.<sup>[137]</sup> Therefore, the compound stabilizes a ternary complex between those proteins, resulting in the subsequent polyubiquitination of the POI due to the close proximity to the E3 ligase. Followed by the shuttling to the proteasome, where the POI gets degraded (Fig. 9 A). Most commonly, two E3-ligases are targeted for the PROTAC strategy. The labs of Crews and Ciulli made major contributions in identifying and developing potent small molecules binding to the Von-Hippel-Lindau (VHL) E3 ligase (Fig. 9 B).<sup>[138]</sup> The other E3-ligase that is hijacked for the PROTAC approach is cereblon (CRBN). This ligase is potently bound by thalidomide and its analogs (Fig. 9 B).<sup>[139]</sup> Another less targeted E3-ligase, but with high-affinity ligands available, is MDM2.<sup>[140]</sup> Despite those, finding new potent E3-ligase binding molecules has been challenging. However, intense research efforts are made to expand the E3-ligase toolbox.<sup>[141]</sup>

## Introduction

The overall degradation activity of a PROTAC does not rely on the potency of its ligands alone, but rather on the optimal formation of the ternary complex between the two proteins.<sup>[142]</sup> The properties of the PROTAC linker are crucial to verify optimal protein-protein interaction. Those parameters are: Its chemical composition, length, hydrophobicity and rigidity of the linker, which can heavily influence the molecules binding kinetics, potency and selectivity.<sup>[143]</sup>

As bifunctional molecules have been proven to address proteins that lack well-defined binding pockets and are therefore classified as “undruggable” with conventional small molecule inhibitors, the PROTAC strategy gained substantial therapeutic interest over the recent years, with the first molecules advancing to clinical trials.<sup>[144]</sup> In addition, PROTACs allow the investigation of non-enzymatic effects of their targets on cellular pathways. These effects depend on the interaction of the POI with other proteins or substrates. Whereas the probes mentioned above are limited to only study the catalytic activity of their respective targets. The rapid depletion of the targets allows the investigations of proteins with slow turnover rates and avoids unwanted adaptation events in comparison to RNA-based or genome editing tools.<sup>[145]</sup> Furthermore, non-covalent PROTAC molecules are not affected by the proteasome. As a result, the same molecule catalyzes several cycles of bridging the POI to the E3-ligase. Therefore, low molecule concentrations often yield high cellular and *in vivo* efficacy.<sup>[146]</sup>

It was not before 2022 that two groups almost simultaneously published the first-in-class PROTAC molecules to target a DUB for degradation.<sup>[147]</sup> Both molecules consist of well-established, potent and selective USP7 binders to target the POI. These binders are connected to a ligand for attaching to the E3 ligase cereblon (CRBN). *Y. Pei et al.* identified a PEG3 unit as their preferred linker, whereas *A. Murgai et al.* utilized a short alkyl chain. Both groups report a sufficient degradation of USP7 and antiproliferative effects in both p53 wild-type and mutant cancer cells.

In contrast to PROTACs, another class of heterobifunctional molecules was introduced in 2022, termed deubiquitinase-targeting chimeras (DUBTACs).<sup>[148]</sup> This compound class includes a ligand to target an allosteric non-catalytic site at a DUB to recruit it in its active form. This recruiter is connected to another ligand independently binding the POI. The targeted protein gets stabilized due to deubiquitination, whereas it would be degraded otherwise in a ubiquitin-dependent manner. *Henning et al.* introduced a ligand that is binding to the non-catalytic Cys23 of the Lys48-ubiquitin specific DUB OTUB1. They linked the molecule to lumacraftor, a drug critical for the treatment of cystic fibrosis and binding to the  $\Delta$ Phenylalanin(Phe)508-cystic fibrosis transmembrane conductance regulator (CFTR). The treatment with the DUBTAC results in

## Introduction

robustly stabilized protein levels of  $\Delta$ Phe508-CFTR. This led to improved chloride channel conductance in a disease-relevant cellular model.

## 2. Motivation and Aims

The complex network of interactions that deubiquitinases are involved in has not been fully elucidated yet. As a result, there exists a lack of understanding the interplay of DUBs in cellular systems. In addition, the number of small molecule inhibitors for the specific targeting of DUBs remains low. This is due to three primary reasons: A limited number of DUB inhibitors that can be used as tool compounds has been reported. Most of them are published in patent literature and lack selectivity profiling or a general cellular characterization. Secondly, only a tiny subset of DUBs is well described regarding their cellular functions, behavior in pathological states or targetability by small molecule inhibitors. Thirdly, the genetic manipulation of DUBs can cause uncontrollable side effects because the RNA knockdown/out of proteins is a relatively slow process compared to direct inhibition of the DUB of interest. Further studies are required to understand how DUBs impact specific cellular pathways and what are their critical roles, particularly in disease states at the protein and genetic levels. To overcome this hurdle, new, potent and specific tool compounds for investigating DUBs in a cellular environment must be developed.

The aim of this thesis is the discovery, synthesis and evaluation of such probe compounds. This goal was accomplished by a top-down approach, further divided into four sub-objectives:

I) To enable the investigation of DUBs, the design and synthesis of small molecule probe compounds based on literature known DUB inhibitors will be performed. The probes will consist of an electrophilic warhead for the covalent modification of their targets and an alkyne moiety to use them in a two-step ABPP approach. Suitable exit vectors, for the attachment of the alkyne moiety will be identified. To obtain those molecules, synthesis will be planned and optimized.

II) The small molecule probes derived from I) are tested in a complex proteome for their ability to covalently modify DUBs. Promising hit molecules are selected and the modified DUB(s) are identified via proteomics based ABPP. These probes are then characterized in a cellular setting for their potency and specificity against the identified DUB(s). To accomplish this, several chemical biology and cellular assays have to be developed and established.



## Motivation and Aims

**III)** The most specific small molecule probes of **II)** will be used as tool compounds to investigate phenotypes resulting from inhibition of the targeted DUB in different cell lines. Furthermore, the compounds will be used in different cellular assays to elucidate the substrate spectrum of the DUB

**IV)** To be able to observe changes in a proteome not only after the inhibition of DUBs but after their depletion, PROTAC molecules will be synthesized. These compounds will be either based on the characterized probes obtained from **II)** & **III)** or from other non-covalent and specific inhibitors derived from the literature. The synthesized molecules will be characterized for the induced degradation of DUBs in cellular systems.

## 3. Results

### 3.1 Synthesis of a focused deubiquitinase probe library

This chapter describes the chemical synthesis and analysis of a DUB probe library derived from literature known inhibitors (Aim I). This includes the synthesis of the parent inhibitors and the associated alkyne-tagged derivatives thereof. In addition, a set of probes with a minimalistic binding scaffold were synthesized as control compounds. These molecules were mandatory for the further investigation of DUBs in a cellular context.

#### 3.1.1 Finding suitable molecular scaffolds for probe design

When the project was started in 2019, only very few small molecules targeting deubiquitinases were published in the academic literature. The proper molecular scaffolds suitable for probe design were primarily derived from patent literature. The research was based on the following criteria: The molecular scaffold had to be described to address at least one DUB, consist of an electrophilic warhead for the covalent modification of the DUB of interest and had to present suitable regions to install an alkyne handle for the attachment of a reporter (Fig. 10A). Surprisingly, the literature search revealed that most molecules described for the covalent attachment to DUBs feature a nitrile functionality as their warhead. The nitrile group reacts with the catalytic cysteine of the DUB in a nucleophilic addition ( $A_N$ ) to form a thioimidate adduct (Fig. 10B). Since the main scaffolds of the inhibitors were diverse in their structures, no direct similarities could be identified that would favor binding to a DUB. At this early stage, no DUB was prioritized for investigation, therefore the different scaffolds should be used to investigate which DUBs could be targeted. Nevertheless, the main scaffold should provide a certain selectivity within the DUB family to establish different probes, each targeting another DUB.

## Results

**a**

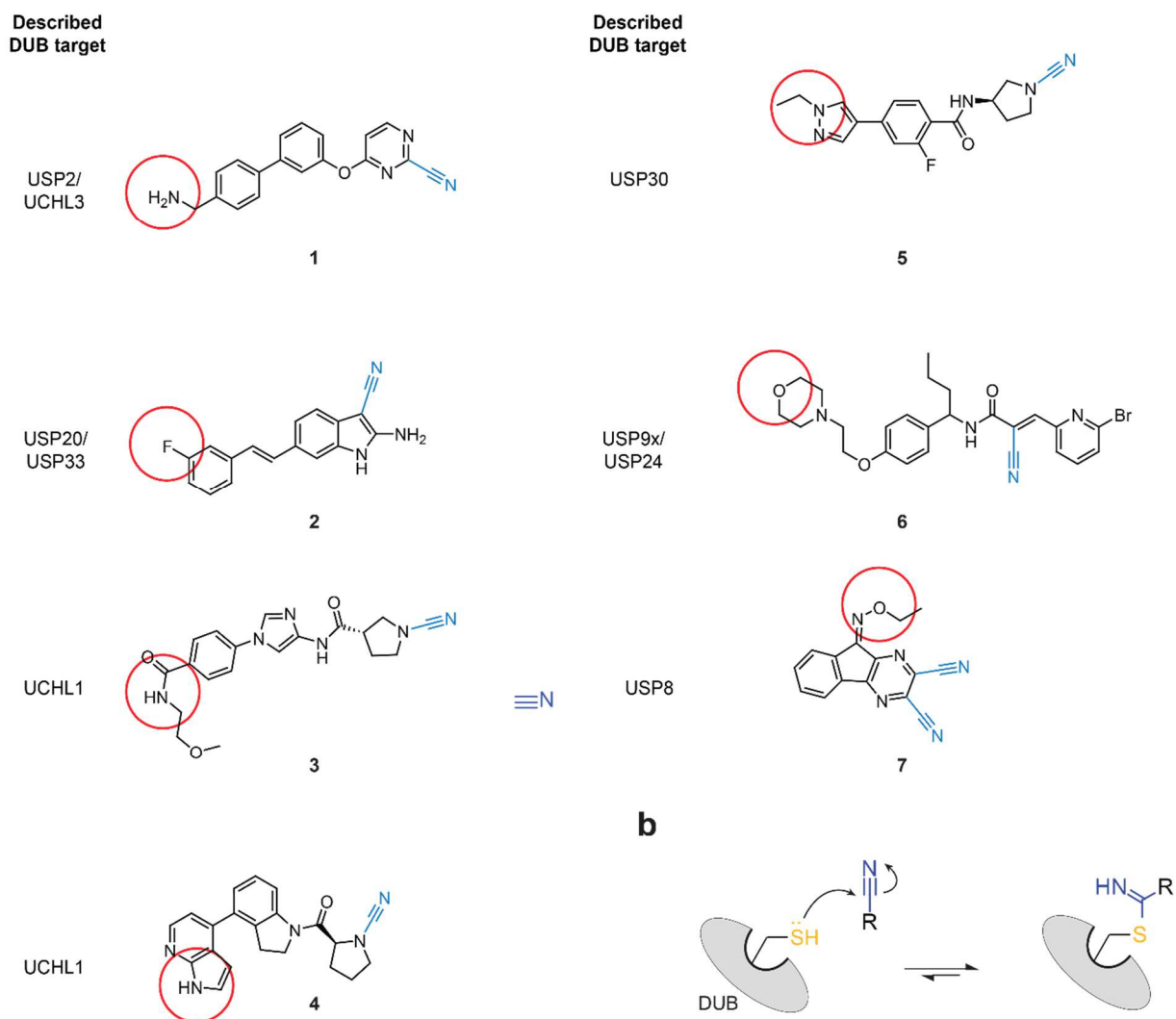


**Fig. 10 | Starting point for the design of a DUB-focused probe library. a)** Structures of patent-derived small molecule inhibitors described to target different DUBs. All structures consist of a nitrile as the electrophilic warhead for covalent modification of their target (blue). The red circle highlights possible sites to install the alkyne handle synthetically. **b)** Depiction of the nucleophilic addition of the thiol group (yellow) from catalytic cysteine with the electrophilic nitrile group (blue) of the compound.

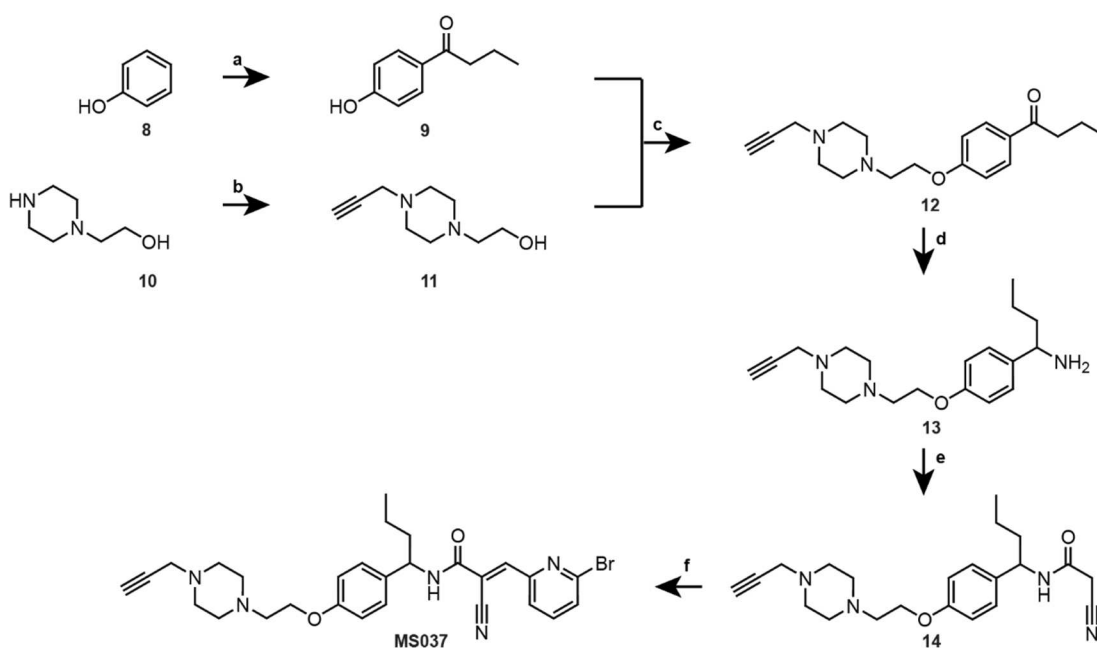
Potencies between 10 nM and 10  $\mu\text{M}$  were reported for the selected inhibitors. Structure-activity relationships (SAR) for some molecules provided insight into the correct placement of the alkyne handle without losing too much of the compound's activity. As a starting point, seven inhibitors with aliphatic nitriles, aryl nitriles and cyanamides were chosen, to target various DUBs from the USP and UCH family. Compound **1** was published in a patent by Novartis in 2010. The molecule is described as a USP2 and/or UCHL3 inhibitor for treating proliferative diseases such as cancer.<sup>[149]</sup> GSK found molecule **2** in a screening campaign against USP20 and reported an  $\text{IC}_{50}$

## Results

value of 160 nM.<sup>[150]</sup> Cyanopyrrolidines **3**, **4**, **5** all come from a patent submitted by Mission Therapeutics and were described to have utilities in various therapeutic areas, including cancer and diseases associated with mitochondrial dysfunction.<sup>[151]</sup> Compound **6** displays a derivative of the inhibitor **WP1130**. This USP9x inhibitor was originally identified by the Donato group, which screened for a Janus kinase 2 (JAK2) inhibitor. Later, it turned out that the molecule was not binding to JAK2, but to a deubiquitinase, which is capable of modulating the kinases ubiquitination.<sup>[152]</sup> Hybrigenics described compound **7** as one of many from a series of fused tri- and tetra-cyclic molecules inhibiting USP8 in a wide range of disease models.<sup>[153]</sup> For the insertion of the alkyne group, easily accessible functional groups were selected, which can be modified by simple chemical reactions, such as amide coupling or nucleophilic substitution.

This collection of molecules, described for targeting DUBs worked as the foundation for small molecule probe synthesis. In addition, suitable exit vectors for the attachment of the alkyne moiety were identified and considered during synthesis planning.

### 3.1.2 Synthesis of an aliphatic nitrile probe

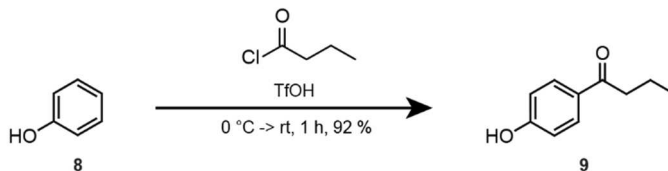


**Scheme 1 | Synthesis of probe MS037.** a) butyryl chloride, TfOH b) propargyl bromide, K<sub>2</sub>CO<sub>3</sub> c) PPh<sub>3</sub>, DIAD d) NaBH<sub>3</sub>CN, ammonium acetate e) cyanoacetic acid, HATU, HOAt, DIPEA f) 6-bromo-2-pyridinecarboxaldehyd, β-alanine.

## Results

The probe **MS037** is based on compound **6** and features a nitrile near a Michael acceptor. The exact role of either of these electrophiles in the covalent reaction with the target protein remains unknown. The retrosynthetic planning of **MS037** foresaw the early introduction of the alkyne functionality into the left part of the molecule to avoid unnecessary protection of the free amine at the piperazine (Scheme 1). Similarly, a left part was synthesized, which was subsequently connected to the right part via a propane ether linkage. A bromopyridine is bridged through the aliphatic nitrile and the amidic Michael acceptor and represents the most eastern part of the final probe.

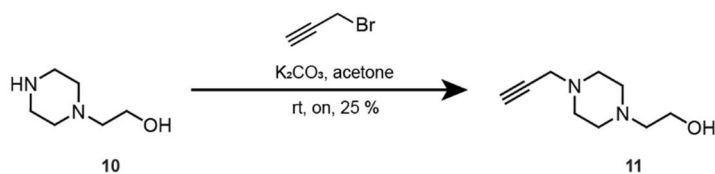
First, molecule **8** is acylated by using butyryl chloride and triflic acid in a Friedel-Crafts reaction (Scheme 2). The strong acid reacts with the acyl halide to form a triflate anhydride, a potent acylating agent. The formed acylium cation reacts in an electrophilic aromatic substitution with **8**. The aromatic ring interacts with the electrophile to form a  $\pi$ -complex. This favors the formation of a positively charged and delocalized arene  $\sigma$ -complex. Aromaticity is reestablished under the collapse of the  $\sigma$ -complex and through the capturing of a proton by the trifluormethane sulfonate. The hydroxy group's positive mesomeric (+M)-effect increases the electron density in the aromatic system and directs the electrophilic attack of the anhydride to the *para*-position.



**Scheme 2 | Representation of 9, starting from 8.** Molecule **9** was synthesized in a Friedel-Crafts acylation from molecule **8** using butyryl chloride and triflic acid.

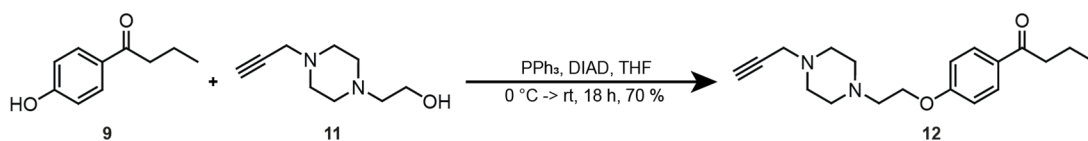
Analogous molecule **10** is alkylated in a  $S_N2$  reaction. The nucleophilic nitrogen of the piperazine attacks the  $\alpha$ -carbon of the alkyl halide (Scheme 3). At the same time, the bromo species is released. The base deprotonates the amine, which leads to the formation of product **11**. The reaction proceeded with a low yield of 25 %, as the product was difficult to purify due to the high polarity of the secondary amines of the piperazine. For the yield determination, only pure fractions were included, whereas many fractions with a low purity of the target structure were discarded. Impurities were detected as unreacted starting material **10**.

## Results



**Scheme 3 | Representation of 11, starting from 10.** Molecule **10** was alkylated in a nucleophilic substitution reaction to yield **11**.

Molecule **12** was obtained by linking **9** and **11** in a Mitsunobu reaction (Scheme 4). In the first step, the triphenylphosphine nucleophilic attacks the diisopropyl azodicarboxylate (DIAD) to yield a betaine intermediate. The so-formed negatively charged nitrogen of the hydrazine deprotonates the hydroxy group of phenol **9**. The triphenyl phosphine forms an oxyphosphonium intermediate with alcohol **11** and the DIAD is released. The attack of the deprotonated phenol upon the oxyphosphonium intermediate results in the collapse of this species and yields the desired product **12** and triphenylphosphine oxide. A yield of 70 % was achieved as difficulties during the purification arose, as the emerging triphenylphosphine oxide was challenging to separate and the repeated chromatographic purification steps resulted in the loss of the product.

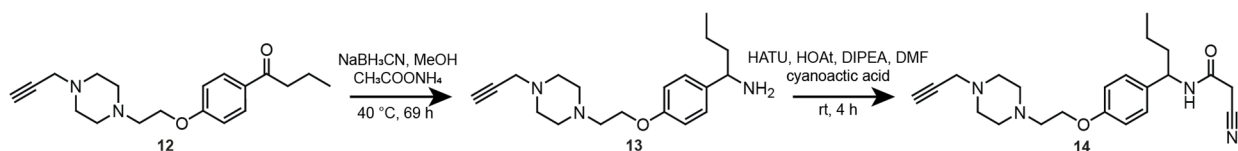


**Scheme 4 | Representation of 12, starting from 9 and 11.** Molecules **9** and **11** are linked together via a Mitsunobu reaction.

To have another site for further modifications available, the ketone of **12** was reduced to a primary amine, which was then acylated to introduce the nitrile warhead of the probe (Scheme 5). In the first step, the ammonium acetate acts as a nitrogen donor. The ketone reacts with the amine of the ammonium acetate to form a hemiaminal species, which collapses under the condensation of water to form an iminium ion. The mild reducing agent transfers the chemoselective hydride to the iminium ion, yielding the primary amine **13**. For the N-acylation of **13**, [O-(7-Azabenzotriazol-1-yl)-N,N,N',N'-tetramethyluronium-hexafluorophosphat] (HATU) was used as the coupling reagent to prevent occurring acid-base reactions, which would inhibit the formation of the desired product. First, the base deprotonates the cyanoacetic acid. The so-formed carboxylate anion attacks the electron-deficient carbon atom at the urea moiety of HATU. The HATU collapses under the release of a 1-hydroxy-7-azabenzotriazole (HOAt) anion. The HOAt anion reacts with the

## Results

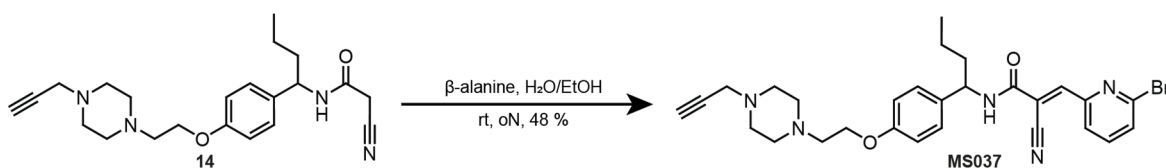
carboxylic acid to form an activated ester species. In a final step, the amine reacts with the activated ester to yield a stable amide bond and the desired product **14**.



**Scheme 5 | Two-step reaction to obtain molecule 14 from 12.** The mild reagent sodium cyanoborohydride reduced the ketone of **12** to obtain a primary amine for further modification. The amine was then coupled to cyanoacetic acid to introduce the nitrile warhead to the probe.

The low yield of 15 % over two steps may depend on several factors: First, the iminium species, in the reductive amination, was only allowed a very short period of time to form by the direct addition of the reducing agent. Indeed, mass spectrometry or other analytical methods could not verify the total conversion of the starting material to the iminium species. Letting the acetate and the ketone **12** stir for several hours could have been critical. Furthermore, the formed water was not removed from the reaction, which might have inactivated the ammonium cyanoborohydride. In addition, the cyanoacetic acid features a very acidic C-H bond at the  $\alpha$ -carbon, which might react with the nitrile group of another cyanoacetic acid molecule or the alkyne moiety of **13**, resulting in unwanted side products.

The 6-bromo-2-pyridinecarboxaldehyde was introduced via a Knoevenagel condensation to obtain the final probe **MS037** (Scheme 6). The  $\beta$ -alanine catalyzes the removal of the acidic proton from the  $\alpha$ -carbon of the cyan acetamide of **14**. The resulting carbanion acts as a nucleophile and attacks the carbonyl carbon of the aldehyde, whereas an alcohol is formed as an intermediate. Water condensation yield the unsaturated Michael acceptor and the final aliphatic probe **MS037**.

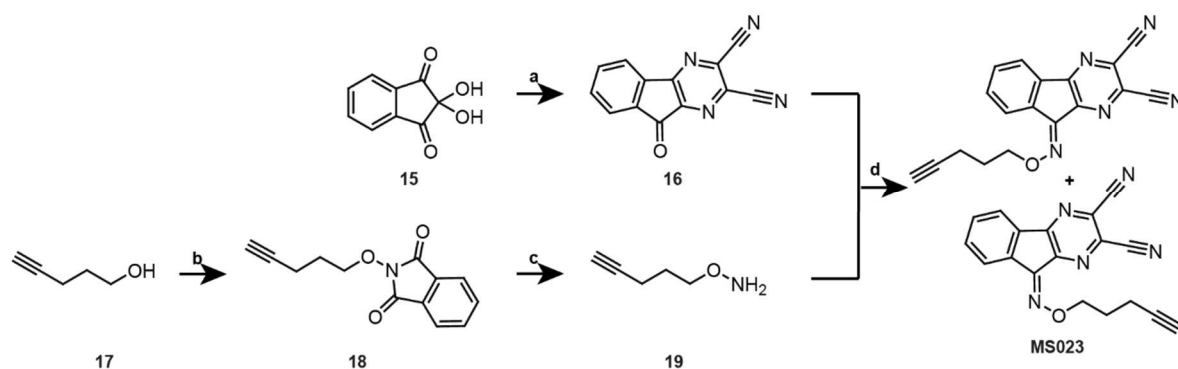


**Scheme 6 | Representation of the final probe MS037, starting from 14.** The Michael acceptor and the eastern part of the final probe were introduced via a Knoevenagel condensation.

## Results

### 3.1.3 Synthesis of aryl nitrile probes

The probe **MS023** was derived from 2,3-dicyanopyrazine inhibitors, such as molecule **7**, designed to target USP7 and USP8. The selectivity towards USP8 was achieved by introducing an alkylated oxime moiety, which represents the only exit vector for the attachment of the alkyne tag available without major changes of the core scaffold. The cyanopyrazine is functionalized with two nitrile groups and the exact covalent mechanism remains unknown. The first step in the synthetic design was the construction of the tricyclic indenopyrazine. Analogously, a hydroxylamine was generated, which is connected to the alkyne via an alkyl chain. Lastly, the hydroxylamine was exchanged with the ketone to form an oxime and to yield the probe **MS037**. The probe was isolated as an *E/Z*-isomeric mixture because of the free rotatability of the C=N bond.



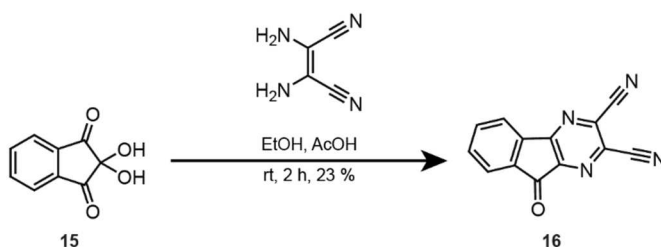
**Scheme 7 | Synthesis of probe MS023.** a) 2,3-diaminosuccinonitrile, EtOH, AcOH b) PPh<sub>3</sub>, DIAD, THF c) 1) N<sub>2</sub>H<sub>4</sub> · H<sub>2</sub>O, EtOH 2) HCl in Et<sub>2</sub>O d) pyridine, molecular sieve

First, ninhydrin **15** forms the heterocyclic indenopyrazine **16** in a condensation reaction with 2,3-diaminosuccinonitrile (DAMN). Ninhydrin exists in equilibrium with the triketone indane-1,2,3-trione, which is susceptible to reactions with nucleophiles. The acidic environment favors the protonation of the carbonyl groups, resulting in the formation of a partially positively charged carbonyl carbon and a hydroxy group. The primary amine of the DAMN acts as a nucleophile and attacks the carbon to form a C-N bond at the carbonyl. Further protonation at the hydroxy group yields the condensation of water and the formation of a Schiff base. Another nucleophilic attack at a second carbonyl carbon and subsequent condensation of water results in the formation of the tricyclic core scaffold **16**, equipped with two nitrile groups as warheads. Many by-products were formed because of the uncontrolled reaction between the DAMN and ninhydrin. The reaction of two DAMN molecules with ninhydrin prevented pyrazine formation. Two ninhydrins can get linked by one DAMN molecule, resulting in further by-products. Therefore, only a low yield of 23 % of



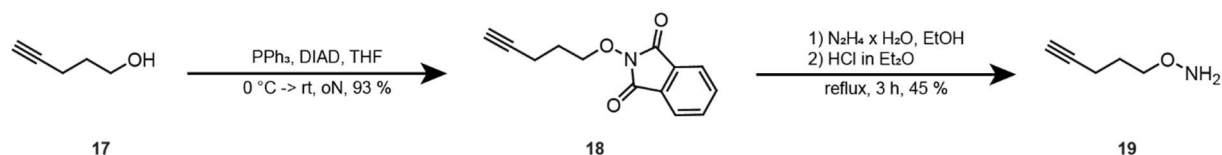
## Results

the desired product was achieved. Due to the fast feasibility, the low effort and the low cost of the starting materials, the reaction was not further optimized.



**Scheme 8 | Representation of 16, starting from 15.** Molecule **16** is obtained in a condensation reaction of ninhydrin with DAMN.

The hydroxylamine, which is later used to connect the alkyne tag to the probe core scaffold via an alkyl chain, was generated in a two-step approach (Scheme 9). First, the hydroxy group of **17** was reacted with *N*-hydroxy phthalimide to introduce the masked nitrogen. Triphenylphosphine was used to form a betaine intermediate from DIAD. This species reacts with the hydroxy group of **17** under the generation of an alcohol-triposponium-ion. The nucleophilic attack of the *N*-hydroxy phthalimide on the alcohol results in the displacement of triphenylphosphine oxide and the formation of the desired *N*-alkoxyphthalimide **18**. The subsequent hydrazinolysis of **18** followed by an acidic workup, yields the desired hydroxylamine **19** as an HCl salt. The lone pair of the hydrazine's nitrogen nucleophilic attacks the carbonyl carbon of **18**. Another nucleophilic attack of the free amine of the hydrazine to the second carbonyl resolves in the formation of phthalhydrazide and the displacement of the desired hydroxylamine **19**. The increased kinetic due to the  $\alpha$ -effect of the hydrazine favors the formation of the thermodynamically favored product.

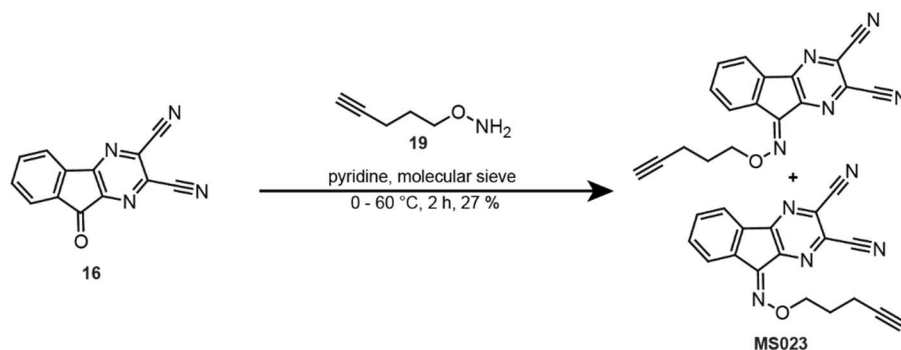


**Scheme 9 | Representation of 19, starting from 17.** The activation of pentynol with *N*-hydroxy phthalimide and the subsequent hydrazinolysis results in the generation of hydroxylamine **19**.

The ketoxime, linking the alkyne tag to the recognition element of the probe, was built up by the condensation of the ketone **16** with hydroxylamine **19** (Scheme 10). The reaction was initiated by a nucleophilic attack of the hydroxylamine to the carbonyl carbon. Reprotonation yielded a *N*-hydroxy hemiaminal. Proton transfer resulted in the elimination of the former carboxy group as water, yielding a carbenium ion. This was mesomerically stabilized through an *N*-hydroxyiminium ion. Deprotonation resulted in the formation of the desired oxime **MS023**. Molecular sieves were

## Results

used to prevent hydrolysis of the resulting oxime by the attack of water released during the reaction. Despite the separability of both isomers on a HPLC prep column, an equilibrium of both isomers was established again after a short period of time since the *E*-isomer can transfer into the *Z*-isomer and *vice versa* due to the free rotability of the C=N bond.



**Scheme 10 | Representation of the final probe MS037.** The oxime, which links the alkyne tag to the probe's core scaffold, was generated via a condensation reaction, yielding the probe MS023 as an *E/Z* isomeric mixture.

The aryl nitrile probes **CG017** and **CG041** were synthesized by Dr. Christian Grethe, and their chemical synthesis is discussed in detail elsewhere.<sup>[154]</sup> In brief, **CG017** was started from 4-bromobenzyl amine. The primary amine was protected with di-*tert* butyl dicarbonate (Boc<sub>2</sub>O) to prevent unwanted side reactions. Next, a phenol was introduced as a boronic acid via palladium-catalyzed Suzuki coupling, whereas the halide of the Boc-protected bromobenzyl amine served as the leaving group. The resulting biphenyl core acts as the recognition element of the final probe. The hydroxy group of the phenol is further modified with 2,4-chloropyrimidine in a nucleophilic aromatic substitution. The nitrile warhead was installed at the chloropyrimidine through another nucleophilic aromatic substitution, using the chloro-substituent in 2-position as the leaving group. The alkyne tag was introduced through an amide coupling to yield the final probe **CG017** (Supplementary Scheme 1).

**CG041** was synthesized starting from Boc-protected 4-bromoethyl aniline, which is transformed into a phosphonate intermediate in a Michaelis-Arbuzov reaction using triethyl phosphite. The Horner-Wadsworth-Emmons reaction was used to link the phosphonate intermediate and a benzaldehyde through an *E*-alkene. The resulting molecule presents the recognition element of the probe **CG041**. The cyanoindole warhead was accessed through the nucleophilic aromatic substitution with malononitrile and a reductive workup. An amide coupling was used to install the alkyne reporter and to obtain the final probe **CG041** (Supplementary Scheme 2).

### 3.1.4 Synthesis of cyanopyrrolidine probes

The synthesis of the cyanopyrrolidine probes **GK13S**, **CG173**, **CG050R** was carried out by Dr. Christian Grethe with the help of MSc. Gian Kipka. These probes are fundamental for this work and their chemical design is described briefly: The probes **GK13S** and **CG173** are based on the compounds **3** and **4**, which are patented as UCHL1 inhibitors. **CG050R** is based on compound **6**, described to target USP30. The molecules contain a cyanopyrrolidine moiety, which could function as a milder warhead regarding reactivity and lead to less off targets compared to more reactive covalently modifying groups. At the other end, the structures of **4** and **5** contain a pyrrolopyridine and a pyrazole, in which various nitrogens were identified that could point out of the catalytic pocket and be solvent exposed to attach the alkyne handle to further install the reporter group. The structure of **3** includes a methoxyethyl group, which is connected via an amide bond with the core scaffold to increase the inhibitor's solubility. The same amide bond was exploited to install the alkyne at the final probe. The synthesis of **GK13S** starts with the *N*-nitration of 3-nitroimidazole, which further reacts with 4-aminobenzoate to yield a biaryllic methyl ester. The nitro group is then reduced to the primary amine using palladium, which is then coupled to the enantiomerically pure (*S*)-1-*N*-*boc*-pyrrolodine-3-carboxylic acid. The methoxy ester was deprotected and the alkyl chain with the terminal alkyne was introduced via amide coupling. The warhead was finalized by deprotecting the pyrrolidine and a subsequent reaction with cyanic bromide to yield the final probe **GK13S** (Supplementary Scheme 3). The minimal probe **GK16S**, the parent inhibitor and other derivatives of **GK13S** were prepared following a similar synthesis strategy, which is discussed in detail elsewhere.<sup>[154]</sup>

The core scaffold of the probe **CG050R** was generated by conjugating a 1-*boc*-pyrazole-4-boronic acid pinacol ester to methyl-4-bromo-2-fluorobenzoate in a Suzuki coupling. After deprotecting the pyrazole under acidic conditions, the so-formed free amine is alkylated with propargyl bromide to introduce the alkyne handle. Base-mediated deprotection yields a free carboxylic acid, available for amide coupling to install the enantiomerically pure (*R*)-1-*boc*-3-aminopyrrolidine. The cyanopyrrolidine warhead is finalized by acidic deprotection and reaction with cyanic bromide (Supplementary Scheme 4). While the probes **GK13S** and **CG50** feature a cyanopyrrolidine as their warhead, the structures contain opposing stereochemistry and reversed connectivity of the heterocycles and the benzene. These design choices should address different DUBs despite the same warhead.

The *boc*-protected pyrrolidine of the probe **CG173** was installed at the bromoindoline core scaffold via amide coupling. Following the transformation of the halide to a boronic acid pinacol ester for

the introduction of the southern part of the core scaffold via Suzuki coupling. The alkyne handle was attached to the secondary amine of the pyrrolopyridine as a propargyl residue. Subsequently, the pyrrolidine was deprotected under acidic conditions and reacted with cyanic bromide to generate the cyanopyrrolidine warhead and to obtain the final probe **CG173**.

### **3.2 Biological characterization of tool compounds to study deubiquitinases**

This chapter describes the biochemical and cellular investigation of the synthesized probes (Aim II). This includes the general evaluation of the probe library for binding in a lysis-based DUB profiling assay. Probes targeting at least one DUB were further characterized regarding their target spectrum, potency, specificity and mechanism of binding in an *in vitro* and cellular setting.

#### **3.2.1 Evaluation of activity-based probe library identifies GK13S as a specific DUB binder**

Since most of the parent inhibitors were poorly characterized with regard to their mode of inhibition and target spectrum, an *in vitro* assay was carried out to ensure that the alkyne-tagged versions of these compounds (Fig. 11 A) could be attached to the reporter group and that they were able to modify their described DUB covalently. The probe **CG50R** was used as a model compound to find suitable conditions for follow-up experiments. Since **CG50R** was described to bind to USP30, the catalytic domain of this enzyme was used in this test experiment. The covalent modification was analyzed by LCMS. The spectrum recorded from the probe/DUB complex shows a mass shift that corresponds precisely to the molecular weight of the probe, proving that covalent modification with the molecules is detectable (Fig 11 B). A gel-based assay was executed to provide information on whether the covalent bond between compound and protein is also stable in buffer medium and whether the reporter group could subsequently be linked to the bound probe (Fig. 11 C). The biorthogonal copper-catalyzed azide-alkyne cycloaddition (CuAAC) was used to link the alkyne of the probe with the azide of the reporter group. Cu(I) ions were utilized as the catalytic species. The Cu(I) catalysis accelerates the reaction to as much as  $10^7$  times faster than the uncatalyzed reaction at ambient temperature.<sup>[155]</sup> The Cu(I) was generated

## Results

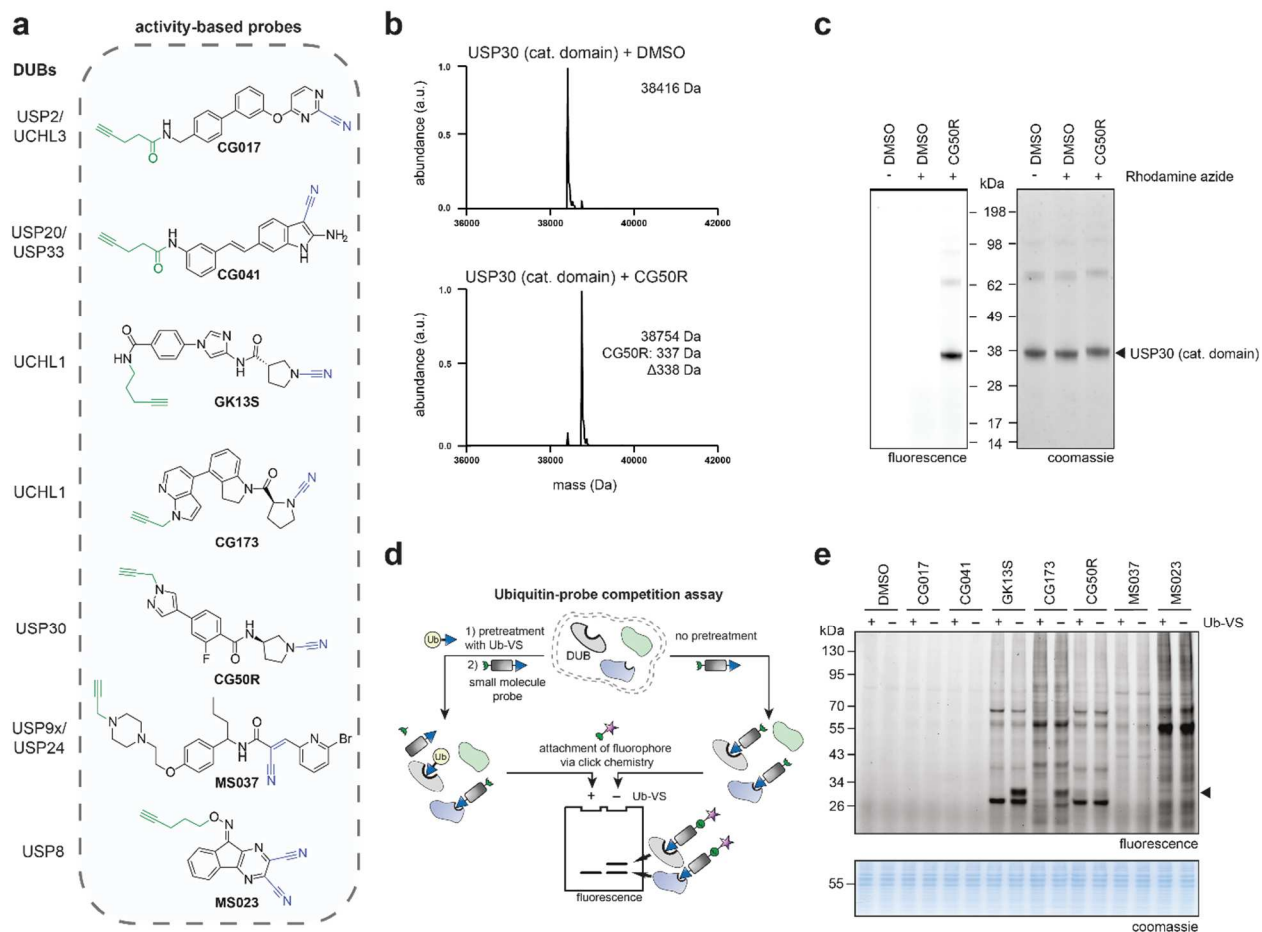


**Fig. 11 | DUB profiling with synthesized probe library.** **a)** Selected probes for characterizing DUB binding in a complex proteome. The possible warhead moiety for the covalent modification of their targets is highlighted in blue. The alkyne moiety for the biorthogonal functionalization is colored green. DUBs the parent inhibitors are reported to bind to are annotated left. **b)** Covalent modification of the catalytic domain of USP30 was demonstrated using CG50R as a model compound. **c)** The catalytic domain of USP30 can be fluorescently labeled and visualized using CG50R. **d)** Schematic workflow to identify covalently bound DUBs by the probes. A complex proteome was either incubated with a Ub-VS probe followed by small molecule probe treatment (left path) or treated with the probe only (right path). The band disappears on the lanes incubated with the Ub-VS first, indicating a modified DUB. **e)** DUB profiling in HEK293 cell lysates treated with indicated compounds (1  $\mu$ M, 1 h). Lysates were preincubated with Ub-Vs where shown. The black arrow hints that a Ub-VS competitive protein target is also modified by activity-based probes GK13S and CG173

*in situ* by the reduction of copper(II) sulfate pentahydrate ( $\text{CuSO}_4 \times 5 \text{H}_2\text{O}$ ) with sodium ascorbate. To inhibit the disproportionation of the Cu(I) species, specialized ligands are used for stabilization. The first applied ligand was Tris((1-benzyl-4-triazolyl)methyl)amine (TBTA). However, TBTA is poorly soluble in water, so that available ligands were improved for better biocompatibility. Since in the present work, the CuAAC was mainly performed in aqueous buffers, 2-(4-((Bis((1-(*tert*-butyl)-1*H*-1,2,3-triazol-4-yl)methyl)amino)methyl)-1*H*-1,2,3-triazol-1-yl)acetic acid (BTAA) was

## Results

the Cu stabilizing ligand of choice, due to its improved solubility compared to TBTA. A fluorophore-azide reporter was used for the visualization of bound proteins. Indeed, a fluorescence band appeared only on the lane where the catalytic domain of USP30 was treated with the probe **CG50R** (Fig 11C, left image, last lane). This demonstrates the ability of **CG50R** to form a covalent conjugate with the catalytic domain of USP30. In addition, the alkyne functionality of the probe is generally amenable to the cycloaddition with the reporter azides under the tested conditions. No band appeared on the lanes treated with the DMSO, excluding the non-specific labeling of the catalytic domain of USP30 not modified with the probe and proves the biocompatibility of the CuAAC. In the coomassie gel, a slight upshift of the band is observable, where the sample was treated with the small molecule probe (Fig 11C, right image, last lane). This small size shift results from the covalent modification with the probe and the conjugation with the reporter group, corroborating a full conversion of the CuAAC. It was unlikely that this shift was due to the modification with the probe alone, as the mass of the compound was too small to cause a visible shift. The successful establishment of the CuAAC act as a basis for the coming up ABPP experiments.

To follow up with the complete library to characterize the small molecule probes for the covalent modification of DUBs and other cellular proteins unbiasedly, a ubiquitin probe competition experiment was performed (Fig 11 D, E). A whole proteome lysate, generated from HEK293 cells, was split up. One half was treated with the small molecule probe library, modifying DUBs and other non-DUBs they bind to. The other half was preincubated with an Ub-VS suicide probe, binding covalently and unspecific to all DUBs in a given proteome. The same samples were treated with the small molecule probes afterward. In those samples, the small molecule probes were unable to bind to a DUB since the Ub-probe blocked the binding site. All molecules are fused to the fluorophore reporter to visualize all protein-probe conjugates. Comparison of Ub-VS treated and Ub-VS non-treated samples reveals covalent modification of a DUB by the small molecule probe because the fluorescent band visualizing the deubiquitinase disappears only where the samples were preincubated with the Ub-VS probe. This pattern is remarkably observable for a DUB of approx. 30 kDa in the samples treated with the cyanopyrrolidine probes **GK13S** and to a lesser extent, with **CG173**. These findings elevated those probes to candidates for in-depth characterization and tools to study the bound deubiquitinase (Fig 11 E). Other probes (**CG017**, **CG041**) failed to modify any proteins or were incompatible with the CuAAC due to steric hindrance upon binding to their protein targets, making the alkyne less available for the cycloaddition. The small molecule probes **CG50R**, **MS037** and **MS023** showed many fluorescently labeled proteins within the HEK293 proteome. However, the pattern suggesting the covalent modification of a DUB

## Results

by these probes was not detectable. Treatment with **MS023** resulted in an intense fluorescence signal at approx. 55 kDa, suggesting the modification of non-DUB protein, which might be relevant in other experimental settings. Even though the binding of **CG50R** to the purified catalytic domain of USP30 was confirmed, no binding to USP30 with the probe was detectable in a complex proteome. However, in a later assay, focusing on detecting USP30 with small molecule probes in a living environment, the binding of **CG50R** to the DUB was established and visualized (see Fig. 30 E). In the underlying assay, the targeted DUBs may be too low abundant and the fluorescence of other non-DUB proteins obscures their detection.<sup>[156]</sup>

Collectively, the established assay for testing the probe library for DUB modification resulted in the identification of a bound DUB by the probe **GK13S**. A similar pattern, suggesting the modification of a DUB, was visible for the probe **CG173**, but also the fluorescence background resulting from bound off-targets were much higher compared to **GK13S**. Other probes did bound to a lot of non-DUB proteins but did not show the desired pattern that suggested the covalent modification of a DUB. Still other did not show any fluorescence bands, suggesting that either no protein was modified by the probe or the CuAAC failed. Reasons for this could be inaccessibility of the alkyne at the probe or the conditions used did not lead to a sufficient reaction.

As the small molecule probe **GK13S** showed the most promising fluorescence pattern for covalently modifying a DUB, the following characterization was focused on this probe. To establish a stable CuAAC for all advanced ABPP experiments a dedicated click reagent screening was carried out (Supplementary Fig. 1). This was to find the best possible conditions first with purified protein, to then transfer them to a cellular context. Since the parent inhibitor of **GK13S** was described to inhibit UCHL1, purified UCHL1 was used in all test experiments. Initially, 1 mM  $\text{CuSO}_4 \times 5 \text{H}_2\text{O}$ , 1 mM BTAA, 5 mM sodium ascorbate and 10  $\mu\text{M}$  fluorophore azide were used as a standard condition. Based on this standard condition, the concentration of one reagent per sample was varied. To cover a range of concentrations, each reagent was used in five times higher (H, high) and five times lower (L, low) concentrations compared to the standard concentration (Supplementary Fig. 1 A). In addition, TCEP, TBTA and a rhodamine azide were tested as alternatives for sodium ascorbate, BTAA and the TAMRA fluorophore, respectively. The CuAAC with purified UCHL1 under standard conditions resulted in a double band after the fluorescence readout. By using a lowered copper concentration, the equilibrium was shifted to the upper band. Increased copper concentration might damage or attach to the protein, affecting its running behavior in the gel and causing multiple fluorescence bands to appear. An increased BTAA as well as an increased azide concentration resulted in increased fluorescence intensity.

## Results

Changing the sodium ascorbate concentration did not appear to affect the reaction. Using TCEP as a reducing agent does not result in any fluorescence and therefore was not used for further experiments. Also, the use of TBTA as an alternative ligand, as well as the rhodamine fluorophore had no positive effect on the reaction. The testing of different conditions resulted in increased fluorescence intensity compared to the standard when 5 mM BTTAA and 100  $\mu$ M of the azide were used. In addition, lowering the copper concentration to 0.2 mM resulted in the disappearance of two fluorescently labeled UCHL1 species.

These data led to a second round of optimization comparing the best conditions of each reagent from the first round (Supplementary Fig. 1 B, C). This optimization established the use of 5 mM BTTAA, 0.2 mM  $\text{CuSO}_4 \times 5 \text{H}_2\text{O}$ , 100  $\mu$ M TAMRA/Biotin azide, 5 mM sodium ascorbate as the improved conditions for the CuAAC with purified UCHL1. Next, these conditions were used to link **GK13S** to the reporter after it bound to endogenous UCHL1 in a cellular setting (Supplementary Fig. 1 D). However, the high concentration of the fluorophore azide resulted in unspecific modification of proteins within the cell lysate. This observation led to a third round of optimization on the CuAAC in cell lysates. Initially, different azide and copper concentrations were investigated in the background of constant BTTAA and sodium ascorbate concentrations (Supplementary Fig. 1 E, F). It was found that a low copper concentration was not sufficient to link bound **GK13S** to the reporter, as the copper may have been quenched by components in the cell lysate. Azide concentrations up to 40  $\mu$ M could be applied without excessive occurrence of non-specific labeling. However, since concentrations above 20  $\mu$ M did not further increase the fluorescence intensity of the UCHL1 band, an azide concentration of 10 – 20  $\mu$ M was chosen for further experiments. In the further course of the project, the CuAAC was further investigated in the context of small molecule probes (see Fig. 28 B, C).

Collectively, a screen for improved reagent conditions in the CuAAC resulted in the use of 5 mM BTTAA, 0.2 mM  $\text{CuSO}_4 \times 5 \text{H}_2\text{O}$ , 100  $\mu$ M TAMRA/Biotin azide and 5 mM sodium ascorbate for linking the reporter to GK13S bound to purified UCHL1. Since those conditions led to unspecific labeling in cell lysates, the conditions were adjusted. Optimizations in HEK293 lysates led to improved reagent concentrations of 5 mM BTTAA, 1 mM  $\text{CuSO}_4 \times 5 \text{H}_2\text{O}$ , 10-20  $\mu$ M TAMRA/Biotin azide, and 5 mM sodium ascorbate for attaching the reporter to GK13S modified UCHL1 in complex protein mixtures via the CuAAC.

Furthermore, the covalent modification of UCHL1 by the probes **GK13S** and the successful CuAAC under the established conditions were investigated in more detail via intact mass spectrometry (Fig 12A). This reporter group allows the side-by-side fluorescent visualization and



## Results

the enrichment of probe-bound proteins. At a concentration of 10  $\mu\text{M}$ , **GK13S** almost completely modifies UCHL1 after one hour of incubation time. After two hours, 100 % of the purified UCHL1 is bound by the probe (Fig. 12A, bottom spectrum). Also, the CuAAC with the TAMRA/Biotin reporter shows full conversion. The formation of copper adducts during the measurement leads to a broadening of the peak and results in deviations from the calculated mass of the complex. However, the absence of unmodified or the **GK13S** bound species demonstrates the successful and biorthogonal course of the reaction. In addition, these data suggest that a suitable position for the attachment of the alkyne group was identified.

To further investigate the ability of **GK13S** and **CG173** to covalently modify UCHL1 in complex protein mixtures, cell lysates from other cell lines were incubated with the probes (Fig. 12B). Samples generated from PC-3 cells, a cell line endogenously expressing UCHL1, showed a prominent fluorescent band upon compound treatment of the same height as seen before in HEK293 cells. Upon pretreatment with the Ub-VS probe, the band disappears, indicating that a DUB was covalently modified. Cell lysates generated from MCF-7 and HeLa cells, both cell lines which are known to have a shallow UCHL1 expression level<sup>[157]</sup>, lacking the band of approx. 30 kDa. This corroborates that the deubiquitinase bound by **GK13S** and **CG173** is indeed UCHL1.

Despite the presence of a large number of other active DUBs in the sampled cell lysates<sup>[158]</sup>, no other ubiquitin-competitive bands were observed. Other non-ubiquitin competitive bands indicating non-DUB targets that were covalently modified by the cyanopyrrolidine probes. Whereas the most prominent one appeared just below the DUB target. Since this band gets more intense in the absence of UCHL1, it is reasonable to assume first the DUB target and then the unknown non-DUB target was modified less abundantly by the probes.

Taken together, the pattern of protein targets is similar throughout all tested cell lines for both compounds, but the fluorescence ratio for the DUB-probe competitive signal is stronger for the probe **GK13S**. From here on, the research was focused on the small molecule-based probe **GK13S** to characterize it as a tool compound to study the DUB UCHL1.

## Results

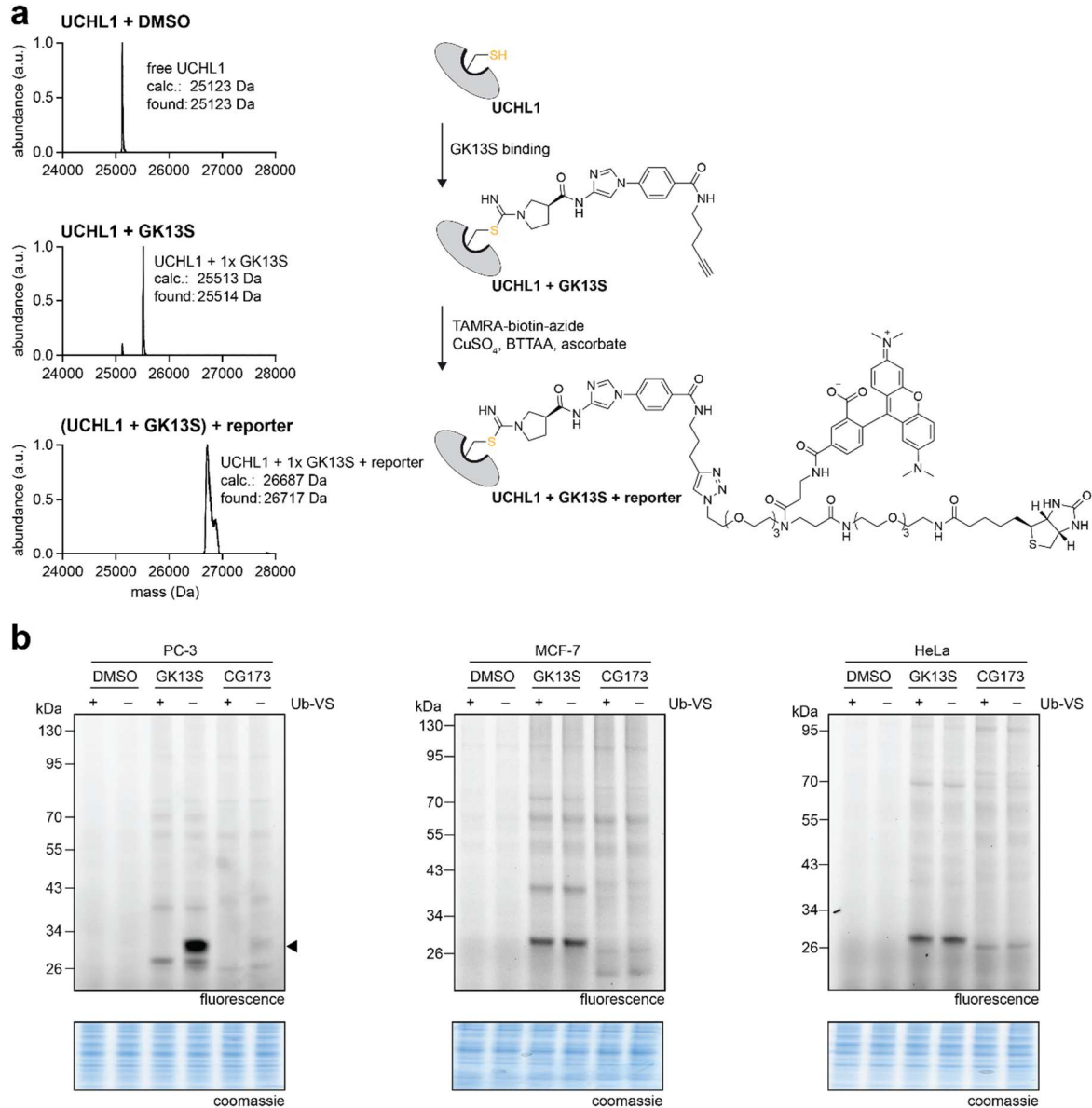


**Fig. 12 | GK13S shows a stable modification of UCHL1. a)** The small molecule-based probe GK13S was incubated with the purified DUB UCHL1 and conjugate formation was read out via intact mass (left panel). The shift in molecular mass indicates the covalent modification with the compound (middle spectrum). The second shift proves the successful cycloaddition and the linkage of the reporter with the probe (bottom spectrum). UCHL1 and the molecular structures of GK13S and the used reporter are shown schematically (right panel) **b)** The binding of the probe to UCHL1 was tested in cell lysates generated from three different cell lines. The black arrow indicates the height of the UCHL1 band. MCF-7 and HeLa cells were known not to express UCHL1.

### 3.2.2 Cellular characterization yields a pair of chemogenomic probes for UCHL1

After confirming the covalent modification of a DUB by **GK13S**, a set of control compounds were included for further characterization of the probe. Those compounds were synthesized by Dr. Christian Grethe with the help of MSc. Gian Kipka (Fig. 13 A). This includes an inactive control compound that lacks the nitrile warhead at the pyrrolidine. As a result, this compound can not modify any of its targets covalently. Additionally, probe **GK16S** was synthesized. **GK16S** represents a minimalistic version of **GK13S**, lacking the central recognition element but still consisting of the cyanopyrrolidine warhead and the alkyne moiety. This class of probes was termed “minimal probes”. **GK16S** acts as a control compound to distinguish between targets that were covalently engaged by the reactivity of the cyanopyrrolidine warhead alone and targets that interact with the recognition element non-covalently and then are modified by the nitrile group of the warhead. Since the structures contain a chiral center at the cyanopyrrolidine, the S- and the R-stereoisomer were prepared. Thus, the influence of the chiral center on the potency of the molecules could be investigated.

In order to find a suitable compound concentration needed for sufficient inhibition, cell lysates were treated with the probes and their derivatives in various concentrations (Supplementary Fig. 2). This was followed up by activity-based protein profiling in intact cells to investigate the cell permeability and the specificity of the probes at different concentrations (Fig. 13 B). The cells were incubated for 24 h after which all probe modified proteins were visualized through TAMRA fluorescence. As expected, the control probes **GK12S** and **GK12R** failed to modify any proteins in a complex environment by lacking the electrophilic warhead. A slight fluorescent background is visible due to the non-specific attachment of the fluorophore to highly abundant proteins rather than the modification with the control compounds (Supplementary Fig. 2, Fig. 13 B). Only the probe **GK13S** shows a concentration-dependent band at approx. 30 kDa. Visible at 0.1  $\mu\text{M}$  exclusively for **GK13S**, it was also visible at higher concentrations for the other probes. Corroborating that the modification with **GK13S** was much better tolerated than with the stereoisomer **GK13R** and that the choice of the chiral center influenced the probes potency towards this protein. The same effect was observable for the epimers **GK16S** and **GK16R**, because at a concentration of 1  $\mu\text{M}$ , the modification with the S-isomer results in a more intense fluorescence intensity than with the R-isomer. The intensity of this band in samples

## Results

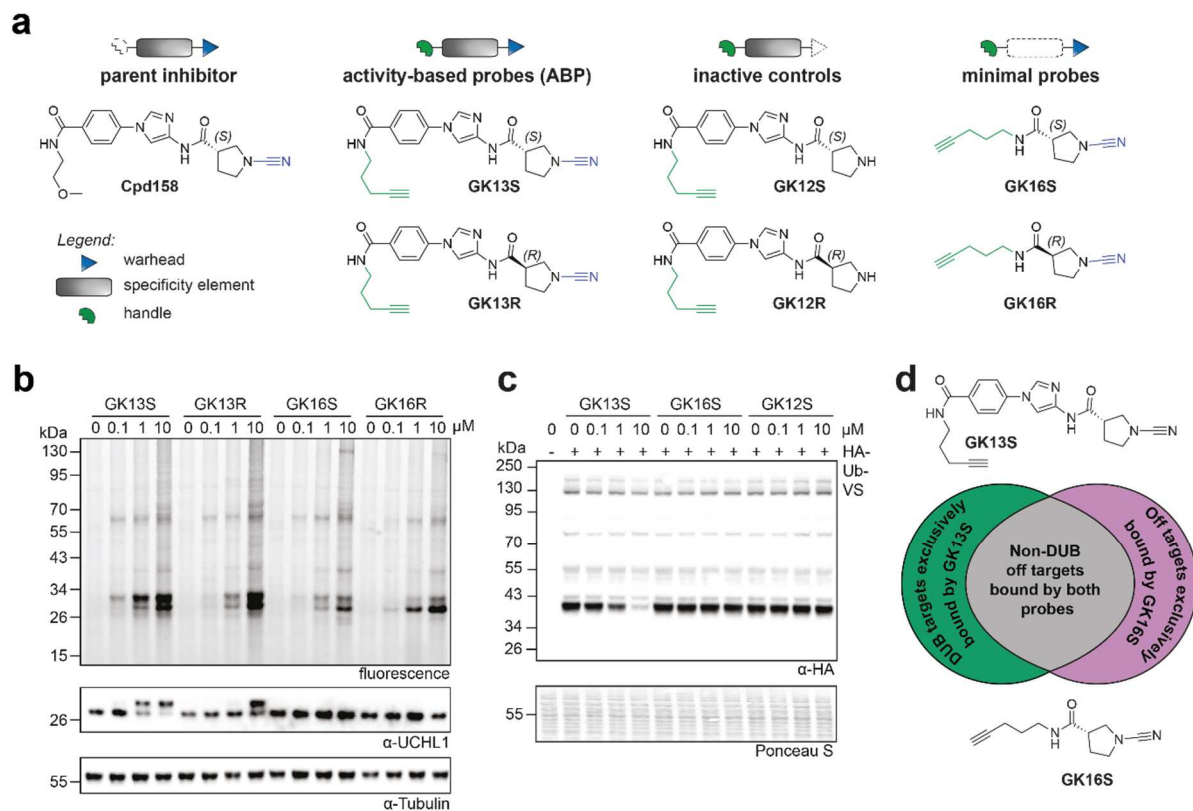


**Fig. 13 | Cellular characterization of pair of chemogenomic probes.** **a)** Overview of synthesized GK13S derivatives for cellular characterization. Schematic representation of the parent inhibitor, consisting of the recognition element (grey) and the warhead (blue) only, the activity-based probe bearing an additional alkyne moiety (green), the inactive control probe lacking the warhead and the minimal probe lacking the recognition element (upper panel). Molecular structures of each derivative in the S-conformation (middle panel) and the R-configuration (lower panel). **b)** Activity-based profiling in intact HEK293 (24 h treatment) cells visualize the specificity and the reactivity of the probes GK13 and Gk16 within a complex proteome. **c)** Counter assay to verify the binding of GK13S to a DUB in intact cells. HEK293 cells were treated with indicated compounds (24 h), lysed and treated with an Ub-VS probe. A decrease in band intensity indicates probe binding to a DUB. **d)** GK13S and GK16S present a set of chemogenomic pair of probes. Schematic Venn diagram describes the pool of proteins in complex mixtures to which both probes bind.

treated with the minimal probe **GK16S** appears much weaker than **GK13S**, indicating that the recognition element positively influences the binding of the probe to the protein. Just below this band appears another band of a low molecular protein modified by all compounds. Already observable in the DUB profiling assay (Fig. 12 E), this band represents a non-DUB off target. This protein is modified with **GK13S** at 1  $\mu\text{M}$  less potent than the upper band. The bands indicate only a slight stereo preference of the R- of the S-isomere. The minimal probe, in contrast, shows a more potent binding, resulting in increased fluorescence intensity of the lower band. Furthermore, the band intensity highlights a clear stereo preference of the R-isomer over the S-isomer of **GK16**.

## Results

A protein between 55 – 70 kDa represents another non-DUB off-target, covalently modified by all probes.

To confirm the fluorescent band of approx. 30 kDa belongs to the DUB targeted by **GK13S** in the DUB profiling assay, a counter screen was carried out (Fig. 13C). In this assay, intact HEK293 cells were treated with the S-isomers of the probes, which appeared to be more potent against the DUB of interest. The cells were lysed and the proteome was incubated with an HA-Ub-VS probes, binding to the catalytic center of all active cysteine DUBs within the complex mixture that was not occupied by any of the probes. Anti-HA western blotting revealed the concentration-dependent signal decrease for a DUB of approx. 30 kDa (the band appears at ~40 kDa, which is the DUB's molecular weight, plus the HA-Ub-VS), only for samples that were treated with the probe **GK13S**. This decrease was not observable for any other DUB, visualized in this assay. Interestingly, treatment with the minimal probe **GK16S** results in no decrease of the band corresponding to the DUB of interest. Taken together, **GK13S** covalently modifies a DUB in a living environment. **GK16S** is not binding to this DUB but modifies all off-targets bound by **GK13S**. This highlights the importance of using a pair of chemogenomic probes for the specific investigation of a non-overlapping target to distinguish between phenotypes that result from inhibiting the protein of interest or an off-target (Fig. 13D). The term “chemogenomic” describes well-defined tool compounds, that can be used to assign specific phenotypes to their target proteins upon inhibition.<sup>[159]</sup>

To identify the modified DUB and to corroborate that the minimal probe **GK16S** has the same target spectrum except the DUB of interest as **GK13S**, a proteomics-based target identification for both probes was carried out. Intact cells were treated with the alkyne-tagged probes. After covalent modification of their targets, the cells were lysed and a biotin azide was fused to the alkyne handle via the CuAAC. These protein-probe-biotin conjugates were separated from the remaining proteome by the enrichment on streptavidin beads. All targets got digested on the beads and subsequently identified via liquid chromatography-mass spectrometry (Fig. 14 A). As already speculated, treatment with 5  $\mu$ M **GK13S** results in the identification of the DUB UCHL1 being the most enriched protein. Around 3000 times (logarithmic enrichment factor of 11.5) more UCHL1 was captured in the **GK13S** samples compared to the DMSO treated samples (Fig. 14 B). This is consistent with the band intensity at approx. 30 kDa from the previous experiments (see Fig. 11 E and 13 B).

The enrichment with 5  $\mu$ M of the probe results in the enrichment of two major off-targets: PARK7 and C21orf33. PARK7, also known as DJ1 is a multifunctional protein with a molecular weight of

## Results

20 kDa. It is described to play an important role in cell protection against oxidative stress.<sup>[160]</sup> The loss of function of the PARK7 gene results in early-onset PD. The exact role ascribed to DJ-1 in PD patients is unknown, but the connection to this disease demonstrates its relevance as a therapeutic target.<sup>[161]</sup> The structure includes an active site with a catalytic dyad,

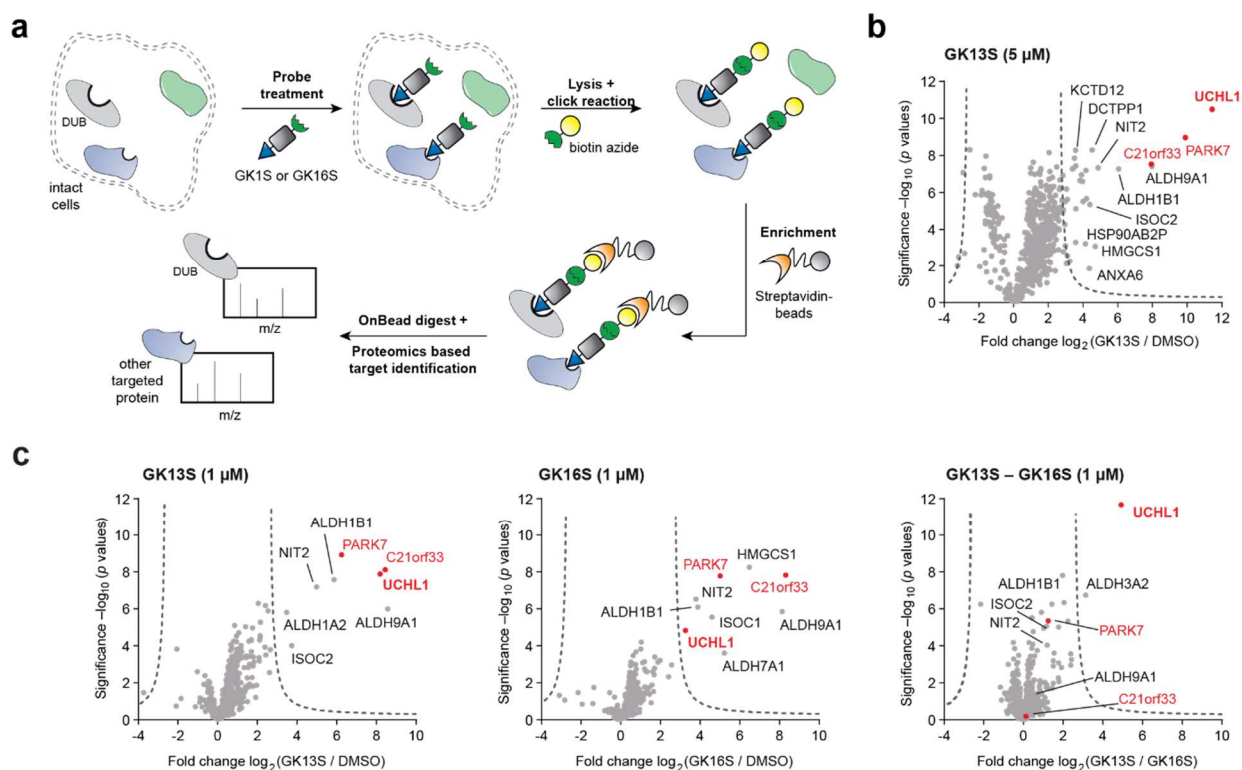


**Fig. 14 | Proteomics-based ABPP reveals UCHL1 as the DUB target of GK13S.** **a)** Schematic procedure of the proteomics-based ABPP. Intact cells get treated with the probe, the cells get lysed and the biotin handle was installed via CuAAC. Covalently modified proteins were captured on streptavidin beads. The enriched proteins were digested and the resulting peptides were subsequently analyzed by mass spectrometry. **b, c)** Target spectrum of indicated probes visualized as volcano plots. The x-axis indicates the relative label-free abundance ratio (fold change) of proteins between compound-treated samples and the DMSO control (**b, c**) or the minimal probe GK16S (**c**), right panel.

consisting of Cys106 and His126. PARK7 displays a low glyoxalase- and a deglycase activity.<sup>[162]</sup> The PARK7 homolog C21orf33 also annotated as GATD3, is a 28 kDa protein that serves as a mitochondrial glutamine amidotransferase.<sup>[163]</sup> Other prominent enriched off-targets include several aldehyde dehydrogenases and the omega-amidase NIT2. Since all of these proteins feature catalytic cysteines, it is not surprising that they were addressed by the electrophilic warhead of the probes and thus enriched on the beads. The family of the aldehyde dehydrogenases includes several members that have a mass above 55 kDa and could thus be assigned to the band fade band between 55-70 kDa, visible for both probes (see Fig. 13 B).

## Results

Furthermore, a large number of proteins were enriched less abundantly, which is consistent with the slight fluorescent smear, observable in previous experiments with **GK13S** at higher concentrations (see Fig. 13 B). This number of proteins drastically decreased when the probe was used at a lower concentration, highlighting the importance to find the appropriate concentration window (Fig. 14 C). At a concentration of 1  $\mu$ M, UCHL1 still belongs to the most abundantly enriched proteins of **GK13S** (enrichment factor  $\sim$ 8). However, the off-targets mentioned above were also still covalently modified at this lower concentration. The major off-targets, PARK7 and C21orf33 present a high enrichment factor of 6-8. Importantly, all non-DUB off-targets, but not the DUB UCHL1, were also prominently enriched by the minimal probe. Subtraction of the spectra of both probes at 1  $\mu$ M leaves the DUB UCHL1 as the only significant enriched protein (Fig 14 C, right plot). This finding strongly supports the hypothesis to use **GK13S** and **GK16S**, as a pair of chemogenomic probes to enable the specific investigation of the UCHL1 in a living environment to distinguish between phenotypes that result from inhibiting either the DUB or one or more of the non-DUB targets. The stereoisomer **GK13R** also enriches the off-targets PARK7, C21orf33, NIT2 and several aldehyde dehydrogenases with an equal potency as **GK13S**. However, the volcano plot also shows that UCHL1 is significantly less enriched. Thus, highlighting once again the importance of the stereocenter of the probe to modify the DUB of interest (Supplementary Fig. 3 A).

Collectively, the DUB bound by the probe GK13S, but not by GK16S was identified as UCHL1. Treatment with GK13S at a concentration of 5  $\mu$ M, resulted in UCHL1 being the most enriched protein, but also various other non-DUB proteins were isolated. This number drastically decreased when the concentration was lowered. Treatment with GK16S resulted in a similar target spectrum and subtraction of the fold change values (GK13S-GK16S) resulted in UCHL1 being the only protein significantly enriched with GK13S. The proteomics based ABPP revealed the target spectrum of both probes, identified the bound DUB as UCHL1 and demonstrated that the click can be utilized to introduce a biotin moiety for the enrichment of DUBs with the probes. Furthermore, this experiment corroborated the finding, that both probes can be used as a chemogenomic pair of probes, which is of immense value for the specific study of UCHL1 in order to precisely trace possible phenotypes after inhibition to the modified DUB.

A genetic knockdown (kd) of UCHL1 and PARK7 in HEK293 cells validated the results from the proteomics-based target identification. RNA interference was used to determine which fluorescence band corresponds to which protein found by mass spectrometry (Fig. 15A). Knockdown of UCHL1 resulted in decreased fluorescence intensity of the upper band where

## Results

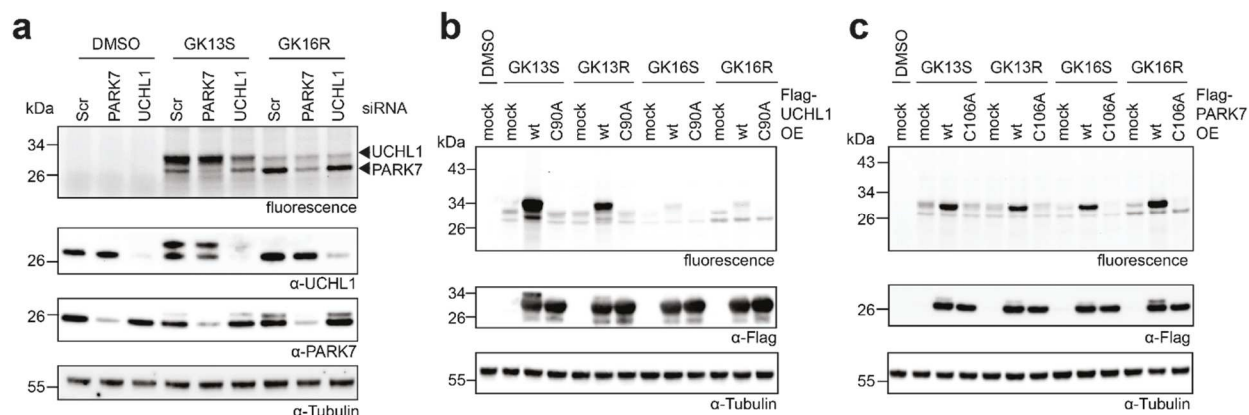


**Fig. 15 | Genetic perturbation to validate the results of the proteomics-based ABPP. a)** siRNA knockdown of UCHL1 and PARK7 in HEK293 cells. Cells were treated with indicated compounds to unravel that UCHL1 corresponds to the upper and PARK7 to the lower fluorescence signal. **b,c)** Overexpression (OEx) of a catalytically inactive C90A Flag-UCHL1 mutant (**b**), a catalytically inactive C106A Flag-PARK7 mutant (**c**) and the wild type of both proteins uncovers the probe modification sites for the proteins.

samples were treated with **GK13S**. Therefore, the upper band can likely be assigned to UCHL1. Even though the western blot proves the complete depletion of UCHL1, a fluorescence signal on the height of UCHL1 is still visible. Since C21orf33, the second major off-target of the probes, has a similar molecular weight as UCHL1, both proteins likely run on the same height. Therefore, the misleading fluorescence signal corresponds to modified C21orf33 rather than UCHL1. This hypothesis is supported by the presence of a weak upper band in samples treated with **GK16R** that does not change in intensity upon the depletion of UCHL1. As labeling with the R-isomer of the minimal probe resulted in a stronger fluorescence signal of the lower band, it was used in this experiment (see Fig. 13B). The kd of PARK7 resulted in a decrease of the lower bands after the labeling with both probes, clarifying that this band corresponds to the protein.

To elucidate if the catalytic cysteines are the covalent modification sites of both proteins, a wild type and a catalytic cysteine deficient mutant (C90A for UCHL1 and C106A for PARK7) were overexpressed in HEK293 cells (Fig. 15 B, C). In the case of UCHL1, Cys152, located at the cross-over loop, presents another reactive site the probe might covalently modify. This cysteine functions as a reactive oxygen species (ROS) scavenger, protecting the catalytic cysteine from oxidation.<sup>[164]</sup> Overexpression of the catalytically inactive mutant abolished the fluorescence signal, whereas the overexpression of the wild type resulted in a strong fluorescence band. This confirmed the catalytic cysteine of UCHL1 as the labeling site of **GK13S**. The DUB is not only labeled but also inhibited in its catalytic activity by the probe. The R-isomer shows a comparable trend, although the fluorescence band for the wild type is weaker due to the lower potency of the



## Results

probe (Fig. 15 B). The minimal probes show only weak binding to the over-expressed wild-type construct, affirming the weak potency towards UCHL1. However, overexpression of the wild-type PARK7, but not the catalytic inactive mutant, led to covalent modification of all probes. This not only confirms the catalytic cysteine as the covalent modification site, but also the acceptance of warheads with five-membered ring systems within the catalytic pocket, irrespective of their stereo configuration.

### 3.2.3 GK13S shows exquisite binding parameters for UCHL1

Now that mass spectrometry-based proteomics aided the identification of the modified DUB as UCHL1 and the cellular targets of **GK13S** were known, the specificity and the binding affinity of the probe for UCHL1 was investigated in more detail. Those *in vitro* experiments were carried out with recombinant proteins. To determine concentrations at which the S-isomer of **GK13** shows superior binding to UCHL1 over the R-isomer, intact mass spectrometry was used. Furthermore, the concentration window that results in binding to the pronounced off-target PARK7 was investigated for both isomers of the probes and the minimal probes (Fig. 16). At a lower concentration of 1  $\mu\text{M}$  the more potent S-isomer is still modifying UCHL1, resulting in a mass shift compared to the DMSO spectrum, which corresponds to the exact molecular weight of the probe. At the same concentration, the R-isomer does not show this characteristic mass shift. Therefore, it can be assumed that the R-isomer is not inhibiting UCHL1 at 1  $\mu\text{M}$  (Fig 16A). The intact mass also shows that the incubation of the probe with the protein results in a complex following a 1:1 stoichiometry. This, together with the results from the overexpression of the inactive mutants, corroborates that **GK13S** exclusively reacts with the catalytic Cys90. At higher concentrations (10  $\mu\text{M}$ ), no stereo preference for the covalent modification is observed since both **GK13** isomers show complete modification of UCHL1 and PARK7 in a 1:1 complex.

## Results

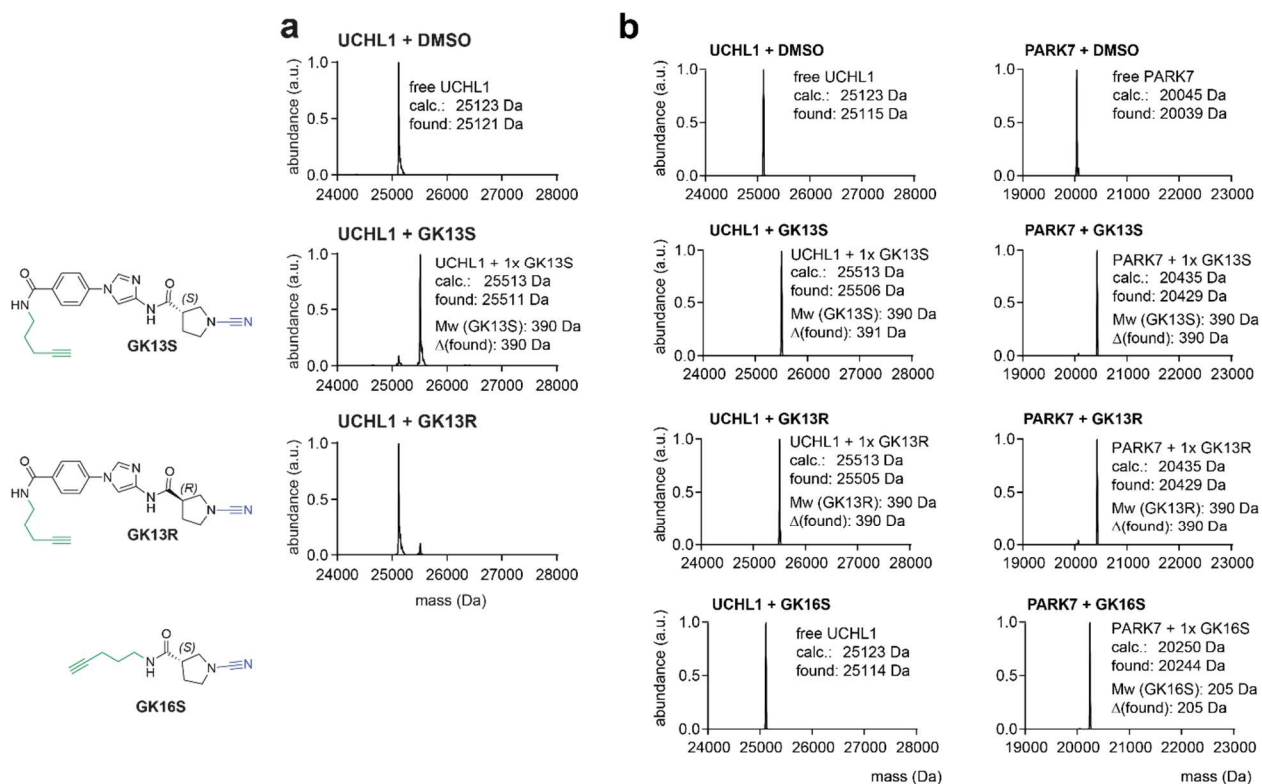


**Fig. 16 | GK13S shows superior binding towards UCHL1 at 1  $\mu$ M. a)** Intact protein mass spectra of the probes GK13S and GK13R incubated with recombinant UCHL1. The S-isomer shows potent binding at 1  $\mu$ M, whereas the R-isomer does not. **b)** Intact protein mass spectra of both GK13 isomers and the minimal probe GK16S at 10  $\mu$ M were incubated with recombinant UCHL1 and PARK7. Higher concentrations resulted in the modification of UCHL1 by both GK13 isomers but not by the minimal probe GK16S. The molecular structures of used probes are shown on the left. Data was recorded and analyzed by Dr. Christian Grethe.

However, even at high concentrations, the minimal probe **GK16S** does not bind to recombinant UCHL1 but is still active against the major off-target protein PARK7 (Fig. 16B). Incubation with the stereoisomers of the inactive probe analog **GK12** did not result in a mass shift for either UCHL1 or PARK7 (Supplementary Fig. 4). Highlighting the use of these analogues as control compounds and the need of electrophilic warheads to probe for deubiquitinases. Together, **GK13S** and **GK16S** can be used as a pair of chemogenomic probes to covalently modify the DUB UCHL1 and discriminate off-targets such as PARK7 up to a concentration of 10  $\mu$ M. To exploit the stereo preference of the S-configuration towards UCHL1, a probe concentration of 1  $\mu$ M should be used.

To understand the probe's inhibitory potency, several *in vitro* experiments were carried out by Dr. Christian Grethe. A Ub-rhodamine cleavage assay was performed to determine the potency of the parent molecule **Cpd158**, the probe **GK13S**, the minimal probe **GK16S**, the inactive control

## Results

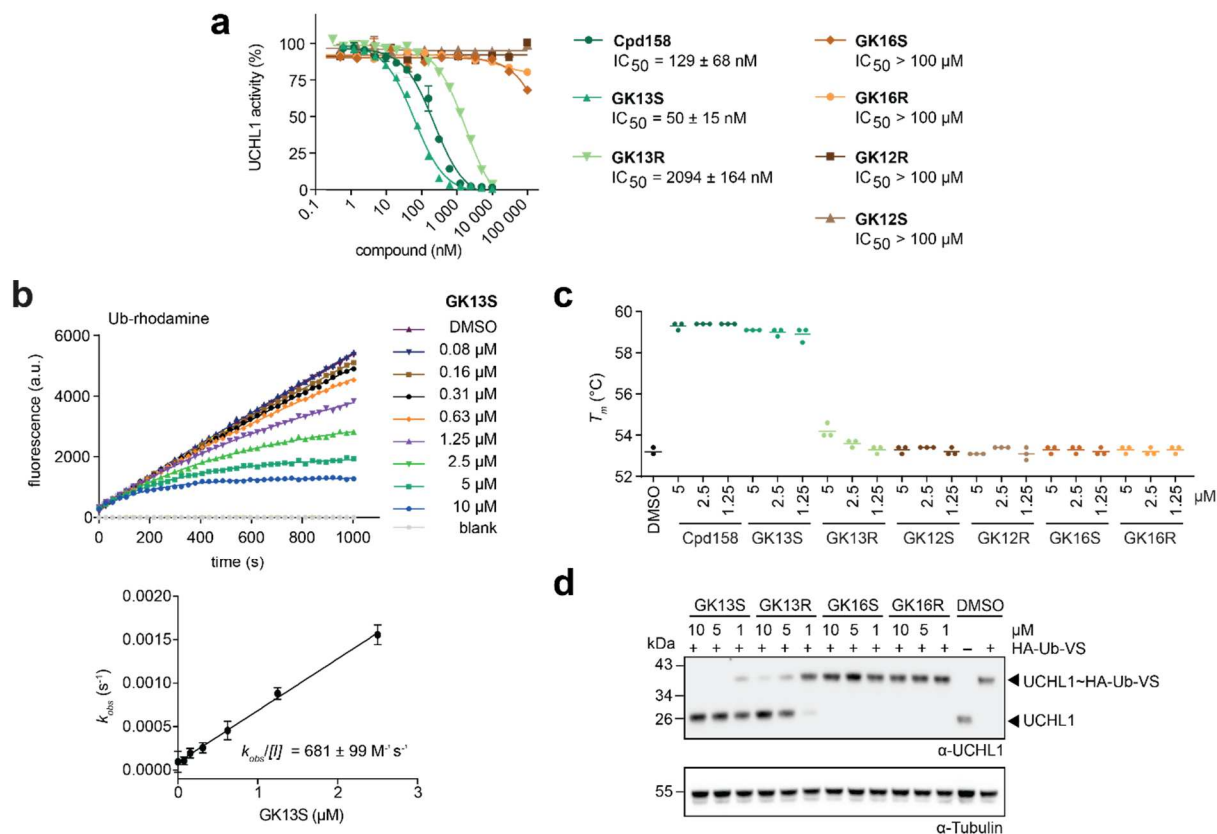


**Fig. 17 | GK13S potently binds UCHL1 *in vitro* and in cells.** All *In vitro* assays were performed by Dr. Christian Grethe<sup>[154]</sup> **a)** A Ub-rhodamine cleavage assay was carried out to determine the inhibitory potencies from all probes and corresponding analogs. **b)** Kinetic assay to determine the  $k_{obs}/[I]$  value for GK13S covalently modifying UCHL1 at indicated concentrations. DMSO and a blank well were used as controls. The rate constant  $k_{obs}$  was determined from the upper plot. To obtain  $k_{obs}/[I]$  value, the rate constant was plotted against the used probe concentrations and calculated from the resulting slope. **c)** Thermal shift assay to demonstrate the melting temperature ( $T_m$ ) of UCHL1 preincubated with the indicated compounds. **e)** Cellular Ub-probe competition assay demonstrates UCHL1 target engagement by the probes in a complex environment. Data was recorded and analyzed by Dr. Christian Grethe.

compound **GK12S** and their respective stereoisomeric counterparts against UCHL1 (Fig. 17 A). In this assay, a ubiquitin is conjugated to a rhodamine-glycine fluorophore at its C-terminus (Ub-Rh). This macromolecule mimics a substrate, which was recognized by deubiquitinases. The enzyme cleaves the amide bond between the rhodamine-glycine and the C-terminus of ubiquitin, generating free ubiquitin and rhodamine-glycine. While the Ub-Rh is non-fluorescent, the cleaved and de-quenched version exhibits intense fluorescence at 485 nm.<sup>[165]</sup> Catalytic active DUBs show a massive increase in fluorescence intensity over time, whereas inhibition results in low fluorescence intensity.

The obtained IC<sub>50</sub> values for the parent inhibitor (129 ± 68 nM) and the probe **GK13S** (50 ± 15 nM) indicate a comparable potency of both compounds. Furthermore, this data proves that the

## Results

decoration of the structure with the alkyne tag does not interfere with the potency of the probe. The measurement with **GK13R** results in an  $IC_{50}$  value ( $2094 \pm 164$  nM) that demonstrates approx. 40 times worse inhibition of UCHL1 compared to the *S*-configuration. Using either the minimal probes **GK16S/R** or the inactive control probes **GK12S/R** in this assay resulted in no quantifiable inhibition of UCHL1 ( $>100$   $\mu$ M). This demonstrates the need for a recognition element within the probes to enable sufficient binding towards UCHL1 for covalent modification.

As the binding behavior of covalent compounds is described more accurately by the time-independent kinetic parameter  $k_{obs}/[I]$ , an assay was carried out to determine the  $k_{obs}/[I]$  for **GK13S** and **GK13R** (Fig. 17 B and Supplementary Fig. 5). The rate constant  $k_{obs}$  was determined by incubating UCHL1 with the probe at a variety of concentrations without preincubation. The rate constant was calculated from the resulting graph and plotted against the inhibitor concentration to determine the kinetic parameter  $k_{obs}/[I]$ . This parameter describes the inactivation efficiency ( $M^{-1}s^{-1}$ ) of a given covalent inhibitor. The resulting value of  $681 \pm 99 M^{-1}s^{-1}$  describes a rather slow inactivation efficiency, consistent with the comparatively weak electrophilicity of the cyanopyrrolidine warhead. However, the *S*-configuration shows an approx. 40 times more efficient inactivation of UCHL1 compared to the *R*-isomer.

To test whether a binding by the probe results in enhanced UCHL1 stability and therefore increases its melting temperature ( $T_m$ ), a thermal shift assay (TSA) was carried out (Fig. 17 C). In this assay, samples with recombinant UCHL1, either treated with the compounds or DMSO as a control, were heated up until the protein unfolded. The fluorescent dye SYPRO orange was used for detection, which binds nonspecifically to hydrophobic surfaces. Its fluorescence emission was highly quenched by water. Upon unfolding, the dye attaches to the hydrophobic center parts of the protein, resulting in an increased fluorescence emission by excluding water. The so-calculated  $T_m$  describes the midway point of the stability curve. The parent inhibitor, as well as **GK13S**, led to the stability of UCHL1 by increasing its melting temperature by approx. 6 °C. **GK13S** showed the same stabilization at a concentration of 1.25  $\mu$ M, as well as at a concentration of 5  $\mu$ M. Incubation with **GK13R**, on the other hand, only resulted in a slight increase in melting temperature of 2 °C at the highest concentration of 5  $\mu$ M. Since the increase in the melting temperature does not change over the selected concentration window, it can be assumed that **GK13S** completely modified the used UCHL1, even at a concentration of 1.25  $\mu$ M. In line with the results from the Ub-Rh cleavage assay, incubation with the stereoisomers of the minimal probe and the inactive control probe does not result in stabilization of UCHL1.

## Results

In order to test whether the findings of the *in vitro* experiments are translatable to a complex proteome, the degree of UCHL1 inhibition was investigated in a living environment via the Ub-VS target engagement assay (Fig. 17 D). HEK293 cells were treated with different probe concentrations for 24 h, lysed and incubated with the Ub-VS suicide probe. The Ub-VS probe covalently modifies the catalytic cysteine of all UCHL1 that was not already occupied by the small molecule-based probes. That results in the upshift of the UCHL1 band of approx. 8 kDa, which corresponds to the molecular weight of Ub. Cells treated with 5 and 10  $\mu\text{M}$  of **GK13S** show complete inhibition of endogenous UCHL1, as no upshift of the corresponding band was visible. Even at 1  $\mu\text{M}$  an almost complete inhibition of the DUB can be observed. The *R*-configuration does not show complete inhibition at the highest concentration of 10  $\mu\text{M}$  and close to no occupation of the catalytic cysteine at 1  $\mu\text{M}$ . Consistent with the findings from the *in vitro* assays, the minimal probes **GK16S** and **GK16R** showed no response in competition with the Ub-VS probe for binding to UCHL1.

Nevertheless, the cellular potency of **GK13S** does not coincide with the  $\text{IC}_{50}$  value determined *in vitro*. This could be mainly because other factors, such as off-target binding and cell permeability, have to be considered in a complex environment. It also proves that other data besides the  $\text{IC}_{50}$  value, should be examined to evaluate covalent compounds. In addition, the specificity window of the probe **GK13S** vs. the minimal probe **GK16S** largely differs from what was observed *in vitro* (50 nM vs. >100  $\mu\text{M}$ ) and in cells. Even though the Ub-VS probe outcompetes **GK16S** in the cellular target engagement assay (Fig. 17 D), binding of the minimal probe leads to the pull down of a small fraction of cellular UCHL1 in the proteomics-based ABPP (Fig. 14 C). Since covalent compounds react with their targets in a time-dependent manner, it is not surprising that **GK16S** also bound a small amount of UCHL1 in cellular experiments. The samples in these experiments were incubated significantly longer (24 h) than in the *in vitro* assays (1 h). However, based on the proteomics data, UCHL1 is 32-fold more enriched with **GK13S** than with the minimal probe. Furthermore, the fraction of UCHL1 bound by **GK16S** represents only a small part of the total amount of the protein in the cell. This is why complete inhibition of the enzyme by **GK16S** can not be assumed, but explains the rather reduced specificity window of **GK13S** vs. **GK16S** in a cellular context. In contrast, the data suggest that the same specificity window is very narrow for **GK13S** vs. **GK13R** since inhibition of UCHL1 with **GK13R** is observable even in the target engagement assay at 1 – 5  $\mu\text{M}$  concentrations.

## Results

Taken together the findings from the *in vitro* evaluation, as well as the cellular characterization corroborates the use of the minimal probe, but not the stereoisomer **GK13R**, as a suitable chemogenomic control to disentangle phenotypes resulting from the specific inhibition of UCHL1.

### 3.2.4 Crystal structure reveals hybrid conformation of UCHL1 after modification with **GK13S**

As the potent inhibition of UCHL1 by **GK13S** was verified *in vitro* and in a cellular context, a more in-depth focus was put on the exact binding mode between the probe and the deubiquitinase (Fig 18). For that purpose, the crystal structure of UCHL1 in co-complex with **GK13S** was solved by Dr. Christian Grethe and the detailed procedure can be found elsewhere.<sup>[154]</sup> The co-complex was solved with an approach where all surface lysine residues were methylated. This increased the overall hydrophobicity of the protein since various soaking efforts in different buffers and additives failed to obtain compound containing crystals. Methylation led to conditions where the crystal structure was solved to 2.24 Å resolution with a comprehensible density of the small-molecule probe. The co-complex confirms the binding of the cyanopyrrolidine warhead of **GK13S** to the catalytic Cys90 of UCHL1, forming an isothioureia bond. The small molecule probe disrupts the interaction with ubiquitin and inhibits the catalytic activity of UCHL1 by binding through a narrow cleft that leads to the active center. This is normally used to channel the C-terminal end of Ub to the catalytic triad of the deubiquitinase (Fig. 18 A-C). After covalent modification, the isothioureia bond is stabilized by the oxyanion hole, formed by the amino acid side chains of Gln84 and Gly87. The covalent bond was further stabilized by a hydrogen bond between the catalytic His161 and the compound (Fig 18 D). Similar to the C-terminal end of Ub, the amide of **GK13S**, which linked the cyanopyrrolidine to the imidazole core, interacts with the backbone of Phe160 and Met6 via hydrogen bonding. The nitrogen of the imidazole ring was stabilized by Ile8, a residue that coordinates Ub after binding to UCHL1 (Fig 18 E, F). Superposition of the **GK13S** and Ub-VME bound structures shows that the C-terminal end of Ub and **GK13S** present hydrogen acceptors and donors at a similar position to interact with UCHL1. This favors a comparable geometry of

## Results

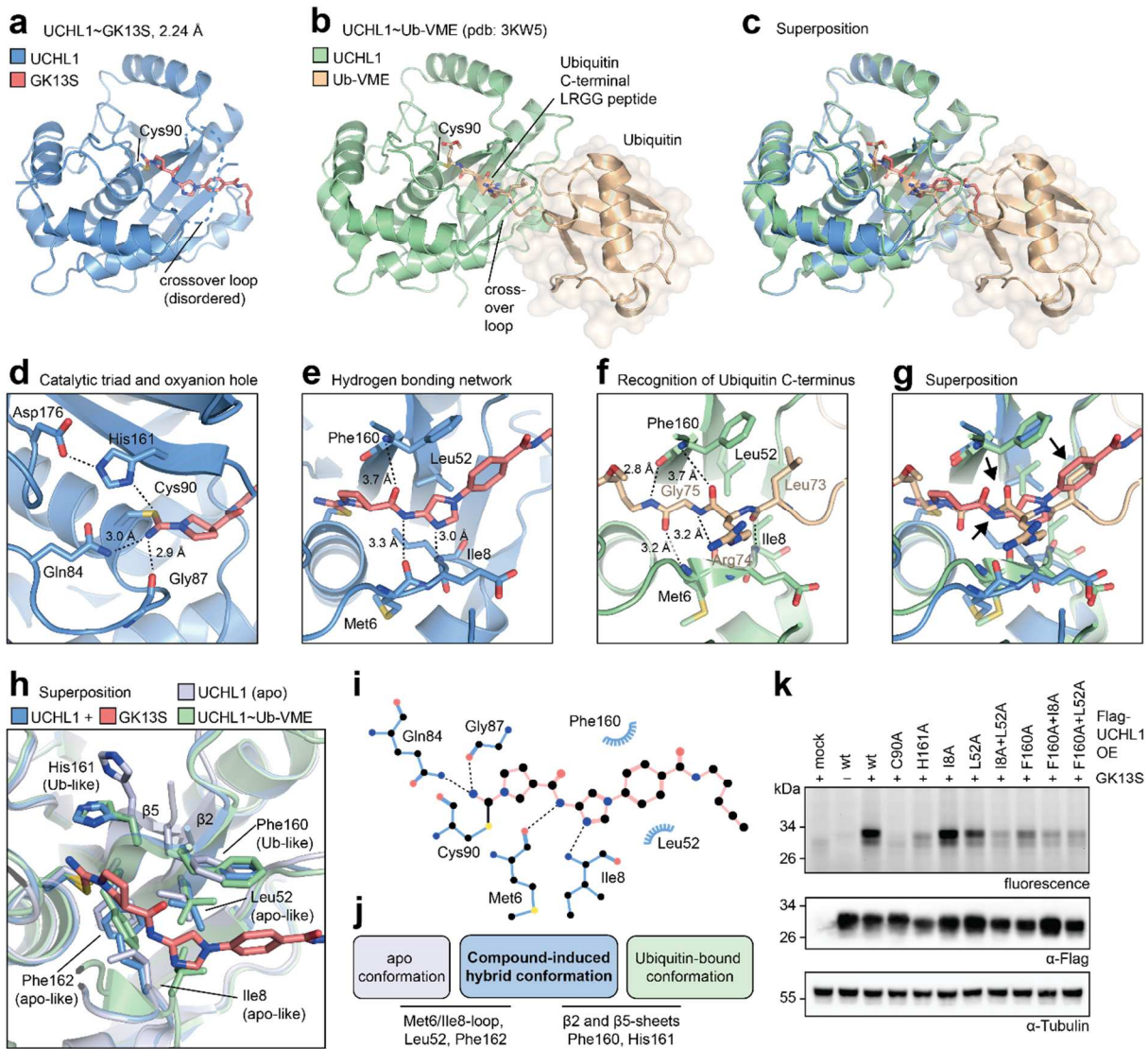


**Fig. 18 | Co-complex structure highlights the hybrid conformation of UCHL1 after inhibition with GK13S. a)** Overview of the co-complex of Gk13S (red) covalently bound to UCHL1 (blue). Annotated are the catalytic Cys90 and the disordered crossover loop (PDB: 7ZM0). **b)** Structure of ubiquitin-VME (light brown) covalently bound to UCHL1 (green). The C-terminal end (LRGG, amino acids (AA) 73-76) of ubiquitin reaching the active site is shown in sticks (PDB: 3KW5). **c)** Superposition of a) and b), indicating that GK13S occupies the same cleft as the C-terminal end of ubiquitin. **d)** Close-up view of the active center of UCHL1 occupied by GK13S. The catalytic Cys90 forms the isothioureia with the compound. The nitrogen of the isothioureia points into the oxyanion hole, interacting with Gln84 and Gly87 via hydrogen bonds. The isothioureia was further stabilized via the aligned catalytic triad. Hydrogen bonds are illustrated as dotted lines. **e)** Close up view to highlight interactions between UCHL1 residues and the recognition element of GK13S, important for potent binding. **f)** Close-up view to indicate interactions of the C-terminal end of ubiquitin with UCHL1. **g)** Superposition of e) and f) shows that GK13S partly adopts a similar conformation in the cleft to the catalytic center as the C-terminal end of Ub. Overlapping interactions are indicated by black arrows. **h)** Superposition of the apo- (violet, PDB: 2ETL), a Ub-VME bound- (green, PDB: 3KW5) and the GK13S bound (blue, PDB: 7ZM0) structure

## Results

of UCHL1. Different residues of the GK13S-bound structure show an orientation corresponding to either the apo- or the Ub-VME bound structure and are labelled accordingly. **i)** 2D illustration of the most critical interactions between GK13S and UCHL1. **j)** Schematic overview of residues and protein features that undergo structural changes upon the binding of GK13S, inducing the hybrid conformation of UCHL1. **k)** Cellular validation of residues involved in the interaction with GK13S. HEK293 cells were used to overexpress indicated Flag-UCHL1 constructs, which bear mutations in the GK13S binding site.

both ligands upon binding to the DUB. The phenyl ring of **GK13S** acts as a hydrophobic interactor, which is otherwise represented by the side chain of leucine (Leu) 73 of Ub and recognized by Phe160 of UCHL1 (Fig. 18 G). At first glance, the compound-bound structure appears to have many structural similarities with the Ub-bound structure. Clear differences become apparent, however, when the focus is on the binding site of the compound. The residues of Phe162, Ile8 and Leu52 of the **GK13S** bound co-complex structurally align analogous to the same residues in the apo UCHL1 structure. Those side chains formed a hydrophobic pocket, which stabilized the pyrrolidine of **GK13S**. The residues of His161 and Phe160, and the  $\beta$ -sheets 5 and 2 adjust to a conformation observable in the Ub-bound structure. Only those conformations allow the interaction of the phenyl ring in **GK13S** with Phe160. The co-complex structure demonstrates that UCHL1 adopts a hybrid conformation after modification with **GK13S**, which includes structural changes of the apo and the Ub-bound state (Fig. 18 H). Only this hybrid conformation of UCHL1 was able to stabilize **GK13S** in its binding pocket, otherwise Ile8 in the Ub-bound state would sterically clash with the imidazole of the compound. On the other hand, the distance of Phe160 in the apo form would be too far to enable sufficient  $\pi$ - $\pi$  stacking with the phenyl ring of **GK13S** (Fig. 18 I, J).

To confirm that the same amino acid residues also involved in essential interactions with the compound in a living environment, various UCHL1 constructs with mutations in the **GK13S** binding site were overexpressed in HEK293 cells (Fig. 18 K). After incubation with the probe and subsequent attachment of the reporter, the fluorophore intensity was read out to visualize the impact of the indicated mutation on the binding of **GK13S**. The mutant of the catalytic cysteine was used as a positive control. The mutation of the His161 results in dealignment of the catalytic triad and therefore also abolishes binding of the compound. Mutation of Ile8 does not destabilize the binding of **GK13S** to UCHL1, since the interactions with Leu52 and Phe160 compensate the loss. Mutations of either Leu52 or Phe160 resulted in a drastic decrease in the binding efficiency, thus highlighting the importance of the hydrophobic environment around the phenyl ring of **GK13S**. Double mutants of all the aforementioned amino acids led to a massive decrease in fluorescence signal and therefore, compound binding. Collectively, **GK13S** binds UCHL1 through



## Results

a small cleft, which is normally occupied by the C-terminal peptide (LRGG) of the natural substrate ubiquitin. Upon binding, the compound forces UCHL1 in a hybrid conformation, in resulting structural changes of key amino acids that arise partly from the apo- and partly from the Ub-bound state of UCHL1. Leu52 and Phe160 form a hydrophobic pocket around the phenyl ring of **GK13S**, which is important for stabilizing the compound inside the binding site.

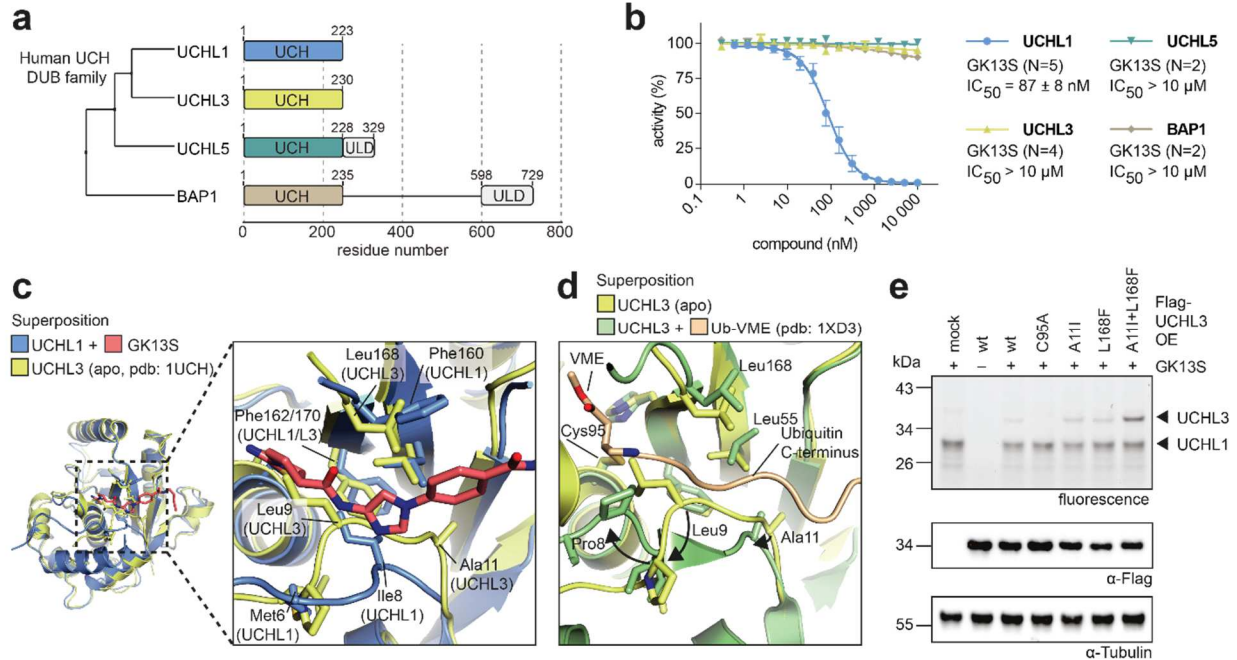


**Fig. 19 | Structural basis for the specific in-class inhibition of UCHL1.** **a**) Schematic overview of the domain architecture of all UCH family members **b**) Ub-Rh cleavage assay with the purified catalytic domains of enzymes of the UCH family, preincubated with GK13S for 1 h. **c**) Alignment of the apo UCHL3 structure (yellow, PDB: 1UCH) with the Gk13S bound UCHL1 structure (blue, PDB: 7ZM0) and close-up of the probes binding pocket. Highlighted amino acid residues are shown as sticks. **d**) Superposition of the apo UCHL3 and UCHL3 (green) in the Ub-VME (light orange) bound state (PDB: 1XD3). This structure was used as a proxy to illustrate the UCHL3 binding site. The C-terminal of Ub is shown and conformational changes upon binding are indicated with black arrows. **e**) Flag-UCHL3 constructs bearing indicated mutations were overexpressed in HEK293 cells. Introduced mutations should mimic the GK13S binding site derived from the UCHL1 structure.

Next, the in-class selectivity of the probe was investigated in more detail (Fig. 19). UCHL1 belongs to the UCH family, which comprises three other members: the closest homolog UCHL3, the proteasome associated UCHL5 and the tumor suppressor BAP1. The structure of all family members contains the characteristic UCH domain, varying in length across the different DUBs. UCHL5 and BAP1 also feature a C-terminal extension involved in regulatory functions (Fig. 19 A). To test the potency of **GK13S** against the other family members, a Ub-Rh cleavage assay with the purified catalytic domains of the individual DUBs was carried out (Fig. 19 B). **GK13S** shows

## Results

specific binding only to UCHL1 (catalytic domain: 87 nM), whereas the  $IC_{50}$  value for all other family members was determined to be over 10  $\mu$ M. This results in a minimum specificity window for the binding of **GK13S** to UCHL1 compared to the other family members of approx. 115-fold. To explain this structurally, the co-complex of UCHL3 with Ub-VME (PDB: 1XD3), and apo UCHL3 (PDB: 1UCH) were used for comparison. The superposition of these structures revealed that not only the apo form of UCHL3 but also the Ub-bound state varies in conformations, especially in their N-terminal region compared to UCHL1. A closer look at the superposition of the **GK13S**/Ub binding site, displays that Leu9 in apo UCHL3 (Met6 in UCHL1) would sterically clash with the compound (Fig 19 C, D). Even more striking is the lack of the hydrophobic pocket present in UCHL1, which explains the weak binding of the probe to UCHL3. Mainly, Ala11 and Leu166 in UCHL3 (Ile8 and Phe160 in UCHL1) present another microenvironment within the binding site, which does not promote the stabilization of **GK13S**. This led to the hypothesis that the interactions in the hydrophobic pocket formed from the residues of Phe160 and Ile8, among others were fundamental residues for the binding of **GK13S** to UCHL1. To test this, several Flag-UCHL3 mutants bearing the critical amino acids identified from the UCHL1 binding site were overexpressed in HEK293 cells and treated with the probe. Compound binding to any of the mutants was verified via InGel fluorescence in an ABPP approach (Fig. 19 E). A negligible low fluorescence signal compared to the signal from UCHL1 is also evident from the binding of the probe to the wild type of UCHL3. Mutation of the catalytic cysteine abolishes the signal, proving that the catalytic cysteine also functions in UCHL3 as an anchor point for covalent modification by the probe. Introducing either the isoleucine in position 11 or the phenylalanine in position 168 only increases the fluorescence signal and therefore, binding of **GK13S** slightly. Only the positioning of both residues drastically increases the fluorescence intensity on the height of UCHL3 after incubation with the probe. This corroborates the need for a hydrophobic environment within the binding surface of UCH proteins for the binding of small molecules with a recognition element based on **GK13S**. Furthermore, this structural analysis explains the in-class specificity of **GK13S** for UCHL1.

### 3.2.5 GK13S and GK16S as tools to unravel UCHL1 substrates

With the binding mode of the small molecule probe **GK13S** towards UCHL1 understood, the third objective (Aim III) was tackled. This part includes identifying possible interaction partners and substrates of UCHL1, as well as characterizing phenotypes after the inhibition of the DUB using the chemogenomic pair of probes **GK13S** and **GK16S**.

#### 3.2.5.1 Inhibition of UCHL1 in glioblastoma cells results in reduced mono ubiquitin levels

As dysregulation of UCHL1 is associated with neurological diseases, human glioblastoma cells U-87 MG were chosen as a model cell line to screen for interaction partners of UCHL1 or phenotypes occurring after its inhibition.<sup>[166]</sup> In addition, U-87 MG cells were selected due to their high expression level of UCHL1 in brain tissue.<sup>[167]</sup> To ensure the successful and non-toxic inhibition of UCHL1 by the probe in the model cell line, validation experiments were performed first (Fig. 20, Supplementary Fig. 6). To demonstrate the use of **GK13S** and **GK16S** as a chemogenomic pair of probes, covalently bound probes were visualized via in gel fluorescence in an ABPP approach (Fig. 20 A). At concentrations of 1 and 5  $\mu\text{M}$  **GK13S** shows a similar binding pattern as observed in HEK293 cells (compare with Fig. 13 B). The most prominent and concentration-dependent band in samples treated with **GK13S** appears on a height of approx. 28 kDa. Based on the previous characterization, this band was assigned to UCHL1. This assignment was supported by the faint appearance of the same band in samples treated with 5  $\mu\text{M}$  of the minimal probe. Just below the UCHL1 band, another fluorescence band appears after the treatment with **GK13S** and **GK16S**, which corresponds to PARK7. Based on the proteomics analysis of modified proteins in HEK293 cells (Fig. 14 C), the bands below 70 kDa correlate most likely to modified aldehyde dehydrogenases. This demonstrates the utility of the probes as a pair of chemogenomic probes in U-87 MG cells. Furthermore, the data proves that the binding behavior of the probes does not fundamentally change across different cell lines. In addition, the isatin *O*-acyl oxime LDN-57444, described as a potent UCHL1 inhibitor, was characterized in U-87 MG cells to use it as a positive control potentially.<sup>[168]</sup> Even though it is widely used in the cellular and *in vivo* examination of UCHL1, its overall activity could not be confirmed recently.<sup>[129a, 129b]</sup> Since it lacked an alkyne handle, its target spectrum in a cellular context could not be verified via in-gel fluorescence. The cellular inhibition of UCHL1 by **GK13S** was verified via a target engagement assay (Fig. 20 C). Incubation with the HA-Ub-VS probes revealed that only **GK13S** covalently modifies UCHL1 in U-87 MG cells. Even after one hour of incubation, a concentration of 5  $\mu\text{M}$  is sufficient to inactivate most of the endogenous UCHL1. Treatment for 24 hours results

## Results

in complete inhibition at 5  $\mu\text{M}$  of the probe. Neither **GK16S** nor **LDN-57444** could outcompete the ubiquitin suicide probe for UCHL1 binding. To exclude cellular toxicity of the probes, cells were stained with propidium iodide (PI) and analyzed via microscopy after compound treatment (Supplementary Fig. 6). Both **GK13S** and the minimal probe **GK16S** did not show any cellular toxicity after 72 hours of incubation and a concentration up to 5  $\mu\text{M}$ .

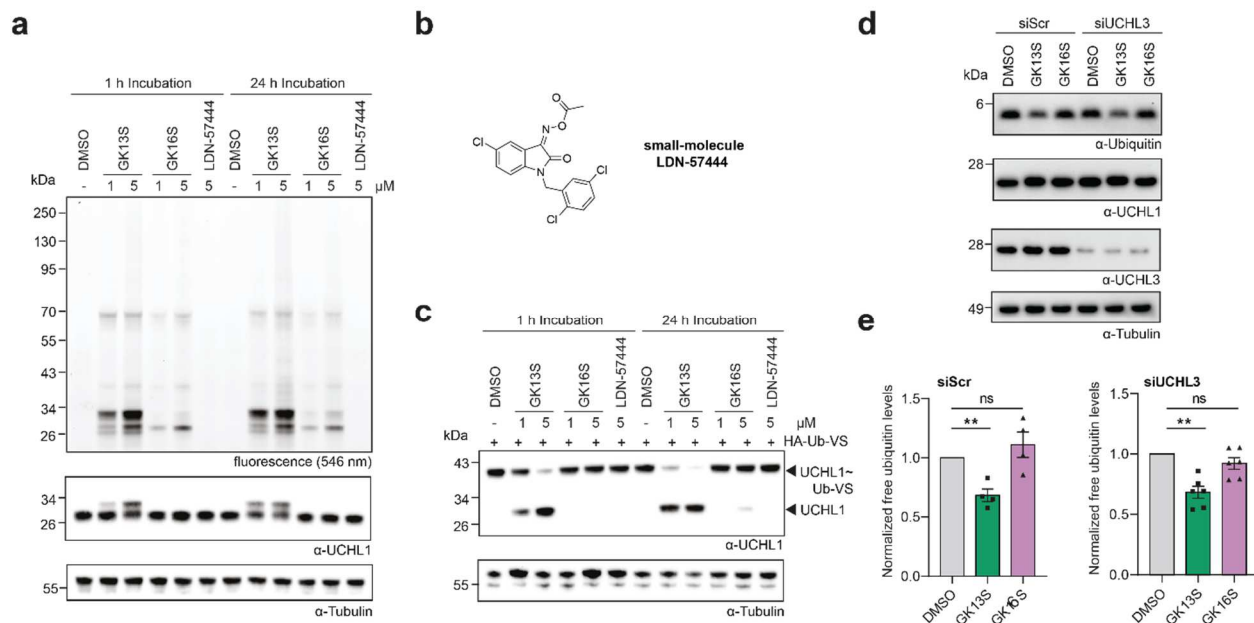


**Fig. 20 | GK13S covalently modifies UCHL1 in human glioblastoma cell line U-87 MG, leading to reduced mono Ub levels.** **a)** Activity-based protein profiling in glioblastoma cells to visualize UCHL1 binding. U-87 MG cells were treated with indicated compounds and concentrations. The cells were harvested and the reporter fluorophore was attached via CuAAC. **b)** Molecular structure of the small molecule inhibitor LDN-57444. **c)** Analysis of successful inhibition of endogenous UCHL1 in U-87 MG cells. The proteome was incubated with a HA-Ub-VS suicide probe after the cellular treatment with the indicated compounds. Target engagement was verified via western blot analysis. **d)** Western blot analysis of mono ubiquitin levels in U-87 MG cells after the treatment with indicated probes in an unmanipulated or UCHL3 knockdown background. **e)** Quantification of mono-ubiquitin intensity on western blots shown in d). Values correspond to the mean of four or six individual experiments for control or UCHL3 knockdown, respectively (ns, not significant). Experiments for detecting changes in the mono-Ub pool were carried out with the help of MSc. Kai Gallant.

Mutations of the UCHL1 gene in mice led to gracile axonal dystrophy.<sup>[169]</sup> In addition, reduced mono ubiquitin levels in mice brain tissues are another phenotype associated with the dysregulation of UCHL1.<sup>[170]</sup> An opposite effect was observed by the overexpression of UCHL1 in the monkey cell line COS-7.<sup>[171]</sup> Since this phenotype has so far only been shown by genetic manipulation of UCHL1, the small molecule-based probes **GK13S** and **GK16S** were used as a chemogenomic pair to stimulate the reduction of the mono-Ub level in human glioblastoma cells

## Results

(Fig. 20 D, E). To rule out the possibility that the phenotype was a rather slow process, U-87 MG cells were treated with the compounds over 48 h. To ensure the full inhibition of newly synthesized UCHL1 over a long period, the cell medium was supplemented with fresh compound every 24 h. During cell lysis, chloroacetamide (CAA) was used to inactivate all endogenous DUBs, which could counteract the inhibition of UCHL1. Western blot analysis of mono ubiquitin levels revealed that the free mono Ub pool is indeed reduced after the treatment of U-87 MG cells with **GK13S** but not with the minimal probe **GK16S**. To exclude the involvement of other family members of the UCH family, the same conditions were studied in a UCHL3 knockdown background. In this environment, the same degree of reduction on the mono Ub level was only observed when cells were treated with **GK13S**. This corroborates the presumed non-redundant functions of UCHL1 and UCHL3.<sup>[172]</sup> Further cellular characterization of **GK13S** and **GK16S** validated its functionality in human glioblastoma cells. In addition, the probes were used to copy a phenotype upon the inhibition of UCHL1 in U-87 MG that had previously only been shown with genetic alterations in mice. Furthermore, these findings prove that a chemogenomic pair of small molecule-based probes is suitable for investigating DUBs in a complex environment.

Next, the phenotype was validated by the posttranscriptional perturbation of UCHL1 in glioblastoma cells (Fig. 21 A, B). Si-RNA-mediated depletion of UCHL1 in U-87 MG cells was used to disentangle if the mono ubiquitin is still bound to substrate proteins or larger Ub aggregates due to the missing deubiquitinase activity of UCHL1. U-87 MG cells were lysed and treated with various exogenous DUBs to rescue the phenotype after the knockdown of UCHL1 (Fig 21 C, D). In order to cleave the Ub-conjugates that may have formed from the inhibition of UCHL1 and thus equalize the free mono Ub pool, DUBs with different chain specificities were selected. OTUB1 mediates the specific deubiquitination of Lys48-linked polyubiquitin chains, whereas AMSH shows specific recognition of Lys63 chains.<sup>[173]</sup> This covered the two most common linkage types and might shed light on the possibly chain specificity of UCHL1. To cover the condensation of the global ubiquitome bound to substrates, the DUB USP2 was used. The addition of hydroxylamine should condensate possible ubiquitin molecules bound to the hydroxy group of serine or threonine residues, but does not cleave those linked via an isopeptide bond.

Unfortunately, neither the addition of hydroxylamine nor any of the exogenous DUBs could equalize the free mono-Ub pool. Interestingly, OTUB1 cleaved most of the visualized Ub-conjugates, even though annotated to be specific for Lys48 polyubiquitin chains. As expected, USP2 condensed all ubiquitinated species in the high molecular weight range. However, even after the cleavage of those species, the free mono Ub pool is still reduced by almost 50 % in the

## Results

UCHL1 knockdown fraction compared to the scrambled control. In samples treated with OTUB1 and AMSH, a slight equalization of the mono ubiquitin level is observable. However, this fluctuation could be due to the non-natural environment after cell lysis, as the DUBs continue to cleave polyubiquitin conjugates. Nevertheless, the released ubiquitin is not used for further conjugation to other substrates and is thus mistakenly added to the free mono-Ub pool.

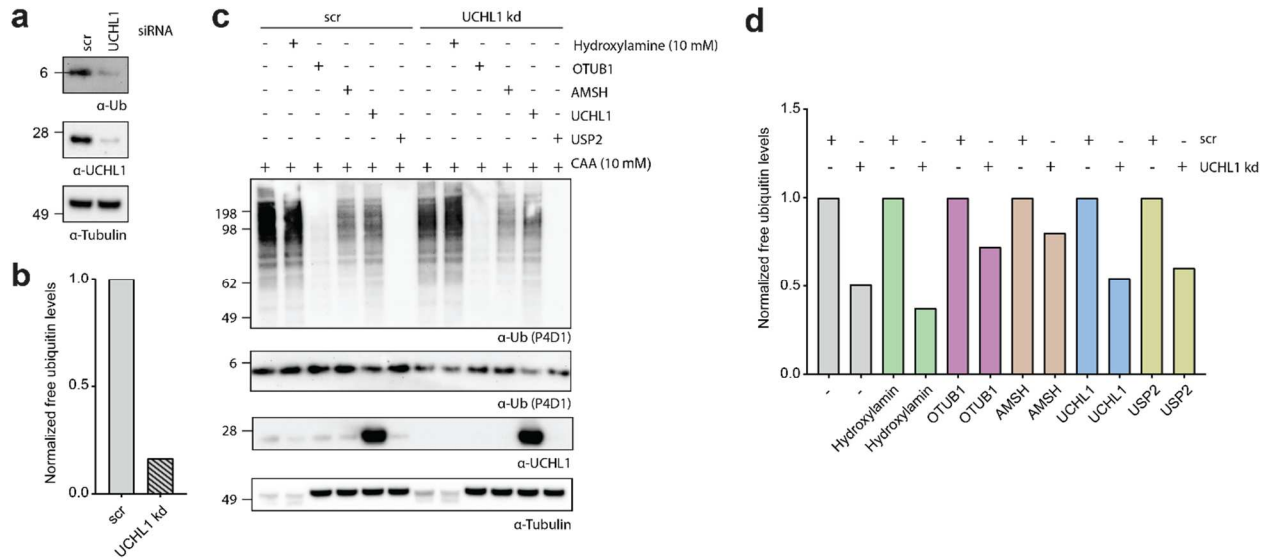


**Fig. 21 | Various DUBs are insufficient in rescuing the reduced mono-Ub pool after UCHL1 knockdown.** **a)** si-RNA-mediated knockdown of UCHL1 reduces mono ubiquitin levels in human U-87 MG cells. **b)** Quantification of mono-ubiquitin intensity on western blots shown in a). **c)** Rescue experiment to equalize the mono ubiquitin pool after depletion of UCHL1 or the incubation with a scrambled si-RNA (scr). U-87 MG cells were lysed and treated with indicated DUBs after the knockdown of UCHL1 and levels of mono ubiquitin were subsequently analyzed via western blotting. **d)** Quantification of mono-ubiquitin intensity on western blots shown in c).

The tubulin bands from samples treated with hydroxylamine appeared faint, resulting from a technical error where no reducing agent was added to the LDS-sample buffer prior to the SDS-PAGE. Collectively, the inhibition by the probes **GK13S** and **GK16S** and the knockdown confirms the UCHL1 dependent maintenance of the free mono-Ub pool in human glioblastoma cells. Catalytic inactivation of the DUB led to the loss of free mono-Ub inside the cell. However, the mono-Ub that was reduced from the pool was most likely not only conjugated to protein substrates or polyubiquitin chains since the addition of endogenous DUBs could not equalize the amount of missing mono-Ub by trimming down higher molecular Ub-conjugates. The fact that even after the addition of USP2, the ubiquitin pool was not equalized suggests that inhibition of UCHL1 may not only affect the free-mono Ub pool but the entire free Ub-pool. The missing ubiquitin molecules seem to be irreversibly lost, but further experiments are needed to support this hypothesis.

### 3.2.5.2 Whole proteome digestion revealed reduced RAC1 protein levels after GK13S cell treatment

UCHL1 is associated with many regulatory functions in different signaling pathways, but its verified protein substrates remain scarce.<sup>[75]</sup> To elucidate possible interaction partners of UCHL1 a proteomics-based whole proteome digestion approach of the human glioblastoma cell line U-87 MG was carried out (Fig. 22). This experiment was based on the fact that UCHL1 stabilizes its protein substrates by removing ubiquitin from them, which would otherwise result in their degradation by the proteasome. If UCHL1 was inhibited by the small molecule probe **GK13S**, the deubiquitinase activity is no longer present, inevitably leading to the degradation of the protein substrates. This leads to a decreased substrate level within the cell, which can be analyzed via digestion and measurement of the entire proteome using mass spectrometric methods (Fig. 22 A). The inhibition of UCHL1 could also trigger other signaling pathways so that some proteins might be upregulated indirectly. The absolute protein levels of the probe-treated samples were compared with a DMSO control to get a general overview of the changes in the proteome. A comparison between the sample treated with **GK13S** and the one treated with the minimal probe **GK16S** provides information about which changes in the proteome result from the inhibited activity of UCHL1 and which are due to the modification of other off-target proteins. Due to the covalent nature of **GK13S**, UCHL1 is irreversibly inactivated, so that even proteins with a low turnover rate were degraded. As an additional control, the changes in the absolute protein levels were quantified upon the knockdown of UCHL1 in U-87 MG cells (Fig. 22 B, Supplementary Fig. 7).

After label-free quantification, the levels of 21 proteins were significantly changed (fold change of  $< -1.5$  for decreased levels,  $> 1.5$  for increased levels) compared to the scrambled control. Those proteins were clustered by classes using the online classification system Protein ANalysis THrough Evolutionary Relationships (PANTHER).<sup>[174]</sup> The hits whose levels were altered belong to various different protein classes and a clear connection between the knockdown of UCHL1 and the altered level of a specific protein class is not apparent. Proteins, whose levels were decreased led to division into the following classes: structural proteins (TTN), metabolic interconversion enzymes (RABGGTB, COX20), adaptor proteins (CD81) and transporter proteins (ATP6AP1). Those with elevated levels involve RNA metabolism proteins (SRSF5, RBM17, LEMD3) and membrane trafficking proteins (SDCBP, CADPS). Protein classes that include both decreased and increased levels were protein modifying enzymes (HtrA2, CDK2) and cytoskeletal proteins

## Results

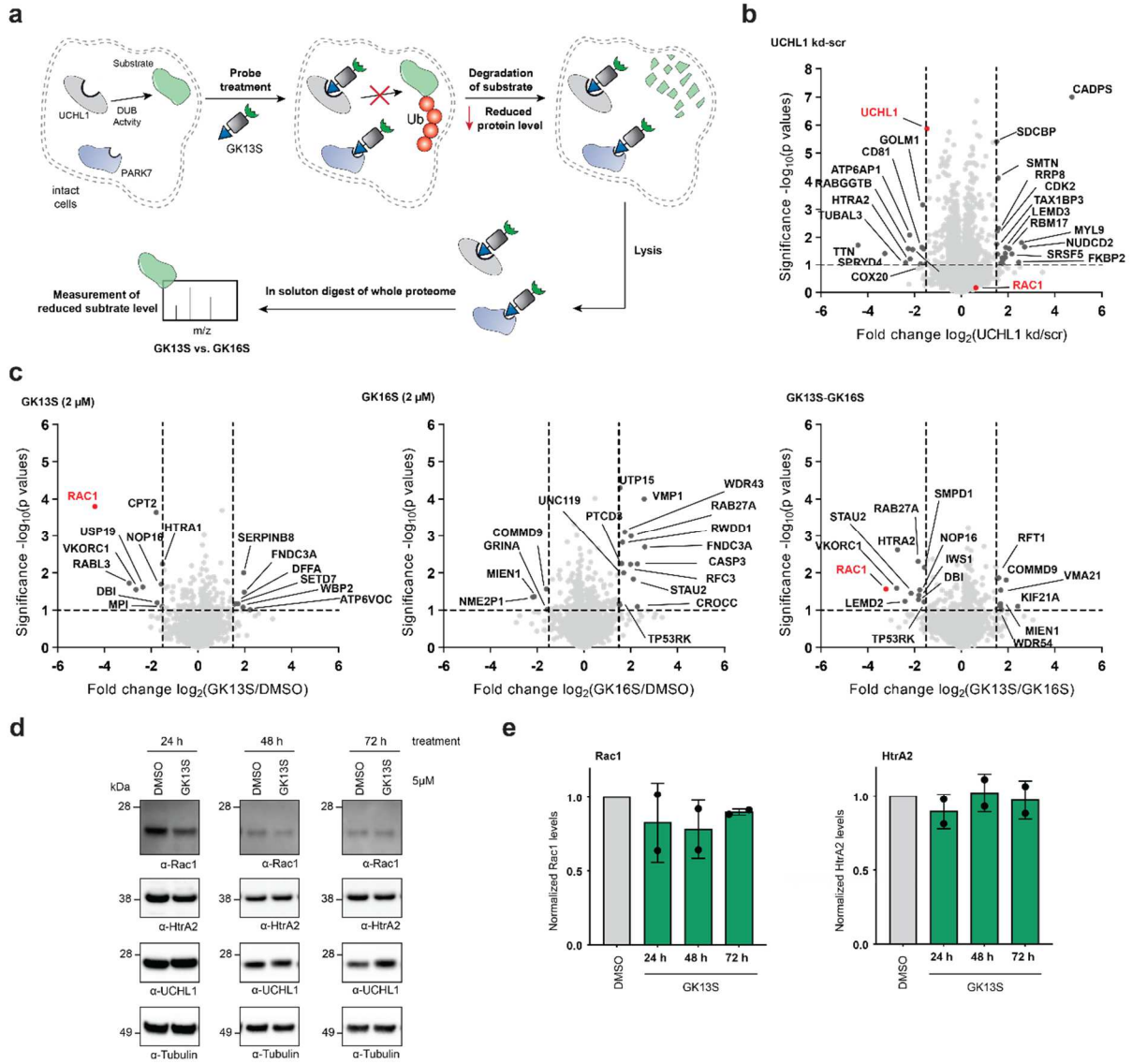


**Fig. 22 | Cellular treatment with GK13S results in reduced levels of RAC1 and other important regulators. a)** Schematic overview of the proteomics-based whole proteome digestion workflow. In a normal cell state, DUBs stabilize their substrates via their deubiquitinase activity. The inhibition of UCHL1 by GK13S results in the ubiquitination of the DUBs substrates and the subsequent degradation by the proteasome. This results in an overall reduced substrate level. The whole proteome was measured by mass spectrometry and changes in protein levels are analyzed to find UCHL1 substrates. **b)** Abundance of proteins that either decreased or increased after the knock down of UCHL1 in U-87 MG cell are visualized as a volcano plot. The x-axis indicates the relative label-free abundance ratio (fold change) of proteins between the UCHL1 knockdown sample and the scrambled control. **c)** Abundance of proteins that either decreased or increased after the treatment of U-87 MG cells with GK13S (left plot) or GK16S (middle plot) are visualized as a volcano plot. The x-axis indicates the relative label-free abundance ratio (fold change) of proteins between compound-treated samples and the DMSO control (left and middle plot) or the minimal probe GK16S (right plot). **d)** Western blot analysis of RAC1 protein levels after treatment of U87-MG cells with GK13S. **e)** Quantification of RAC1 band intensity of western blots shown in d). Values correspond to the mean of two individual experiments



## Results

(TUBAL3, MYL9, NUDCD2). Some others were not annotated to any protein class (TAX1BP3, RRP8, FKBP2, GOLM1, SPRYD4) (Supplementary Fig. 7). The UCHL1 protein level was decreased approx. 3-fold (fold change of 1.5) due to the knockdown. The protein most abundantly destabilized in the UCHL1 knockdown background is titin (decreased protein level of approx. 21-fold compared to the scrambled control). It is the critical component of cardiac and skeletal muscles, controlling the correct assembly and function of this tissue.<sup>[175]</sup> The calcium-dependent secretion activator 1 (CADPS) level was significantly upregulated upon knockdown of UCHL1 (increased protein level of approx. 128-fold compared to the scrambled control). CADPS or CAPS1 is involved in the calcium-dependent exocytosis of vesicles that are important transporting of neurotransmitters and neuropeptides.<sup>[176]</sup> Of particular note is the altered protein level of HtrA2 (approx. 4.5-fold decreased level compared to the scrambled control). HtrA2 belongs to the serine protease family and is involved in initiating apoptosis by either direct binding and inhibition of BIRC proteins or through protease activity-dependent mechanisms. Under normal conditions the enzyme is localized at the mitochondria, but in response to various cellular stresses, HtrA2 is recruited to the cytosol.<sup>[177]</sup> Furthermore, the gene coding for HtrA2 was suspected to belong to a group of genes responsible for the development of Parkinson's disease. The gene alias is PARK11 (genes of UCHL1 and DJ1 belonging to the same group, termed PARK5 and PARK7, respectively).<sup>[178]</sup> Besides the link to PD, HtrA2 interacts with UCHL1 under apoptotic conditions.<sup>[177]</sup> In addition, the overall protein level of HtrA2 was also decreased upon the inhibition of UCHL1 by **GK13S** (approx. 6.5-fold decreased in comparison with the **GK16S** treated proteome), but not in the cells treated with the minimal probe **GK16S** (Fig. 22 C).

Comparison of altered protein levels in a UCHL1 knock down background and the compound-treated samples revealed that HtrA2 was the only protein whose levels significantly changed upon both manipulations, indicating a strong UCHL1 dependency (Supplementary Fig. 8). As in the UCHL1 knockdown sample, the treatment with neither **GK13S** nor **GK16S** led to the reduction of a specific class of proteins (Supplementary Fig. 9). The incubation of the cells with the small molecule probes instead resulted in the alteration of protein levels from various families. Among the proteins with reduced levels were metabolite interconversion enzymes (SMPD1, VKORC1), a carrier protein (DBI), small GTPases (RAB27A, Rac1) and protein modifying enzymes (HtrA2, TP53RK). The hits that show an increased protein level belong to the transporter (RFT1) and cytoskeletal (KIF21A, WDR54) class of proteins.

Significantly Rac1 was destabilized after the inhibition of UCHL1 by **GK13S** (approx. 9-fold decreased in comparison with the **GK16S** treated proteome) (Fig. 22 C). Rac1 belongs to the Rho

## Results

family of small GTPases, which regulate key interactions in the cytoskeleton and gene expression pathways. Its correct function is necessary in various cellular downstream functions, all central for normal cell physiology.<sup>[179]</sup> Deregulation of Rac1 activity can have a tremendous impact on the cellular state and lead to various diseases with cancer, cardiovascular diseases, neurodegenerative disorders and pathological inflammatory responses, among them.<sup>[180]</sup> To confirm the observed effects, the band intensity of Rac1 and HtrA2 on western blots after the inhibition of UCHL1 by **GK13S** was analysed (Fig. 22 D, E). In order to map a more significant time window, the cells were incubated with the probe for up to 72 h. The western blot analysis of Rac1 levels revealed a slight reduction at 24 h after the treatment with **GK13S**. At 48 h the Rac1 level further decreased until, after 72 h, a rebound of the protein level was observed. The recovery of Rac1 could be triggered by other deubiquitinases that stabilized the protein. Analysis of HtrA2 protein levels showed only minimal changes in protein levels after the treatment with **GK13S** over time, so western blot could not confirm the effect that occurred after digestion of the proteome.

Collectively, a proteomics-based whole proteome digestion approach of human glioblastoma cells treated with the small molecule probe **GK13S** and the corresponding minimal probe **GK16S** revealed two possible substrates of UCHL1. Both the small GTPase Rac1 and the serine protease HtrA2, also suspected of being involved in the development of PD, showed altered protein levels after the inhibition of UCHL1 with the probe **GK13S**, but not with the minimal probe **GK16S**. A connection between UCHL1 and mitochondrial HtrA2 in a PD- and a non-PD background was also drawn by others.<sup>[177, 181]</sup> The reduced levels of HtrA2 were also verified with the si-RNA mediated knock down of UCHL1 in the same cell line after whole proteome digestion. However, verifying reduced protein levels of Rac1 and HtrA2 after the treatment with **GK13S** by western blot analysis did not lead conclusive results. Further experiments are necessary to identify the mentioned proteins as substrates of UCHL1 and to clarify mechanistic relationships.

### 3.2.6 Utilizing an inactive UCHL1 mutant for substrate trapping

The proteomic-based whole proteome approach only reveals changes in total protein levels that were dependent on a deubiquitinase activity involved in manipulating a degradation signal. Many deubiquitinases are not only involved in stabilizing their substrates since different ubiquitin linkage types can trigger different cellular events other than being a signal for protein degradation. Furthermore, UCHL1 could transmit signals via protein-protein interactions (PPI). These types of interaction partners could also not be detected with the method described in 3.2.5.2. Therefore,

## Results

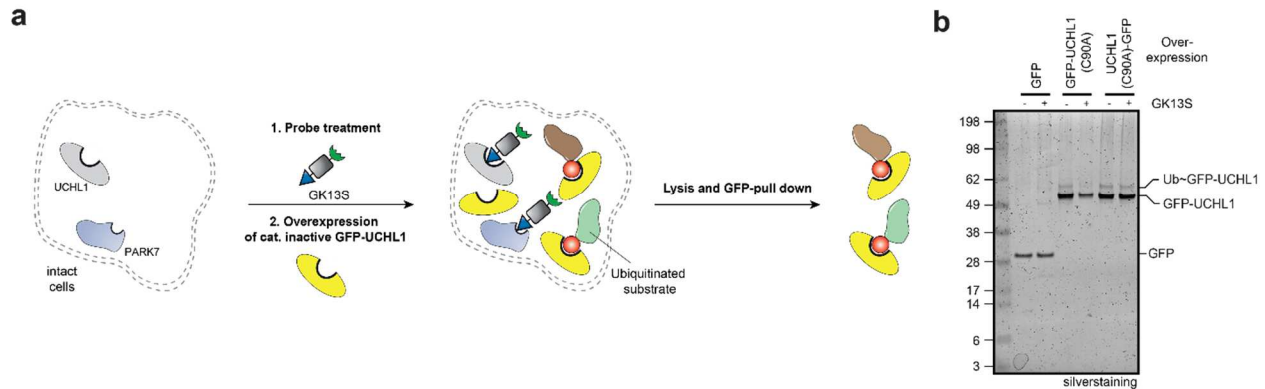


**Fig. 23 | Utilizing a catalytic inactive UCHL1 variant for substrate trapping. a)** Schematic overview of the UCHL1 substrate trapping strategy. Intact cells were treated with GK13S to abolish the catalytic activity of endogenous UCHL1. A catalytic inactive and GFP-tagged UCHL1 mutant (C90A) was overexpressed. This UCHL1 variant was used as a bait to fish for ubiquitinated substrates. The GFP-tag was used as a pull-down handle to isolate the bound substrates. **b)** Silver stain analysis of GFP pull-down fractions. Indicated proteins were used as baits. Samples were incubated with the probe GK13S where indicated.

a substrate trapping approach was carried out to identify possible UCHL1 substrates in an unbiased manner (Fig 23). In order to fully inhibit endogenous UCHL1 and to enrich for ubiquitinated substrates of the DUB, intact cells were treated with the probe **GK13S**. An inactive mutant was introduced via overexpression to exploit UCHL1 as a bait for substrate trapping. In this construct, the catalytic Cys90 was mutated to an alanine. This mutation abolishes the catalytic efficiency. However, the DUB was still able to bind to ubiquitin. The approach was published for other DUBs recently and the authors suggest that an active site alanine mutation enhances the enzyme's affinity for ubiquitin.<sup>[182]</sup> The exogenous UCHL1 variant was further tagged with GFP to utilize anti-GFP beads in a pull-down strategy to isolate the bound substrates (Fig 23 A). Two bait variants were introduced to allow the interaction of possible substrates with either the N- or C-terminus of UCHL1. One bearing the GFP tag N-terminal, the other at the C-terminus. The pull downed proteins were analyzed via silver staining to visualize low-abundant species. Unfortunately, the most abundant bands after the pull-down, corresponded to the bait proteins (lane 5-8) or the GFP alone, which was used as negative control (lane 2-3) (Fig. 23 B). A weak band above the UCHL1 mutants was visible, which could correspond to the ubiquitinated forms of the baits. It was reported that UCHL1 is regulated via mono ubiquitination and thus also possesses an auto-deubiquitinase activity.<sup>[183]</sup> The catalytic inactive mutant cannot deubiquitinate itself, resulting in the stable mono ubiquitination and upshift of the bait proteins. The authors suggest further that the mono ubiquitination near the catalytic center prevents UCHL1 from binding to other ubiquitinated substrates. This, and the fact that the interaction of other proteins

## Results

with UCHL1 was not stable enough to isolate them as a complex, could explain why no other bands were visible on the gel.

### 3.3 Structural improvement of GK13S towards selective UCHL1 probes

In an effort to characterize the in-family specificity of GK13S an *in vitro* DUB screen was carried out. **GK13S** was screened against 55 purified DUBs, including representatives of all families except the ZUP1s (Fig. 24).<sup>[184]</sup> The screen revealed reduced activity of UCHL1 of over 90 % after the incubation with the probe. However, treatment with the probe also resulted in a >70 % decrease in activity of the DUBs USP9X/Y, USP30, USP45, and JOSD2. All of these DUBs are cysteine proteases, which makes a covalent modification of the catalytic cysteine of these enzymes by **GK13S** likely. Chemical variation of the warhead of **GK13S** was a promising starting point to optimize the probe for increased target specificity within the DUB family towards UCHL1. Furthermore, efforts in the chemical variation of the warhead structure should result in the discrimination of the most potent off-target PARK7.

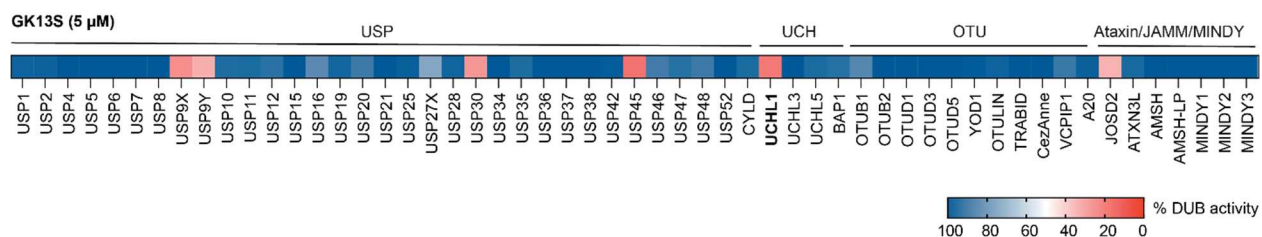


**Fig. 24 | Screening of GK13S against 55 purified DUBs.** *In vitro* DUB screening to determine the in-family specificity of the probe GK13S. Incubation of 55 purified DUBs from various families with GK13S at 5  $\mu$ M, revealed the modification of five other DUBs besides UCHL1. The remaining DUB activity is highlighted with a color gradient ranging from dark blue (full activity, no inhibition) to dark red (no activity, full inhibition). The screen was carried out as a paid service at the MRC protein phosphorylation and ubiquitylation unit at the University of Dundee.

#### 3.3.1 N-cyanopyrrolidines with more complex decorations

The crystal structure of UCHL1 in co-complex with **GK13S** (Fig. 18) showed that there was additional space available where the warhead interacts with the protein that **GK13S** does not structurally occupy. More complex decorations on the five-membered ring of the cyanopyrrolidine should occupy this extra space in the catalytic pocket of UCHL1 and lead to discrimination of binding to other DUBs as well as PARK7 (Fig. 25). These decorations included modifications with a methoxyethyl- (**CG287**) and a methoxymethyl (**CG385**) group in the 5 and 4

## Results

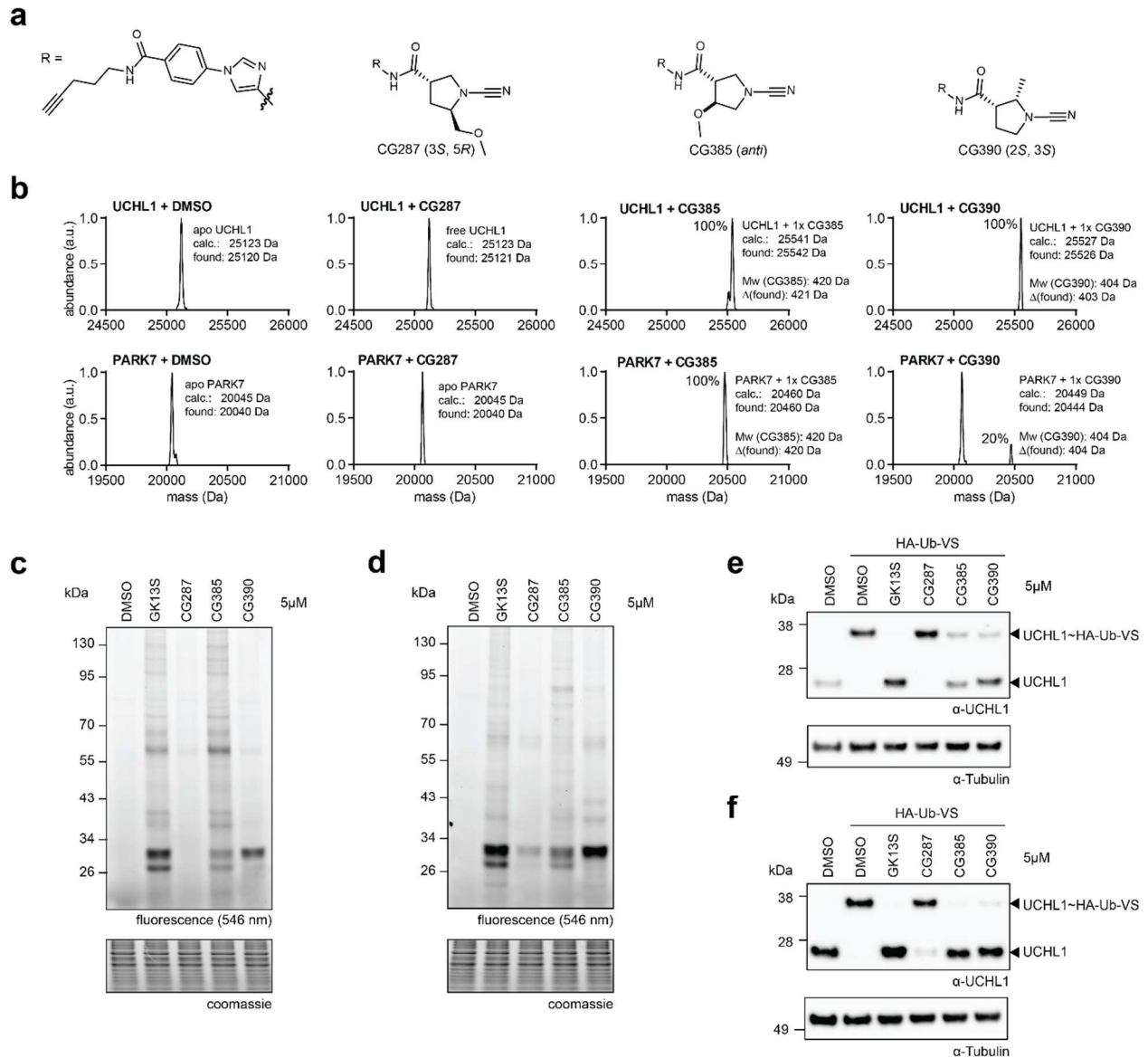


**Fig. 25 | Characterization of modified N-cyanopyrrolidine warheads.** **a**) Molecular structures of the probes CG287, CG385 and CG390. The recognition element was kept from GK13S, but the 5-membered ring of the warhead was further modified with more complex decorations to target an additional space in the catalytic pocket of UCHL1. **b**) Modification of purified UCHL1 and PARK7 with indicated compounds measured by intact protein mass. Covalent binding to UCHL1 or PARK7 results in a mass shift corresponding to the mass of the used compounds. All spectra were recorded and analyzed by Dr. Christian Grethe. **c, d**) Activity-based protein profiling with the indicated compounds to visualize their target spectrum in either cell lysates (**c**) or intact HEK293 cells (**d**) via InGel fluorescence. **e, f**) Covalent modification of UCHL1 by the indicated compounds in either cell lysates (**e**) or HEK293 cells was verified via a target engagement assay. Cell lysates or intact cells were first treated with the compounds and then with a HA-Ub-VS probe. Binding of the Ub-probe resulted in an upshift of the protein band in the gel, if the small molecule compound did not occupy the Ub binding site during the first incubation step.

## Results

positions on the pyrrolidine ring. Modification with a methyl group in the 2 position further resulted in the diastereomer **CG390** (Fig. 25 A). All molecules displayed under section 3.8 were synthesized by Dr. Christian Grethe and a detailed chemical analysis can be found elsewhere.<sup>[154]</sup> The core recognition element of **GK13S** was not changed further, since the possible interactions with the binding pocket of UCHL1 were well covered by the current structure and further interactions in this area, which would lead to enhanced specificity, were not to be expected by a chemical variation of the core element of the probe.

Intact protein mass spectrometry was used to test whether the new cyanopyrrolidines were still able to covalently modify UCHL1. In addition, purified PARK7 was used to determine if a variation of the warhead structure could result in reduced binding to the off-target (Fig. 25 B). Incubation with the diastereomer **CG287** showed no binding, neither to UCHL1 nor to PARK7, verifying that the proteins did not tolerate decorations in the 4-position of the cyanopyrrolidine. In contrast, treatment with **CG385**, bearing a methoxymethyl group in 5-position, resulted in complete modification of both proteins, proving that decorations at the 5-position are generally tolerated, but do not lead to the discrimination of PARK7 binding. Only **CG390** showed total modification of UCHL1, but a reduced binding of the purified PARK7. This confirmed that a chemical optimization of the warhead structure could result in a probe with enhanced specificity towards UCHL1.

To corroborate this finding in a cellular setting, intact HEK293 cells and lysates thereof were treated with the compounds. After the treatment, the alkyne handle of the probes was used to install the rhodamine fluorophore to visualize the covalently modified proteins (Fig. 25 C, D). As expected, no fluorescence bands were visible on the height of UCHL1 and PARK7 for cell lysate samples that were incubated with **CG287**. Faint bands were observable that prove minimal modification of UCHL1 and PARK7 in HEK293 cells. Treatment of lysates as well as intact cells with **CG385** results in a similar target spectrum to that of **GK13S**. However, the higher fluorescence background and the fainter bands between 26 – 34 kDa, for the sample incubated with **CG385**, indicated that the warhead of this probe was more reactive against various off-targets but less reactive against the major targets (UCHL1, PARK7) of **GK13S**. Incubation with **CG390** showed sufficient binding of UCHL1 but less intense fluorescence compared to **GK13S**. Nevertheless, only a faint band corresponding to PARK7 was observable in lysate-treated and intact cell treated samples. The degree of covalent modification of UCHL1 by the probes in cellular systems was tested by a target engagement assay using a HA-Ub-VS as a suicide probe (Fig. 25 E, F). The data is consistent with what was observed for the intact protein mass experiments. In cell lysates, **CG287** is outcompeted by the Ub-probe completely and by treating intact cells, only

## Results

a fragile band was visible. **CG385** and **CG390** showed proper modification of UCHL1 in intact HEK293 cells. A faint upshifted band is observable where cells were incubated with **CG390**, corresponding to not completely modified UCHL1 after 24 h of incubation. Cell lysate-treated samples showed more prominent bands of compound unmodified UCHL1 in samples treated with **CG385** and **CG390**, whereas **GK13S** showed complete modification in cell lysates after 4 h of incubation. This highlights that decorations on the cyanopyrrolidine ring led to slower binding kinetics towards UCHL1.

Taken together, the probe **CG390**, bearing a methyl group in 2 position of the cyanopyrrolidine, confirmed that chemical variations of the warhead were utilized to reduce the binding to off-targets *in vitro* and in a cellular setting. However, the probe was still binding to PARK7 to some extent and reacted much slower with UCHL1 than **GK13S**.

### 3.3.2 Warhead optimization led to N-cyanopiperazine probes with enhanced specificity

Another approach to tackle the structural optimization to occupy additional space in the UCHL1 binding pocket to improve probe specificity was to expand the warhead's ring size. Synthetic efforts yielded the molecules **CG305** and **CG322**, featuring the **GK13S** recognition element but consisting of 6-membered N-cyanopiperidine warheads (Fig. 26 A). **CG305** represents the *S*-isomer and the cyanopiperidine at **CG322** was installed in *R*-configuration to test whether the same stereo preference for UCHL1 also applies after a ring expansion of the warhead. Both molecules were tested for the covalent modification of purified UCHL1 via intact protein mass spectrometry (Fig 26 B). Incubation with the *S*-isomer **CG305** showed almost complete (83 %) modification of expressed UCHL1, whereas no binding to UCHL1 was verified with the *R*-isomer **CG322**. This proves that the stereo preference of the *S*-isomer over the *R*-isomer was intact, even though the ring system of the warhead was expanded. Nevertheless, **CG305** was losing potency to UCHL1 compared to the lead probe **GK13S**. Interestingly, using cyanopiperidines as warhead structures resulted in the discrimination of PARK7 as an off-target.

Motivated by this finding, a series of 6-membered warheads with different heteroatoms and decorations on the ring system was synthesized (Fig. 26 C). This yielded the probes **CG337**, bearing a cyanomorpholine as a warhead and **CG341**, **CG306**, and **CG386**, which feature cyanopiperazines with different modifications as their electrophilic binding element. Since the clear preference for the *S*-configuration was already established, only this isomer of each probe

## Results

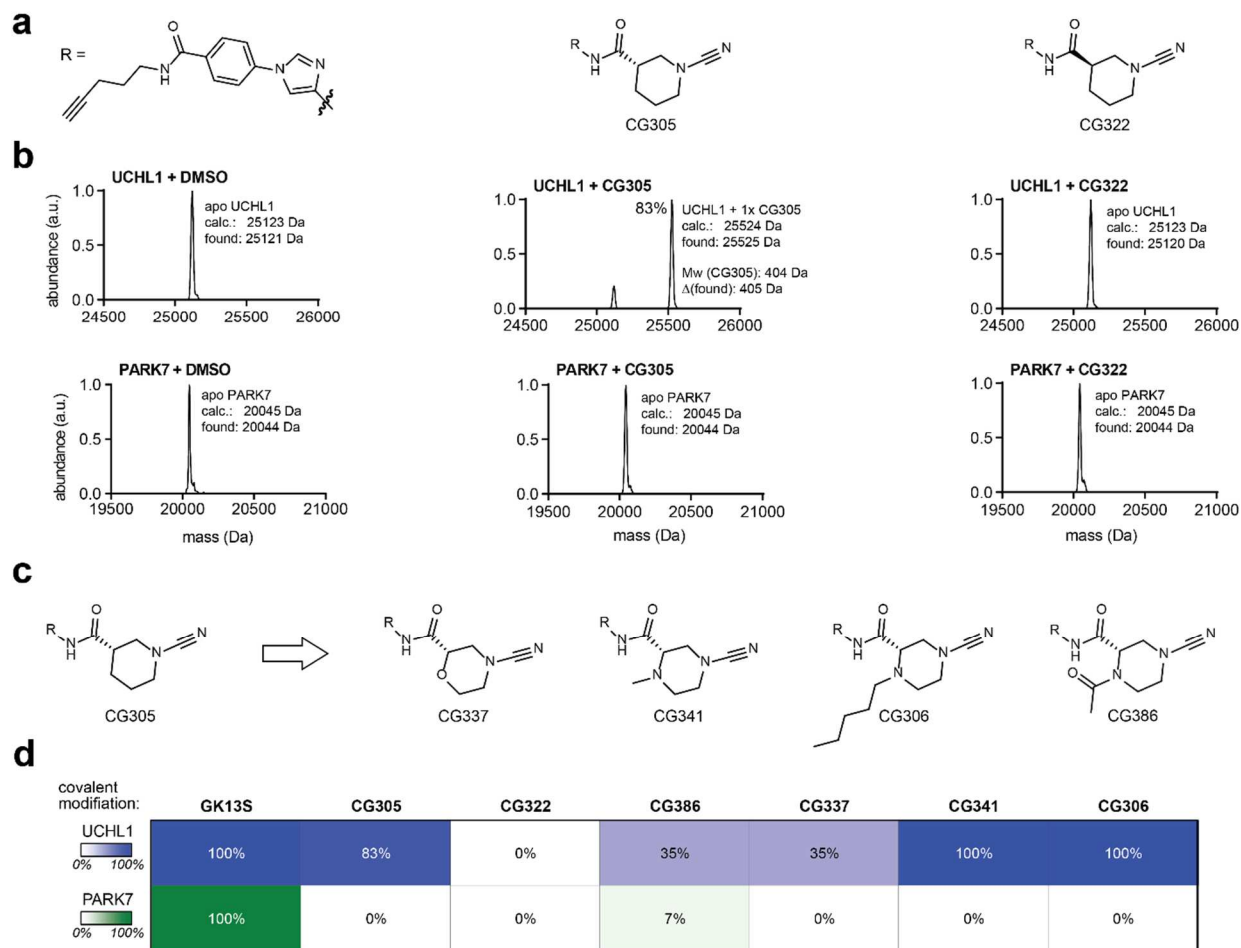


**Fig. 26 | 6-membered warhead structures discriminate PARK7 as an off-target.** **a)** Molecular structures of the recognition element based on GK13S (left), and the cyanopiperidine precursor warheads in *S*-configuration (middle) and in *R*-configuration (right). **b)** Intact protein mass spectra verify binding of indicated probes to purified UCHL1 and PARK7. All spectra were recorded by Dr. Christian Grethe. **c)** Series of further modified 6-membered warheads. Molecular are ordered by increasing complexity. **d)** Summary of covalent modification of UCHL1 or PARK7 with indicated probes in %. Modification is by a color gradient ranging from white (no modification) to dark blue (complete modification of UCHL1) or dark green (complete inhibition of PARK7).

was synthesized and biologically characterized. First, for covalent binding to purified UCHL1 and PARK7 via intact protein mass spectrometry (Fig. 26 D, Supplementary Fig. 10). All of the tested 6-membered warheads showed no binding to PARK7. This established the use of 6-membered cyano warheads as a general probe feature to discriminate the binding to PARK7. Using the cyanomorpholine, and the acylated form of the cyanopiperazine as a warhead results in drastic loss of covalent modification of UCHL1. Probes were the secondary nitrogen of the cyanopiperazine was alkylated, however, demonstrated complete modification of UCHL1.



## Results

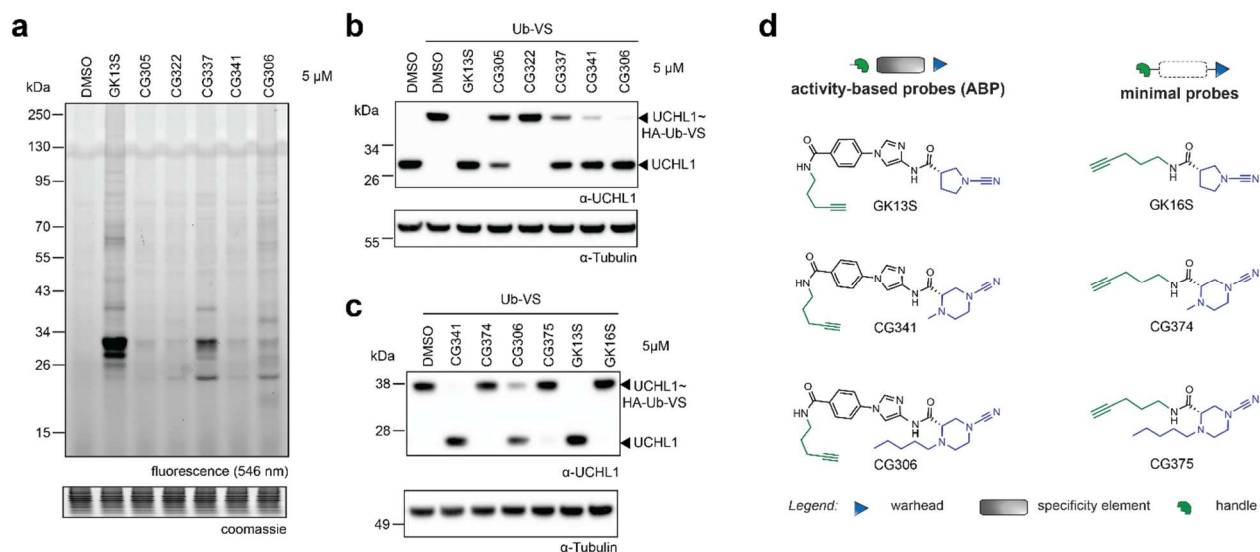


**Fig. 27 | Cellular characterization of 6-membered warhead probes.** **a)** Read out of the in-gel fluorescence after treatment of HEK293 cells with either the indicated compounds (5  $\mu$ M) or DMSO. **b, c)** Target engagement of the 6-membered warhead probes in intact HEK293 cells was investigated via western blot analysis of endogenous UCHL1. Cells were first treated with either the indicated compounds (5  $\mu$ M) or DMSO and after lysis, with an Ub-suicide probe (1  $\mu$ M). **c)** Target engagement of selected cyanopiperazine probes and their corresponding minimal probes in HEK293 cell lysates was visualized via western blot analysis of endogenous UCHL1. **d)** Molecular structures of GK13S, the selected cyanopiperazine probes CG341 and CG306 (left panel) and their corresponding minimal probes (right panel).

Next, to test whether this binding behavior is also stable in a cellular setting, HEK293 cells were incubated with various 6-membered warhead probes at different concentrations (Fig. 27 and Supplementary Data 11). Only probes that did not bind to PARK7 in the previous experiment were selected for this advanced testing. Surprisingly, treatment with the 6-membered warhead probes at a concentration of 5  $\mu$ M and subsequent attachment of the fluorophore reporter via CuAAC resulted in a very poor overall fluorescence intensity compared to the proteome that was treated with **GK13S** (Fig. 27 A). No clear band is recognizable at the height of PARK7 for any of the 6-membered warhead probes. However, only a fragile band was visible on the height of UCHL1, whereas **CG337**, followed by **CG306**, showed the most labeling of the DUB based on fluorescence intensity among all 6-membered warhead probes tested. A similar result is visible when treating the cells with 1  $\mu$ M of each compound (Supplementary Fig. 11 A). The target engagement in HEK293 cells confirmed comparable binding behavior, as observed with the intact protein mass spectrometry (Fig. 26 D). The *in vitro* inactive probe **CG322**, equipped with a cyanopiperidine in the *R*-configuration, also showed no modification of UCHL1 in a cellular setting. Treatment with the corresponding *S*-isomer confirmed more than 50 % covalent modification but no complete inhibition of the available UCHL1. As observed earlier, the cyanomorpholine probe **CG337** revealed less than 50 % covalent modification of the endogenous UCHL1 in HEK293

## Results

cells. Only using the cyanopiperazine probes **CG341** and **CG306** resulted in sufficient covalent modification of endogenous UCHL1 in a living environment. Even though only **CG306** proved complete modification, comparable to the lead probe **GK13S** (Fig. 27B). **CG306** is decorated with a longer N-alkyl chain on the piperazine, resulting in an improved membrane permeability compared to **CG341**, which could explain this different binding behavior. This hypothesis was further corroborated when HEK293 cell lysates were treated with **CG341** and **CG306** (Fig. 27 C). In cell lysates, an enhanced modification of UCHL1 is observed with **CG341** likely due to its higher hydrophilicity and increased water solubility than **CG306**. Similar trends were evident when cells were treated with the identical probes at a concentration of 1  $\mu$ M (Supplementary Fig. 11 B, C). Due to its *in vitro* and cellular binding profile, only the cyanopiperazine probes **CG341** and **CG306** were chosen for further characterization. To further adapt the approach of the chemogenomic pair of probes, successfully established with **GK13S** and **GK16S**, the corresponding minimal probes of **CG341** and **CG306** were synthesized and tested in HEK293 cell lysates (Fig. 27 C, D). As expected, the 6-membered electrophilic cyanopiperazine warhead alone was insufficient to covalently modify the catalytic cysteine of UCHL1.

Collectively, the *N*-cyanopiperazine probes **CG341** and **CG306** show the complete covalent modification of UCHL1 *in vitro* and in intact HEK293 cells but do not bind to PARK7. However, the *in-gel* fluorescence is drastically reduced compared to samples treated with **GK13S**, even though the compounds fully modify UCHL1. In addition, the minimal probes **CG374** and **CG375** were tested in a cellular setting to use them together with **CG341** and **CG306** as pairs of chemogenomic probes.

### 3.3.3 Copper-catalyzed cycloaddition reverses covalent modification with **CG341** and **CG306**

The fluorescence readout after the cellular treatment with **CG306** and **CG341** resulted in a weak intensity compared to **GK13S** (Fig. 27 A). However, the target engagement suggested full labeling of UCHL1 with the probes (Fig. 27 B, C). Therefore, further experiments were carried out to clarify this dichotomy (Fig. 28). Cells were treated with the compounds and lysed to confirm that the probes were stable under lysis conditions. The covalent modification of endogenous UCHL1 in the lysis buffer was monitored by incubating with an Ub-VS probe at different time points (Fig. 28 A). If the probes presented a covalent reversible binding behavior, the Ub-probe could occupy the binding pocket, resulting in an upshift of the UCHL1 band on the western blot. All tested probes

## Results

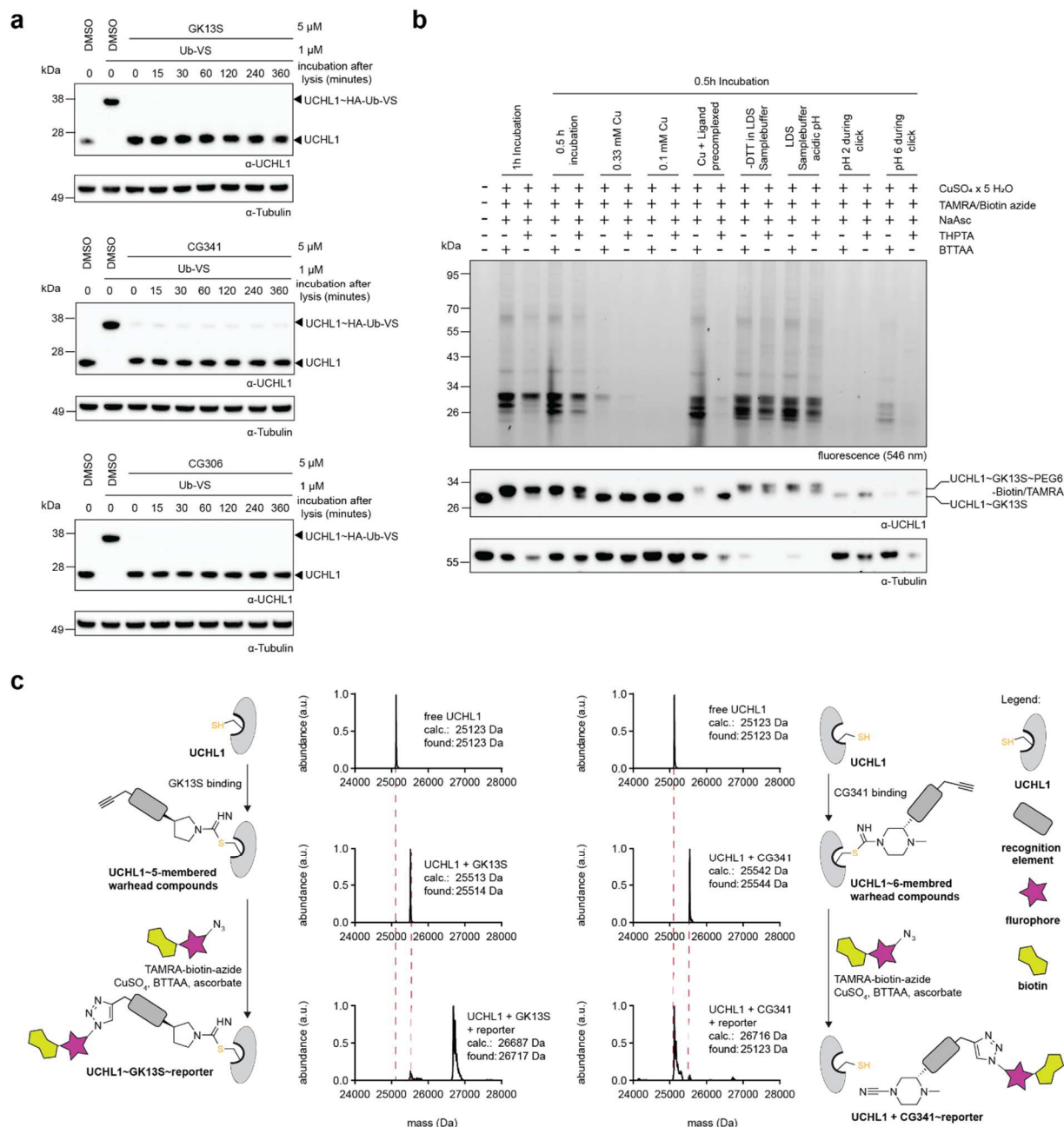


**Fig. 28 | Characterization of covalent reversible behavior of CG306 and CG341. a)** Binding stability of indicated probes after cell lysis. HEK293 cells were treated with GK13S, CG341 and CG306. The cells were lysed and incubated on ice. A sample was taken at different time points and incubated with a Ub-VS probe. A stability readout was done by western blot analysis against UCHL1. **b)** Screening of various conditions to improve the copper-catalyzed cycloaddition in complex proteomes with GK13S as a model compound. **c)** Schematic illustration of the binding behavior of 5-membered warhead probes (left) and 6-membered warhead probes (right), upon initially binding to UCHL1 and after the CuAAC. Intact protein mass spectra (middle panel) of free UCHL1 after covalent binding of the respective probe and after the incubation with reagents for the copper-catalyzed cycloaddition.

## Results

were stable for up to six hours (a timeframe in which experiments were carried out, and lysates never stored longer) in the lysis buffer, irreversibly modifying endogenous UCHL1.

Next, the reversible character of **CG341** and **CG306** in a CuAAC background was investigated. Different conditions for the CuAAC were screened with **GK13S** as a model compound to establish optimized parameters for improved UCHL1 fluorescence intensity (Fig. 28 B). Besides band intensity, the small upshift, triggered by the attachment of the large reporter group (approx. 1.2 kDa) of UCHL1 during western blot analysis, was used to verify click efficiency. Overall, 30 – 60 minutes incubation with the CuAAC reagents was sufficient to completely convert compound bound UCHL1 into the reporter labelled species. Using Tris((1-hydroxy-propyl-1H-1,2,3-triazol-4-yl)methyl)amine (THPTA) results in less intense fluorescence intensity, compared to using BTTAA as the ligand. Whereas using a premixture of all reagents in combination with THPTA results in no labeling. Decreasing the copper concentration results in a drastic loss of the fluorescence signal. The same outcome was observed if the environment during the CuAAC was acidified (pH 2 – 6). Incubation time of 1 hour and final concentrations of 1 mM CuSO<sub>4</sub>, 12.5 μM azide-reporter, 5 mM BTTAA and 15 mM sodium ascorbate as a reducing agent resulted in complete labeling of endogenous UCHL1, using **GK13S** as the alkyne source.

Although the CuAAC efficiency for **GK13S** was increased, the optimized conditions resulted in low in-gel fluorescence intensity when samples were incubated with **CG341** and **CG306**. Therefore, the CuAAC for 5-membered warhead and for 6-membered warhead probes was monitored via intact protein mass spectrometry (Fig. 28 C). The modification of purified UCHL1 with both probe classes was completely established after one hour of incubation. However, the compound bound UCHL1 was only converted to the reporter labeled species when covalently modified with the 5-membered cyanopyrrolidine probe but not with the 6-membered cyanopiperazine probe. Once incubated with the CuAAC reagents, the modification with **CG341** was reversed, resulting in free UCHL1 with an intact thiol in the catalytic center and the free probe modified with the TAMRA/biotin reporter group (Supplementary Fig. 12). This proves that a linkage of **CG341** with the reporter group within the CuAAC was possible. However, this species was not stable under the present conditions. The influence of the individual reagents as well as other parameters such as the unfolding of UCHL1 were investigated in further experiments (Fig. 29). Both **GK13S** and **CG341** were incubated with purified UCHL1 and then either diluted in a 6 M guanidinium hydrochloride buffer or heated for 20 minutes at 95 °C. Both conditions favor the unfolding of the protein (Fig. 29 A). Interestingly, after unfolding of UCHL1, with guanidinium hydrochloride, the modification with **GK13S** was stable whereas the binding of **CG341** was

## Results

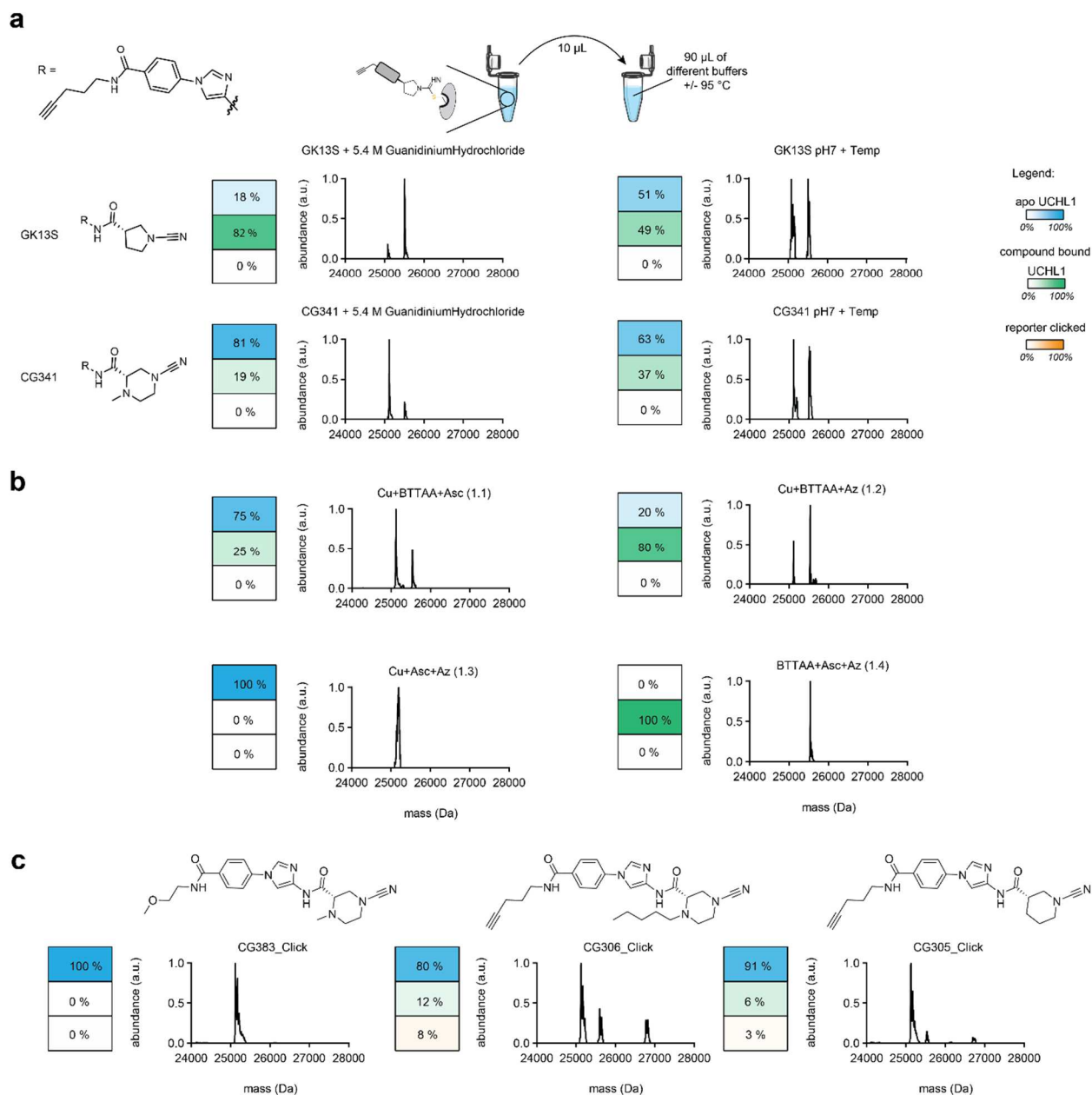


**Fig. 29 | Copper ions reverse modification with CG341. a)** Intact protein mass spectrometry was used to determine the causes of the dissociation of CG341 during CuAAC. GK13S and CG341 were incubated with purified UCHL1, then diluted in 6 M guanidinium hydrochloride, or boiled for 20 minutes. The resulting spectra prove the loss of modification with CG341 after unfolding of UCHL1. **b)** The influence of the individual reagents used in the CuAAC was analyzed. Spectra highlight that exposition of UCHL1 to copper ions results in the dissociation of CG341 **c)** Intact protein mass spectrometry proves that loss of the modification with 6-membered warhead probes is a general feature of this class of compounds when used in the CuAAC.

drastically reduced. The effect of heat caused the dissociation of both probes equally. Investigation of the individual reagents used in the CuAAC revealed that the modification of UCHL1 with **CG341** was reversed as soon as the DUB-probe complex was exposed to copper

## Results

ions (Fig. 29 B, spectra 1.1 – 1.3). The binding was further disrupted in the presence of sodium ascorbate, which reduces the copper (II) to copper (I) ions (spectrum 1.2). If no copper was used, the modification with the probe was stable in the presence of all other reagents (spectrum 1.4). Different molecules were tested for their CuAAC efficiency to confirm that the probe modification of UCHL1 was reversed upon unfolding also when other 6-membered warhead compounds were used (Fig. 29 C). In addition, **CG383**, the non-alkyne derivative of **CG341**, was tested to determine the influence of the triazole formed in the CuAAC on the dissociation of the probe. The dissociation of **CG385** from UCHL1 upon exposure to the CuAAC reagents proves that the forming triazole is not influencing the loss of the modification. Loss of modification was also observed for the molecules **CG306** and the N-cyanopiperidine **CG305**, proving that the dissociation is not specific for one probe but instead a general weakness of 6-membered warhead probes.

Collectively, biochemical analysis of **CG306** and **CG341** confirmed a stable modification of UCHL1 for up to six hours after cell lysis. However, the unfolding of UCHL1, either by copper ions or guanidinium hydrochloride, promotes the dissociation of the probes. This is not only the case for **CG341** and **CG306** but appeared to be a general characteristic of the 6-membered warhead probes. In contrast, the treatment with the 5-membered probe **GK13S** resulted in a stable modification even upon unfolding of UCHL1.

### 3.3.4 N-cyanopiperazine probes usable for the specific investigation of UCHL1

To carry out a small molecule target competition assay, for the further characterization of **CG306** and **CG341**, non-alkyne derivatives (**CG382** and **CG383**, respectively) were used (Fig. 30 A). Those probes were used for a cellular competition assay, which was independent of the fluorescence intensity of the 6-membered warhead probes (Fig. 30 B). Intact HEK293 cells were treated first with the non-alkyne version of **GK13S**, **GK16S**, **CG341** and **CG306**, followed by a second incubation of all cell samples with the probe **GK13S**. Evaluation after cell lysis and CuAAC led to fluorescently labeled proteins through modification of **GK13S**, only where the non-alkyne derivatives did not inhibit a binding. **CG118**, the non-alkyne derivative of **GK13S**, was expected to bind to UCHL1 and PARK7 among other proteins, resulting in reduced fluorescence intensity after the treatment with **GK13S**. In contrast, **CG382** and **CG383** were supposed to bind only to UCHL1, but not PARK7. **CG370S**, the non-alkyne derivative of the minimal probe **GK16S**, was used as a control for the complete modification of PARK7. Even though the fluorescence intensity for UCHL1 was drastically reduced when preincubating cells with **CG118**, **CG382** and **CG383**, the fluorescence band of PARK7 was still clearly visible.

## Results

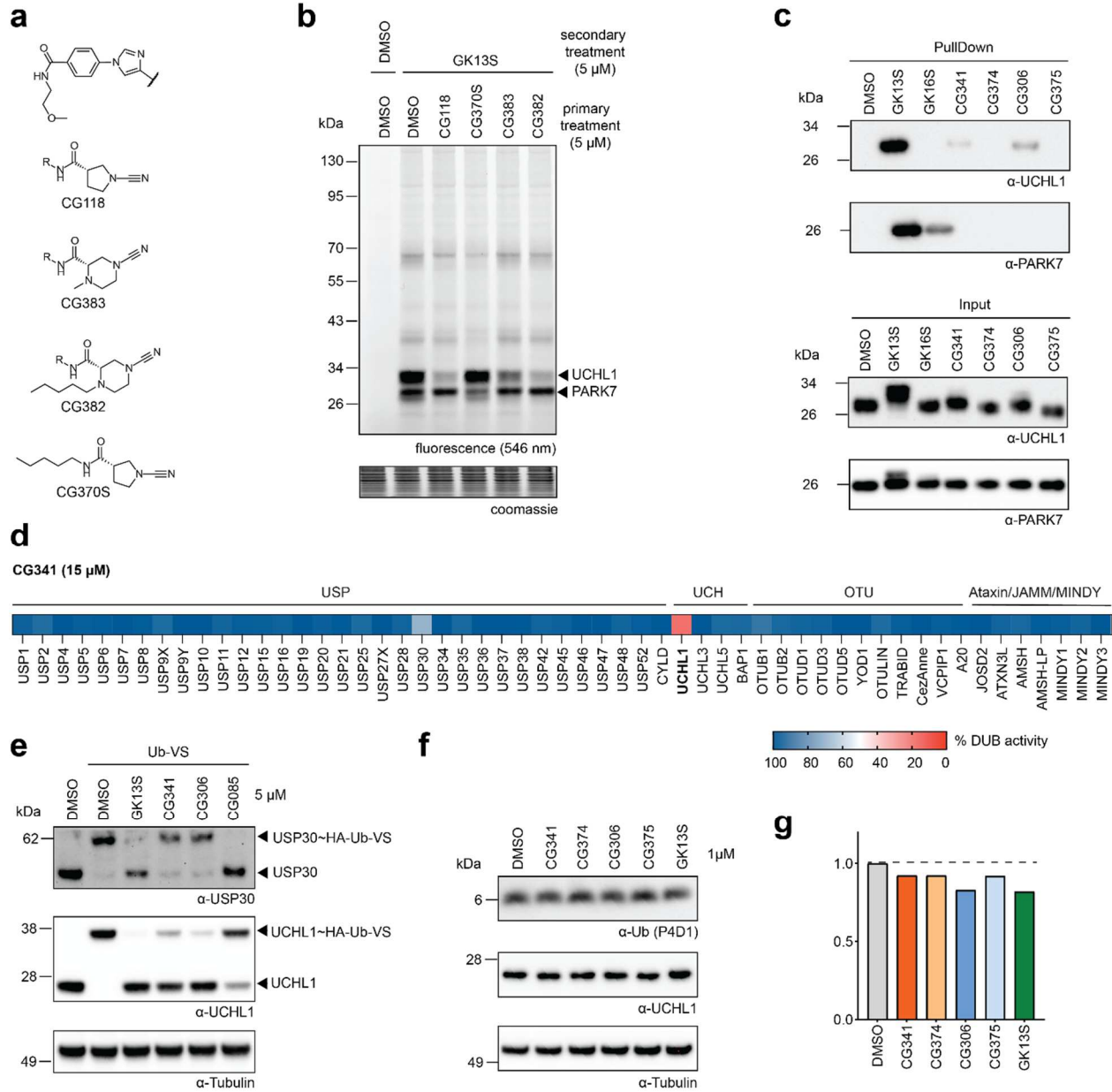


**Fig. 30 | CG341 and GC306 are specific probes for the study of UCHL1 in a cellular context. a)** Molecular structures of non-alkyne derivatives CG118, CG383, CG382 and CG370S. **b)** Cellular small molecule competition assay. Intact HEK293 cells were pretreated with the indicated non-alkyne versions of established small molecule probes, followed by a treatment of the same cells with GK13S. Fluorescence readout revealed which proteins GK13S could modify and which binding sites were occupied by the non-alkyne derivatives. **c)** Gel-based pull-down with the indicated probes and subsequent western blot analysis of pull-downed proteins. **d)** *In vitro* DUB screening with the N-cyanopiperazine probe CG341 reveals in-family specificity for covalent modification of UCHL1. The screen was carried out as a paid service at the MRC protein phosphorylation and ubiquitylation unit at the University of Dundee. **e)** Cellular target engagement assay proves covalent binding of CG341 and CG306 to UCHL1 but not USP30 in a complex proteome. **f)** Treatment of human glioblastoma cells with CG341, CG306, GK13S and the respective minimal probes

## Results

to induce UCHL1-dependent reduction of the mono-Ub pool. **g)** Quantification of mono-Ub band intensity of western blots shown in f).

This may be because the potency of **CG118** was not sufficient to fully modify cellular PARK7. Thus, the remaining protein was labeled by **GK13S**. Only **CG370S** potentially modified PARK7, which led to decreased fluorescence intensity after the labeling with **GK13S**. Comparing the pretreatment with **CG382** and **CG383**, the intensity of the UCHL1 band decreased where the non-alkyne derivative of **CG306** was used. This corroborates the enhanced potency of **CG306** over **CG341** in living cells. The prominent bands below UCHL1 proved the discrimination of **CG341** and **CG306** for PARK7 binding. Since it was not excluded that the cyanopiperazine probes also modify a small proportion of cellular PARK7, a gel-based pull-down was performed (Fig. 30 C). Western blot analysis of the corresponding pull-down fractions confirmed that only UCHL1 was isolated, but not PARK7, when **CG341** and **CG306** were used. The promising specificity profile of the cyanopiperazine probes led to a second DUB selectivity screening with **CG341** (Fig. 30 D). At a concentration of 15  $\mu\text{M}$ , UCHL1 was the only DUB sufficiently (>90 %) inhibited by the probe. This confirmed that variation of the warhead structure could result in a small molecule probe with in-family specificity, even though the compound was bound to the ubiquitin-binding site of a DUB. The screen showed that USP30 was weakly bound by the probe (approx. < 40 % inhibition, second most binding within the DUB family).

To confirm in-family specificity of **CG341** and **CG306** in a cellular setting, a target engagement assay against USP30 was carried out (Fig. 30 E). HEK293 cells were treated with the indicated probes, lysed and incubated with an Ub-VS probe. **CG085**, a confirmed USP30 inhibitor, was used as a control compound. The resulting western blot analysis proved that the *N*-cyanopiperazine probes discriminated USP30 binding but potentially modified UCHL1 in a living environment. *N*-cyanopyrrolidine **GK13S**, on the other hand, showed covalent modification of both USP30 and UCHL1. Next, the probes were applied to human glioblastoma cells to confirm the reduction of the free mono-Ub pool upon specific inhibition of UCHL1 (Fig. 30 F, G).

Treatment with the more cell-permeable cyanopiperazine probe **CG306** (compared to **CG341**), resulted in a similar reduction of free mono-Ub (approx. 20 % at 1  $\mu\text{M}$  compound concentration) as observable after the treatment with **GK13S** (in this assay, compare with 5  $\mu\text{M}$  treatment **GK13S** Fig. 20 D). Treatment with **CG341** resulted in reduction of approx. 10 % of the mono Ub-pool compared to the DMSO control. However, also the treatment with the corresponding minimal probes, which did not bound to UCHL1 (Fig. 27 C), showed a similar reduction of the mono Ub-pool. For this reason, and also because **CG341** does not show complete modification of UCHL1



## Results

in intact cells, the reduction of the free mono-Ub pool after treatment with **CG341** should be viewed critically. Nevertheless, this highlights the use of the small molecule probe **CG306** as an important tool for investigating endogenous UCHL1 in a cellular setting.

Taken together, the 6-membered warhead cyanopiperazine probes showed exquisite in-family specificity for UCHL1 in a dedicated DUB screen and discriminated the major off-target PARK7 that was potentially modified by the forerunner probe **GK13S**. The screen also suggested weak modification of USP30 by **CG306** and **CG341**, but this was not confirmed in a cellular target engagement assay. Furthermore, the probe **CG306** was used to inhibit UCHL1 in U-87 cells, which led to reduced mono-Ub levels similar to the treatment with **GK13S**. Many questions remain unanswered about the substrate spectrum and the mechanistic relationship between UCHL1 and the free mono-ubiquitin pool. However, the biochemically characterized probes **CG306**, **CG341** and **GK13S**, and their corresponding minimal probes, can be used in future experiments to make decisive contributions to answering these questions.

### 3.4 PROTAC tool compounds for the degradation of DUBs

PROTACs are bifunctional molecules that consists of a binder for the protein of interest and a recruiter for an E3-ligase connected by a linker. These molecules are used to induce the specific degradation of the protein of interest. The PROTACs designed to target DUBs, can be utilized as tool compounds to investigate phenotypes or general changes in global protein levels not only after the inhibition but after the induced degradation of the DUB of interest (Aim IV).

#### 3.4.1 Identification and synthesis of suitable USP7 binder for PROTAC generation

PROTAC development requires potent and selective binders to the protein of interest. Even though inhibitors are available that fulfill those criteria, it does not make them suitable molecules for PROTAC design. The compounds need to provide an exit vector for the attachment of the linker to connect the inhibitor to the E3-ligase binder. Furthermore, the exit vector should be solvent-exposed and the linker attachment should not interfere with the inhibitor's potency and selectivity.

In 2020, when this work was executed, mainly four USP7 inhibitors were published that provided the right potency and selectivity suitable for PROTAC design (Fig 31 A). Compound **41** was characterized with an excellent potency, but based on a complex synthesis strategy, it had no

## Results

obvious exit vector in its structure. The other three inhibitors all indicated a promising exit vector at the western end of the molecular structures. This was confirmed by the published structures of the inhibitors in co-complex with USP7, where the attachment sites for linkers were all solvent-exposed (Fig 31 B, C). The synthesis strategy for the inhibitor XL188 appeared most feasible as the quinazolinone core scaffold was the fastest to build up. Therefore, the inhibitor XL188 was chosen as a starting point for PROTAC development for the targeted degradation of USP7. The synthesis of the selected USP7 ligand starts with 4-nitro anthranillic acid, which reacts in a condensation reaction to yield the bicyclic nitroquinazolinone. Simultaneously, a boc-protected piperidone was used to generate a highly reactive epoxide, which is conjugated to the quinazolinone to obtain the centric scaffold of the ligand. The eastern part of the molecule is introduced by a chiral phenylbutanoic acid and coupled to the core scaffold via the secondary nitrogen of the piperidone. The (*R*)-stereoisomer is crucial for the inhibitors binding capacity since it appears to be 100-fold more potent than the (*S*)-stereoisomer.<sup>[103]</sup>

## Results

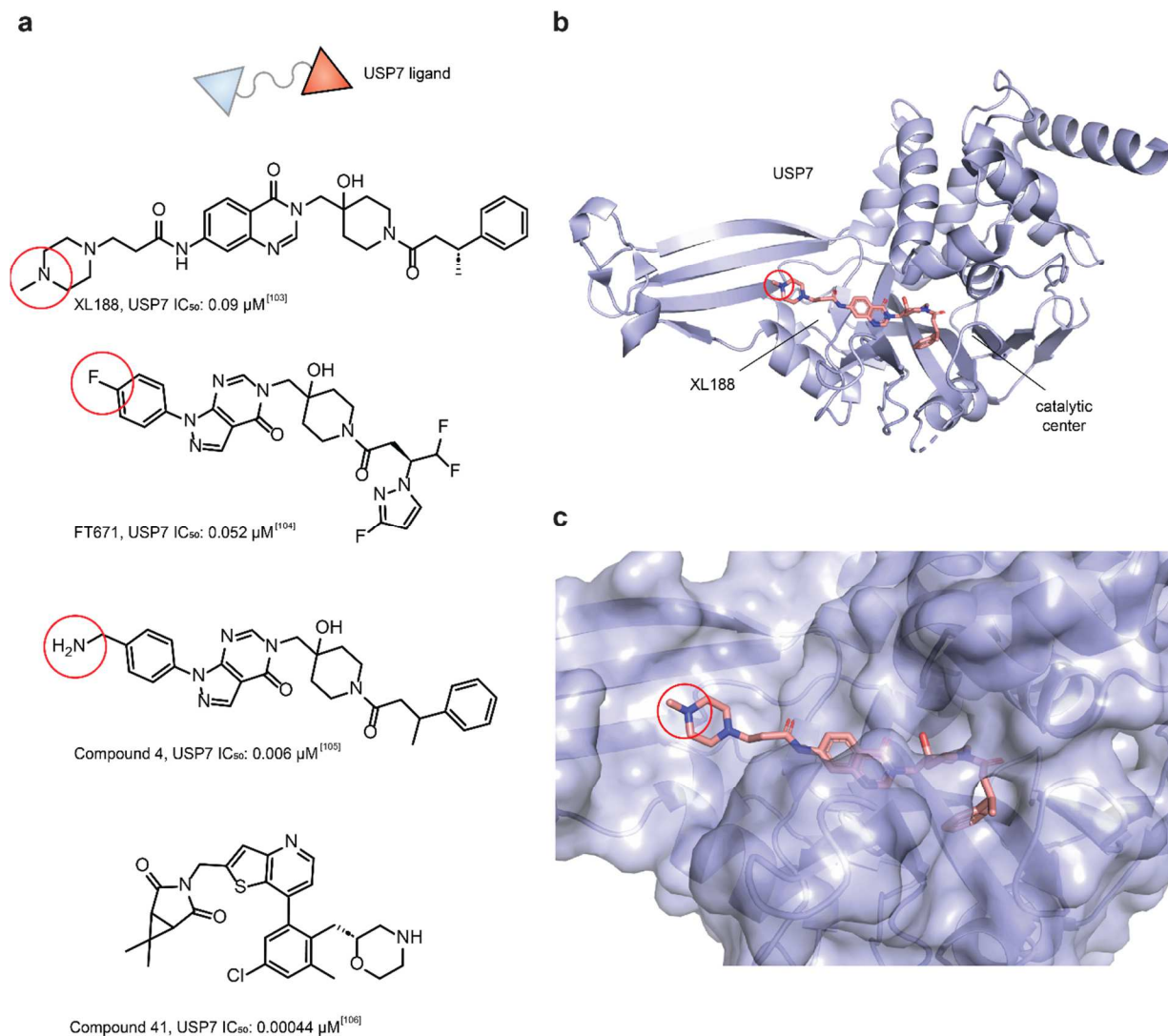
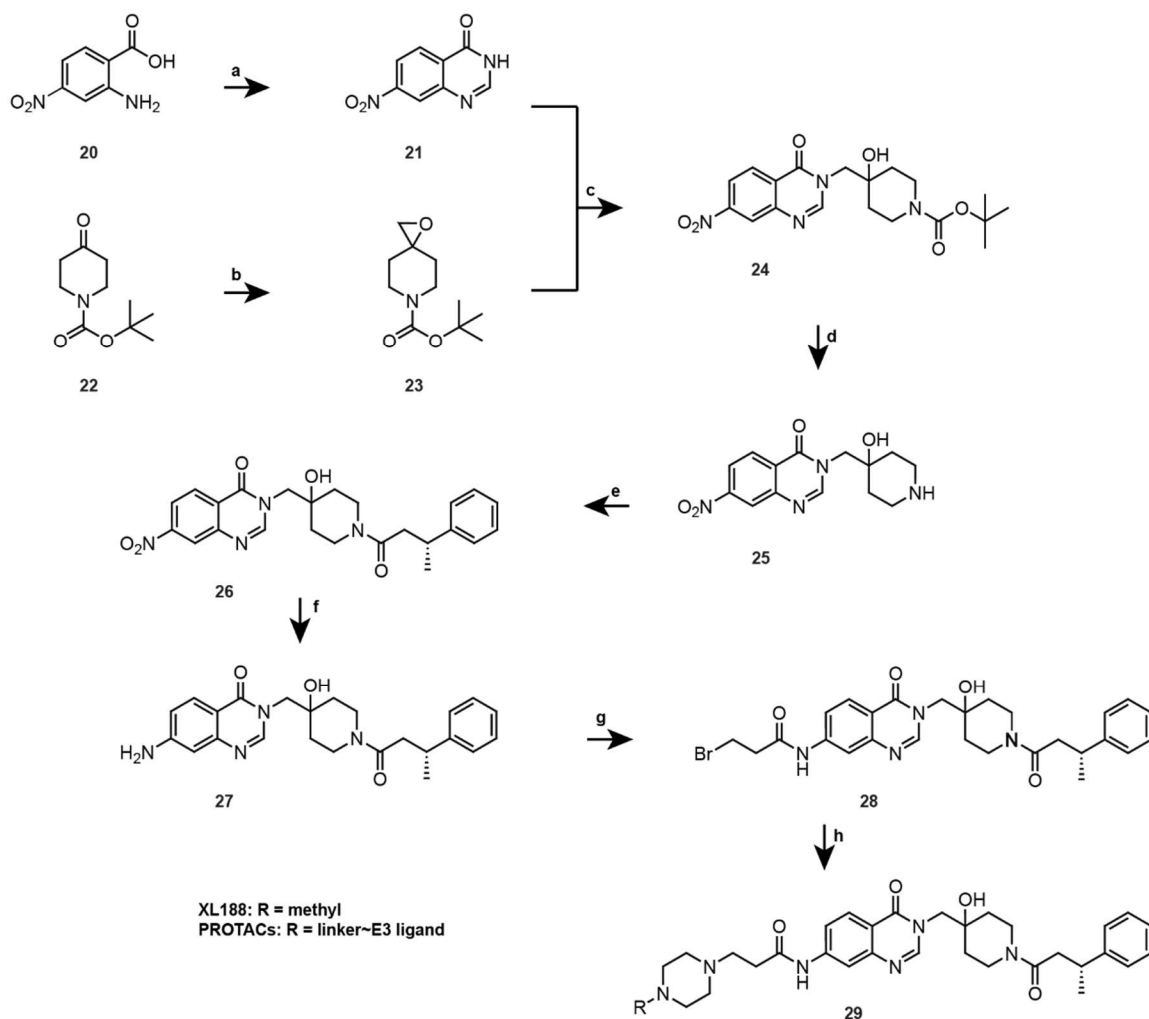


**Fig. 31 | Possible USP7 inhibitors for the development of PROTACs. a)** Molecular structures of published USP7 inhibitors suitable for PROTAC design. The red circle indicates solvent-exposed positions and was accessible for the chemical modification to install the linker. **b)** Overview of the crystal structure (PDB: 5VS6) of the inhibitor XL188 non-covalently bound to the catalytic center of USP7. **c)** Zoom in to the catalytic pocket occupied by XL188: the eastern part of the molecule is buried in the catalytic cleft, whereas the piperazine moiety is fully solvent exposed.

The nitro group of the quinazolinone was reduced to introduce the western part. The corresponding primary amine was conjugated with a short linker to introduce the piperazine. The original synthesis of XL188 involves the attachment of a methyl piperazine as a solubility group. For the design of the PROTAC, an N-Boc-protected piperazine was chosen, which could be further modified with the linker after deprotection (Scheme 11).

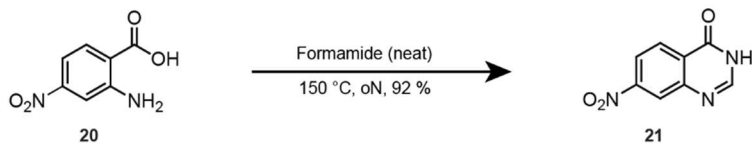
## Results



**Scheme 11 | Synthesis route of the USP7 binder XL188 and derivatives thereof for generating PROTACs.** a) Formamide b) NaH, TMSOI c) Cs<sub>2</sub>CO<sub>3</sub> d) 10 % TFA in DCM e) (*R*)-Phenylbutyric acid, HATU, Et<sub>3</sub>N f) Fe, HCl g) 3-Bromopropionyl chloride, Et<sub>3</sub>N h) methyl piperazine, Et<sub>3</sub>N

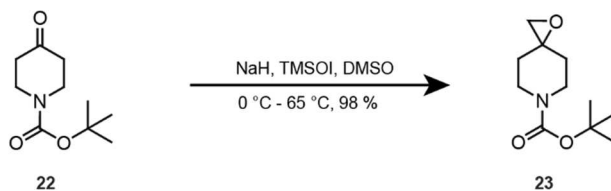
A Niementowski reaction prepared quinazolinone **21** from anthranilic acid **20** and formamide (Scheme 12). The first step of this cyclization involves the nucleophilic addition of the nitrogen of the anthranilic acid to the carbonyl group of the formamide. Relocation of electrons results in the release of ammoniac, which attacks the carbonyl group of the anthranilic acid. An endothermic reaction leads to the condensation of water and an amide bond was formed. Another nucleophilic attack of the amidic nitrogen on the opposing carbonyl group results in cyclization and the release of a second water molecule yields the quinazolinone **21**.

## Results



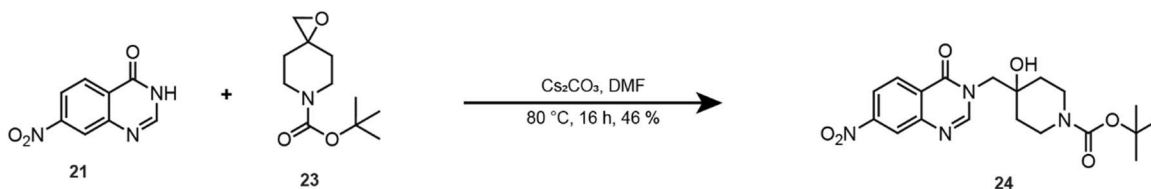
**Scheme 12 | Representation of 21.** A Niementowski condensation yields the quinazolinone **21** from nitroanthranilic acid **20** and formamide.

Simultaneously epoxide **22** was prepared in a Johnson-Corey-Chaykovsky reaction (Scheme 13). The dimethyloxosulfonium methylide is used as a methylene-transfer reagent and was generated by the reaction of trimethylsulfoxonium iodide (TMSOI) with sodium hydride, which abstracts a proton from the methyl group. The ylide reacts in a nucleophilic addition with the carbonyl group of the piperidone **22**. Because the sulfonium cation functions as a good nucleofuge, the negatively charged oxygen of the carbonyl group can attack the methyl group to yield the epoxide.



**Scheme 13 | Representation of 23.** The precursor epoxide **23** was prepared in a Johnson-Corey-Chaykovsky reaction.

The base-catalyzed ring opening of the epoxide enables the linkage of **21** and **23** (Scheme 14). Under basic conditions, the attack of the secondary nitrogen of **21** with the epoxide is shaped by steric repulsions. This favors the reaction with the less substituted C<sup>β</sup>-atom of the epoxide, following a S<sub>N</sub>2 mechanism.<sup>[185]</sup> The resulting alkoxide is subsequently protonated to form molecule **21**. The tertiary hydroxy group has a decisive influence on the potency of the inhibitor. It forms hydrogen bonds with the carboxylic group of Asp295 as well as the nitrogen of the peptide backbone of valine (Val) 296.

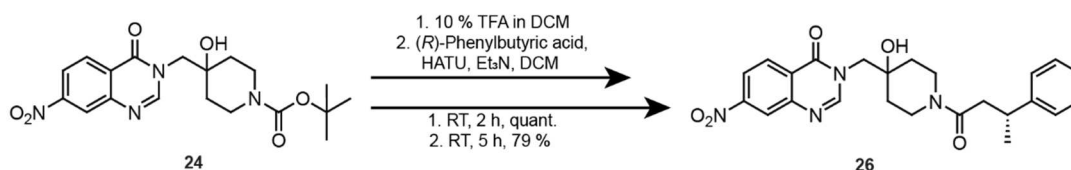


**Scheme 14 | Representation of 24.** The core scaffold **24** was generated via a base-catalyzed epoxide ring opening.

The reaction resulted in a yield of 46 %. Reactant **23** could have been contaminated by DMSO residues from the previous reaction, that were difficult to separate. This hypothesis was corroborated by the observation of unreacted **21** in the LC-spectrum.

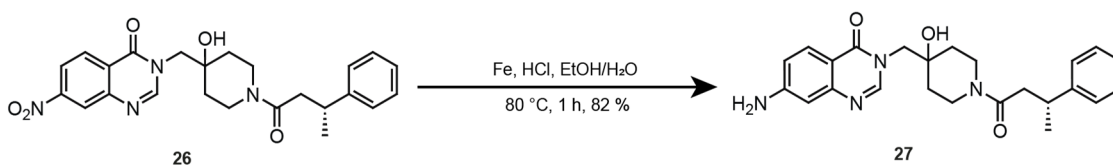
## Results

The piperidine was decarboxylated under acidic conditions to make the secondary nitrogen accessible for further modifications (Scheme 15). The eastern part of XL188 is composed of (*R*)-phenylbutyric acid, which points into the catalytic pocket of USP7 and is involved in various crucial interactions: The phenyl ring is stabilized by hydrophobic interactions with the aromatic systems of tyrosine (Tyr) 514, His456, Phe409 and the aliphatic chains of Lys420 and arginine (Arg) 408. The methyl group at C<sup>α</sup> to the phenyl ring is involved in multiple van der Waals interactions with the backbone of asparagine (Asn) 460, among others. In addition, the connection of the acid with the piperidine via an amide bond is important since the oxygen of the carbonyl group interacts with Tyr495 as a proton acceptor.<sup>[103]</sup> HATU was used as a coupling reagent to convert the acid into the activated uranium salt intermediate. This intermediate facilitates the nucleophilic attack of the nitrogen and collapses to release the amide **26** and a triazolopyridinol as a by-product.



**Scheme 15 | Representation of 26.** The eastern part of **XL188** was introduced via acetylation of piperidines secondary amine

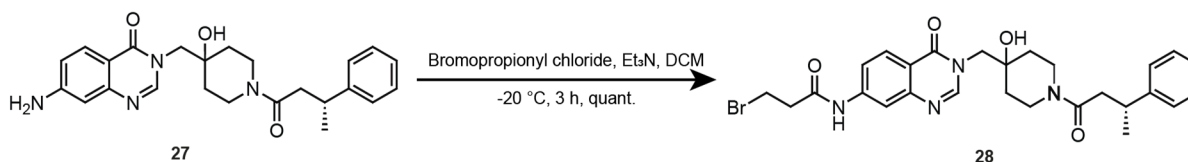
To prepare an aniline at the quinazolinone to attach the E3-binder/linker conjugate, the nitro group was converted via the Béchamp reduction (Scheme 16). Acid catalysis triggers the electron transfer from the iron to the nitro group of **26**, resulting in its protonation and the condensation of water. The so-formed nitroso group gets hydrated at the double bond, which condenses another water molecule. An electron transfer leads to the accumulation of a negative charge at the nitrogen. As a result, another proton was bound to form the primary amine **27**. Throughout this process, the iron scavenges several hydroxy ions, forming iron hydroxide. The hydroxide was released and recovered as water, leaving the iron as an iron oxide by-product. Also other reducing agents, such as palladium on charcoal and tin(II)chloride, were applied in test reactions. However, only the use of iron led to sufficient yields of the desired product.



**Scheme 16 | Representation of 27.** The nitro group of **26** is transferred to the corresponding primary amine **27** via a Béchamp reduction.

## Results

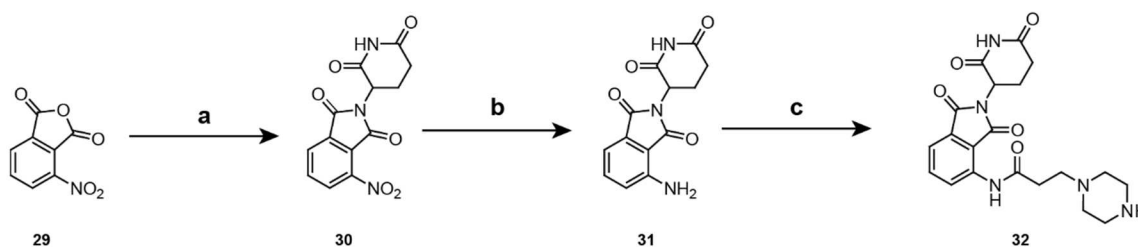
The solvent-exposed piperazine moiety was attached to the core scaffold **27** via a short propionyl linker. The linker was introduced as a highly reactive acyl chloride (Scheme 17). The base was used to activate the carbonyl group in a nucleophilic catalysis mechanism. The amine of the base attacks the carbonyl bond upon which a tetrahedral intermediate was formed. The displacement of the halide results in the formation of a quaternary acyl ammonium salt, which was more susceptible to react with the aniline of the core scaffold.<sup>[186]</sup> To prevent unwanted reactions with the alkyl bromide, the reaction was constantly kept at -20 °C.



**Scheme 17 | Representation of 28.** The alkyl bromide to further attach the E3-binder/linker conjugate was installed via an amide bond with the highly reactive bromopropionyl chloride.

### 3.4.2 Design and synthesis of PROTACs targeting USP7

To exploit the ubiquitination machinery, two recruiters for the E3-ligases CRBN and Von-Hippel-Lindau were used for PROTAC design. The synthetic strategy for the CRBN binder pomalidomide was adapted from the literature and the yield of all intermediates was in agreement with published procedures (Scheme 18).<sup>[187]</sup>



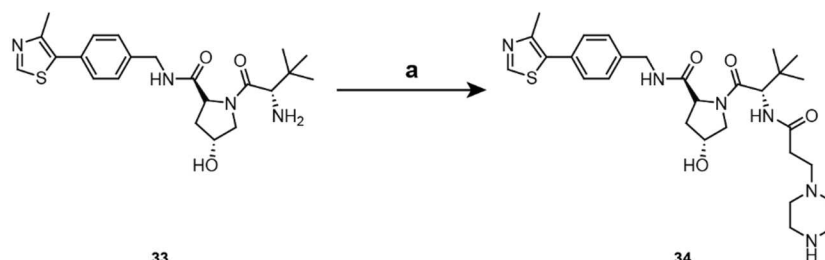
**Scheme 18 | Synthesis and functionalization of the CRBN binder.** **a**)  $\alpha$ -aminoglutarimide hydrochloride, NaOAc, HOAc, **b**) Pd/C, H<sub>2</sub> **c**) 1. 3-bromopropionyl chloride, DMAP; 2. Boc-piperazine, Et<sub>3</sub>N; 3. 20 % TFA in DCM

In brief, the synthesis of the piperazine functionalized pomalidomide **32** was started from a condensation reaction of the nitro phthalic anhydride **29** with alpha-aminoglutarimide to obtain **30**. Palladium on charcoal under a hydrogen atmosphere was used to reduce the nitro group of **30** to an aniline to obtain the thalidomide analog pomalidomide **31**. In order to introduce the symmetric spacer between the CRBN binder and XL188 a short propionyl linker was installed via amide coupling. A boc-protected piperazine was attached to bridge the E3-binder to the USP7 inhibitor

## Results

in a final nucleophilic substitution. The boc group was deprotected, which yielded the functionalized CRBN recruiter **32**.

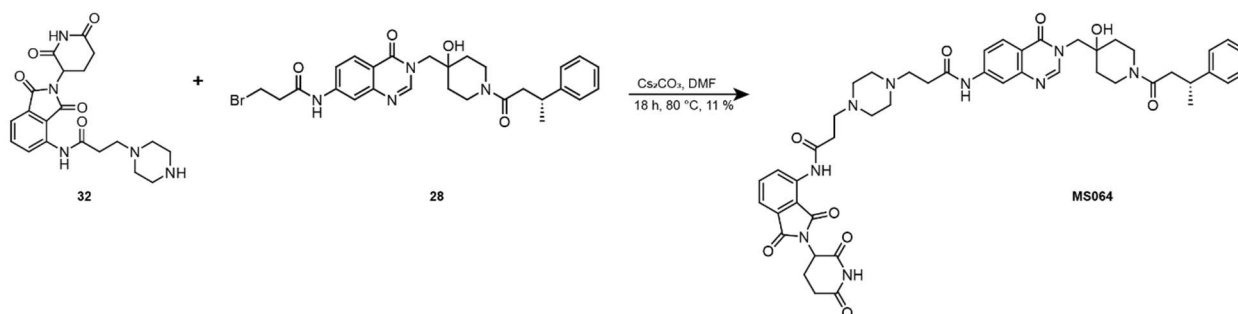
The VHL-binder was commercially available and only functionalized with a short spacer for attachment to the USP7 inhibitor XL188 (Scheme 19).



**Scheme 19 | Last step functionalization of VHL-ligand 31. a)** 1. 3-(4-(tert-butoxycarbonyl)piperazin-1-yl)propanoic acid, DIPEA, HATU; 2. 20 % TFA in DCM.

The symmetric spacer was attached to the eastern end of the VHL-ligand via amide coupling and subsequently deprotected to generate a free amine that was linked to **XL188**. There are various exit vectors described for the design of VHL recruiting PROTACs. Depending on the chosen exit vector, the ternary complex between the E3-ligase, the PROTAC molecule and the POI can vary and therefore, promote or inhibit the transfer of the ubiquitin. Attaching a spacer at the eastern primary amine of the structure was the most used exit vector (87 % of all VHL recruiting PROTACs published). It was therefore chosen for this first generation of USP7 PROTACs.<sup>[188]</sup>

Lastly, the USP7 inhibitor and the E3-ligase binder were combined via a nucleophilic substitution. This resulted in the generation of CRBN recruiting PROTACs **MS062**, **MS064** (Scheme 20) and the VHL recruiting PROTAC **MS067** (Scheme 21).

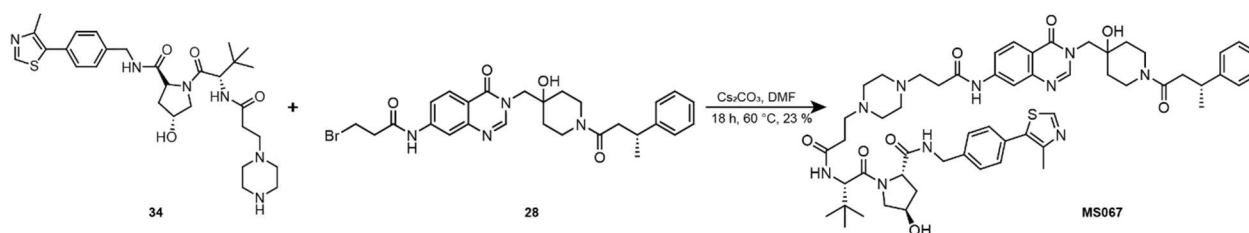


**Scheme 20 | Coupling of the CRBN recruiter to XL188 yielded PROTAC MS064.** The USP7 inhibitor **28** was coupled to **32** via a nucleophilic substitution.



## Results

**MS064** bears the more potent USP7 binder with the methyl group in *R*-configuration, but **MS062**, the racemic derivative, was synthesized according to the same synthetic strategy. Both molecules were obtained in low yield. LC-MS analysis of both crude products revealed major side products, which were not further identified, but side reactions with the pomalidomide in DMF were recently investigated.<sup>[189]</sup> However, the small amount of both PROTACs obtained after HPLC purification was sufficient for biological testing. Nevertheless, the synthesis strategy should be optimized for future reactions. Since there was evidence via LC-MS, that the bromide of **28** was eliminated during the reaction through an E1<sub>cb</sub> mechanism, an alternative linking strategy should be considered. The elimination resulted in the formation of alkene at molecule **28**, which did not react to form the desired product. To prevent the elimination, a screening of the reagents, especially of the solvent and the base, should be carried out. Furthermore, boc-protected 3-(piperidin-4-yl)propanoic acid could be fused to **27** by amide coupling. The piperidine is then deprotected and linked to the E3- recruiter. This strategy would involve the linkage of the DUB binder and the E3-binder in a different order and therefore circumvent any eliminations occurred in the original synthesis strategy. Alternatively, the linker consisting of the piperazine connected to an alkyl spacer at both ends could be synthesized analogous to the DUB binder and the E3-recruiting molecule. The standalone linker is then attached to the CRBN binder and **XL188** in a last step. This would allow multiple molecules to be synthesized in parallel.



**Scheme 21 | Coupling of the VHL recruiter to XL188 yielded PROTAC MS067.** The USP7 inhibitor **28** was coupled to **34** via a nucleophilic substitution.

VHL recruiting PROTAC **MS67** was synthesized using a similar strategy to **MS062**.

### 3.4.3 Biochemical evaluation of synthesized PROTACs reveals potent binding and degradation of USP7 in HEK293 cells

To confirm that the synthesized PROTACs (Fig. 32 A, B) were still able to bind to USP7 and were not sterically hindered by the E3-ligase binder, a Ub-Rh cleavage assay was executed (Fig 32 C). The determined IC<sub>50</sub> indicated whether the PROTACs' potency was in a similar range to the parent

## Results

inhibitor **XL188**. For that purpose, purified USP7 was preincubated with all synthesized PROTAC molecules for one hour and subsequently tested for deubiquitinase activity with and ubiquitin rhodamine fluorophore. For comparability of potencies, the parent inhibitor **XL188** and the racemic analogon were also tested. For both parent inhibitors and VHL-recruiting PROTAC **MS067**, comparable potencies in the sub-micro molar range were determined. This confirms that adding an E3-ligase binder at the structure of **XL188** does not interfere with its inhibition of USP7.

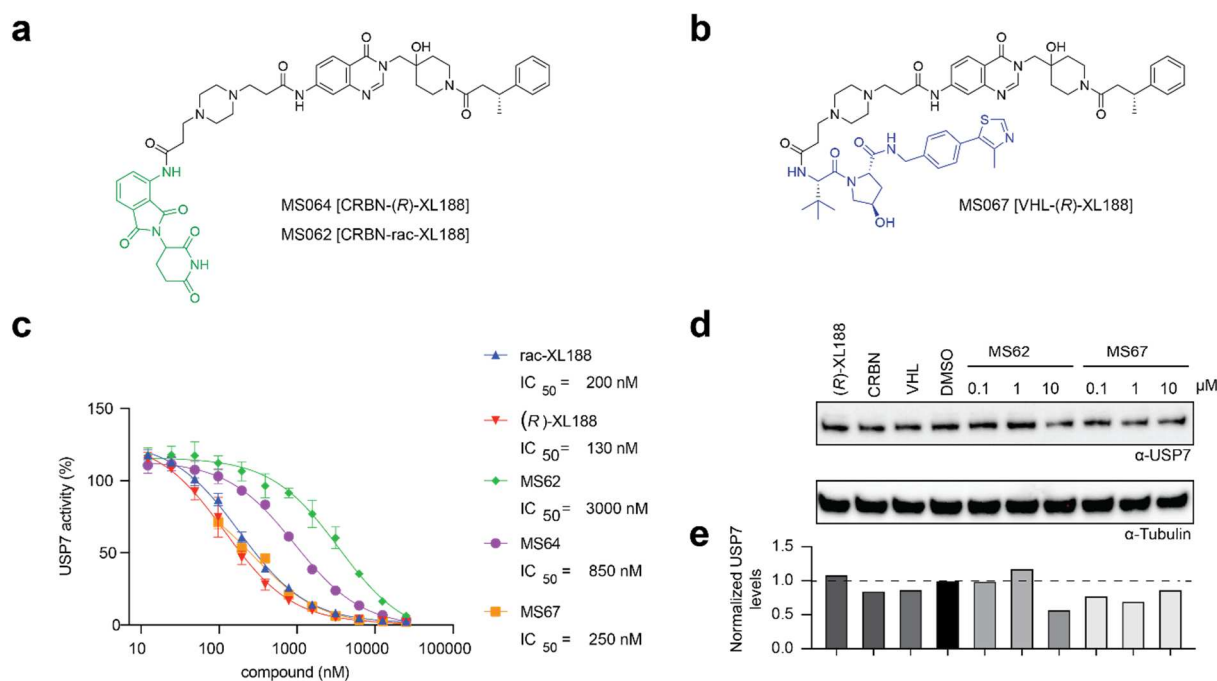


**Fig. 32 | Synthesized PROTACs showed potent binding and induced degradation of cellular USP7. a)** Molecular structure of CRBN recruiting PROTAC **MS064**. **MS062** represents the racemic analogon thereof. **b)** Molecular structure of VHL-recruiting PROTAC **MS067**. **c)** PROTACs were tested for USP7 inhibition in an *in vitro* Ub-Rh cleavage assay. USP7 was preincubated with indicated compounds for 1 h. IC<sub>50</sub> values were determined from three independent experiments for all compounds. **d)** Cellular characterization of induced degradation by indicated compounds in a concentration-dependent manner. Protein levels were analyzed via western blot. **e)** Quantification of USP7 band intensity from western blots depicted in d). All levels were normalized to α-tubulin levels.

Furthermore, this corroborates that a suitable exit vector for the attachment of a linker was identified in the structure of **XL188**, which does not result in a steric clash with the protein surface of USP7. Incubation of USP7 with the CRBN recruiting PROTAC **MS064** led to approx. 6-fold lower potency compared to the parent inhibitor and approx. 3.5-fold lower potency compared to the VHL-recruiting PROTAC. This might result from the poor solubility of the pomalidomide in an

## Results

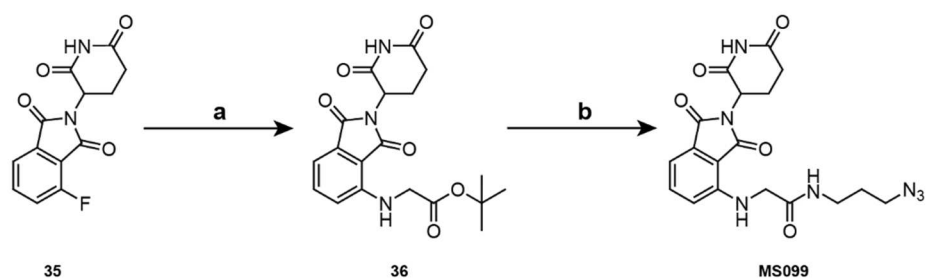
aqueous environment.<sup>[190]</sup> Even though the IC<sub>50</sub> value of the racemic analogon of **MS064** was 15-fold higher than the racemic XL188, all PROTACs showed potent inhibition of USP7 *in vitro*.

To investigate if the PROTACs induce the specific degradation of USP7 in cellular context, HEK293 cells were treated with the compounds in a concentration-dependent manner for 24 h (Fig. 32 D). The abundance of endogenous USP7 was analyzed by western blotting and normalized to endogenous  $\alpha$ -tubulin. XL188, and the recruiter molecules for both E3-ligases were used as controls to confirm that the induced degradation of USP7 is not dependent on any of the molecules alone. Treatment of the cells with **MS067** led to a degradation of endogenous USP7 at all concentrations. This shows that the molecules could penetrate the cell membrane and were able to reach USP7 inside the cell. Treatment with 0.1  $\mu$ M resulted in the reduction of USP7 by approx. 20 %, whereas a concentration of 1  $\mu$ M led to reduced USP7 levels of approx. 30 %. This confirmed that treatment with the VHL-recruiting PROTAC **MS067** can induce the reduction of endogenous USP7 levels in a concentration-dependent manner. Only a concentration of 10  $\mu$ M resulted in less degradation of USP7 than with a 10-fold lower concentration of the PROTAC. Since this concentration corresponds to 40 times the IC<sub>50</sub> value of **MS067**, its very likely that a Hook effect occurred, which inhibited the degradation of USP7. The hook effect describes the cellular concentration of a PROTAC, at which the molecules saturate the binding site either at the E3-ligase or the POI. This auto-inhibits the formation of the ternary complex and results in unproductive binary complexes.<sup>[191]</sup> The racemic derivative of the CRBN recruiting PROTAC **MS062** shows no degradation at a concentration of 1  $\mu$ M or lower. Treatment with 10  $\mu$ M of **MS062** resulted in the degradation of >60 % of endogenous USP7. Recruiting CRBN resulted in an increased degradation of cellular USP7, albeit at higher concentrations of the PROTAC. Since the racemic version of the CRBN recruiting PROTAC was used, it is likely that treatment with **MS064**, the PROTAC with **XL188** in the *R*-configuration, induces the degradation of USP7 at much lower cellular concentrations.

Collectively, the successful synthesis of two PROTACs consisting of different E3-recruiters was shown. The PROTACs were based on the literature known inhibitor **XL188**, whose crystal structure in co-complex with USP7 was used to identify a possible exit vector for the attachment of a linker. Biochemical and cellular characterization of the PROTACs showed potent inhibition of purified USP7 and degradation of the endogenous protein in a living environment. This proves that the chosen linker was sufficient initializing the ternary complex and that USP7 was susceptible to induced degradation by PROTACs.

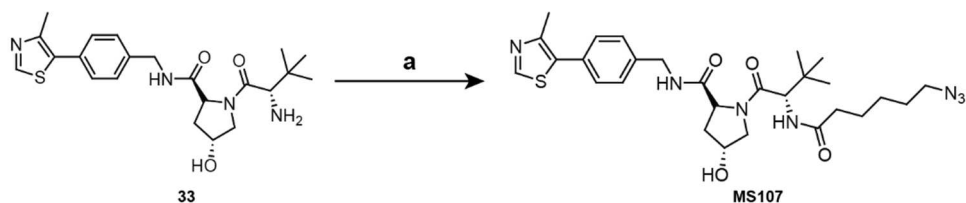
### 3.4.4 Transformation of GK13S into bifunctional molecule to degrade UCHL1

Motivated by the results of the USP7 PROTACs, the copper-catalyzed azide-alkyne cycloaddition was used to install an E3-ligase binder at the alkyne-bearing probe **GK13S**. This resulted in the synthesis of bifunctional molecules targeting UCHL1 for degradation. For that purpose, the already synthesized CRBN- and VHL-binder were equipped with an azide moiety. To install the alkyl linker with the terminal azide functionality by amide coupling, a *tert*-butyl protected glycinate spacer was added to the pomalidomide derivative **32** via nucleophilic aromatic substitution ( $S_NAr$ ) reaction. After deprotection of the ester, the carboxyl group was exploited for amide coupling to obtain the azide-modified CRBN binder **34** (Scheme 22).



**Scheme 22 | Synthesis of azide functionalized CRBN-binder.** a) *tert*-butyl glycinate, DIPEA b) 1. 20 % TFA in DCM, 2. 3-azidopropan-1-amine, HATU, DIPEA

Due to the free carboxylic acid, a direct coupling of the azide alkyl chain to the VHL-binder was possible (Scheme 23). A slightly longer alkyl chain was used to ensure comparability of the linker length between the VHL- and CRBN recruiter.

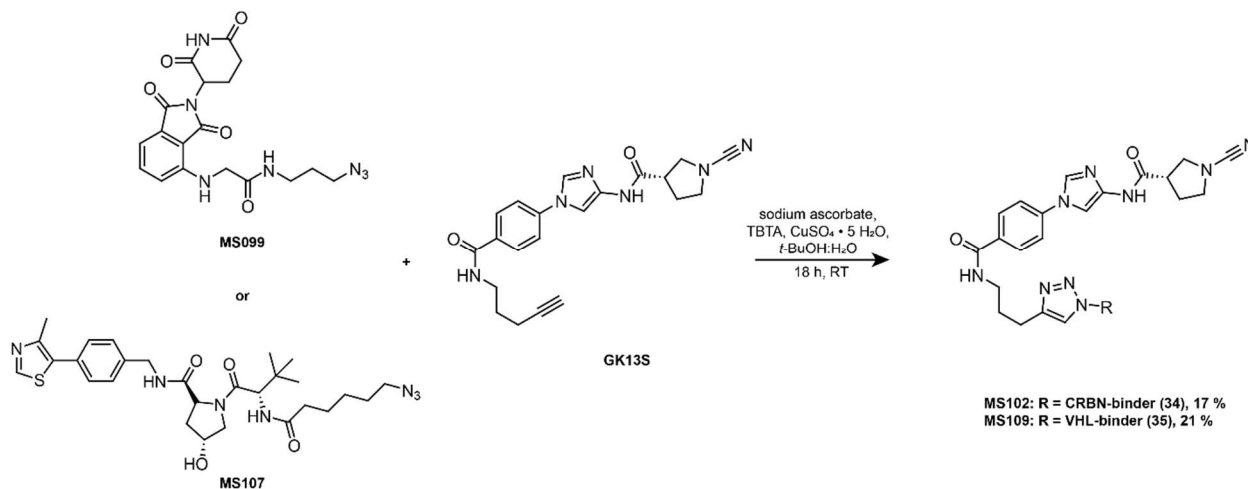


**Scheme 23 | Synthesis of azide functionalized VHL-binder.** a) 6-azidohexanoic acid, HATU, DIPEA

Since the small molecule probe **GK13S** was already equipped with an alkyne functionality, the E3-ligase recruiter was conjugated in a final synthesis step via copper-catalyzed alkyne-azide cycloaddition (Scheme 24). The Cu (II) was reduced by sodium ascorbate to the reactive Cu(I). The proposed mechanism involves the addition of one copper ion to the alkyne via a  $\sigma$ -complex, resulting in the formation of a copper-acetylide intermediate. Next, a second copper ion is recruited to form the catalytically active complex. The azide is coordinated to the  $\pi$ -bound copper

## Results

complex. This complex collapses under the stepwise formation of the triazole moiety.<sup>[192]</sup> TBTA was used as a ligand to prevent the disproportionation of Cu(I) ions. A mixture of *tert*-butanol and water was necessary to solve the copper source and the reducing agent in the aqueous phase, but also to solve the other reagents in the organic phase. The reaction successfully conjugated the probe with the E3-ligase binder, usable for biological evaluation (Fig. 33 A).



**Scheme 24 | Synthesis of PROTACs MS102 and MS109.** Copper-catalyzed cycloaddition was utilized to conjugate GK13S with CRBN and VHL-recruiter.

To test whether the PROTACs **MS102** and **MS109** could bind to UCHL1, a target engagement assay in HEK293 cell lysates was performed. The lysate was treated with the compounds at different concentrations to detect a concentration range suitable for UCHL1 modification (1 h). All samples were incubated with a HA-Ub-V5 probe and analyzed for UCHL1 band upshifts by western blot, indicating no compound binding (Fig. 33 B). The probe **GK13S** was used as a control to confirm the covalent binding at UCHL1. **MS107** and **MS099**, the azide-conjugated E3-recruiter for the respective PROTACs, were used as controls to confirm that binding the E3-ligase alone does not result in the degradation of UCHL1. As expected, the incubation with **GK13S** led to complete modification of UCHL1 and no upshift of the corresponding band. Treatment with the E3-binder-azide conjugates **MS099** and **MS107** resulted in no modification of UCHL1. The VHL-recruiting PROTAC **MS109** showed binding of UCHL1 in a concentration range from 2.5 to 10  $\mu$ M concentration. Whereas only at 10  $\mu$ M the available UCHL1 was almost wholly modified. At 5  $\mu$ M more than 50 % of the endogenous UCHL1 was bound. The CRBN-recruiting PROTAC showed more potent binding than **MS109**, with concentrations of 5-10  $\mu$ M entirely modifying UCHL1 from HEK293 lysates. Concentrations as low as 625 nM resulted in partial modification and 1.25  $\mu$ M in binding of approx. 50 % of the present UCHL1. To test the degradation efficiency of both

## Results

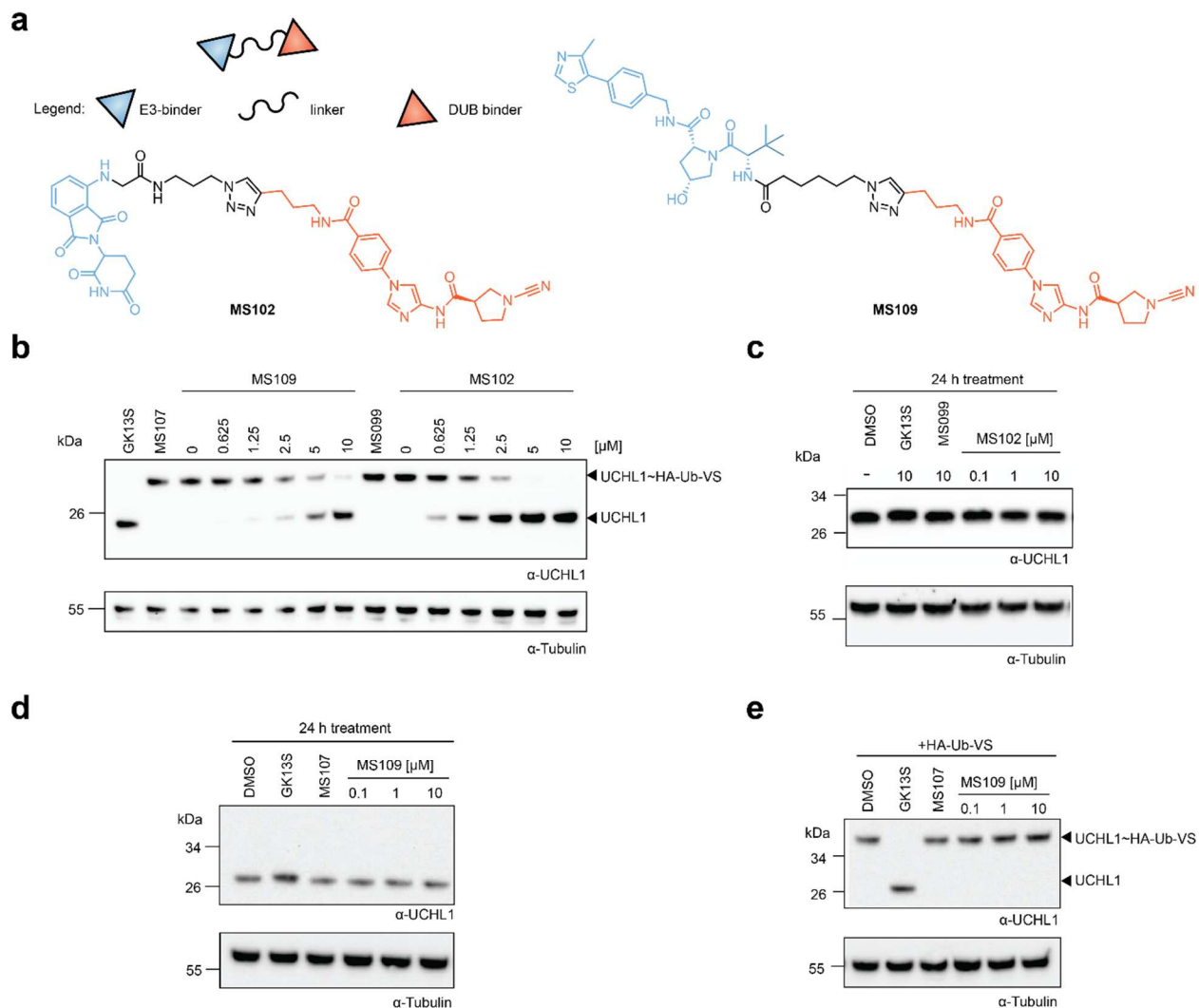


**Fig. 33 | PROTACs MS102 and MS109 show binding towards UCHL1 but lack membrane permeability. a)** Schematic representation of a PROTAC molecule with E3-binder (light blue), linker (curved line), and DUB binder (orange) (top left corner) and the molecular structures of the UCHL1 targeting PROTACs MS102 and MS109. **b)** UCHL1 engagement assay in HEK293 cell lysates. Cells were treated with the indicated compounds for 1 h, following the incubation with a HA-Ub-VS probe. All samples were analyzed by western blot analysis. **c, d)** UCHL1 degradation assay in intact HEK293 cells. Cells were incubated with MS102 (c) or MS109 (d) for 24 h with indicated concentrations, harvested and subsequently analyzed by western blotting. **e)** UCHL1 target engagement assay in intact HEK293 cells. Cells were treated with MS109 for 24 h, lysed and treated with a HA-Ub-VS probe. Samples were analyzed by western blotting.

PROTACs, intact HEK293 cells were treated for 24 h. A range between 0.1 – 10  $\mu\text{M}$  was chosen to observe a compound concentration-dependent degradation. After the incubation period, the cells were harvested and UCHL1 levels were subsequently analyzed for induced degradation (Fig. 33 C, D). Unfortunately, the treatment with either **MS102** or **MS109** resulted in no changes of the endogenous UCHL1 levels at any concentration. Since only two PROTACs design to target

## Results

UCHL1 with slight linker variation were tested, the composition of the linker might not be sufficient to induce a stable ternary complex. Another critical parameter is the cell membrane permeability, as many PROTACs fail to pass this barrier due to their molecular size and multiple hydrogen bond donors.<sup>[193]</sup> To test whether **MS109** could pass the cell membrane to reach UCHL1, HEK293 cells were treated with the PROTAC (Fig. 33 E). Following incubation with the HA-Ub-VS probe revealed no labeling of cellular UCHL1 with the PROTAC at concentrations up to 10  $\mu$ M.

Taken together, the copper-catalyzed 1,3-cycloaddition was successfully employed to conjugate binders for the E3-ligases CRBN and VHL to the characterized UCHL1 probe **GK13S**. Biological evaluation in HEK293 cell lysates confirmed stable binding of the PROTACs to UCHL1 in the low micromolar range. However, treatment of intact cells resulted in no degradation of cellular UCHL1 due to cell membrane permeability issues of the molecules. This was conformed with a target engagement assay in intact cells so that a synthetic revision of the molecules is necessary to enable the degradation of cellular UCHL1.

## 4. Discussion and Conclusion

Ubiquitylation as a post translational modifier for signal transduction is used in most pathways throughout the cell.<sup>[13]</sup> The specific reversal of various ubiquitin species is a fundamental regulatory switch executed by deubiquitinases. The dysregulation of DUBs results in many specific diseases, with cancer, cardiovascular diseases and neurological disorders among them.<sup>[112]</sup> This protein class represents an important target for therapeutic applications, due to the association of DUBs with these diseases. However, not many DUBs were exploited for drug discovery approaches, due to the overall insufficient understanding of their substrate spectrum, localization and interaction partners in different signaling pathways.<sup>[194]</sup>

This thesis described the synthesis of a dedicated library of small molecules targeting deubiquitinases. These compounds were further equipped with electrophilic warheads to utilize them as probes for the covalent modification of DUBs. The future use of the fully characterized probes should work as a foundation to enhance the understanding about this enzyme class in regards to the above-mentioned points. Most probes of the library presented in this thesis, contained a nitrile or cyanopyrrolidine as their electrophilic moiety, a feature that was commonly described in the patent literature for the covalent modification of DUBs. However, a recent publication by the Buhrlage lab suggests that small molecule probes bearing different electrophilic moieties show the ability to selectively target different DUBs.<sup>[113]</sup> Using chloroacetamide as the warhead structure resulted in the covalent modification of various USP DUBs that were not bound with any other electrophilic warheads. Furthermore, only the use of acrylamides and sulfonamides as a warhead resulted in the modification of USP15 and USP22 respectively.<sup>[113]</sup>

The here described library consisted of seven compounds derived from literature known inhibitors against DUBs suitable for the use as probes. This compound collection was assembled as a proof of concept to use small molecule probes for the cellular investigation of DUBs. The introduction of the alkyne at specially identified sites within the molecule made proteomics based ABPP in intact cell and other cellular assays possible. The ABP library represents an extension of the toolbox to study deubiquitinases. They can be used complementary to Ub based probes, with which cellular experiments are difficult to realize. However, the attachment of the alkyne at specific areas within the molecule made rapid derivatization of the core scaffold and thus expansion of the library difficult to achieve. To circumvent this limitation, improved synthesis



## Discussion and Conclusion

strategies are required, which involves the preparation of building block suitable for several probes. To accomplish this, the warhead and the moiety bearing the alkyne tag have to be synthesized separately from the core scaffold of the final probe. If the warhead and the alkyne structure are connected with the core scaffold as a final synthesis step the high throughput screening for potent core scaffolds against different DUBs is possible. The best core scaffolds would be selected to allow the rapid buildup of small molecule probe libraries. Taken together, the variation of the electrophilic warhead structure and the ease of the chemical synthesis of the compounds are important considerations for the future assembly of small molecule probe libraries for the investigation of DUBs.

The biochemical evaluation of the probe library resulted in the identification of the 3-carboxy-*N*-cyanopyrrolidine probe **GK13S** covalently modifying the DUB UCHL1 *in vitro* as well as in different cellular systems. For the other synthesized probes, no clear binding to a DUB in a complex proteome was observed. The synthesized probes were tested in a DUB profiling assay. This assay presents a rapid and powerful approach which utilizes the use of Ub-suicide probes to detect for probe binding in cell lysates. However, the assay is limited for the detection of low abundant DUBs that are easily overshadowed by higher abundant proteins with a similar molecular weight. This may have resulted in some of the probes tested being classified as unusable, although low abundant DUBs may have been modified. Work of the Ovaa lab suggest the enrichment of a DUBtome from a complex mixture by the use disulfide Ub-Probes, from which the release under mild reducing condition is possible.<sup>[195]</sup> In isolation, the binding behaviors of the small molecule probes to the DUBs of interest can be investigated in more detail. This would circumvent the obstacles of off-target fluorescence caused by the binding of the probes to non-DUBs, otherwise not allowing the detection of low abundant DUBs with the presented assay from a complex proteome.

UCHL1, a DUB that is predominantly expressed in neurons, is associated with cancer and neurological disorders such as Parkinson's disease. Its catalytic center is covered by the so called cross over loop, a structural feature that restricts larger substrates from binding to the catalytic cleft. Its substrate spectrum remained therefore elusive.<sup>[67]</sup> The activity of UCHL1 is regulated by conformational plasticity. In the inactive apo form, the catalytic triad is unaligned, which abolishes any catalytic activity. The binding of ubiquitin results in a conformational change, which aligns the catalytic triad, widens the cleft leading to the catalytic cysteine and stabilizes the Ub C-terminal LRGG peptide for cleavage.<sup>[69]</sup> The covalent modification with the probe **GK13S**, locks UCHL1 in a hybrid conformation, with some amino acid residues displaying conformations found in the apo

## Discussion and Conclusion

structure and some adopt conformations from the ubiquitin bound state. The structure of **GK13S** adopts a similar orientation as the C-terminal peptide of ubiquitin, through key hydrogen bonding and hydrophobic interactions. Interestingly, its specificity for UCHL1 over most other DUBs results from alignment of its pyrrolidine in a pocket that only forms in the apo state of UCHL1. Other working groups have reported DUB inhibitors exclusively stabilizing their targets in either the active or the inactive forms.<sup>[104, 196]</sup> The co-complex structure of UCHL1 with **GK13S** highlights that the newly observed hybrid conformation can lock deubiquitinases in an inhibited state induced by small molecule binding. This finding can add another layer of specific inhibition of DUBs with small molecules. The principle can be adapted by compounds binding to other DUBs by exploiting their conformational flexibilities. Furthermore, the crystal structure, solved by Dr. Christian Grethe, was the first of UCHL1 solved in co-complex with a small molecule probe and enabled important insights into the binding behavior of **GK13S**. The structure allows conclusions about the covalent modification of the catalytic cysteine and highlights important interactions sites between the molecule's recognition element and the protein. In addition, the structure provides a conclusive explanation for the preference of the *S*-isomer over the *R*-configuration of **GK13S**. Those insights will pave the way for the rational synthesis of UCHL1 inhibitors with enhanced potency and selectivity profiles.

The covalent modification of UCHL1 with **GK13S** was confirmed via the pull down of the DUB in an activity-based protein profiling approach. This target validation highlighted PARK7 (DJ-1) as the major off-target of the probe **GK13S**. Other off-targets were identified as C21orf33, a PARK7 family associated protein, as well as the proteins ISOC1, NIT2 and different aldehyde dehydrogenases. Most of these off-target proteins feature a catalytic cysteine and a covalent modification of them were also confirmed by others in target validation experiments using cyanopyrrolidine based probes.<sup>[129a, 129b, 197]</sup> As a control, the minimal probe **GK16S** was synthesized. This probe lacks the specificity element, consisting of a direct conjugation of the alkyne handle to the cyanopyrrolidine warhead. The enrichment of UCHL1 was drastically reduced when **GK16S** was used. Besides UCHL1, **GK16S** showed a similar off-target spectrum as **GK13S**. This finding was further corroborated *in vitro* by determining the IC<sub>50</sub> value of >100 μM for the binding of **GK16S** to UCHL1. In addition, cellular investigation confirmed no covalent modification of endogenous UCHL1 with **GK16S**. Biochemical evaluation of both probes showed major differences in potency towards UCHL1, which allowed to apply the probes in a concentration range where **GK13S**, but not **GK16S** was able to bind UCHL1 and both probes modified the same off-target spectrum. By binding to the same off-targets but not UCHL1, **GK16S** can be utilized to distinguish between phenotypes that result from the inhibition of UCHL1 and

## Discussion and Conclusion

*vice versa*. This resulted in the use of **GK13S** and **GK16S** as chemogenomic pair of probes for the specific investigation of UCHL1.

Target identification experiments with **GK13R** resulted in drastically decreased enrichment of UCHL1 compared to the *S*-configuration. Nevertheless, only the treatment of a complex proteome with **GK13R**, resulted in the weak isolation of USP10 (Supplementary Fig 3 B), another DUB not identified in the original DUB profiling assay. This highlights that warheads in different stereo configurations can influence the DUB target spectrum of a probe. Furthermore, **GK13R** presents a starting point for the design and synthesis of small molecule probes for USP10. Further investigation such as target engagement assay are necessary that prove that **GK13R** is able to covalently modify USP10 in cellular setting.

Even though UCHL1 is one of the most studied DUBs in scientific literature<sup>[198]</sup>, the phenotypes resulting from the interactions of UCHL1 in various signaling pathways, as well as its role in associated diseases are controversial.<sup>[71]</sup> One reason for this may be the use of the small molecule **LDN-57444**, which is often incorrectly utilized as a specific UCHL1 inhibitor.<sup>[199]</sup> The experiments presented in this thesis, in agreement with data from others,<sup>[129b]</sup> suggest that **LDN-57444** is not sufficiently characterized to allow the specific study of UCHL1 in a cellular environment.

UCHL1 is an extremely abundant protein in the brain, where it is estimated to count for 1-5 % of the total soluble neuronal protein.<sup>[75]</sup> Genetic deletions or engineered alterations of UCHL1 in mice highlighted important functions of the DUB in neurodegeneration and maintenance of the free mono-Ub pool.<sup>[87, 200]</sup> Stabilization of mono-Ub by UCHL1 was previously investigated in the context of a monkey cell.<sup>[183]</sup> Curious, if a similar phenotype is observable in a human cell line the chemogenomic pair of **GK13S** and **GK16S** was used to reconstitute this effect in glioblastoma cell line U-87 MG. The data presented in this thesis suggests the reduction of free mono-Ub after the inhibition of UCHL1 by **GK13S**. This does not only demonstrate the utility of **GK13S** and **GK16S** as a chemogenomic pair of probes, but also establishes the U-87 MG cell line for the study of effects on the mono-Ub pool associated with UCHL1. To further understand the source of the disturbance of the mono-Ub pool a rescue experiment was performed. This involved the addition of different DUBs to replenish the mono-Ub pool, in case the lost mono Ub was conjugated to other substrates. Even though exogenous DUBs with and without different linkage specificities were used, the mono-Ub pool could not be adjusted to samples in which the endogenous UCHL1 was not inhibited. Further experiments are needed to clarify the cause of this irreversible loss of mono-Ub.

## Discussion and Conclusion

**GK13S** was further used to inhibit endogenous UCHL1, to employ an exogenous catalytic inactive UCHL1 mutant for the pull down of substrates and interaction partners. Unfortunately, no proteins were isolated. Besides the points made in the results section variation of the isolation tag could lead to improved outcomes. Since GFP is a rather large tag, that could clash with the interaction or binding of possible substrate, smaller tags like FLAG, biotin or HA could be utilized. Cross-linkers could be employed to stabilize the weak interaction between UCHL1 and other interactors. To distinguish between substrates that bind to the catalytic pocket and interactors that bind on the surface of the protein, cross-linking groups could either be attached to UCHL1 directly or fused to **GK13S** (Fig. 34).

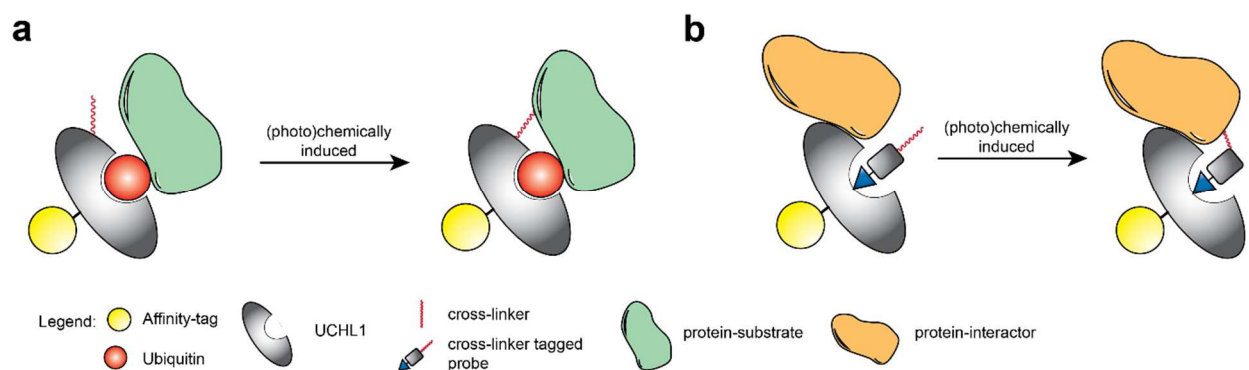


**Fig. 34 | Utilizing cross-linkers to stabilize interaction between UCHL1 and other proteins. a)** A cross-linking group is directly attached to the DUB to stabilize interactions with a substrate. **b)** A crosslinker modified probe derivative is used to capture non-catalytic interaction partners of UCHL1. Both complexes are enriched via an affinity tag.

In an approach to identify changes on a proteome wide level upon the inhibition of UCHL1 with **GK13S** in human glioblastoma cells, a proteomics based whole proteome digest was carried out. This was based on the hypothesis that under normal conditions UCHL1 stabilizes its substrates by deubiquitination. Inhibition of UCHL1 led to destabilization and thus to reduced levels of these substrates. Changes were detected with mass spectrometry assisted methods on a proteome wide scale. Evaluation revealed decreased levels of the small Rho-GTPase Rac1 and the serine protease HtrA2 among others. Especially the destabilization of Rac1 is of therapeutic interest, since the overexpression of the GTPase is implicated in different types of cancer.<sup>[201]</sup> To corroborate this finding decreasing levels of Rac1 were verified via western blot analysis. After 24 hours of treatment with **GK13S**, the level of Rac1 is slightly decreased. After 48 hours, the decrease continues to increase again after 72 hours. At this point, other DUBs may compensate for the loss of UCHL1 activity. More data remains to corroborate the association between inhibition of UCHL1 and the loss of Rac1 and to shed light on the mechanism the DUB might be involved in. However, especially the indirect destabilization of RAC1 by inhibiting UCHL1 opens

## Discussion and Conclusion

new therapeutic opportunities to interfere with an otherwise undruggable class of proteins that play major roles in various diseases. Unfortunately, it was not possible to confirm reduced HtrA2 levels after the inhibition of UCHL1 with GK13S via western blotting. Since HtrA2 is located to the mitochondrial membrane under normal cellular conditions and is only released to the cytosol under apoptotic conditions, reduced levels of HtrA2 after inhibition of UCHL1 might become more distinct in different cellular states.<sup>[181a]</sup> Under normal conditions the change in protein level might be too sensitive to be quantified via western blotting.

Surprisingly, an *in vitro* DUB profiling with **GK13S** revealed the covalent modification of five other DUBs besides UCHL1, which were not identified in the original cellular DUB profiling (Fig. 11 E). One reason for this could be the low abundance of the DUBs in the lysate, which were therefore not detectable. Furthermore, the fluorescence bands from other modified off-target proteins with similar might have overshadowed them. The screening carried out at MRC Protein Phosphorylation and Ubiquitylation unit, used only the purified catalytic domain for some DUBs. **GK13S** might have a better accessibility to the amino acid residue the probe reacted with, when only the structure of the catalytic center rather than the full-length protein is present. In addition, other reasons might be that some DUBs were not transferred to the soluble protein fraction due to insufficient lysis conditions, which came therefore not in contact with the probe in the lysis-based assay.

Nevertheless, the *in vitro* targeting of other DUBs by **GK13S** resulted in the chemical optimization of the probe with the aim to reach in-DUB family specificity and to discriminate the most abundant off-target PARK7. Further evaluations of the crystal structure of UCHL1 in co-complex with **GK13S**, demonstrated unoccupied space in the binding pocket of UCHL1. This led to optimization efforts, involving the synthesis of different variations of the warhead structure. Cyanopyrrolidines with decorations in 2-position of the ring system, already resulted in decreased modifications of PARK7, but also in decreased potency against UCHL1 compared to **GK13S**. Structural improvement and biological characterization resulted in the 6-membered cyanopiperazine probes **CG306** and **CG341**. Both were covalently modifying UCHL1, but no other DUBs or PARK7. These probes show comparable potencies towards UCHL1, but an increased specificity profile compared to **GK13S**. This not only confirmed the rational that occupying additional space in the catalytic pocket of UCHL1 led to increased specificity of the probe over other off-targets. But also, that the specific targeting of DUBs with small molecules was possible, even though the molecule binds to the ubiquitin binding site, a structural feature that is contained in all DUBs. The probes feature a N-alkylation at the warhead, whereas **CG341** is methylated and **CG306** contains a pentyl

## Discussion and Conclusion

chain at the piperazine. Interestingly, the methylated probe presents a more potent modification of UCHL1 in cell lysates due to its better solubility in aqueous media, whereas the pentylated probe demonstrates an enhanced membrane permeability, resulting in increased covalent modification of UCHL1 in intact cells.

Target engagement assays *in vitro* and in intact cells with **CG341** and **CG306** at 5  $\mu\text{M}$ , confirmed full covalent modification of endogenous UCHL1, comparable to the results observed with **GK13S**. But even though the DUB was fully modified, the fluorescence intensity or the enrichment of UCHL1 after attaching the reporter group via CuAAC remained low. Extensive investigation demonstrated, that the covalent bond formed between the probes and the DUBs was stable under lysis conditions for several hours, but upon addition of the CuAAC reagents the modification with **CG341** and **CG306**, but not with **GK13S** was abolished. Screening the reagent spectrum made it most likely that the addition of Cu ions led to the unfolding of UCHL1 and the destabilization of the cyanopiperazine probes. Addition of sodium ascorbate enhances this effect even further. The use of **CG306** and **CG341** for ABPP is therefore limited.

To circumvent this limitation, **CG341** and **CG306** could pre-clicked and incubated with the cells in a copper free environment. But whether the molecules are able to pass the cell membrane in this state remains questionable. The strain-promoted azide-alkyne cycloaddition (SPAAC) demonstrates another possibility to utilize the probes in ABPP experiments. The SPAAC, developed by Bertozzi and coworkers, presents a copper-free version of the CuAAC. Instead of using Cu(I) ions to activate the alkyne, a strained cyclooctyne is used. The ring strain destabilizes the alkyne, increasing the reaction force to proceed the [3+2] cycloaddition with the azide. This allows not only the attachment of the reporter after lysis, but in intact cells cells under physiological conditions.<sup>[202]</sup> However, further synthetic effort is needed to replace the alkyne with a cyclooctyne. The full target spectrum of the cyanopiperazines should be elucidated in regards to fully characterized the synthesized probes. A chemical optimization of the probes, which results in the availability for target ID experiments is therefore inevitable.

In order to investigate phenotypes that were enabled by interaction of UCHL1 with other macromolecules, but not by its catalytic activity, PROTACs based on **GK13S** were synthesized. The PROTACs are designed to promote the degradation of cellular UCHL1, which is no longer available for non-catalytic interactions. Since the probe **GK13S** already contained an azide, the CuAAC was used to enable the rapid linkage with azide conjugated E3-recruiters. However, biological evaluation showed that although the PROTACs were able to bind endogenous UCHL1, they were unable to penetrate the cell membrane due to their size and the triazole moiety. For

## Discussion and Conclusion

the application of UCHL1 PROTACs based on **GK13S**, utilization of the SPAAC would be advantageous to introduce the E3-binder. With this method, **GK13S** alone is used completely modify UCHL1, so that in a second step the E3-binder is conjugated via SPAAC in a living environment. Furthermore, the cyanopiperazine probes **CG341** and **CG306** could be converted into specific UCHL1 PROTACs. The reversibility after unfolding of UCHL could be exploited. Thus, the molecules would be released from the DUB upon unfolding at the proteasome. This would release the PROTACs for another modification cycle.

That the induced degradation of DUBs is possible was demonstrated by the design, synthesis and biological characterization of PROTACs targeting USP7. USP7 is a well-studied DUB and therapeutically interesting in the context of the p53/MDM2 axis. Just recently two other groups published PROTACs against USP7 that are structurally similar to the molecules presented in this thesis.<sup>[147]</sup> Both PROTACs consist of a pomalidomide analogon to recruit CRBN to USP7. This corroborates the finding, that recruiting CRBN results in increased degradation of USP7 when treated with **MS062** at higher concentrations, compared to recruiting VHL. The here presented USP7 PROTAC molecules work as chemical tool compounds for the investigation of USP7 in cellular settings and with further improvement, present a promising strategy to intervene with p53 in cancer relevant settings.

The tool compounds described in this thesis will help to elucidate and understand the mechanisms, interaction partners and substrates of deubiquitinases. Furthermore, they will serve as a basis for developing and improving active compounds for the targeting of DUBs in order to make this important class of proteins accessible for therapeutically interventions.

## 5. Methods

Parts of the methods described below were already been published as excerpts or in their entirety.<sup>[203]</sup>

### 5.1 Biology

#### 5.1.1 Biochemical assays

##### Cloning and constructs

Human UCHL1 (uniprot: P09936, residues: 1-223) and PARK7 (uniprot: Q99497, residues: 1-189) sequences were cloned from cDNA templates for bacterial expression into the pOPIN-B vector (for UCHL1 and PARK7, N-terminal His<sub>6</sub>-3C-tag, an additional GS linker was used for UCHL1) and into the pOPIN-E vector for mammalian cell transfection (with an N-terminal Flag-GS tag and no C-terminal tag) using the In-Fusion HD Cloning Kit (Takara Clontech). Site-directed mutagenesis was carried out by splicing-by-overlap extension PCR using Phusion Polymerase (New England BioLabs).

##### Protein expression and purification

For bacterial expression of proteins, Rosetta2(DE3) pLacI cells were transformed with the respective vector. Overnight cultures were diluted 1:100 into 2xTY medium, and suitable antibiotics were added to the medium. Then cultures were grown shaking at 37 °C. As soon as a  $A_{600}$  of 0.8 was reached, cultures were cooled to 18 °C, isopropyl-1-thio- $\beta$ -D-galactopyranoside (IPTG) was added (0.5 mM final concentration) and cultures were grown overnight. Cells were harvested by centrifugation and stored at -80 °C. The pellets were thawed, resuspended in lysis buffer (50 mM H<sub>2</sub>NaPO<sub>4</sub>, 300 mM NaCl, 20 mM imidazole, pH 8.0, supplemented with lysozyme and DNase) and lysed by sonication on ice for 5 min. The cell debris was cleared by centrifugation at 22000xg for 30 min at 4 °C and sterile filtered. The clear lysate was then passed through a 5 mL HisTrap column (GE Healthcare), preequilibrated with buffer A (50 mM H<sub>2</sub>NaPO<sub>4</sub>, 300 mM NaCl, 20 mM imidazole, pH 8.0), using an ÄKTA Pure System (GE Healthcare). The protein was then eluted into buffer B (50 mM H<sub>2</sub>NaPO<sub>4</sub>, 300 mM NaCl, 500 mM imidazole, pH 8.0). Protein containing fractions were pooled and concentrated. For UCHL1 and PARK7, GST-3C protease



## Methods

was added and the sample was dialyzed into buffer C (20 mM Tris pH 8.0, 100 mM NaCl, 4 mM DTT) overnight. These proteins were further purified by size exclusion chromatography using a HiLoad 16/600 Superdex 75 pg column (GE Healthcare) with buffer C. PARK7 was dialyzed subsequently into buffer D (20 mM  $\text{KH}_2\text{PO}_4$  pH 7.0 and 5 mM DTT). Dialysed samples were passed through a pre-equilibrated HisTrap column and the eluate was diluted into low salt buffer (25 mM Tris pH 8.5, 50 mM NaCl, 4 mM DTT). These proteins were further purified by anion exchange chromatography on a ResQ column (GE Healthcare) by elution into high salt buffer (25 mM Tris pH 8.5, 500 mM NaCl, 4 mM DTT) over 20 column volumes. Pure protein containing fractions were collected, concentrated and buffer exchanged into buffer C + 5% glycerol. The final protein concentrations were measured by UV absorbance on a Nanodrop 2000.

### **Intact protein mass spectrometry**

Recombinant protein was diluted to a final concentration of 3  $\mu\text{M}$  in PBS (1.8 mM  $\text{KH}_2\text{PO}_4$ , 10 mM  $\text{Na}_2\text{PO}_4$  pH 7.4, 137 mM NaCl, 2.7 mM KCl) and treated with either DMSO or compound. The compound was diluted from a 10 mM stock to a final concentration of 10  $\mu\text{M}$ . The protein compound mixtures were allowed to incubate for 1 h at room temperature. In case CuAAC was carried out,  $\text{CuSO}_4 \cdot 5 \text{H}_2\text{O}$  (1 mM), BTAA (5 mM), 5/6-TAMRA-Azide-Biotin (20  $\mu\text{M}$ ) (Jena Bioscience), and sodium ascorbate (5 mM, all final concentrations) was added and incubated for 1 at RT and protected from light. The samples were either run through a MassPrep Online Desalting 2.1x10 mm cartridge (Waters, flow rate 0.5 mL/min, runtime 7.00 min, column temperature 30 °C) or an AdvanceBio DesaltingRP 2.1x12.5 mm cartridge (Agilent, flow rate 0.4 mL/min, runtime 6 min, column temperature 32 °C) with solvents A = HPLC-grade  $\text{H}_2\text{O}$  + 0.1% formic acid and solvent B = HPLC-grade acetonitrile + 0.1% formic acid as mobile phases. A gradient from 20-90% solvent B (MassPrep Online Desalting cartridge) or 5-95% solvent B (AdvancedBio DesaltingRP) was programmed. The samples were either analyzed on a Velos Pro Dual-Pressure Linear Ion Trap mass spectrometer (ThermoFisher), equipped with an electrospray ion source in positive mode (capillary voltage 5 kV, desolvation gas flow 40 L/min, temperature 275 °C) or on an Agilent 1260 II Infinity system (Agilent), equipped with an electrospray ion source in positive mode (capillary voltage 4 kV, desolvation gas flow 80 L/min, temperature 350 °C). Spectra were deconvoluted with ProMass (Enovatia).

### Fluorescence labeling of USP30 in vitro

Either the compound (from 10 mM stock) or DMSO was diluted to a final concentration of 10  $\mu$ M in PBS buffer. Purified USP30 (residues 64-502) (3  $\mu$ M final conc.) was added to each sample and incubated for 1 h at RT. Then  $\text{CuSO}_4 \cdot 5 \text{H}_2\text{O}$  (0.25 mM), BTAA (1 mM), Rh-azide (20  $\mu$ M) and sodium ascorbate (5 mM, all final concentrations) were added to each sample and incubated for 1 h protected from light. The click reaction was quenched by the addition of 4 x LDS-sample buffer. Samples were resolved by SDS-PAGE using a 4-12% Bis-Tris gel (Invitrogen, NuPAGE) with MES SDS running buffer for 50 min at 180 V. Fluorescence was read out using the Alexa488 ( $\lambda_{\text{ex/em}}$  490/525 nm, for Rhodamine) channel on a ChemiDoc MP Imaging System (BioRad).

### Ub-Rhodamine assay

Reactions were performed in black 384 well low volume non-binding surface plates (Greiner 784900) in a final volume of 20  $\mu$ L. USP7 was diluted in reaction buffer H (20 mM Hepes pH 8.0, 50 mM NaCl, 0.05 mg/ml BSA) to a 4x stock (75 nM final concentration). DUBs were mixed in a 1:1 ratio with 4x PROTACs dissolved in reaction buffer (final DMSO concentration: 0.1-1%). To each well was added 10  $\mu$ L of DUB-compound solution in triplicates, followed by 1 h incubation time. Reactions were initiated by the addition of 10  $\mu$ L Ub-Rhodamine 110 (Biomol, final concentration: 50 nM, diluted into reaction buffer supplemented with 5 mM DTT) and fluorescence (excitation = 492 nm, emission = 525) was read on a Tecan Spark plate reader for 1 h in 1.5 min intervals at room temperature. Biochemical  $\text{IC}_{50}$  values were calculated using GraphPad Prism.

### Reversibility measurements of N-cyanopiperazine probes

Purified UCHL1 was diluted in HEPES buffer (20 mM HEPES pH 8.0, 50 mM NaCl) to 10  $\mu$ M (2x stock). Indicated compounds were diluted to 40  $\mu$ M (2x stock) in HEPES buffer. 100  $\mu$ L of the UCHL1 stock was incubated with 100  $\mu$ L of each compound or DMSO for 1 h at RT. Then, 10  $\mu$ L of each UCHL1/compounds solution were incubated in 90  $\mu$ L of indicated buffers for 1 h at RT. For testing the reversibility upon addition of click reagents, 80  $\mu$ L of the UCHL1/compound solution were incubated with 5  $\mu$ L of each click reagent in different compositions and incubated for 1 h at RT protected from light. Samples were analyzed via intact mass spectrometry as described above.

### 5.1.2 Cellular assays

#### Cell culture

Cell lines were obtained from the American Type Culture Collection (ATCC) or the Leibniz Institute DSMZ-German Collection of Microorganisms and Cell Cultures GmbH. All cell lines were cultivated in a humidified incubator at 37 °C and 5% CO<sub>2</sub>. HEK293, HeLa, MCF-7 and U-87 MG cells were cultivated in Dulbecco's modified Eagle's medium (DMEM) supplemented with 10% fetal bovine serum (FBS) and 2% penicillin-streptomycin. PC-3 cells were cultivated in F-12K Nut Mix media supplemented with 10% FBS and 2% penicillin-streptomycin. Cells were tested negative for mycoplasma contamination.

#### Transfection

For overexpression, HEK293 cells ( $7 \times 10^5$ ) were seeded in six-well plates and cultivated for 24 h. 200  $\mu$ L OPTI-MEM medium was mixed with PEI transfecting reagent (Polysciences) and the vectors and preincubated for 15 minutes. Cells were then transfected with vectors and incubated for 24 h. Following the treatment with either compounds or DMSO in fresh media for an additional 24 h, cells were processed as described below. All siRNA (scrambled: siGENOME Non-Targeting siRNA Control Pools, D-001206-13-05; UCHL1 smart pool: siGENOME Human UCHL1 siRNA, M-004309-00-0005; PARK7 smart pool: siGENOME Human PARK7 siRNA, M-005984-00-0005; UCHL3 smart pool: siGENOME Human UCHL3 siRNA, M-006059-02-0005) were obtained from Dharmacon. Cells were seeded as described above. 2  $\mu$ L of 10  $\mu$ M siRNA was diluted in 100  $\mu$ L OPTI-MEM medium. Additionally, 6  $\mu$ L RNAiMAX (Thermo Fisher) were diluted with 100  $\mu$ L OPTI-MEM medium. Both solutions were combined, incubated for 5 min, and added dropwise to the cells. 24 h after transfection, cells were treated with the compounds or DMSO in fresh media for 24 h. Cells were subsequently processed as described below.

#### DUB profiling for synthesized small molecule probe library

HEK 293 cells ( $4 \times 10^6$ ) were seeded in 10 cm dishes and grown to 90% confluency. The medium was aspirated, cells were washed with ice-cold PBS, treated with 600  $\mu$ L ABP lysis buffer (1% (v/v) IGEPAL, 50 mM Tris, 150 mM NaCl, 5% glycerol, pH 8, cOmplete protease inhibitor cocktail) and incubated on ice for 15 min. The lysed cells were scrapped off the dish and the cell debris were removed by centrifugation. Total protein concentration was determined via a Bradford assay and the cell lysate was diluted to a protein concentration of 2-4 mg/mL with ABP lysis buffer, split

## Methods

in half, and one half treated with HA-Ub-VS (1  $\mu$ M final concentration, 37°C, 30 min). Compounds were diluted to a 2x concentration in PBS buffer from a 10 mM stock in DMSO (final concentration: 1  $\mu$ M). Then each compound dilution or a DMSO dilution was mixed with cell lysate and incubated for one hour at room temperature. Afterwards 1  $\mu$ L of each click reagent (final concentration of 0.5 mM CuSO<sub>4</sub>·5 H<sub>2</sub>O, 1 mM BTTAA, 4  $\mu$ M 5/6-TAMRA-Azide-Biotin (Jena Bioscience), 5 mM sodium ascorbate, each from 100x stocks) were added to each sample, followed by an incubation period of one hour at room temperature with protection from light. Samples were resolved by SDS-PAGE using a 4-12% Bis-Tris gel (Invitrogen, NuPAGE) with MES SDS running buffer for 50 min at 180 V. Fluorescence was read out using the Alexa564 ( $\lambda_{ex/em}$  520-545/577-613 nm, for TAMRA) and Alexa680 ( $\lambda_{ex/em}$  650-675/700-730 nm, for the PageRuler Prestained NIR Protein Ladder (Thermo Scientific)) channels on a ChemiDoc MP Imaging System (BioRad).

### Cellular activity-based protein profiling

Cells ( $7 \times 10^5$ ) were seeded in six well plates and cultivated for 24 h or 48 h. Cells were then incubated in fresh DMEM supplemented with compound or DMSO for 24 h. The cells were washed with ice-cold PBS and harvested in 150  $\mu$ L (experiments with U-87 MG cells) or 200  $\mu$ L ABP lysis buffer as described above. The cell lysate was diluted to a protein concentration of 2 mg/mL with ABP lysis buffer. 1  $\mu$ L of each click reagent (final concentration of 1 mM CuSO<sub>4</sub>·5 H<sub>2</sub>O, 5 mM BTTAA, 10  $\mu$ M 5/6-TAMRA-Azide-Biotin (Jena Bioscience), 5 mM sodium ascorbate, each from 100x stocks) were added to each sample, followed by an incubation period of one hour at room temperature and protected from light. Samples were separated by SDS-PAGE and analyzed for fluorescent protein-compound conjugates as described above.

### Western Blotting

Proteins were transferred to a polyvinylidene fluoride (PVDF) or nitrocellulose membrane using a Trans-Blot Turbo system (BioRad, 1.3 A, 25 V, 10 min). The membranes were blocked with 5% (m/v) nonfat milk in PBS-T buffer and incubated with indicated primary antibodies (anti-UCHL1, 1:1000, Cell Signaling, D3T2E; anti-PARK7, 1:1000, Cell Signaling, D29E5; anti-Tubulin, 1:4000, Sigma, T6199; anti-Hemagglutinin, 1:1000, BioLegend, 16B12; anti-flag, 1:2000, Sigma, F3165; anti-Ubiquitin, 1:1000, Cell Signaling, P4D1; anti-Ubiquitin, 1:300, Santa Cruz, P4D1, sc-8017; anti-UCHL3, 1:1000, Proteintech, 12384-1-AP, anti-USP30, Sigma Aldrich, HPA016952, 1:1000, anti-Rac1 1:1000, Millipore, 05-389, anti-HtrA2 1:1000, Proteintech, 15775-1-AP, anti-USP7,

## Methods

1:1000, Abcam, ab190183) over night. Then the membranes were incubated with the respective secondary antibody (anti-mouse, 1:5000, Sigma, NXA931; anti-rabbit, 1:5000, Sigma, GENA934) coupled to horseradish peroxidase. The chemiluminescent reaction was initiated using a Clarity Western ECL substrate (BioRad) and images were taken on a ChemiDoc MP Imaging System (BioRad).

### **Cellular Ub-probe competition**

Cells were cultured, treated with compound, and lysed as described above. The total protein concentration was adjusted to 2 mg/ml by diluting each sample with ABP lysis buffer. A final concentration of 1  $\mu$ M HA-Ub-VS probe was added, followed by an incubation for 10 min (All experiments with N-cyanopiperazine warhead probes) or 30 min (All other experiments) at 37 °C. The labelling reaction was quenched by the addition of 4x LDS sample buffer. The samples were separated via SDS-PAGE and further analyzed via western blotting as described above.

### **Identification of probe-labelled proteins with mass spectrometry**

Cells were cultured, treated with compound, and lysed as described above. The cell lysate was diluted to a protein concentration of 2 mg/mL with ABP lysis buffer. 1  $\mu$ L of each click reagent (see above) were added to each sample, followed by an incubation period of one hour at room temperature with protection from light. The sample volume was adjusted to 1000  $\mu$ L with PBS and 30  $\mu$ L of a NeutrAvidin (ThermoFisher) bead slurry (prewashed 3x with PBS) were added to each sample. The samples were incubated for one hour to overnight on a rotator at 15 rpm at 4 °C. Beads were pelleted by centrifugation, the supernatant was discarded, and the beads were washed six times (1x with  $\frac{1}{2}$ x lysis buffer, followed by five washes with PBS). After removing the washing solution completely, the beads were subjected to reduction with dithiothreitol (1 mM), alkylation with chloroacetamide (5 mM) and on-bead digestion with first LysC (Serva Biotech, 1 h, 37 °C) followed by trypsin (Sigma Aldrich, 1 h, overnight). Tryptic peptides were desalted with C18 StageTips and analyzed by nano-HPLC-MS/MS. An Ultimate 3000 RSLC nano-HPLC system and a Hybrid-Orbitrap mass spectrometer (Q Exactive Plus) equipped with a nano-spray source (ThermoFisher Scientific) was used. The protein fragments were enriched on a C18 PepMap 100 column (5  $\mu$ m, 100 Å, 300  $\mu$ m ID \* 5 mm, Dionex) using 0.1% TFA, at a flow rate of 30  $\mu$ L/min, for 5 min and separated on a C18 PepMap 100 column (3  $\mu$ m, 100 Å, 75  $\mu$ m ID \* 50 cm) using a linear gradient (5-30% ACN/H<sub>2</sub>O + 0.1% formic acid over 90 min) with a flow rate

## Methods

of 300 nL/min. The nano-HPLC apparatus was coupled online with the mass spectrometer using a standard coated Pico Tip emitter (ID 20  $\mu\text{m}$ , Tip-ID 10  $\mu\text{M}$ , New Objective). Signals in the mass range of  $m/z$  300 to 1650 were acquired at a resolution of 70,000 for full scan, followed by ten high-energy collision-dissociation (HCD) MS/MS scans of the most intense at least doubly charged ions at a resolution of 17,500. Proteins were relatively quantified by using MaxQuant<sup>[204]</sup> v.2.0.3.1, including the Andromeda search algorithm and searching the *Homo sapiens* reference proteome of the UniProt database. Briefly, an MS/MS ion search was performed for enzymatic trypsin cleavage, allowing two missed cleavages. Carbamidomethylation was set as a fixed protein modification, and oxidation of methionine and acetylation of the N-terminus were set as variable modifications. The mass accuracy was set to 20 parts per million (ppm) for the first search, and to 4.5 ppm for the second search. The false discovery rates for peptide and protein identification were set to 0.01. Only proteins for which at least two peptides were quantified were chosen for further validation. Relative quantification of proteins was performed by using the label-free quantification algorithm implemented in MaxQuant. Statistical data analysis of pulldown samples was performed using Perseus<sup>[205]</sup> v.1.6.15.0 including proteins which were identified in at least four of the five biological replicates which were used per condition. Label-free quantification (LFQ) intensities were log-transformed ( $\log_2$ ); replicate samples were grouped together. Pairwise comparisons of groups were performed separately. Missing values were imputed using small normally distributed values (width 0.3, down shift 1.8) and a two-sided  $t$ -test ( $s_0=5$ , FDR=0.001) was performed. Enrichment numbers of different proteins are difficult to compare as some (e.g. UCHL1) were measured in the DMSO control samples (owing e.g. to high abundance in proteome) while for others the enrichment number is a result of the imputation as the protein was not quantified in the control condition. The three enriched proteins for GK13S (UCHL1, PARK7 and C21orf33) were observed not only in the shown experiment with biological replicates, but also in two other fully independent experiments.

### **Quantification of monoubiquitin levels in U-87 MG cells**

U-87 MG cells ( $5 \times 10^5$  / well) were seeded in six well plates and cultivated for 8 h. Cells were transfected with siRNA as described above. On the next day, cells were cultured in fresh media supplemented with either compounds (final conc. 5  $\mu\text{M}$ ) or DMSO, where indicated, for further 48 h. The media was replaced with fresh medium supplemented with compounds (final conc. 5  $\mu\text{M}$ ) or DMSO every 24 h. Cells were washed with ice cold PBS (1x) and lysed for 15 min at 4 °C in 100-200  $\mu\text{L}$  ABP lysis buffer (50 mM Tris pH 7.5, 150 mM NaCl, 5% (w/v) glycerol, 1%

## Methods

(v/v) IGEPAL, cOmplete protease inhibitor cocktail supplemented with 2 mM EDTA, 10 mM chloroacetamide (CAA). Lysed cells were scrapped off the dish, cleared by centrifugation and the protein concentration was determined via a Bradford assay. The cell lysate was diluted to a protein concentration of 1.3-2.0 mg/mL with ABP lysis buffer. Proteins were separated via SDS-PAGE and analyzed via western blot as described above. Densitometric quantification of bands was carried out using ImageJ (version 1.53o). Monoubiquitin band intensities were first normalized to  $\alpha$ -tubulin and subsequently normalized to the intensities of monoubiquitin bands in the sample treated with DMSO or siScr (where no DMSO was used) which was set to '1'.

### Rescue of mono-Ub levels

U-87 MG cells ( $4 \times 10^5$  / well) were seeded in six well plates and cultivated for 8 h. Cells were transfected with siRNA as described above. On the next day, cells were cultured in fresh media for further 48 h. Cells were washed with ice cold PBS (1x) and lysed for 15 min at 4 °C in 100-200  $\mu$ L ABP lysis buffer (50 mM Tris pH 7.5, 150 mM NaCl, 5% (w/v) glycerol, 1% (v/v) IGEPAL, cOmplete protease inhibitor cocktail, 10 mM chloroacetamide (CAA), NO EDTA was added. Cells were harvested as described above. The total protein concentration in each sample was adjusted to 2 mg/mL. CAA was quenched by the addition of DDT (20 mM) and indicated DUBs (2  $\mu$ M final concentration) or hydroxylamine were added to the lysate and incubated for 1 h at 4 °C. Proteins were separated via SDS-PAGE and analyzed via western blot as described above. Densitometric quantification of bands was done as described above.

### Proteomics based whole proteome digestion

U-87 MG cells ( $5 \times 10^5$  / well) were seeded in six well plates and cultivated for 24 h. Cells were treated with either the indicated compounds (2  $\mu$ M final concentration) or DMSO and incubated for 48 h. The medium was replaced every 24 h with fresh medium supplemented with compound (2  $\mu$ M final concentration) or DMSO. The cells were washed with ice cold PBS and stored at -80 °C until sample preparation. The sample preparation, LC-MS/MS measurements and data processing were done at the Analytics Core Facility Essen (ACE). The SP3 bead capture and digestion of the proteome was done according to a recently published SP3 protocol.<sup>[206]</sup> A volume that includes a total amount of 15  $\mu$ g protein per sample was taken up in 100  $\mu$ L SP3 lysis buffer (5 % (w/v) SDS, 10 mM TCEP, 40 mM chloroacetamide, 200 mM HEPES pH 8) and heated for 5 min at 90 °C. After cooling the samples to room temperature, a mixture of 150  $\mu$ g each hydrophilic

## Methods

and hydrophobic SeraMag Speed Beads (Cytiva) were added to the lysate (bead to protein ratio 10:1). One volume EtOH (100 %, v/v) was added to the suspension and incubated for 20 min, 24 °C, 1200 rpm (Thermomixer, Eppendorf). The beads were collected on a magnet and washed with EtOH (80 %, v/v, 4x). The beads were taken in a 25 mM ammoniumbicarbonate solution supplemented with 1 µg trypsin and sonicated for 5 min at 37 °C. Samples were incubated overnight, 37 °C, 1300 rpm (Thermomix). The trypsin was quenched by adding concentrated formic acid (FA, final conc. 1 % v/v). The beads were collected on a magnet and the supernatant was collected in a fresh Eppendorf cup. The samples were desalted via C18 StageTip desalting according to a procedure described previously.<sup>[207]</sup> After elution the samples were dried in a vacuum concentrator (Eppendorf) and the peptides were taken up in 0.1 % FA solution (10 µL) which was completely used for LC-MS/MS measurements. MS Experiments were performed on an Orbitrap Fusion LUMOS instrument (Thermo) coupled to an EASY-nLC 1200 ultra-performance liquid chromatography (UPLC) system (Thermo). The UPLC was operated in the one-column mode. The analytical column was a fused silica capillary (75 µm × 41 cm) with an integrated fritted emitter (CoAnn Technologies) packed in-house with Kinetex 1.7 µm C18-XB core shell beads (Phenomenex). The analytical column was encased by a column oven (Sonation PRSO-V2) and attached to a nanospray flex ion source (Thermo). The column oven temperature was set to 50 °C during sample loading and data acquisition. The LC was equipped with two mobile phases: solvent A (0.2% FA, 2% Acetonitrile, ACN, 97.8% H<sub>2</sub>O) and solvent B (0.2% FA, 80% ACN, 19.8% H<sub>2</sub>O). All solvents were of UPLC grade (Honeywell). Peptides were directly loaded onto the analytical column with a flow rate of 0.4 – 0.6 µL/min. Peptides were subsequently separated on the analytical column by running a 105 min gradient of solvent A and solvent B (start with 3% B; gradient 3% to 9% B for 6:30 min; gradient 9% to 30% B for 62:30 min; gradient 30% to 50% B for 24:00 min; 50% to 100% B for 2:30 min; 100% for 9:30 min) at a flow rate of 300 nL/min. The mass spectrometer was controlled by the Orbitrap Fusion Lumos Tune Application (version 3.3.2782.28) and operated using the Xcalibur software (version 4.3.73.11). The mass spectrometer was set in the positive ion mode. The ionization potential (spray voltage) was set to 2.5 kV. Source fragmentation was turned off. Precursor ion scanning was performed in the Orbitrap analyzer (FT; fourier transform mass spectrometer) in the scan range of m/z 375-1500 and at a resolution of 240000 with the internal lock mass option turned on (lock mass was 445.120025 m/z, polysiloxane) AGC (automatic gain control) was set to “standard” and acquisition time to “auto”. Product ion spectra were recorded in a data dependent fashion in the IT (ion trap) in a variable scan range (“auto”) and at “rapid” scan rate. Peptides were analyzed using a “top speed” regime (repeating cycle of full precursor ion scan (AGC target “standard”); acquisition time



## Methods

“auto”) followed by dependent MS2 scans for 3 seconds (minimum intensity threshold  $4 \times 10^3$ ). The MS2 precursor ions were isolated using the quadrupole (isolation window 1.6 m/z) and fragmentation was achieved by stepped Higher-energy C-trap dissociation (sHCD) (normalized collision mode set to “stepped” and normalized collision energy set to “27, 32, 40%”). During MS2 data acquisition dynamic ion exclusion was set to 60 seconds with mass tolerance  $\pm 10$  ppm. Only charge states between 2-7 were considered for fragmentation. RAW spectra were submitted to an Andromeda<sup>[208]</sup> search in MaxQuant (v2.0.3.0)<sup>[204]</sup> using the default settings. The MS/MS spectra data were searched against the Uniprot *H. sapiens* reference database. All searches included a contaminants database search. Enzyme specificity was set to “Trypsin/P” with two missed cleavages allowed. The instrument type in Andromeda searches was set to Orbitrap and the precursor mass tolerance was set to  $\pm 20$  ppm (first search) and  $\pm 4.5$  ppm (main search). The MS/MS match tolerance was set to  $\pm 0.5$  Da. Minimum peptide length was 7 aa. For protein quantification unique and razor peptides were allowed. Modified peptides were allowed for quantification. The minimum score for modified peptides was 40. Label-free protein quantification was switched on, and unique and razor peptides were considered for quantification with a minimum ratio count of 2. Retention times were recalibrated based on the built-in nonlinear time-rescaling algorithm. MS/MS identifications were transferred between LC-MS/MS runs with the “match between runs” option in which the maximal match time window was set to 0.7 min and the alignment time window set to 20 min. The quantification is based on the “value at maximum” of the extracted ion current. At least two quantitation events were required for a quantifiable protein. Further analysis and filtering of the results was done in Perseus<sup>[209]</sup> v1.6.10.0. For quantification related biological replicates were combined to categorical groups. Only those proteins that were found in at least one categorical group in a minimum of 3 out of 4 biological replicates were investigated. Comparison of protein group quantities (relative quantification) between different MS runs is based solely on the LFQ’s as calculated by MaxQuant, MaxLFQ algorithm.

### **Quantification of Rac1 and HtrA2 levels in U-87 MG cells**

U-87 MG cells ( $7 \times 10^5$  / well) were seeded in six well plates and cultivated for 24 h. The medium was aspirated and replaced with fresh medium supplemented with either GK13S or DMSO (5  $\mu$ M final concentration) and incubated for 24-72 h. The medium was replaced every 24 h for fresh medium supplemented with the probe or DMSO. Cells were lysed and harvested as described above. The cell lysate was diluted to a protein concentration of 3.0 mg/mL with ABP lysis buffer. Proteins were separated via SDS-PAGE and analyzed via western blot as described above.

## Methods

Densitometric quantification of bands was carried out using ImageJ (version 1.53o). Rac1 and HtrA2 band intensities were first normalized to  $\alpha$ -tubulin and subsequently normalized to the intensities of Rac1 and HtrA2 bands in the sample treated with DMSO which was set to '1'.

### **Substrate trapping**

HEK293 cells ( $6 \times 10^5$  / well) were seeded in six well plates and cultivated for 24 h. The medium was aspirated and replaced with fresh medium supplemented with either GK13S or DMSO (5  $\mu$ M final concentration) and incubated for 4 h. GFP alone or GFP-tagged UCHL1 versions were overexpressed as described above. The medium was replaced every 24 h with fresh medium supplemented with GK13S or DMSO and cells were cultivated for 48 h. Cells were harvested as described above. Cell lysates were diluted to a total protein concentration of 2 mg/mL. Each sample was further diluted in dilution buffer (10 mM Tris pH 7.5, 150 mM NaCl, 0.5 mM EDTA) to 0.5 mg/mL total protein concentration. GFP-Trap<sup>®</sup> Agarose bead (chromotek) were equilibrated according to the user manual. 25  $\mu$ L of bead slurry was added to each sample and rotated for 1 h at 4 °C. Beads were sedimented by centrifugation and the supernatant was aspirated. Beads were washed in wash buffer (50 mM Tris pH 8.0, 150 mM NaCl, 0.1 % (v/v) IGEPAL) (500  $\mu$ L, 3x). Beads were boiled for 5 min at 95 °C in 4 x LDS sample buffer. Eluted proteins were separated via SDS-PAGE as described above. To visualize trapped proteins, gels were silver stained using a kit (BioRad) and following the user instructions.

### **Target engagement in cell lysates**

Cells were seeded in 10 cm dishes and cultured to 90 % confluency. Cells were harvested and lysed as described above. Lysates were treated with the compounds and incubated for 1 h or 4 h (all experiments with N-cyanopiperazine warhead probes). Then, all samples were incubated with the HA-Ub-VS probes as described above. The reaction with the Ub-probe was quenched by the addition of 4xLDS-sample buffer. Proteins were separated via SDS-PAGE and analyzed via western blot as described above.

### **Non-alkyne compound competition**

HEK293 cells ( $6 \times 10^5$ /well) were seeded in 6-well plates and cultured for 24 h. Cells were treated with the indicated non-alkyne derivatives or DMSO and incubated for 24 h. The same cells were

## Methods

then treated with either GK13S or DMSO and incubated for 24 h. Cells were lysed and harvested as described above. The CuAAC was initiated following the procedure described above. Proteins were separated via SDS-PAGE and the fluorescence was read out using the Alexa564 ( $\lambda_{\text{ex/em}}$  520–545/577–613 nm, for TAMRA) and Alexa680 ( $\lambda_{\text{ex/em}}$  650–675/700–730 nm, for the PageRuler Prestained NIR Protein Ladder (Thermo Scientific)) channels on a ChemiDoc MP Imaging System (Bio-Rad).

### **Gel-based pull-down assay**

HEK293 cells ( $6 \times 10^5$ /well) were cultured and treated with indicated compounds as described above. Cells were lysed for 15 min, 4 °C with HEPES based ABP lysis buffer (150  $\mu$ L) (50 mM HEPES pH 8.0, 150 mM NaCl, 5 % (v/v) Glycerol, 1 % (v/v) IGEPAL + 1 x PIC). Lysate was harvested by scraping and cell remnants were removed by centrifugation at 14 000 rpm, 15 min, 4 °C. The total protein concentration was determined via Bradford assay and 400  $\mu$ L of each sample was diluted to 4 mg/mL with ABP lysis buffer. The copper-catalyzed alkyne-azide cycloaddition was initiated by adding 952  $\mu$ L PBS, 8  $\mu$ L Biotin/TAMRA-PEG6-azide (12.5  $\mu$ M final conc., from 100 x stock in water), 80  $\mu$ L BTTAA (5 mM final conc., from 20 x stock in water), 80  $\mu$ L  $\text{CuSO}_4 \times 5 \text{H}_2\text{O}$  (1  $\mu$ M final conc., from 20 x stock in water), 80  $\mu$ L sodium ascorbate (15 mM final concentration, from 20 x stock) were added to each sample and incubated for 60 min at room temperature, protected from light. NeutrAvidin agarose beads were washed with ice cold PBS (3 x 1 mL, 0.5 g, 1 min) and 60  $\mu$ L of bead slurry was added to 100  $\mu$ L of each sample. Samples were incubated on a rotator at 10 °C, 15 rpm, overnight. The supernatant was aspirated and the Proteins were eluted in 50  $\mu$ L LDS-sample buffer at 95 °C for 10 minutes. Proteins were separated via SDS-PAGE and further analysed by western blotting.

### **Lysate compound reversibility**

HEK293 cells ( $3 \times 10^5$  / well) were cultured, treated with indicated compound and harvested as described above. The lysate was diluted to a total protein concentration of 2 mg/mL. The lysate was incubated on ice and a sample for HA-Ub-VS treatment was taken at the indicated time points. Proteins were separated via SDS-PAGE and further analyzed via western blotting.

### Induced degradation of DUBs

HEK293 cells ( $7 \times 10^5$ ) were cultured for 48 h. Cells were either treated with the PROTACs or controls compounds at indicated concentrations for 24 h. The cells were harvested and lysed as described above. Total protein concentration was adjusted to 2 mg/mL and proteins were separated via SDS-PAGE. Samples were further analyzed via western blotting for either decreased USP7 or UCHL1 band intensity. In case of USP7, band intensities were first normalized to  $\alpha$ -tubulin and subsequently normalized to the intensities of USP7 bands in the sample treated with DMSO which was set to '1'.

### 5.2 Chemical synthesis

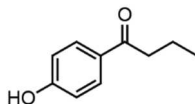
Chemicals and solvents were used without further purification, and purchased from companies such as Acros, Activate Scientific, Alfa Aesar, Fluorchem, Merck, Novabiochem, Roth, Sigma-Aldrich, TCI and VWR. Solvents used for all synthetic steps were named as follows. EA: ethyl acetate, DCM: dichloromethane, MeOH: methanol, PE: petroleum ether, CH: cyclohexane, DMF: dimethylformamide, THF: tetrahydrofuran, ACN: acetonitrile, H<sub>2</sub>O: water, EtOH: ethanol. Thin-layer chromatography was carried out using silica gel aluminum plates (silica gel 60 F254, Merck). The detection was carried out using UV light ( $\lambda = 254/366$  nm) and potassium permanganate or ninhydrin solution as staining reagents. For purification via column chromatography, silica gel 60 (60Å, 0.035-0.070 mm, Sigma Aldrich) was used. Automated column chromatographic purification was carried out on a Pure C-850 FlashPrep system or a Pure-C-810 Flash system (Büchi). For preparative HPLC, an 1260/1290 Infinity II series system (Agilent Technologies) with a VP125/21 Nucleodur C18 Gravity column (5  $\mu$ m, Macherey Nagel) was used. For low resolution LC-MS analysis, a 1200 series HPLC system (Agilent Technologies) with a ZORBAX Eclipse XDB column (C18 80 Å; 4.6 x 150 mm; 5  $\mu$ m) was used. High resolution mass spectrometry (HRMS) was carried out with an LTQ Orbitrap (Thermo Fisher). NMR spectra were recorded on the following devices (all from Bruker): AV 400 Avance III HD (400 MHz for <sup>1</sup>H and 101 MHz for <sup>13</sup>C-NMR), AV 500 Avance III HD (500 MHz for <sup>1</sup>H and 125 MHz for <sup>13</sup>C-NMR), AV 600 Avance III HD (600 MHz for <sup>1</sup>H and 151 MHz for <sup>13</sup>C NMR) and AV 700 Avance III HD (700 MHz for <sup>1</sup>H and 176 MHz for <sup>13</sup>C NMR). The chemical shifts of all spectra are specified in ppm. The coupling constants *J* are given in Hertz (Hz). Peaks are referenced to used deuterated solvent (DMSO-*d*<sub>6</sub>:  $\delta = 2.50$  ppm / 39.52 ppm; CDCl<sub>3</sub>:  $\delta = 7.26$  ppm / 77.16 ppm; MeOH-*d*<sub>4</sub>:  $\delta = 4.87$  ppm / 49.15 ppm). The

## Methods

multiplicities of the signals in the  $^1\text{H}$  spectra are abbreviated as follows. s (singlet), d (doublet), dd (doublet of doublets), t (triplet), td (triplet of doublets), q (quartet), m (multiplet) and b (broad).

### 5.2.1 Preparation of probe molecules MS037 and MS023

#### 1-(4-Hydroxyphenyl)butan-1-one (9, MS005)



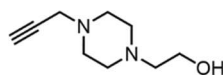
Phenol (500 mg, 5.31 mmol, 1.0 eq) was dissolved in neat triflic acid (TfOH, 4 mL) at 0 °C. The solution was stirred for 10 min. Butyryl chloride (550  $\mu\text{L}$ , 5.31 mmol, 1.0 eq) was added dropwise at 0 °C. The ice bath was removed, and the reaction mixture was stirred for 1 h at room temperature. The reaction mixture was then poured into cold  $\text{H}_2\text{O}$  and extracted with EA (3x10 mL). The organic layers were combined and washed with aq. 1 M HCl solution (1x10 mL), sat.  $\text{NaHCO}_3$  (1x10 mL) and brine (1x10 mL). The organic phase was dried over  $\text{MgSO}_4$  and the solvent was evaporated under reduced pressure. The crude product was purified by column chromatography (0-40% EA in PE) to yield MS05 (800 mg, 4.87 mmol, 92%) as a white solid.

$^1\text{H NMR}$  (600 MHz,  $\text{DMSO}-d_6$ )  $\delta$  (ppm) = 10.30 (s, 1H), 7.87-7.82 (m, 2H), 6.87-6.82 (m, 2H), 2.88 (t,  $J = 7.2$  Hz, 2H), 1.61 (h,  $J = 7.3$  Hz, 2H), 0.92 (t,  $J = 7.4$  Hz, 3H).

$^{13}\text{C NMR}$  (151 MHz,  $\text{DMSO}-d_6$ )  $\delta$  (ppm) = 198.11, 161.85, 130.39, 128.42, 115.17, 39.52, 17.54, 13.73.

**LC-MS**  $m/z$  for  $\text{C}_{10}\text{H}_{13}\text{O}_2^+$  ( $[\text{M}+\text{H}]^+$ ) calculated: 165.08, found: 165.10.

#### 2-(4-(Prop-2-yn-1-yl)piperazin-1-yl)ethan-1-ol (11, MS006)



2-(Piperazin-1-yl)ethan-1-ol (50 mg, 0.38 mmol, 1.0 eq) was dissolved in acetone (2 mL).  $\text{K}_2\text{CO}_3$  (52 mg, 0.38 mmol, 1.0 eq) was added and the reaction mixture was cooled to 0 °C. Propargyl bromide (32  $\mu\text{L}$ , 0.38 mmol, 1.0 eq) was dissolved in acetone (2 mL) and added dropwise to the reaction mixture. The ice bath was removed, and the reaction mixture was allowed to stir overnight at room temperature. The solvent was evaporated under reduced pressure. The crude product

## Methods

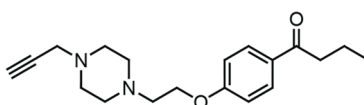
was purified by column chromatography (aluminum oxide, 0-10% MeOH in DCM) without aqueous work up, to yield MS06 (16.4 mg, 0.1 mmol, 25%) as a light-yellow solid.

**<sup>1</sup>H NMR** (400 MHz, DMSO-*d*<sub>6</sub>) δ (ppm) = 4.35 (t, *J* = 5.4 Hz, 1H), 3.47 (td, *J* = 6.3, 5.3 Hz, 2H), 3.22 (d, *J* = 2.4 Hz, 2H), 3.12 (t, *J* = 2.4 Hz, 1H), 2.48-2.30 (m, 10H).

**<sup>13</sup>C NMR** (101 MHz, DMSO-*d*<sub>6</sub>) δ (ppm) = 79.45, 75.57, 60.23, 58.55, 53.03, 51.15, 46.00.

**HRMS** *m/z* for C<sub>9</sub>H<sub>17</sub>N<sub>2</sub>O<sup>+</sup> ([M+H]<sup>+</sup>) calculated: 169.1335, found: 169.1333.

### 1-(4-(2-(4-(Prop-2-yn-1-yl)piperazin-1-yl)ethoxy)phenyl)butan-1-one (12, MS016)



2-(4-(Prop-2-yn-1-yl)piperazin-1-yl)ethan-1-ol (214 mg, 1.27 mmol, 1.0 eq), 1-(4-hydroxyphenyl)butan-1-one (209 mg, 1.27 mmol, 1.0 eq) and triphenylphosphine (PPh<sub>3</sub>) (400 mg, 1.53 mmol, 1.2 eq) were dissolved in anhydrous THF (5 mL) under argon atmosphere. The mixture was cooled to 0 °C. Diisopropyl azodicarboxylate (DIAD) (400 μL, 2.04 mmol, 1.6 eq) was dissolved in anhydrous THF (7.5 mL) and added dropwise to the reaction mixture. The solution was stirred for 10 min at 0 °C. The ice bath was removed, and the reaction was allowed to stir for 18 h at room temperature. The solvent was evaporated under reduced pressure. The resulting residue was washed with brine (1x20 mL). The aqueous phase was extracted with EA (3x20 mL). The crude product was purified by column chromatography (0-40% EA in PE and 0-10% MeOH in DCM) to obtain MS16 (279 mg, 0.89 mmol, 70%) as a white solid.

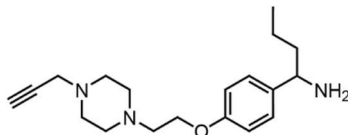
**<sup>1</sup>H NMR** (400 MHz, CDCl<sub>3</sub>) δ (ppm) = 7.95 (d, *J* = 8.9 Hz, 2H), 6.92 (d, *J* = 8.9 Hz, 2H), 4.50-4.41 (m, 2H), 3.72 (d, *J* = 2.6 Hz, 2H), 3.69-3.39 (m, 10H), 2.90 (t, *J* = 7.3 Hz, 2H), 2.59 (t, *J* = 2.5 Hz, 1H), 1.75 (h, *J* = 7.4 Hz, 2H), 1.00 (t, *J* = 7.4 Hz, 3H).

**<sup>13</sup>C NMR** (101 MHz, CDCl<sub>3</sub>) δ (ppm) = 199.23, 160.64, 131.70, 130.65, 114.30, 78.85, 72.46, 62.88, 56.15, 50.75, 48.09, 46.03, 40.45, 18.06, 14.03.

**HRMS** *m/z* for C<sub>19</sub>H<sub>27</sub>N<sub>2</sub>O<sub>2</sub><sup>+</sup> ([M+H]<sup>+</sup>) calculated: 315.2067, found: 315.2069.

## Methods

### 1-(4-(2-(4-(Prop-2-yn-1-yl)piperazin-1-yl)ethoxy)phenyl)butan-1-amine (13, MS024)



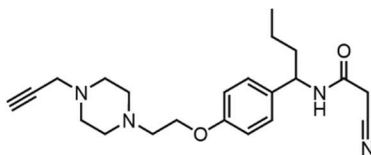
1-(4-(2-(4-(Prop-2-yn-1-yl)piperazin-1-yl)ethoxy)phenyl)butan-1-one (588 mg, 1.87 mmol, 1.0 eq) was dissolved in MeOH (20 mL) and ammonium acetate (4.325 g, 56.10 mmol, 30.0 eq) was added. The flask was charged with argon and a 1 M solution of NaBH<sub>3</sub>CN in dry THF (9 mL, 9.35 mmol, 5.0 eq) was added dropwise to the reaction mixture at room temperature. The mixture was heated to 40 °C and allowed to stir for 69 h. Thereafter the reaction was cooled to room temperature and diluted with EA (30 mL). The mixture was then washed with sat. NaHCO<sub>3</sub> solution (2 x 20 mL) and brine (1 x 20 mL). The aqueous phases were combined, and the pH was adjusted to 10 using aq. 2 M NaOH solution. Then the aqueous phase was extracted with EA (1 x 30 mL). The organic phases were combined, dried over MgSO<sub>4</sub> and the solvent was evaporated under reduced pressure. The crude product was isolated as a sticky yellow oil and was used for the next reaction without further purification.

<sup>1</sup>H NMR (500 MHz, DMSO-*d*<sub>6</sub>) δ (ppm) = 8.07 (s, 2H), 7.35 (d, *J* = 8.7 Hz, 2H), 7.00 (d, *J* = 8.8 Hz, 2H), 4.16 (dd, *J* = 9.4, 5.6 Hz, 1H), 4.07 (t, *J* = 5.8 Hz, 2H), 4.03 (q, *J* = 7.1 Hz, 2H), 3.24 (d, *J* = 2.4 Hz, 2H), 3.15 (t, *J* = 2.4 Hz, 1H), 2.68 (t, *J* = 5.4 Hz, 4H), 2.45 (s, 4H), 1.84-1.67 (m, 2H), 1.23 (s, 2H), 0.84 (t, *J* = 7.4 Hz, 3H).

<sup>13</sup>C NMR (126 MHz, DMSO-*d*<sub>6</sub>) δ (ppm) = 158.65, 131.55, 128.75, 114.70, 79.43, 75.72, 65.62, 59.79, 56.49, 53.65, 52.94, 45.99, 40.11, 39.85, 18.44, 14.11.

LC-MS *m/z* for C<sub>19</sub>H<sub>30</sub>N<sub>3</sub>O<sup>+</sup> ([M+H]<sup>+</sup>) calculated: 316.2383, found: 316.2385.

### 2-Cyano-*N*-(1-(4-(2-(4-(prop-2-yn-1-yl)piperazin-1-yl)ethoxy)phenyl)butyl)-acetamide (14, MS035)



## Methods

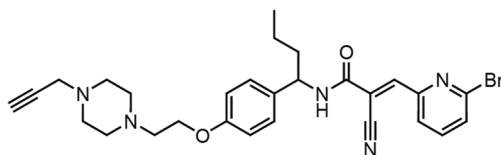
Cyanoacetic acid (95 mg, 1.12 mmol, 1.0 eq) was dissolved in dry DMF (2 mL) to which HATU (425 mg, 1.12 mmol, 1.0 eq) and HOAt (152 mg, 1.12 mmol, 1.0 eq) were added. The mixture was stirred for 30 min at room temperature, then cooled to 0 °C. 1-(4-(2-(4-(Prop-2-yn-1-yl)piperazin-1-yl)ethoxy)phenyl)butan-1-amine (353 mg, 1.12 mmol, 1 eq) was dissolved in dry DMF (2 mL) and added dropwise to the ice cold reaction mixture, followed by addition of DIPEA (419  $\mu$ L, 2.46 mmol, 2.2 eq). The ice bath was removed, and the reaction was allowed to stir for 4 h at room temperature. Afterwards the reaction mixture was diluted with EA (10 mL) and washed with sat. NaHCO<sub>3</sub> solution (2x10 mL) and brine (1x10 mL). The organic phase was dried over MgSO<sub>4</sub> and the solvent was evaporated under reduced pressure. The crude product was purified by column chromatography (0 – 15 % MeOH in DCM) to yield MS35 (68 mg, 0.18 mmol, 15% over two steps) as a sticky yellow oil.

**<sup>1</sup>H NMR** (500 MHz, DMSO-*d*<sub>6</sub>)  $\delta$  (ppm) = 8.58 (d, *J* = 8.3 Hz, 1H), 7.19 (d, *J* = 8.7 Hz, 2H), 6.89 (d, *J* = 8.7 Hz, 2H), 4.69 (q, *J* = 8.2 Hz, 1H), 4.07 (t, 2H), 3.71-3.57 (m, 2H), 3.27 (s, 2H), 3.18 (s, 1H), 2.63 (dt, *J* = 3.6, 1.8 Hz, 2H), 2.53-2.45 (m, 8H), 1.60 (dddd, *J* = 22.5, 15.5, 8.7, 5.0 Hz, 2H), 1.25 (ddd, *J* = 19.6, 15.4, 7.0 Hz, 2H), 0.85 (t, *J* = 7.4 Hz, 3H).

**<sup>13</sup>C NMR** (126 MHz, DMSO-*d*<sub>6</sub>)  $\delta$  (ppm) = 161.26, 157.25, 135.16, 127.57, 116.31, 114.30, 75.90, 54.95, 52.72, 52.30, 45.86, 38.23, 25.37, 19.08, 13.59.

**HRMS** *m/z* for C<sub>22</sub>H<sub>31</sub>N<sub>4</sub>O<sub>2</sub><sup>+</sup> ([M+H]<sup>+</sup>) calculated: 383.2442, found: 383.2443.

### **(E)-3-(6-Bromopyridin-2-yl)-2-cyano-N-(1-(4-(2-(4-(prop-2-yn-1-yl)piperazin-1-yl)ethoxy)phenyl)butyl)acrylamide (MS037)**



2-Cyano-*N*-(1-(4-(2-(4-(prop-2-yn-1-yl)piperazin-1-yl)ethoxy)phenyl)butyl)acetamide (58 mg, 0.15 mmol, 1.0 eq) was dissolved in EtOH (99%, absolute). Beta-alanine (203 mg, 2.27 mmol, 15 eq) and ddH<sub>2</sub>O (2 mL) were added, followed by 6-bromo-2-pyridinecarboxaldehyde (113 mg, 0.61 mmol, 4 eq). The reaction mixture was stirred for 18 h at room temperature. Afterwards the reaction mixture was diluted with EA (6 mL) and washed with sat. NaHCO<sub>3</sub> solution (2x10 mL) and brine (1x10 mL). The organic phase was dried over MgSO<sub>4</sub> and the solvent was evaporated under reduced pressure. The crude product was isolated as a crystalline yellow solid. The crude



## Methods

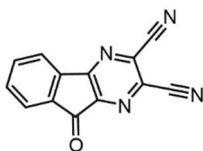
material was further purified by preparative HPLC (gradient B) to obtain MS37 (40 mg, 0.07 mmol, 48%) as a pale-yellow TFA salt. Synthesis route of probe **MS037** was based on patent WO2015054555A1.

**<sup>1</sup>H NMR** (500 MHz, CDCl<sub>3</sub>) δ (ppm) = 8.15 (s, 1H), 7.70 – 7.62 (m, 1H), 7.61 – 7.52 (m, 2H), 7.26 (d, *J* = 8.6 Hz, 2H), 6.89 – 6.81 (m, 2H), 4.98 (q, *J* = 7.5 Hz, 1H), 4.40 – 4.22 (m, 2H), 3.81 – 3.74 (m, 2H), 3.70 (s, 4H), 3.57 – 3.47 (m, 6H), 2.62 (s, 1H), 1.94 – 1.76 (m, 2H), 1.44 – 1.17 (m, 2H), 0.94 (t, *J* = 7.4 Hz, 3H).

**<sup>13</sup>C NMR** (126 MHz, CDCl<sub>3</sub>) δ (ppm) = 162.00 (q, *J* = 38.3 Hz), 158.97, 156.49, 150.88, 148.50, 142.51, 139.35, 135.39, 130.87, 128.20, 125.81, 115.85, 115.79 (d, *J* = 288.0 Hz), 114.82, 109.35, 79.45, 71.69, 62.49, 56.15, 54.26, 50.27, 47.81, 45.89, 38.02, 19.52, 13.80.

**HRMS** *m/z* for C<sub>28</sub>H<sub>33</sub>BrN<sub>5</sub>O<sub>2</sub><sup>+</sup> ([M+H]<sup>+</sup>) calculated: 550.1812, found: 550.1823.

### 9-Oxo-9*H*-indeno[1,2-*b*]pyrazine-2,3-dicarbonitrile (16, MS003)

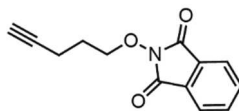


Ninhydrin (100 mg, 0.56 mmol, 1.0 eq) and diaminomaleonitrile (DAMN) (30 mg, 0.5 eq, 0.28 mmol) were dissolved in anhydrous EtOH (5 mL) and acetic acid (0.5 mL) was added. The mixture was stirred for 2 h at room temperature. The precipitated solid was filtered and washed with cold EtOH, to obtain MS03 (30 mg, 0.13 mmol, 23%) as a yellow solid. The product was used for the following reactions without further purification.

**<sup>1</sup>H NMR** (400 MHz, DMSO-*d*<sub>6</sub>) δ (ppm) = 8.11 (d, *J* = 7.5 Hz, 1H), 8.00-7.89 (m, 2H), 7.82 (td, *J* = 7.5, 1.1 Hz, 1H).

**<sup>13</sup>C NMR** (176 MHz, DMSO-*d*<sub>6</sub>) δ (ppm) = 186.49, 160.75, 150.86, 138.58, 137.83, 136.29, 135.29, 134.57, 132.44, 125.55, 124.11, 114.83.

**LC-MS** *m/z* for C<sub>13</sub>H<sub>5</sub>N<sub>4</sub>O<sup>+</sup> ([M+H]<sup>+</sup>) calculated: 233.04, found: 233.00.

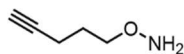
**2-(Pent-4-yn-1-yloxy)isoindoline-1,3-dione (18, MS015)**

4-Pentyn-1-ol (55  $\mu$ L, 0.59 mmol, 1.0 eq), *N*-hydroxyphthalimide (116 mg, 0.71 mmol, 1.2 eq) and triphenylphosphine (PPh<sub>3</sub>) (203 mg, 0.77 mmol, 1.3 eq) were dissolved in anhydrous THF (2 mL) under argon atmosphere. The mixture was then cooled to 0 °C. Diisopropyl azodicarboxylate (DIAD) (187  $\mu$ L, 0.95 mmol, 1.6 eq) was dissolved in anhydrous THF (2 mL) and added dropwise. The reaction mixture was stirred for 10 min at 0 °C, until complete dissolution. The ice bath was removed, and the reaction was allowed to stir overnight at room temperature. The solvent was evaporated under reduced pressure. The crude product was purified by column chromatography (0-40% EA in PE) to obtain MS15 (127 mg, 0.55 mmol, 93%) as a pale-yellow solid.

**<sup>1</sup>H NMR** (700 MHz, DMSO-*d*<sub>6</sub>)  $\delta$  (ppm) = 7.86 (s, 4H), 4.21 (t, *J* = 6.3 Hz, 2H), 2.81 (t, *J* = 2.7 Hz, 1H), 2.39 (td, *J* = 7.2, 2.6 Hz, 2H), 1.85 (p, *J* = 6.7 Hz, 2H).

**<sup>13</sup>C NMR** (176 MHz, DMSO-*d*<sub>6</sub>)  $\delta$  (ppm) = 163.34, 134.77, 128.61, 123.23, 83.53, 76.34, 71.63, 26.91, 14.24.

**LC-MS** *m/z* for C<sub>13</sub>H<sub>12</sub>NO<sub>3</sub><sup>+</sup> ([M+H]<sup>+</sup>) calculated: 230.07, found: 230.10.

**O-(Pent-4-yn-1-yl)hydroxylamine hydrochloride (19, MS020)**

2-(Pent-4-yn-1-yloxy)isoindoline-1,3-dione (300 mg, 1.31 mmol, 1.0 eq) was dissolved in anhydrous EtOH (10 mL). Hydrazine hydrate (63  $\mu$ L, 1.96 mmol, 1.5 eq) was added, the reaction mixture was heated to reflux and stirred for 3 h. The reaction was quenched by adding a solution of sat. NaHCO<sub>3</sub>. The aqueous phase was extracted with DCM (3x10 mL). The combined organic layers were washed with brine and dried over Na<sub>2</sub>SO<sub>4</sub>. The solvent was removed under reduced pressure. The resulting slurry was dissolved in 2 N HCl in Et<sub>2</sub>O (2 mL) and the solvent was removed *in vacuo*. The formed precipitate was washed with cold Et<sub>2</sub>O and collected by vacuum

## Methods

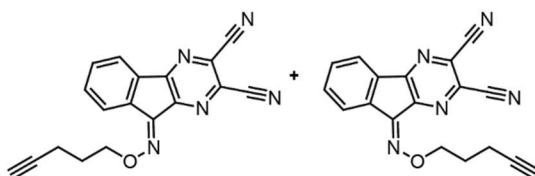
filtration to yield MS20 (59 mg, 0.60 mmol, 45%) as a white solid. The product was used for the next reaction without further purification.

**<sup>1</sup>H NMR** (500 MHz, DMSO-*d*<sub>6</sub>) δ (ppm) = 11.05 (s, 2H), 4.07 (t, *J* = 6.4 Hz, 2H), 2.88 (t, *J* = 2.7 Hz, 1H), 2.24 (td, *J* = 7.2, 2.7 Hz, 2H), 1.78 (p, *J* = 6.8 Hz, 2H).

**<sup>13</sup>C NMR** (126 MHz, DMSO-*d*<sub>6</sub>) δ (ppm) = 83.76, 73.16, 72.40, 26.73, 14.70.

**LC-MS** *m/z* for C<sub>5</sub>H<sub>10</sub>NO<sup>+</sup> ([M+H]<sup>+</sup>) calculated: 100.07, found: 100.07.

### 9-((Pent-4-yn-1-yloxy)imino)-9*H*-indeno[1,2-*b*]pyrazine-2,3-dicarbonitrile (MS23)



9-Oxo-9*H*-indeno[1,2-*b*]pyrazine-2,3-dicarbonitrile (30 mg, 0.13 mmol, 1.0 eq) was dissolved in pyridine (5 mL). The mixture was cooled to 0 °C and *O*-(pent-4-yn-1-yl)hydroxylamine hydrochloride (53 mg, 0.39 mmol, 3.0 eq) was added. The reaction mixture was warmed to room temperature and molecular sieves (3 Å) were added. The reaction mixture was heated to 60 °C and stirred for 2 h. Afterwards the mixture was cooled to room temperature and the pyridine was evaporated under reduced pressure. The residue was dissolved in sat. aq. NH<sub>4</sub>Cl (10 mL) solution and the aqueous phase was extracted with EA (3x10 mL). The organic layers were combined, dried over Na<sub>2</sub>SO<sub>4</sub> and the solvent was evaporated under reduced pressure. The crude product was purified by preparative HPLC (Gradient A) to obtain MS23 (11 mg, 0.04 mmol, 27%, anti/syn-mixture) as a pale-yellow solid.

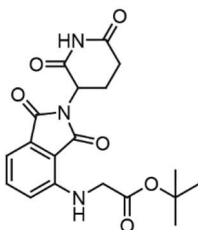
**<sup>1</sup>H NMR** (500 MHz, DMSO-*d*<sub>6</sub>) δ (ppm) = 8.42 (d, *J* = 7.0 Hz, 1H), 8.22 (d, *J* = 6.9 Hz, 1H), 8.12 (d, *J* = 7.1 Hz, 1H), 7.97 (d, *J* = 7.3 Hz, 1H), 7.92-7.80 (m, 2H), 7.80-7.70 (m, 2H), 4.67 (t, *J* = 6.3 Hz, 2H), 4.61 (t, *J* = 6.4 Hz, 2H), 2.87 (t, *J* = 2.6 Hz, 1H), 2.85 (t, *J* = 2.6 Hz, 1H), 2.43 - 2.37 (m, 2H), 2.37-2.33 (m, 2H), 2.10-2.03 (m, 2H), 2.02-1.96 (m, 2H).

**<sup>13</sup>C NMR** (126 MHz, DMSO-*d*<sub>6</sub>) δ (ppm) = 155.70, 155.09, 151.28, 145.93, 145.33, 145.20, 136.72, 134.58, 134.16, 133.77, 133.18, 132.77, 132.38, 132.28, 131.99, 131.68, 131.01, 130.71, 128.79, 123.53, 123.48, 121.83, 114.80, 114.67, 114.54, 83.57, 83.53, 76.37, 75.95, 71.99, 71.86, 39.85, 27.90, 27.69, 14.53, 14.27.

**HRMS** *m/z* for C<sub>18</sub>H<sub>12</sub>N<sub>5</sub>O<sup>+</sup> ([M+H]<sup>+</sup>) calculated: 314.1036, found: 314.1034.

### 5.2.2 Preparation of UCHL1 PROTACs

#### *tert*-butyl (2-(2,6-dioxopiperidin-3-yl)-1,3-dioxoisindolin-4-yl)glycinate (**36**, MS095)



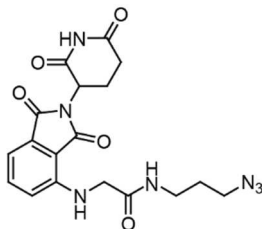
2-(2,6-Dioxopiperidin-3-yl)-4-fluoroisindoline-1,3-dione (550 mg, 2.0 mmol, 1.0 eq.) and *tert*-butyl glycinate (272  $\mu$ L, 2.0 mmol, 1.0 eq.) were dissolved in dry DMSO (20 mL). DIPEA (677  $\mu$ L, 4.0 mmol, 2.0 eq.) was added and the reaction mixture was allowed to stir for 18 h at 90 °C. The reaction was diluted with ethyl acetate (10 mL), washed with water (10 mL) and brine (10 mL) and dried over Na<sub>2</sub>SO<sub>4</sub>. The crude product was purified by column chromatography (normal phase 50 % EA in DCM), to yield the title compound (504 mg, 1.3 mmol, 65 %) as a yellow oil.

**<sup>1</sup>H NMR** (500 MHz, DMSO-*d*<sub>6</sub>)  $\delta$  (ppm) = 11.12 (s, 1H), 7.79 (d, *J* = 7.3 Hz, 1H), 7.61 – 7.56 (m, 1H), 6.97 (d, *J* = 8.6 Hz, 1H), 5.07 (dd, *J* = 12.8, 5.4 Hz, 1H), 4.09 (d, *J* = 6.0 Hz, 2H), 2.89 (ddd, *J* = 17.1, 13.9, 5.4 Hz, 2H), 2.05 (ddd, *J* = 13.0, 7.6, 2.2 Hz, 2H), 1.43 (s, 9H).

**<sup>13</sup>C NMR** (126 MHz, DMSO)  $\delta$  (ppm) = 173.33, 170.55, 170.18, 169.73, 146.34, 136.61, 132.47, 118.22, 111.67, 110.20, 81.75, 60.25, 44.89, 31.44, 28.19, 21.24.

**LC-MS** *m/z* for C<sub>19</sub>H<sub>21</sub>N<sub>3</sub>O<sub>6</sub>Na<sup>+</sup> ([M+Na]<sup>+</sup>) calculated: 410.1, found: 410.0.

#### *N*-(3-azidopropyl)-2-((2-(2,6-dioxopiperidin-3-yl)-1,3-dioxoisindolin-4-yl)amino)acetamide (MS099)



## Methods

MS095 (504 mg, 1.3 mmol, 1.0 eq.) was dissolved in DCM (20 mL) supplemented with 20 % TFA. The reaction mixture was allowed to stir for 2 h at RT. After full conversion the solvent was evaporated under reduced pressure. This intermediate was used for the next reaction step without further purification.

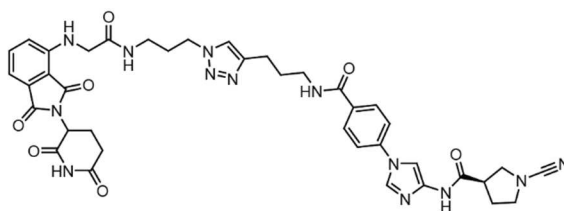
Deprotected MS095 (80 mg, 0.24 mmol, 1.2 eq) was dissolved in dry DMF (1 mL). DIPEA (136  $\mu$ L, 0.8 mmol, 4.0 eq.) and HATU (152 mg, 0.4 mmol, 2.0 eq.) were added. The mixture was allowed to stir for 10 minutes at RT. 3-Azidopropan-1-amine (20 mg, 0.2 mmol, 1.0 eq.) was dissolved in dry DMF (1 mL) and added dropwise to the reaction. The mixture was allowed to stir for 4 h at RT. The reaction was diluted with EA (20 mL), washed with brine (3 x 20 mL) and dried over MgSO<sub>4</sub>. The crude product was purified via column chromatography (normal phase, 0 – 20 % MeOH in DCM) and afterwards by preparative chromatography (reversed phase, 20 – 90 % ACN in H<sub>2</sub>O). This resulted in the title compound (18 mg, 0.04 mmol, 22 %) as a yellow solid.

**<sup>1</sup>H NMR** (700 MHz, Chloroform-*d*)  $\delta$  (ppm) = 8.07 (s, 1H), 7.60 – 7.53 (m, 1H), 7.25 (s, 1H), 6.82 (d, *J* = 8.4 Hz, 1H), 4.94 (dd, *J* = 12.6, 5.4 Hz, 1H), 3.97 (d, *J* = 6.1 Hz, 2H), 3.51 – 3.48 (m, 1H), 3.37 (dt, *J* = 7.9, 6.8 Hz, 2H), 2.94 – 2.72 (m, 4H), 1.99 – 1.94 (m, 1H), 1.77 (p, *J* = 6.7 Hz, 2H).

**<sup>13</sup>C NMR** (151 MHz, Chloroform-*d*)  $\delta$  (ppm) = 170.89, 169.51, 169.20, 168.31, 167.38, 145.98, 136.84, 132.69, 117.10, 113.89, 112.14, 49.60, 47.44, 43.45, 37.45, 31.64, 28.87, 22.93.

**LC-MS** *m/z* for C<sub>18</sub>H<sub>20</sub>N<sub>7</sub>O<sub>5</sub><sup>+</sup> ([M+H]<sup>+</sup>) calculated: 414.2, found: 414.0.

**(3S)-1-Cyano-N-(1-(4-((3-(1-(3-(2-((2-(2,6-dioxopiperidin-3-yl)-1,3-dioxoisindolin-4-yl)amino)acetamido)propyl)-1*H*-1,2,3-triazol-4-yl)propyl)carbamoyl)phenyl)-1*H*-imidazol-4-yl)pyrrolidine-3-carboxamide (MS102)**



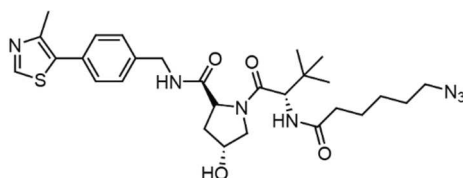
GK13S (5.7 mg, 14.51  $\mu$ mol, 1.0 eq.) was dissolved in THF (500  $\mu$ L). TBTA (1.5 mg, 2.90  $\mu$ mol, 0.2 eq.), CuSO<sub>4</sub> x 5 H<sub>2</sub>O (0.72 mg, 2.90  $\mu$ mol, 0.2 eq.), MS099 (6 mg, 14.51  $\mu$ mol, 1.0 eq.) and sodium ascorbate (8.6 mg, 43.54  $\mu$ mol, 3.0 eq.) were added to the solution. A few drops of water were added to the mixture and the reaction was stirred for 16 h at RT under argon atmosphere. The reaction was diluted with EA (5 mL) and washed with brine (3 x 5 mL). The organic phase

## Methods

was dried over MgSO<sub>4</sub> and the solvent was evaporated under reduced pressure. The crude product was purified by flash chromatography (normal phase, 0 – 20 % MeOH in DCM), which resulted in the title compound (2 mg, 2.49 μmol, 17 %) as a white solid.

**HRMS** m/z for C<sub>39</sub>H<sub>42</sub>N<sub>13</sub>O<sub>7</sub><sup>+</sup> ([M+H]<sup>+</sup>) calculated: 804.3324, found: 804.3336

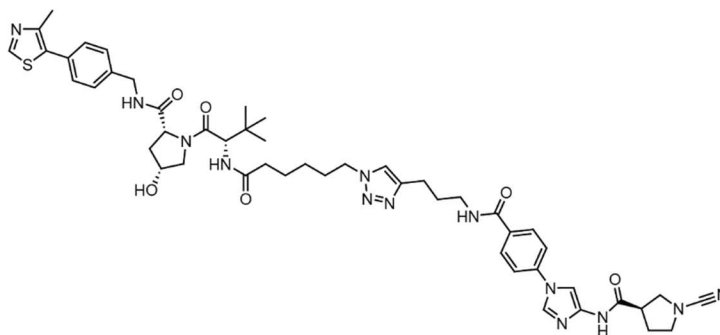
### **(2*S*,4*R*)-1-((*S*)-2-(6-azidohexanamido)-3,3-dimethylbutanoyl)-4-hydroxy-*N*-(4-(4-methylthiazol-5-yl)benzyl)pyrrolidine-2-carboxamide (MS107)**



6-azidohexanoic acid (15 mg, 0.10 mmol, 1.5 eq.) was dissolved in DCM (1 mL). DIPEA (44 μL, 0.26 mmol, 4.0 eq.) and HATU (49 mg, 0.13 mmol, 2.0 eq.) were added and the mixture was allowed to stir for 10 min at RT. The VHL-ligand (30 mg, 0.06 mmol, 1.0 eq.) was added and the reaction was further stirred for 4 h at RT. The reaction was diluted with DCM (10 mL) and washed with a sat. aq. NH<sub>4</sub>Cl-solution (2 x 10 mL). The organic phase was dried over MgSO<sub>4</sub> and the solvent was evaporated under reduced pressure. The crude product was purified by flash chromatography (normal phase, 0 – 20 % MeOH in DCM), which resulted in the title compound (18 mg, 0.03 mmol, 49 %) as a white solid.

**HRMS** m/z for C<sub>28</sub>H<sub>40</sub>N<sub>7</sub>O<sub>4</sub>S<sup>+</sup> ([M+H]<sup>+</sup>) calculated: 570.2857, found: 570.2853

### **(2*S*,4*R*)-1-((*S*)-2-(6-(4-(3-(4-(4-((*S*)-1-cyanopyrrolidine-3-carboxamido)-1*H*-imidazol-1-yl)benzamido)propyl)-1*H*-1,2,3-triazol-1-yl)hexanamido)-3,3-dimethylbutanoyl)-4-hydroxy-*N*-(4-(4-methylthiazol-5-yl)benzyl)pyrrolidine-2-carboxamide (MS109)**



## Methods

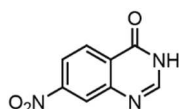
CuSO<sub>4</sub> x 5 H<sub>2</sub>O (3.2 mg, 13 μmol, 0.85 eq.) and sodium ascorbate (9 mg, 46.10 μmol, 3.0 eq.) were dissolved in H<sub>2</sub>O (1 mL). The mixture was flushed with argon and stirred for 10 minutes at RT. GK13S (6 mg, 7.68 μmol, 1.0 eq.) and MS107 (9.6 mg, 15.37 μmol, 1.1 eq.) were dissolved in DMF (1 mL) and added to the aqueous solution. The reaction was stirred over night at RT. The reaction was diluted with EA (5 mL) and washed with brine (3 x 5 mL). The organic phase was dried over MgSO<sub>4</sub> and the solvent was evaporated under reduced pressure. The crude product was purified by flash chromatography (normal phase, 0 – 20 % MeOH in DCM), which resulted in the title compound (3.1 mg, 3.25 μmol, 21 %) as a white solid.

**HRMS** *m/z* for C<sub>49</sub>H<sub>62</sub>N<sub>13</sub>O<sub>6</sub>S<sup>+</sup> ([M+H]<sup>+</sup>) calculated: 960.4661, found: 960.4692

### 5.2.3 Preparation of USP7 PROTACs

The following section describes the chemical synthesis of PROTACs to target and degrade the DUB USP7, which are based on the chiral USP7 Inhibitor XL188. The procedures described in the following yielded the enantiomerically pure compounds, but the racemic counterparts were prepared using the same synthetic strategy as described below. XL188 and precursors were synthesized according to the literature.<sup>[103]</sup>

### 7-Nitroquinazolin-4-one (21, MS041)

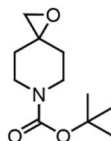


2-amino-4-nitrobenzoic acid (1.8 g, 10.0 mmol, 1.0 eq.) was dissolved in neat formamide. The mixture was heated to 150 °C and stirred for 15 h. The reaction was cooled to rt. The precipitate was filtered and washed with cold ddH<sub>2</sub>O. The product (1.7 g, 9.1 mmol, 92 %) was dried under reduced pressure and used for the next reaction without further purification.

**<sup>1</sup>H NMR** (500 MHz, DMSO-d<sub>6</sub>) δ (ppm) = 12.67 (s, 1H), 8.37 (d, *J* = 2.2 Hz, 1H), 8.35 - 8.31 (m, 1H), 8.28 - 8.22 (m, 2H).

**<sup>13</sup>C NMR** (126 MHz, DMSO-d<sub>6</sub>) δ (ppm) = 159.89, 151.09, 149.18, 147.79, 128.24, 127.02, 122.26, 120.42.

**LC-MS** *m/z* for C<sub>8</sub>H<sub>6</sub>N<sub>3</sub>O<sub>3</sub><sup>+</sup> ([M+H]<sup>+</sup>) calculated: 192.0, found: 192.1.

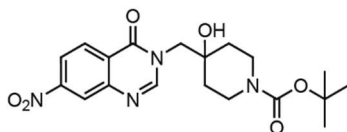
**tert-Butyl 1-oxa-6-azaspiro[2.5]octane-6-carboxylate (23, MS042)**

Sodium hydride (804 mg, 20.1 mmol, 1.1 eq, 60 % dispersion on mineral oil) was suspended in dry DMSO (40 mL) under argon atmosphere. Trimethylsulfoxonium iodide (TMSOI) (4.4 g, 20.1 mmol, 1.1 eq.) was added portion wise at rt. The suspension was allowed to stir for 40 min at rt. Then 1-Boc-4-piperidone (3.6 g, 18.3 mmol, 1.0 eq.) was added portion wise to the reaction and stirred for 1 h at rt. Then the reaction was heated to 65 °C and stirred for 1 h. The mixture was poured on ice cold water (100 mL). The aqueous phase was extracted with EA (3 x 50 mL). The organic phases were combined and washed with brined (1 x 50 mL). The organic phase was dried over MgSO<sub>4</sub> and the solvent was evaporated under reduced pressure. This resulted in an oil, which was further dissolved in H<sub>2</sub>O (5 mL) and lyophilized overnight. The title compound (3.85 g, 18.05 mmol, 98 %) was isolated as pale yellow oil. The product was used for the next reaction without further purification.

<sup>1</sup>H NMR (500 MHz, DMSO-d<sub>6</sub>) δ (ppm) = 3.50 (ddd, J = 12.8, 6.4, 4.3 Hz, 2H), 3.36 (dd, J = 15.3, 6.2 Hz, 2H), 2.65 (s, 2H), 1.64 (ddd, J = 12.9, 8.4, 4.3 Hz, 2H), 1.40 (s, 11H).

<sup>13</sup>C NMR (126 MHz, DMSO) δ (ppm) = 153.86, 78.86, 56.92, 52.83, 32.53, 28.08.

LC-MS *m/z* for C<sub>7</sub>H<sub>12</sub>NO<sub>3</sub><sup>+</sup> ([M-*t*-butyl+H]<sup>+</sup>) calculated: 158.1, found: 158.1.

**tert-Butyl 4-hydroxy-4-((7-nitro-4-oxoquinazolin-3-yl)methyl)piperidine-1-carboxylate (24, MS043)**

MS041 (1.52 g, 8.0 mmol, 1.0 eq.) was dissolved in dry DMF (10 mL). MS042 (1.87 g, 8.8 mmol, 1.1 eq.) and Cs<sub>2</sub>CO<sub>3</sub> (7.8 g, 23.9 mmol, 3.0 eq.) were added to the solution. The reaction mixture



## Methods

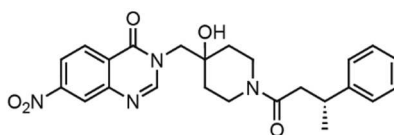
was heated to 80 °C and allowed to stir for 16 h. The reaction was cooled to rt and diluted with EA (3 x 15 mL). The organic phases were combined and washed with brine (1 x 15 mL). The organic phase was dried over MgSO<sub>4</sub> and the solvent was evaporated under reduced pressure. The crude product was purified by column chromatography (normal phase 40 – 100 % EA in PE, reversed phase 5 – 95 % ACN in H<sub>2</sub>O + 0.1 % TFA), to yield MS043 (1.2 g, 2.87 mmol, 36 %) as a pale-yellow solid.

**<sup>1</sup>H NMR** (400 MHz, DMSO-*d*<sub>6</sub>) δ (ppm) = 8.43 – 8.39 (m, 2H), 8.38 (s, 1H), 8.26 (dd, *J* = 8.8, 2.2 Hz, 1H), 4.94 (s, 1H), 4.03 (s, 2H), 3.66 (d, *J* = 12.8 Hz, 4H), 1.50 (td, *J* = 11.9, 11.4, 3.8 Hz, 4H), 1.39 (s, 9H).

**<sup>13</sup>C NMR** (126 MHz, DMSO) δ (ppm) = 160.36, 154.29, 151.65, 151.53, 148.73, 129.19, 126.28, 122.65, 121.03, 79.01, 69.68, 54.56, 34.78, 28.55.

**LC-MS** *m/z* for C<sub>19</sub>H<sub>24</sub>N<sub>4</sub>O<sub>6</sub>Na<sup>+</sup> ([M+Na]<sup>+</sup>) calculated: 427.2, found: 427.1.

### **(*R*)-3-((4-Hydroxy-1-(3-phenylbutanoyl)piperidin-4-yl)methyl)-7-nitroquinazolin-4(3*H*)-one (26, MS045)**



MS043 (668 mg, 1.65 mmol, 1.0 eq.) was dissolved in DCM (8 mL) supplemented with TFA (2 mL). The reaction was allowed to stir for 2 h at RT. The reaction was diluted with DCM (10 mL) and the solvent was evaporated under reduced pressure. The residue was taken up in ddH<sub>2</sub>O (10 mL). The aqueous phase was lyophilized to obtain the Boc-protected intermediate of MS043. This intermediate was used for the next reaction without further purification.

(*R*)-3-Phenylbutyric acid (472 mg, 2.87 mmol, 1.2 eq.) was dissolved in anhydrous DMF (3 mL). HATU (1.8 g, 4.8 mmol, 2.0 eq.) and Et<sub>3</sub>N (1.7 mL, 12.0 mmol, 5.0 eq.) was added to the reaction and allowed to stir for 10 min at rt. Boc-protected MS043 (1 g, 2.39 mmol, 2.39 mmol, 1.0 eq.) was dissolved in anhydrous DMF (3.3 mL) and Et<sub>3</sub>N (1 mL, 7.2 mmol, 3.0 eq.) was added. Both solutions were combined and further stirred for 5 h at RT. The reaction mixture was diluted with EA (15 mL) and washed with brine (3 x 15 mL). The org. phase was dried over MgSO<sub>4</sub> and the solvent was evaporated under reduced pressure. The crude product was further purified via

## Methods

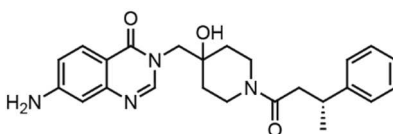
column chromatography (normal phase 0 – 20 % MeOH in DCM). This resulted in the title compound as a pale orange solid (851 mg, 1.89 mmol, 78 % over two steps).

**<sup>1</sup>H NMR** (500 MHz, DMSO-*d*<sub>6</sub>) δ (ppm) = 8.45 – 8.33 (m, 3H), 8.27 (dd, *J* = 8.8, 2.1 Hz, 1H), 7.32 – 7.10 (m, 5H), 4.97 (d, *J* = 5.6 Hz, 1H), 4.11 – 3.90 (m, 4H), 3.26 – 3.11 (m, 2H), 2.65 – 2.55 (m, 2H), 1.99 (s, 1H), 1.50 – 1.22 (m, 4H), 1.20 (d, *J* = 6.9 Hz, 3H).

**<sup>13</sup>C NMR** (126 MHz, DMSO) δ (ppm) = 169.60, 160.35, 151.53, 148.72, 147.17, 147.05, 129.18, 128.71, 128.67, 127.41, 127.37, 126.47, 126.28, 122.65, 121.05, 69.75, 60.24, 54.57, 41.50, 37.36, 36.47, 35.36, 22.36, 14.56.

**LC-MS** *m/z* for C<sub>24</sub>H<sub>27</sub>N<sub>4</sub>O<sub>5</sub><sup>+</sup> ([M+H]<sup>+</sup>) calculated: 451.2, found: 451.2.

### **(*R*)-7-Amino-3-((4-hydroxy-1-(3-phenylbutanoyl)piperidin-4-yl)methyl)quinazolin-4(3*H*)-one (27, MS047)**



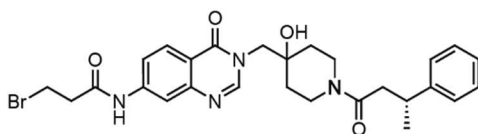
MS045 (200 mg, 0.44 mmol, 1.0 eq.) was dissolved in an EtOH/H<sub>2</sub>O mixture (4:1, 4 + 1 mL) and 1 % (v/v) conc. HCl (50 μL) was added. Iron powder (248 mg, 4.44 mmol, 10.0 eq.) was added in portion to the solution. The reaction was allowed to stir at 80 °C (reflux) for 1 h. The iron powder was removed via filtration through Celite545®. The solvent was evaporated under reduced pressure and the crude product was further purified via column chromatography (normal phase, 0 – 20 % MeOH in DCM) to obtain the title compound (153 mg, 0.36 mmol, 82 %).

**<sup>1</sup>H NMR** (700 MHz, DMSO-*d*<sub>6</sub>) δ (ppm) = 11.95 (s, 3H), 8.02 (d, *J* = 18.9 Hz, 1H), 7.79 (d, *J* = 8.6 Hz, 1H), 7.25 – 7.23 (m, 2H), 7.17 – 7.12 (m, 1H), 6.72 (dd, *J* = 8.7, 2.2 Hz, 1H), 6.61 (d, *J* = 2.2 Hz, 1H), 6.09 (s, 1H), 5.75 (s, 1H), 4.88 (d, *J* = 9.5 Hz, 1H), 4.04 – 3.93 (m, 2H), 3.87 – 3.60 (m, 4H), 3.25 – 3.14 (m, 2H), 1.91 (s, 1H), 1.42 – 1.22 (m, 4H), 1.19 (dd, *J* = 6.9, 3.3 Hz, 3H).

**<sup>13</sup>C NMR** (176 MHz, DMSO) δ (ppm) = 172.47, 169.56, 160.75, 154.81, 150.48, 149.19, 149.17, 147.17, 147.05, 128.68, 128.66, 128.07, 127.36, 126.43, 126.38, 115.43, 107.24, 69.78, 53.69, 41.58, 37.44, 36.68, 22.37, 21.55.

**LC-MS** *m/z* for C<sub>24</sub>H<sub>29</sub>N<sub>4</sub>O<sub>3</sub><sup>+</sup> ([M+H]<sup>+</sup>) calculated: 421.2, found: 421.2.

**(R)-3-Bromo-N-(3-((4-hydroxy-1-(3-phenylbutanoyl)piperidin-4-yl)methyl)-4-oxo-3,4-dihydroquinazolin-7-yl)propanamide (28, MS057)**



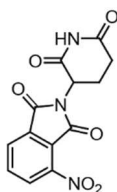
MS047 (220 mg, 0.52 mmol, 1.0 eq.) was dissolved in DCM (10 mL). The mixture was cooled to -20 °C and Et<sub>3</sub>N (145 μL, 1.05 mmol, 2.0 eq.) was added. 3-bromopropionyl chloride (83 μL, 0.78 mmol, 1.5 eq.) was dissolved in DCM (2.5 mL) and added dropwise to the reaction mixture under argon atmosphere. The reaction was allowed to stir for 3 h at 0 °C. The reaction was quenched by adding a few drops of water. The solvent was evaporated under reduced pressure to obtain MS057 (quant. yield) as a crude, which was used for the step without further purification.

**<sup>1</sup>H NMR** (600 MHz, DMSO-*d*<sub>6</sub>) δ (ppm) = 10.52 (s, 1H), 8.19 (d, *J* = 15.8 Hz, 1H), 8.09 (d, *J* = 8.7 Hz, 1H), 8.04 (d, *J* = 1.9 Hz, 1H), 7.25 (d, *J* = 5.3 Hz, 5H), 7.14 (dq, *J* = 6.4, 3.9, 3.0 Hz, 1H), 4.93 (d, *J* = 7.7 Hz, 1H), 4.02 (d, *J* = 13.8 Hz, 2H), 3.95 – 3.87 (m, 2H), 3.76 (t, *J* = 6.4 Hz, 2H), 3.68 – 3.59 (m, 1H), 3.04 (t, *J* = 6.4 Hz, 2H), 2.90 – 2.83 (m, 2H), 1.37 – 1.22 (m, 4H), 1.20 (d, *J* = 2.6 Hz, 3H).

**<sup>13</sup>C NMR** (151 MHz, DMSO) δ (ppm) = 169.59, 169.56, 160.61, 149.92, 149.46, 147.16, 144.48, 128.69, 128.66, 127.81, 127.38, 127.36, 126.44, 118.81, 118.54, 117.24, 115.36, 69.78, 54.04, 46.20, 41.55, 37.41, 36.70, 35.38, 34.82, 29.34, 22.55.

**LC-MS** *m/z* for C<sub>27</sub>H<sub>32</sub>BrN<sub>4</sub>O<sub>4</sub><sup>+</sup> ([M+H]<sup>+</sup>) calculated: 555.2, found: 555.1.

**1-(4-Nitro-1,3-dioxo-2,3-dihydro-1H-inden-2-yl)dihydropyrimidine-2,4(1H,3H)-dione (30, CER01)**



α-Aminoglutarimide hydrochloride (384 mg, 2.3 mmol, 0.9 eq.) was dissolved in glacial acetic acid (7 mL). Anhydrous sodium acetate (195 mg, 2.3 mmol, 0.9 eq.) and 3-nitrophthalic anhydride (500 mg, 2.6 mmol, 1.0 eq.) were added lot wise to the reaction mixture at RT. The reaction was

## Methods

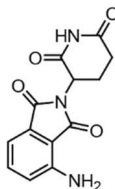
heated to 120 °C and allowed to stir for 18 h. After completion the reaction was cooled to 60 °C and the solvent was reduced under reduced pressure. The residue was dissolved in ddH<sub>2</sub>O (12 mL) and stirred for 1 h at RT. The precipitate was filtered and washed with cold ddH<sub>2</sub>O (2 x 12 mL). The product was dried to obtain the title compound as a pale purple solid (620 mg, 2.0 mmol, 79 %)

**<sup>1</sup>H NMR** (400 MHz, DMSO-*d*<sub>6</sub>) δ (ppm) = 11.16 (s, 1H), 8.35 (dd, *J* = 8.1, 0.8 Hz, 2H), 8.24 (d, *J* = 7.3 Hz, 1H), 8.12 (t, *J* = 7.8 Hz, 1H), 5.20 (dd, *J* = 12.9, 5.4 Hz, 1H), 2.89 (ddd, *J* = 17.2, 13.9, 5.4 Hz, 1H), 2.67 – 2.51 (m, 2H), 2.08 (dtd, *J* = 13.0, 5.3, 2.3 Hz, 2H).

**<sup>13</sup>C NMR** (126 MHz, DMSO) δ (ppm) = 173.18, 169.96, 165.65, 162.99, 144.91, 137.28, 133.47, 129.34, 127.77, 123.02, 49.89, 31.33, 22.19.

**LC-MS** *m/z* for C<sub>13</sub>H<sub>10</sub>N<sub>3</sub>O<sub>6</sub><sup>+</sup> ([M+H]<sup>+</sup>) calculated: 304.1, found: 304.1.

### 1-(4-Amino-1,3-dioxo-2,3-dihydro-1H-inden-2-yl)dihydropyrimidine-2,4(1H,3H)-dione (31, CER02)



CER01 (1 g, 3.3 mmol, 1.0 eq.) was dissolved in DMF (20 mL). Palladium on charcoal (200 mg) and a few drops of water were added to the solution under H<sub>2</sub> atmosphere. The reaction was allowed to stir for 24 h at RT. The palladium was filtered off through Celite545®. Cold ddH<sub>2</sub>O was added to the organic phase and the precipitated product was collected by filtration and dried under vacuum to obtain the title compound as a yellow solid (825 mg, 3.0 mmol, 92 %).

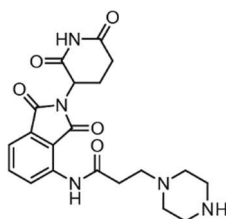
**<sup>1</sup>H NMR** (500 MHz, DMSO-*d*<sub>6</sub>) δ (ppm) = 11.17 (s, 1H), 7.96 (td, *J* = 8.3, 4.5 Hz, 1H), 7.80 (d, *J* = 7.3 Hz, 1H), 7.75 (t, *J* = 8.8 Hz, 1H), 5.17 (dd, *J* = 13.0, 5.4 Hz, 1H), 2.66 – 2.46 (m, 4H).

**<sup>13</sup>C NMR** (126 MHz, DMSO) δ (ppm) = 173.23, 170.18, 166.57, 164.44, 158.31, 156.23, 138.57, 133.91, 123.41, 120.54, 49.53, 31.36, 22.30.

**LC-MS** *m/z* for C<sub>13</sub>H<sub>12</sub>N<sub>3</sub>O<sub>4</sub><sup>+</sup> ([M+H]<sup>+</sup>) calculated: 274.1, found: 274.1.

## Methods

### ***tert*-Butyl 4-(3-((2-(2,4-dioxotetrahydropyrimidin-1(2*H*)-yl)-1,3-dioxo-2,3-dihydro-1*H*-inden-4-yl)amino)-3-oxopropyl)piperazine-1-carboxylate (32, MS060)**



CER02 (400 mg, 1.46 mmol, 1.0 eq.) and DMAP (18 mg, 0.14 mmol, 0.1 eq.) was dissolved in dry THF under argon atmosphere. 3-Bromopropionyl chloride (186  $\mu$ L, 1.76 mmol, 1.2 eq.) was dissolved in dry THF (5 mL) and added dropwise to the reaction mixture under argon atmosphere. The reaction was allowed to stir at 65  $^{\circ}$ C for 4 h. The reaction was quenched by adding a few drops of water. The solvent was evaporated under reduced pressure. The crude product was used for the next step without further purification.

The crude product of the previous step (600 mg, 1.47 mmol, 1.0 eq.) was dissolved in dry DMF (10 mL). Boc-piperazine (355 mg, 1.91 mmol, 1.3 eq.) and Et<sub>3</sub>N (407  $\mu$ L, 2.94 mmol, 2.0 eq.) were added to the mixture. The solution was allowed to stir for 3 h at 60  $^{\circ}$ C. The reaction mixture was diluted with EA (15 mL) and washed with a sat. NH<sub>4</sub>Cl solution (1 x 30 mL). The aqueous phase was extracted with EA (3 x 15 mL). The organic phases were combined and the solvent was evaporated under reduced pressure. The crude product was further purified via column chromatography (normal phase, 0 – 20 % MeOH in DCM) to obtain the title compound as a pale-yellow solid (663 mg, 1.29 mmol, 88 % over two steps).

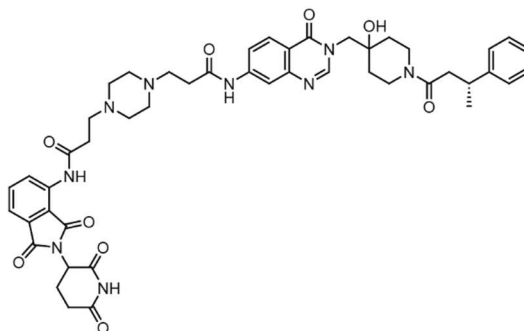
**<sup>1</sup>H NMR** (700 MHz, DMSO-*d*<sub>6</sub>)  $\delta$  (ppm) = 11.14 (s, 1H), 10.36 (s, 1H), 8.55 (d, *J* = 8.4 Hz, 1H), 7.85 – 7.80 (m, 1H), 7.61 (d, *J* = 7.2 Hz, 1H), 5.14 (dd, *J* = 12.9, 5.5 Hz, 1H), 3.34 (d, *J* = 23.6 Hz, 6H), 2.94 – 2.60 (m, 6H), 2.42 (s, 4H), 1.39 (s, 9H).

**<sup>13</sup>C NMR** (176 MHz, DMSO)  $\delta$  (ppm) = 173.21, 171.80, 170.30, 167.92, 167.19, 154.30, 136.91, 136.47, 132.02, 126.97, 118.70, 117.33, 79.20, 53.70, 52.73, 49.37, 34.18, 31.42, 28.54, 22.44.

**LC-MS** *m/z* for C<sub>25</sub>H<sub>32</sub>N<sub>5</sub>O<sub>7</sub><sup>+</sup> ([M+H]<sup>+</sup>) calculated: 514.2, found: 514.2.

## Methods

### ***N*-(2-(2,6-dioxopiperidin-3-yl)-1,3-dioxoisindolin-4-yl)-3-(4-(3-((3-((4-hydroxy-1-((*R*)-3-phenylbutanoyl)piperidin-4-yl)methyl)-4-oxo-3,4-dihydroquinazolin-7-yl)amino)-3-oxopropyl)piperazin-1-yl)propanamide (MS064)**



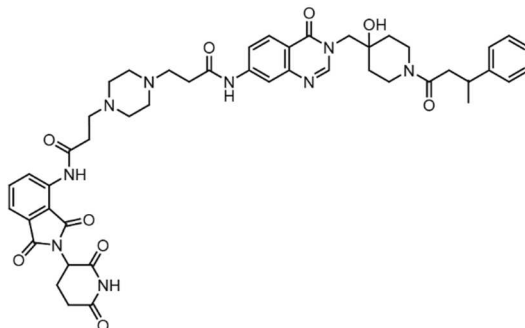
MS060 (663 mg, 1.29 mmol, 1.0 eq.) was dissolved in DCM (7 mL) supplemented with TFA (1.4 mL). The reaction mixture was stirred for 3 h at RT. The reaction was diluted with DCM (10 mL) and the solvent was evaporated under reduced pressure. The residue was diluted in water and lyophilized overnight, which resulted in the title compound as off white solid (TFA salt, 985 mg, 1.54 mmol, quant.). This intermediate was used for the next reaction step without further purification.

The deprotected MS060 (60 mg, 0.11 mmol, 1.0 eq.) and MS057 (70 mg, 0.13 mmol, 1.1 eq.) were dissolved in dry DMF. Cs<sub>2</sub>CO<sub>3</sub> (148 mg, 0.46 mmol, 4.0 eq.) was added to the mixture and the solution was allowed to stir for overnight at 80 °C. The solvent was reduced under reduced pressure. The residue was taken up in water and lyophilized overnight. The crude product was purified by preparative chromatography (reversed phase, 20 – 90 % ACN in H<sub>2</sub>O) to obtain the title compound (11 mg, 10 μmol, 11 %).

**HRMS** *m/z* for C<sub>47</sub>H<sub>54</sub>N<sub>9</sub>O<sub>9</sub><sup>+</sup> ([M+H]<sup>+</sup>) calculated: 888.4039, found: 888.4052

## Methods

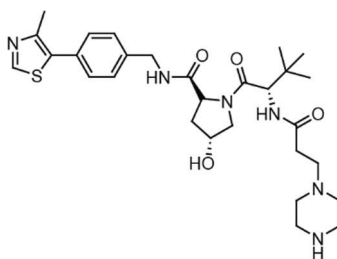
### ***N***-2-(2,6-dioxopiperidin-3-yl)-1,3-dioxoisindolin-4-yl)-3-(4-(3-((3-((4-hydroxy-1-(3-phenylbutanoyl)piperidin-4-yl)methyl)-4-oxo-3,4-dihydroquinazolin-7-yl)amino)-3-oxopropyl)piperazin-1-yl)propenamide (MS062)



MS062 represents the racemate of MS064 and was synthesized and purified similarly as described above. In brief, deprotected MS060 (130 mg, 0.25 mmol, 1.0 eq.) and MS055 (150 mg, 0.27 mmol, 1.1 eq) were dissolved in dry DMF (5 mL). Cs<sub>2</sub>CO<sub>3</sub> (321 mg, 0.99 mmol, 4.0 eq.) was added to the mixture and the solution was allowed to stir for overnight at 80 °C. Purification resulted in the title compound (2.8 mg, 2.51 μmol, 1 %) as a white solid.

**HRMS** *m/z* for C<sub>47</sub>H<sub>54</sub>N<sub>9</sub>O<sub>9</sub><sup>+</sup> ([M+H]<sup>+</sup>) calculated: 888.4039, found: 888.4058

### ***tert***-butyl 4-(3-(((*S*)-1-((2*R*,4*R*)-4-hydroxy-2-((4-(4-methylthiazol-5-yl)benzyl)carbamoyl)pyrrolidin-1-yl)-3,3-dimethyl-1-oxobutan-2-yl)amino)-3-oxopropyl)piperazine-1-carboxylate (34, MS065)



3-(4-(*tert*-butoxycarbonyl)piperazin-1-yl)propanoic acid (28 mg, 0.11 mmol, 1.0 eq.) and the VHL-ligand (50 mg, 0.11 mmol, 1.0 eq.) were dissolved in dry DMF (3 mL) and DIPEA (66 μL, 0.39 mmol, 3.6 eq.) was added. The reaction mixture was cooled to 0 °C and HATU (81 mg, 0.21 mmol, 2.0 eq.) was added. The reaction was allowed to stir for 4 h at RT. After complete conversion the reaction mixture was diluted with sat. aq. HCO<sub>3</sub> solution (15 mL) and extracted with DCM (3 x 15 mL). The organic phases were combined, dried over MgSO<sub>4</sub> and the solvent was evaporated under reduced pressure. The crude product was purified via column chromatography (normal phase, 0 – 20 % MeOH in DCM). This resulted in the title compound (55 mg, 0.08 mmol, 77 %) as a pale-yellow solid.

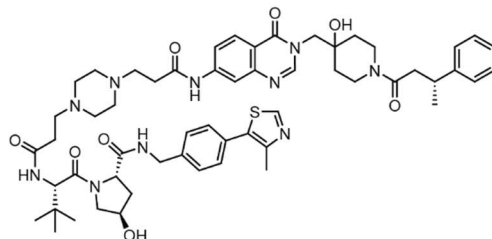
## Methods

**<sup>1</sup>H NMR** (600 MHz, DMSO-*d*<sub>6</sub>) δ (ppm) = 8.97 (s, 1H), 8.61 – 8.49 (m, 2H), 8.20 (d, *J* = 9.1 Hz, 1H), 7.95 (s, 1H), 7.43 (d, *J* = 8.3 Hz, 2H), 5.75 (s, 1H), 4.55 (d, *J* = 9.5 Hz, 1H), 4.44 (dt, *J* = 16.2, 7.3 Hz, 2H), 4.35 (s, 1H), 4.20 (dd, *J* = 16.0, 5.4 Hz, 1H), 3.69 – 3.56 (m, 2H), 3.29 (s, 4H), 2.60 (dd, *J* = 13.0, 4.9 Hz, 2H), 2.43 (s, 3H), 2.42 – 2.36 (m, 2H), 2.35 – 2.22 (m, 4H), 2.06 – 1.87 (m, 2H), 1.34 (s, 9H), 0.94 (s, 9H).

**<sup>13</sup>C NMR** (151 MHz, DMSO) δ (ppm) = 172.44, 171.26, 170.11, 154.21, 151.87, 148.16, 139.96, 131.64, 130.10, 129.06, 127.82, 79.22, 69.36, 59.18, 56.93, 56.63, 54.32, 36.00, 32.66, 28.46, 26.82, 16.38.

**LC-MS** *m/z* for C<sub>34</sub>H<sub>51</sub>N<sub>6</sub>O<sub>6</sub>S<sup>+</sup> ([M+H]<sup>+</sup>) calculated: 671.4, found: 671.4.

**(2*S*,4*R*)-4-Hydroxy-1-((*S*)-2-(3-(4-(3-((4-hydroxy-1-((*R*)-3-phenylbutanoyl)piperidin-4-yl)methyl)-4-oxo-3,4-dihydroquinazolin-7-yl)amino)-3-oxopropyl)piperazin-1-yl)propanamido)-3,3-dimethylbutanoyl)-*N*-(4-(4-methylthiazol-5-yl)benzyl)pyrrolidine-2-carboxamide (MS067)**



MS065 (55 mg, 0.08, 1.0 eq.) was dissolved in DCM (3 mL) supplemented with 20 % TFA. The reaction mixture was allowed to stir for 2 h at RT. After full conversion the reaction was diluted with DCM (15 mL) and the solvent was evaporated under reduced pressure. The residue was taken up in H<sub>2</sub>O (2 mL) and lyophilized overnight. This intermediate was used for the next reaction step without further purification.

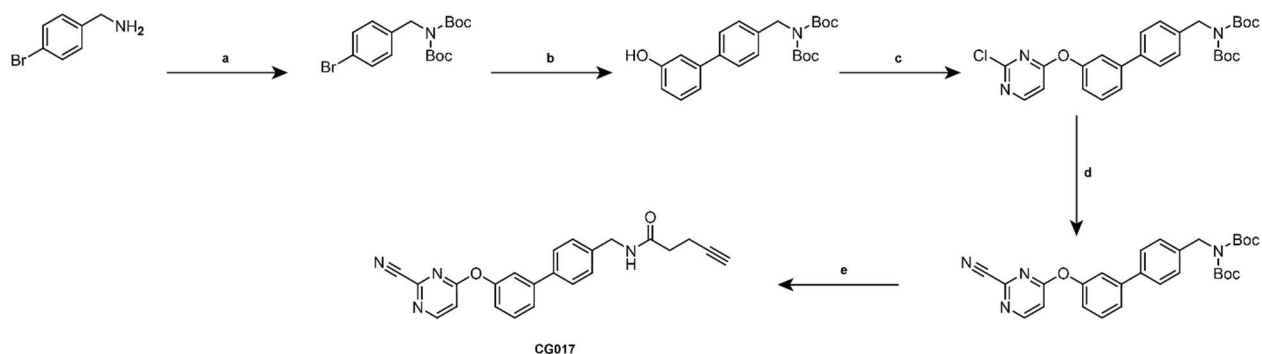
Deprotected MS065 (55 mg, 0.07 mmol, 1.0 eq.) was dissolved in dry DMF (2.5 mL) and Cs<sub>2</sub>CO<sub>3</sub> (179 mg, 0.55 mmol, 8.0 eq.) was added to the solution. MS057 (46 mg, 0.08 mmol 1.2 eq.) was added the reaction was allowed to stir for 3 days at 60 °C. The crude product was purified by preparative chromatography (reversed phase, 20 – 90 % ACN in H<sub>2</sub>O). This resulted in the title compound (20 mg, 0.02 mmol, 23 %)

**HRMS** *m/z* for C<sub>56</sub>H<sub>74</sub>N<sub>10</sub>O<sub>8</sub>S<sup>2+</sup> ([M+2H]<sup>2+</sup>) calculated: 523.2700, found: 523.2696



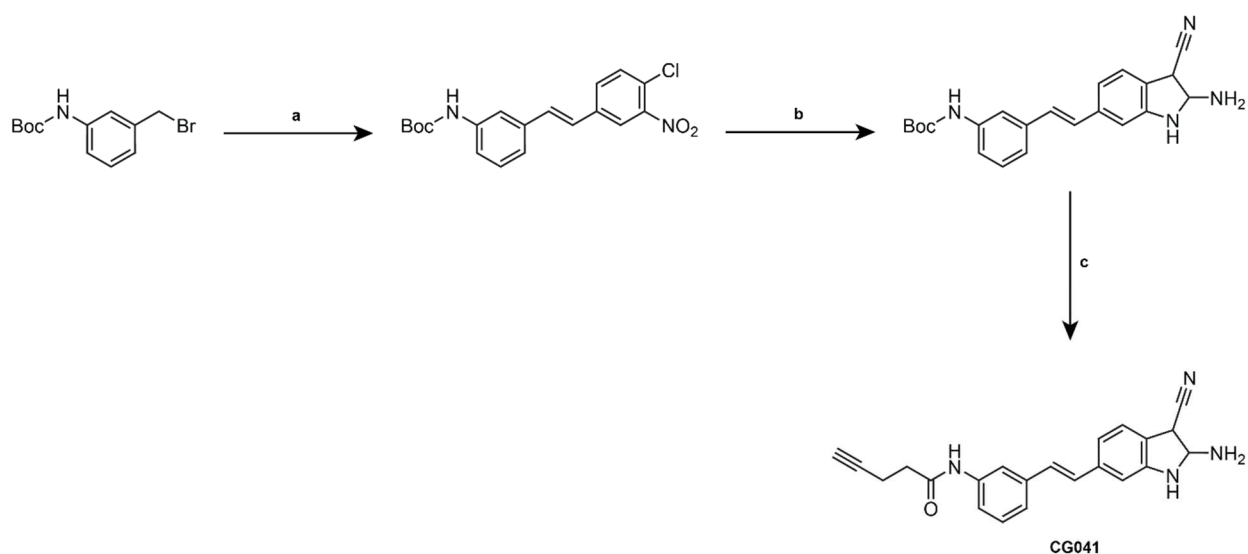
## 6. Supplementary Data

### Synthesis of CG017



**Supplementary Scheme 1 | Synthesis of CG017.** **a)**  $\text{Boc}_2\text{O}$ , DMAP, THF, rt **b)** (3-hydroxyphenyl)boronic acid, super stable Pd(0), DMF:H<sub>2</sub>O = 5:1, 90 °C, 6 h **c)** 2,4-dichloropyrimidine, K<sub>2</sub>CO<sub>3</sub>, DMF, rt, 20 h **d)** Zn(CN)<sub>2</sub>, Pd[(PPh)<sub>3</sub>]<sub>4</sub>, DMF,  $\mu\text{W}$ , 130 °C, 20 min **e)** 1. 20 % TFA in DCM, rt, 4 h; 2. pent-4-ynoic acid, EDC-HCL, DIPEA, DCM, rt, 2 h

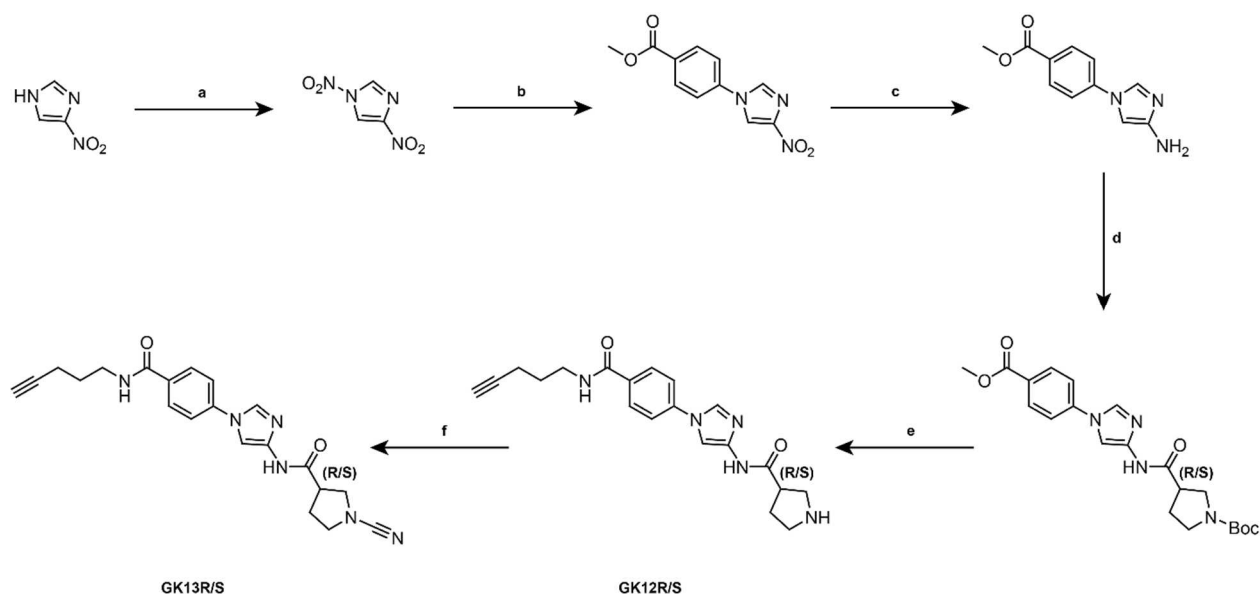
### Synthesis of CG041



**Supplementary Scheme 2 | Synthesis of CG041.** **a)** 1. 4-chloro-3-nitrobenzaldehyde, POEt<sub>3</sub>, 130 °C, 1 h; 2. NaH, DMF, 0 °C, oN **b)** 1. Malononitrile, K<sub>2</sub>CO<sub>3</sub>, DMF, 50 °C, oN; 2. Na<sub>2</sub>S<sub>2</sub>O<sub>3</sub>, DMF, 110 °C, 15 min **c)** 1. 20 % TFA in DCM, rt, 2 h; 2. pent-4-ynoic acid, EDC-HCL, DIPEA, DCM, rt, 4 h

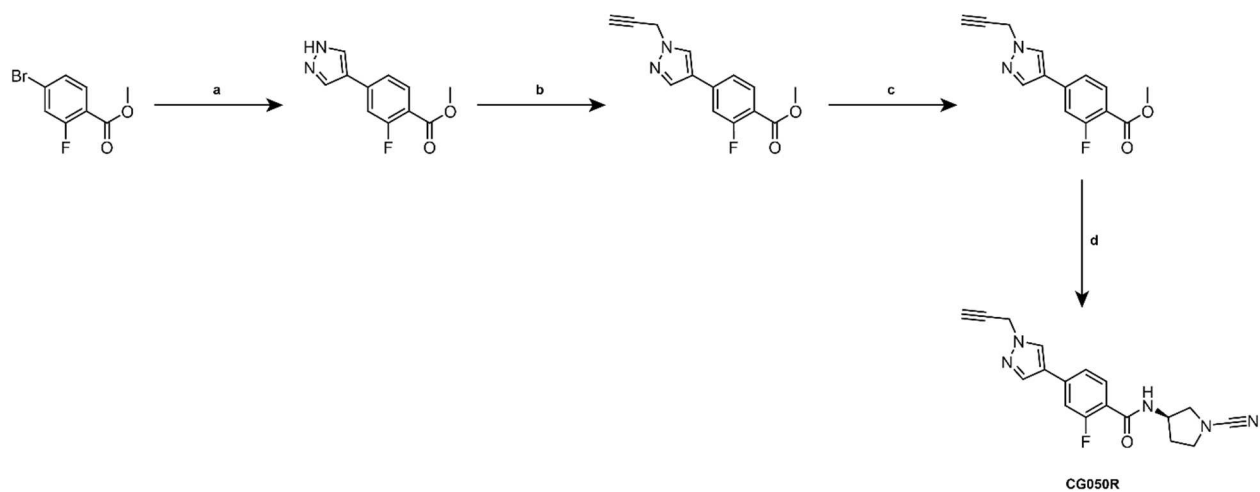
## Supplementary Data

### Synthesis of GK12S/R and GK13S/R



**Supplementary Scheme 3 | Synthesis of GK12S/R and GK13S/R.** a)  $\text{HNO}_3$ ,  $\text{Ac}_2\text{O}$ ,  $\text{AcOH}$ , rt, 5 h b) methyl 4-aminobenzoate,  $\text{MeOH}:\text{H}_2\text{O}$  (1:1), rt, 2 h c)  $\text{Pd/C}$ ,  $\text{H}_2$ ,  $\text{EtOH}$ ,  $\text{H}_2\text{O}$ , rt, 2 h d) (S/R)-1-(tert-butoxycarbonyl)pyrrolidine-3-carboxylic acid, HATU, DIPEA, DCM, rt, 4 h e) 1.  $\text{LiOH}$ ,  $\text{MeOH}$ , rt, 30 h; 2. pent-4-yn-1-amine, HATU, DIPEA, DCM, rt, 1 h; 3. 20 % TFA in DCM, rt, 1 h f)  $\text{BrCN}$ ,  $\text{K}_2\text{CO}_3/\text{DIPEA}$ , DCM/DMF,  $0^\circ\text{C} \rightarrow$  rt, 2 h

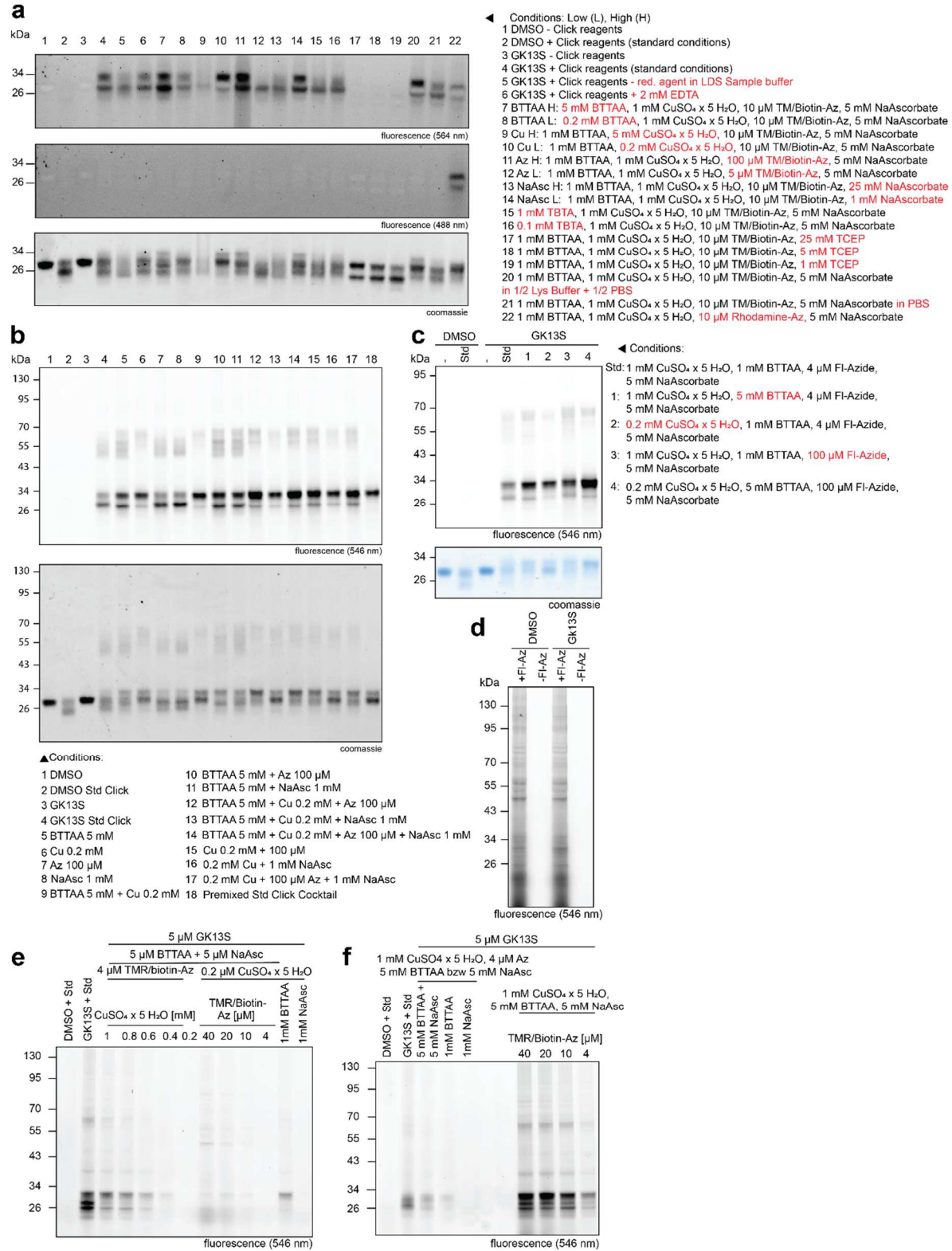
### Synthesis of CG050R



**Supplementary Scheme 4 | Synthesis of CG050R.** a) (1-(tert-butoxycarbonyl)-1H-pyrazol-4-yl)boronic acid,  $\text{Pd}(\text{PPh}_3)_4$ ,  $\text{Na}_2\text{CO}_3$ ,  $\text{Dioxane}:\text{H}_2\text{O} = 5:1$ ,  $90^\circ\text{C}$ , oN b) 3-bromoprop-1-yne,  $\text{K}_2\text{CO}_3$ , acetone, rt, oN c) 1.  $\text{LiOH}$ ,  $\text{MeOH}$ , rt, oN; 2. tert-butyl (R)-3-aminopyrrolidine-1-carboxylate, HATU, DIPEA, DMF, rt, oN; 3. 10 % TFA in DCM, rt, 4 h d)  $\text{BrCN}$ ,  $\text{K}_2\text{CO}_3$ , THF, rt, 2 h

# Supplementary Data

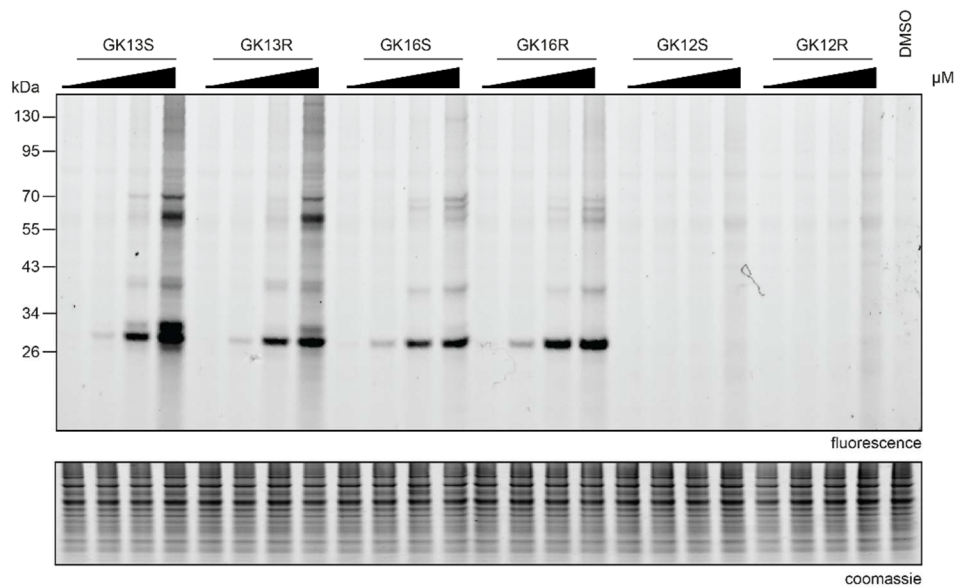
## Supplementary Figure 1



## Supplementary Data

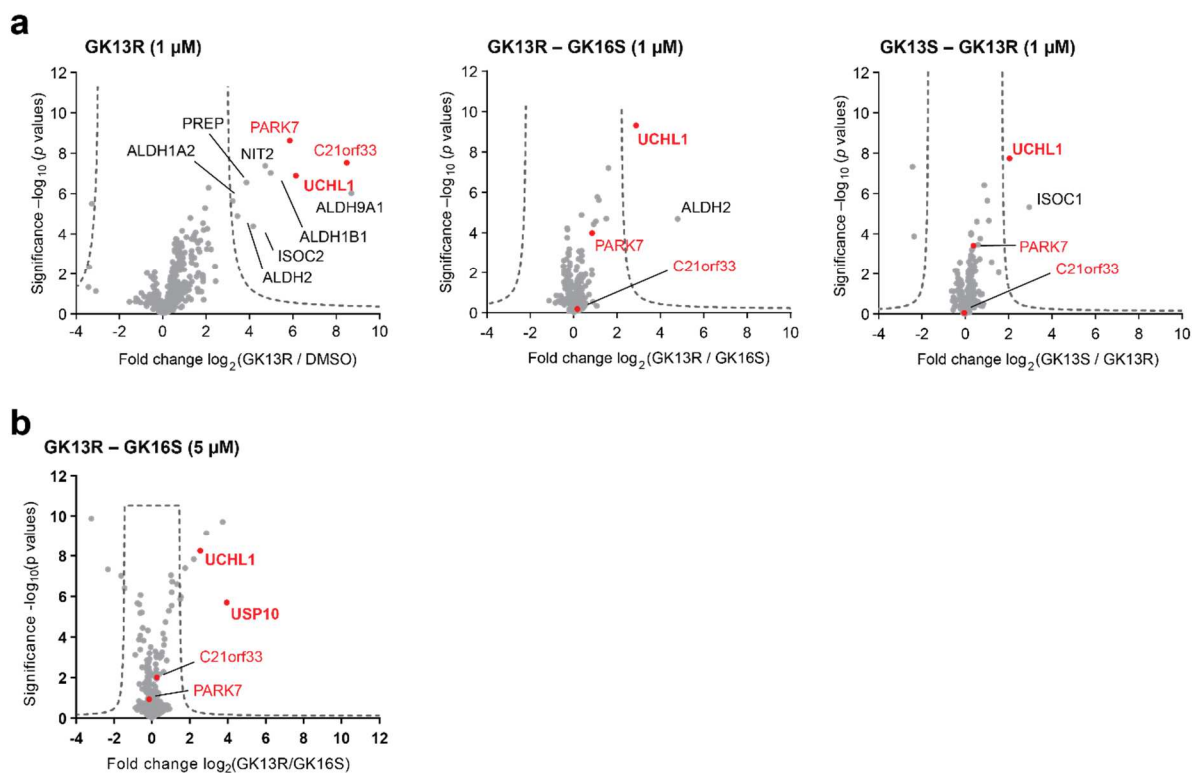
**Supplementary Fig. 1 | Screening of reagent concentration led to improved CuAAC conditions.** **a)** Initial CuAAC screen, where each reagent was tested in a high concentration (5 x higher than the standard concentration) and in a lower concentration (5 x lower than the standard concentration) on purified UCHL1 after the modification with **GK13S**. Additional reagents tested are TCEP, TBTA and a rhodamine azide. Concentrations of 1 mM CuSO<sub>4</sub> x 5 H<sub>2</sub>O, 1 mM BTTAA, 5 mM sodium ascorbate and 10 μM fluorophore azide were used as a standard. Numbers correspond to the condition used on each lane are shown on the right. **b)** Second round of CuAAC optimization with purified UCHL1. Conditions are shown below the gel. When a reagent is not listed, it refers to the standard concentration (only variations are listed). **c)** Summary of conditions in the CuAAC in the presence of purified UCHL1 resulting in enhanced fluorescence intensity compared to the standard conditions. Conditions for each lane are shown on the right with variations highlighted in red. Optimization resulted in 0.2 mM CuSO<sub>4</sub> x 5 H<sub>2</sub>O, 5 mM BTTAA, 5 mM sodium ascorbate and 100 μM fluorophore azide, being improved reagent concentrations to label UCHL1 modified with the reporter. **d)** Optimized reagent concentration for purified UCHL1, resulted in non-specific labeling in cell lysates. **e, f)** Testing different reagent concentration in HEK293 cell lysates led to the identification of CuAAC conditions to label endogenous UCHL1 in complex protein mixtures. 5 mM BTTAA, 1 mM CuSO<sub>4</sub> x 5 H<sub>2</sub>O, 5 mM sodium ascorbate and 10 – 20 μM fluorophore azide resulted in sufficient signal to noise ratio.

## Supplementary Figure 2



**Supplementary Fig. 2 | Lysates treated with GK13S and analogs.** HEK293 cell lysates were treated with the probes GK13S/R, the minimal probes GK16S/R and the negative control probes GK12S/R in a concentration dependent manner (0.01 – 10 μM). Afterward a rhodamine fluorophore was attached via CuAAC and in-gel fluorescence was read out.

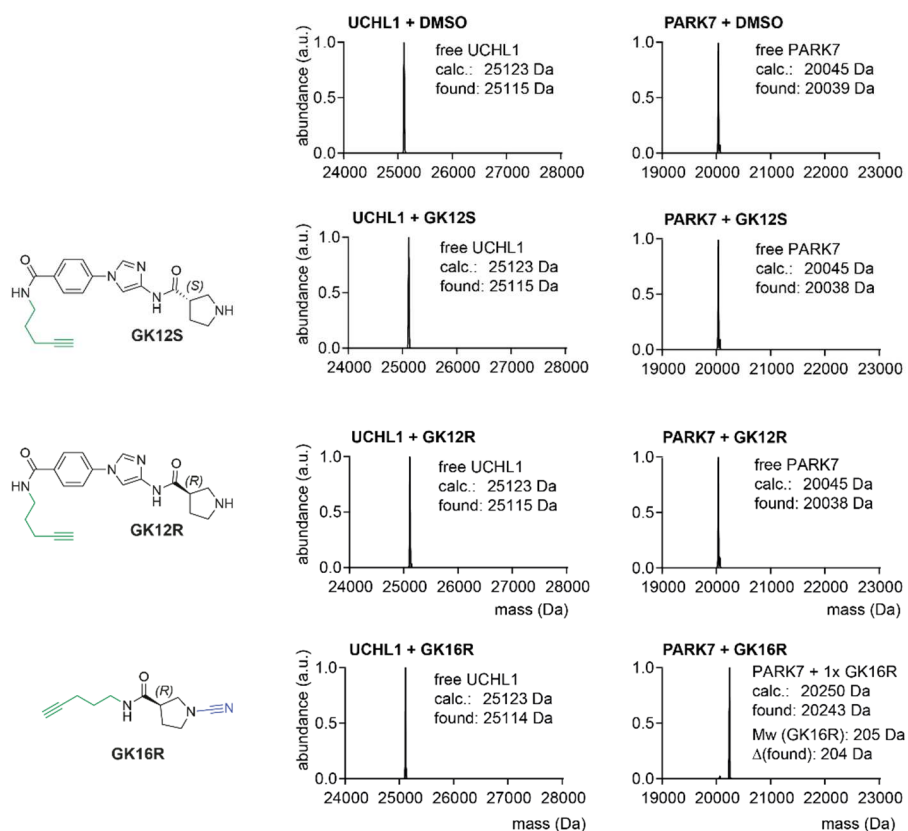
## Supplementary Figure 3



**Supplementary Fig. 3 | GK13R enriches UCHL1 less frequent than GK13S. a)** Target spectrum of GK13R at 1  $\mu$ M visualized as volcano plots. The x-axis indicates the relative label-free abundance ratio (fold change) of proteins between compound-treated samples and the DMSO control or compound treated samples. **b)** Target spectrum of GK13R at 5  $\mu$ M. USP10 is abundantly enriched.

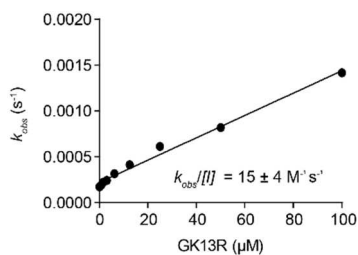
## Supplementary Data

### Supplementary Figure 4



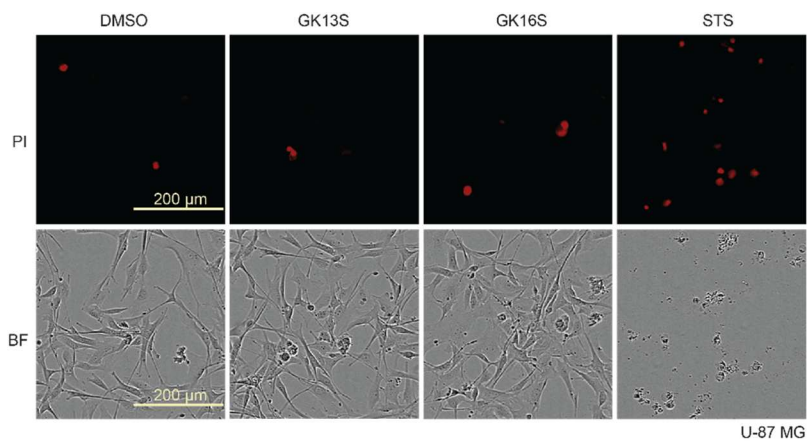
**Supplementary Fig. 4 | Intact protein mass spectra of the probes GK12S/R and GK16R.** Intact protein mass spectra of the probes GK12S/S and GK16R incubated with recombinant UCHL1. No covalent of purified UCHL1 was recorded. The molecular structures of used probes are shown on the left.

### Supplementary Figure 5



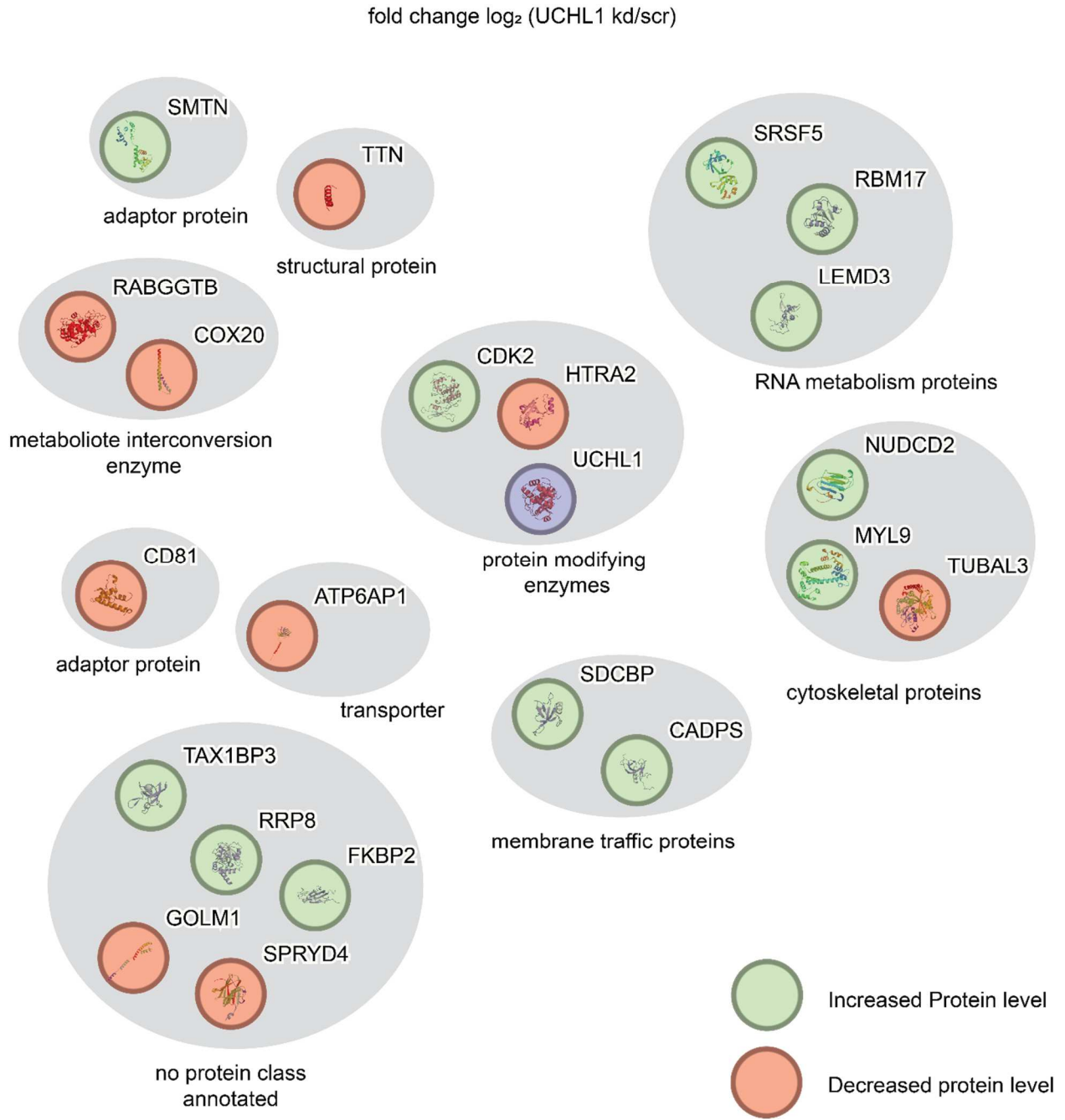
**Supplementary Fig. 5 | Kinetic assay to determine the  $k_{obs}/[I]$  value for GK13R.** DMSO and a blank well were used as controls. The rate constant  $k_{obs}$  was determined from the upper plot. To obtain the value for  $k_{obs}/[I]$ , the rate constant was plotted against the used probe concentrations and calculated from the resulting slope.

## Supplementary Figure 6



**Supplementary Fig. 6 | Compounds show no toxicity upon treatment of U-87 MG treatment.** Microscopy image of U-87 MG cells that were treated with the indicated compounds (1.25 μM) for 72 h. Staurosporin (STS) was used as a control. Effects on the cell growth and viability were analyzed via confluency (bright-field, BF) and apoptosis (propidium iodide staining, PI). All microscopy images were recorded by Dr. Rachel O'Dea.

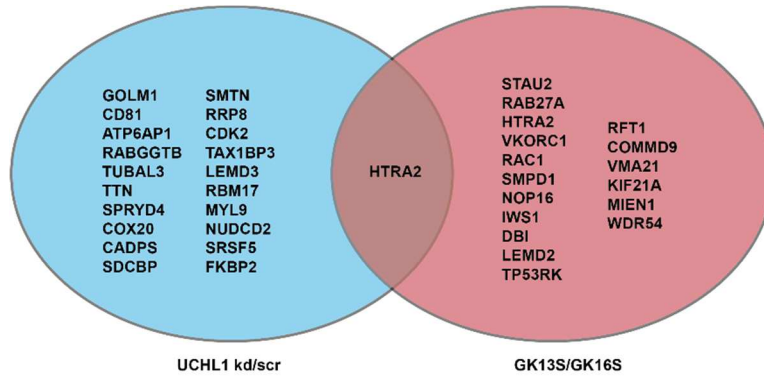
Supplementary Figure 7



**Supplementary Fig. 7 | Clustering of proteins with increased or decreased levels after knockdown of UCHL1.** Identified proteins with altered levels after the knockdown of UCHL1 in U-87 MG cells, were clustered by their protein class using the webtool PANTHER.<sup>[174]</sup>

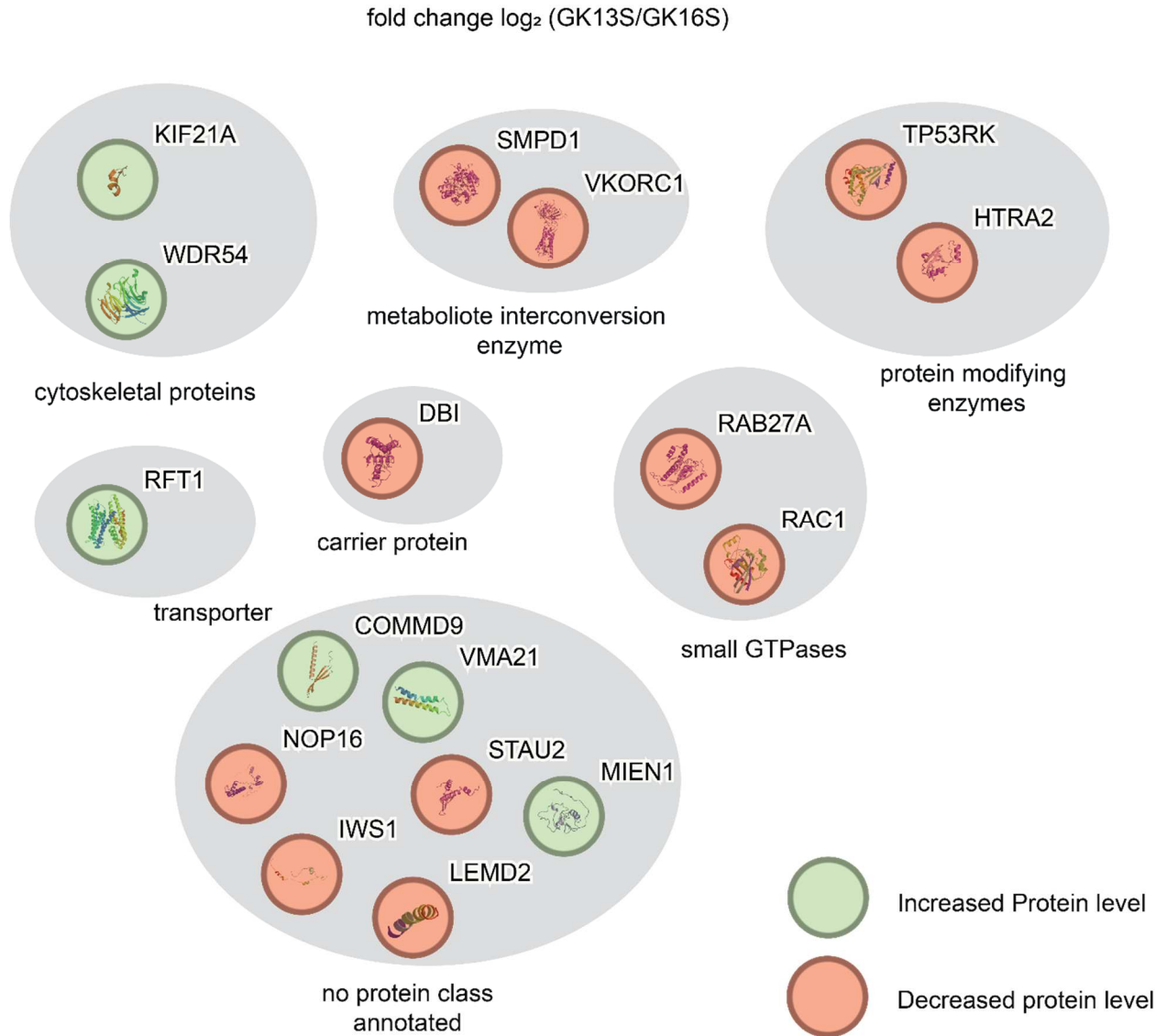


Supplementary Figure 8



**Supplementary Fig. 8 | HtrA2 protein level was altered in the UCHL1 kd and GK13S treated samples.** Venn diagram lists all proteins with altered protein levels identified after digestion of the whole proteome of U87-MG cells. HtrA2 was the only overlapping protein identified with altered levels in the UCHL1 knockdown samples and the GK13S treated samples.

**Supplementary Figure 9**

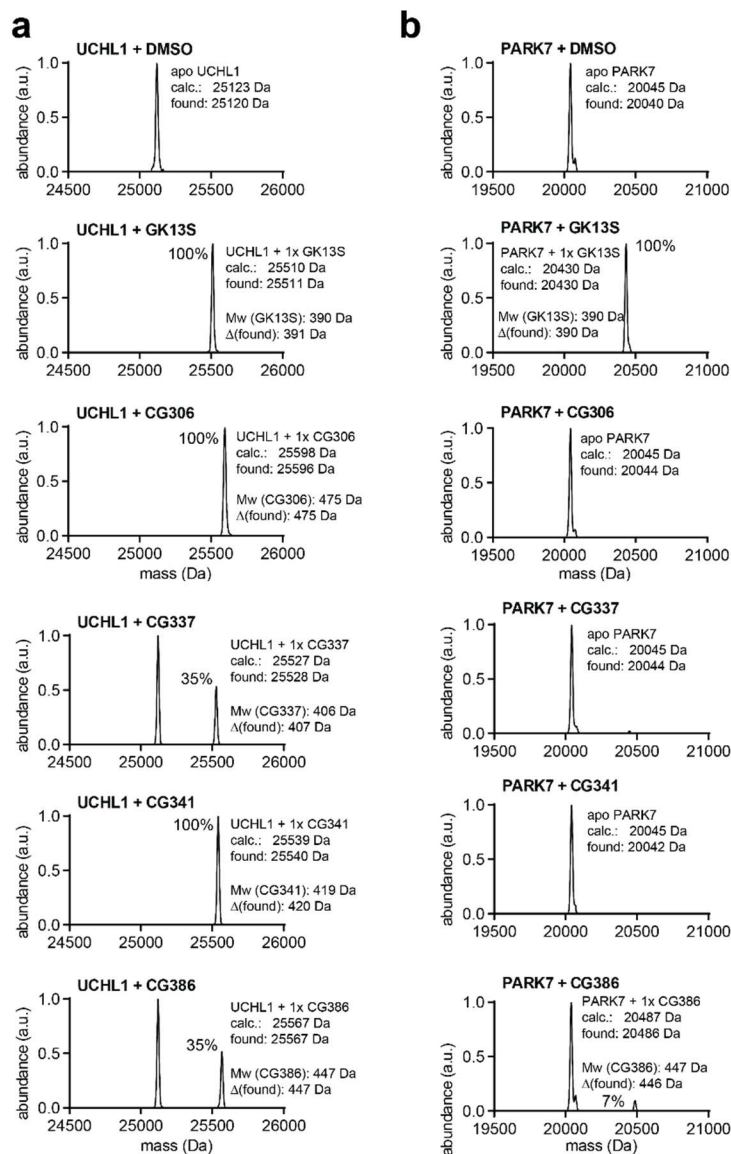


**Supplementary Fig. 9 | Clustering of proteins with increased or decreased levels after treatment with GK13S.**

Identified proteins with altered levels after the treatment of U-87 MG cells with Gk13S, were clustered by their protein class using the webtool PANTHER.<sup>[174]</sup>

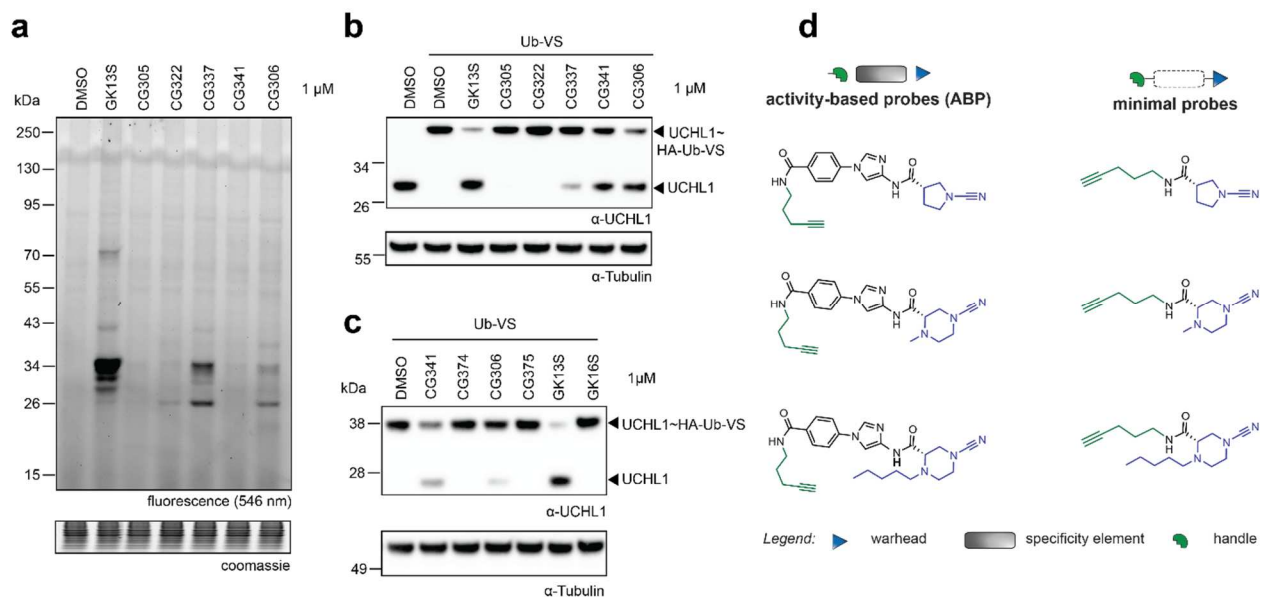
## Supplementary Data

### Supplementary Figure 10



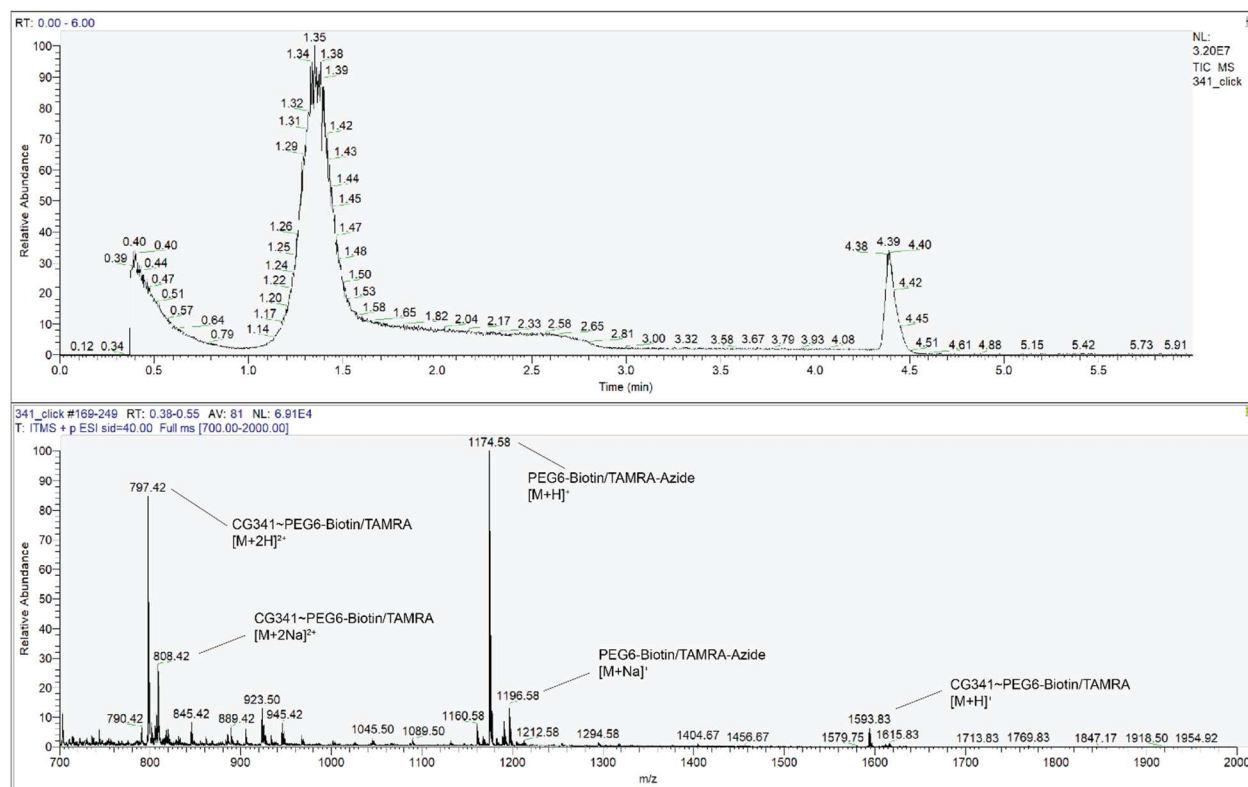
**Supplementary Fig. 10 | Intact protein mass spectra recorded from various N-cyanopiperazine warheads probe.** Either purified UCHL1 or PARK7 was incubated with the indicated N-cyanopiperazine probes and subsequently measured on the LC/MS to test for covalent modification of the proteins. DMSO and GK13S were used as controls.

## Supplementary Figure 11



**Supplementary Fig. 11 | Further cellular characterization of N-cyanopiperazine compounds. a)** in-gel fluorescence was recorded after treatment of HEK293 cells with indicated compounds (1  $\mu$ M). **b, c)** UCHL1 target engagement of indicated probes after treatment of HEK293 cell lysates. **d)** Molecular structures of used probes.

## Supplementary Figure 12



**Supplementary Fig. 12 | Mass spectrum of CG341 and UCHL1 after addition of CuACC reagents. LC/MS confirms the reversibility of CG341 from UCHL1 after the addition of the click reagents.**

Uncropped Gels

Fig. 11 C

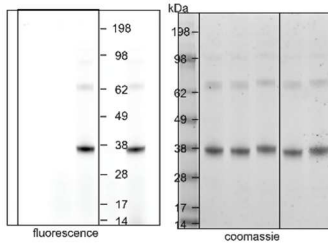


Fig. 11 D

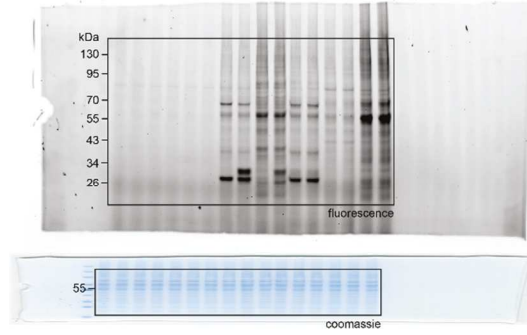
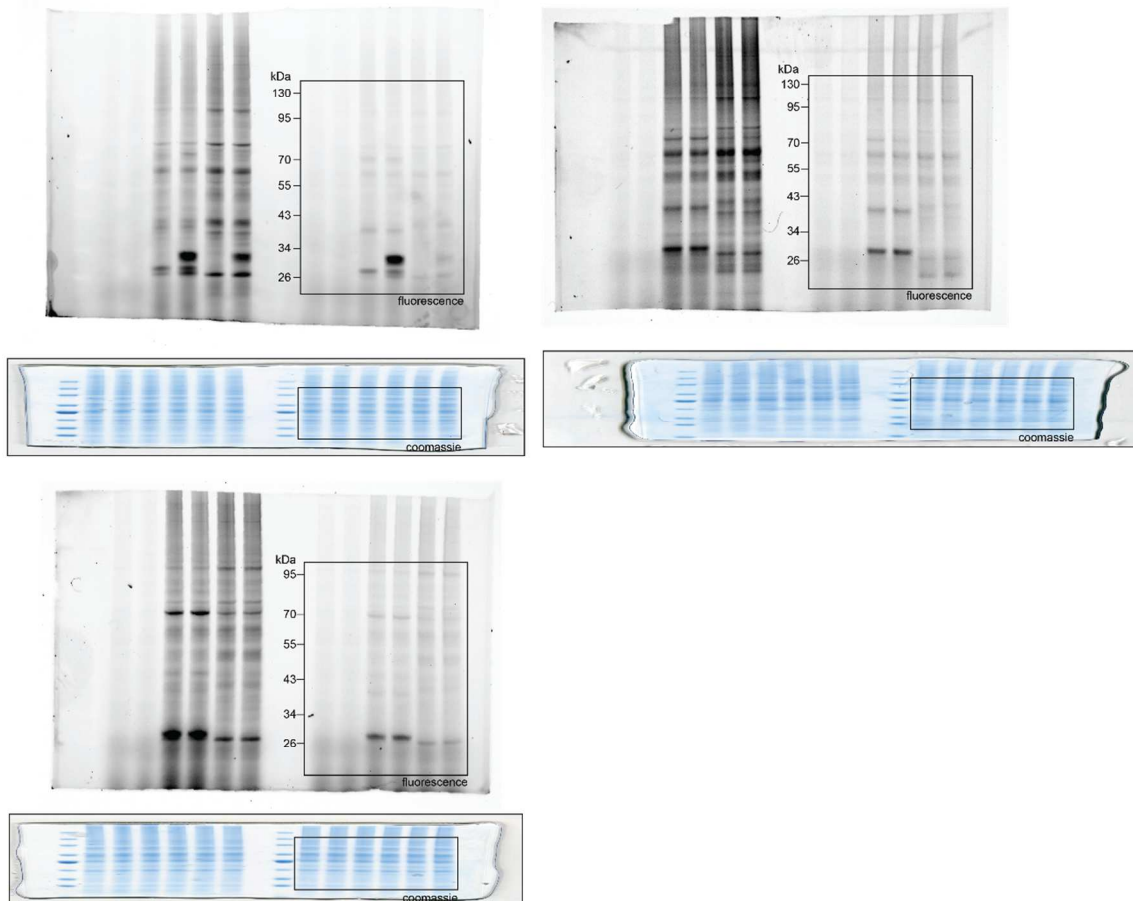
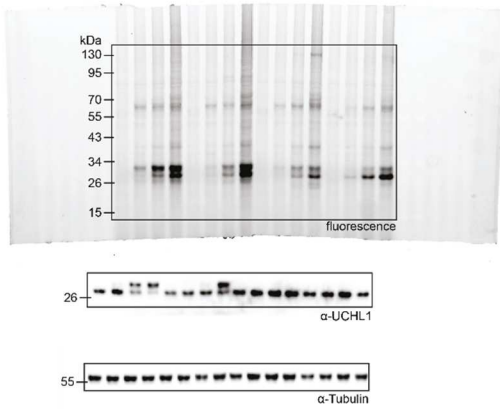


Fig. 12 B



# Supplementary Data

**Fig. 13 B**



**Fig. 13 C**

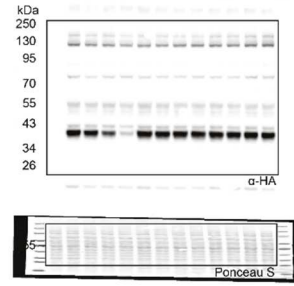


**Fig. 15 A**

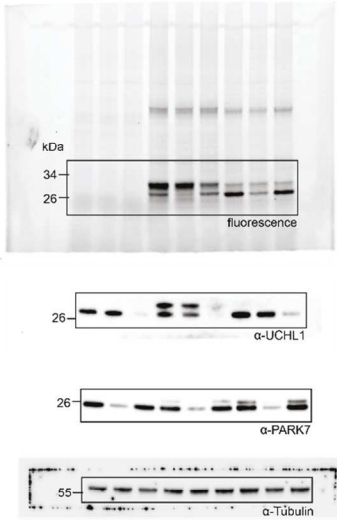


**Fig. 15 B**

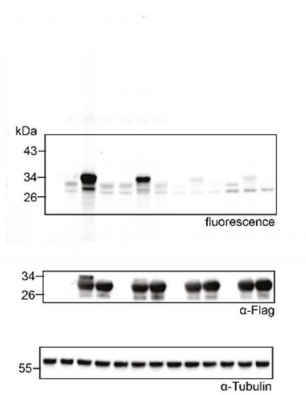


**Fig. 15 C**

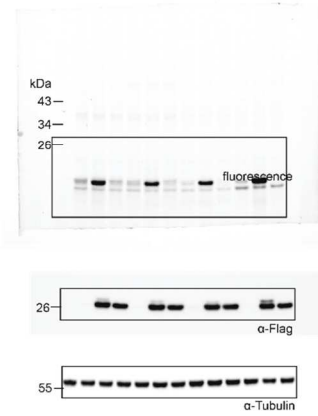


**Fig. 17 D**

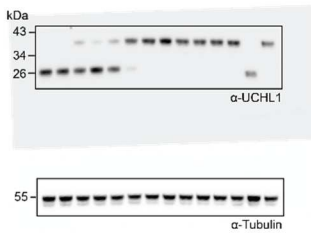
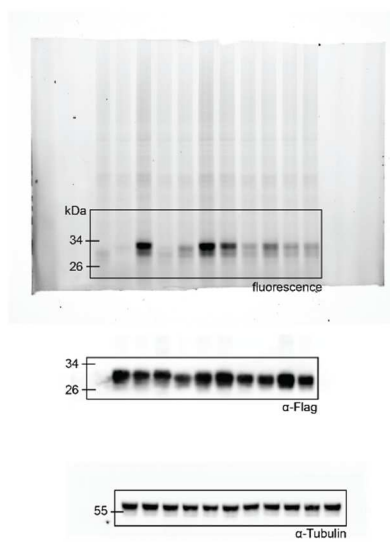


**Fig. 18 K**



Supplementary Data

Fig. 19 E

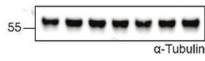
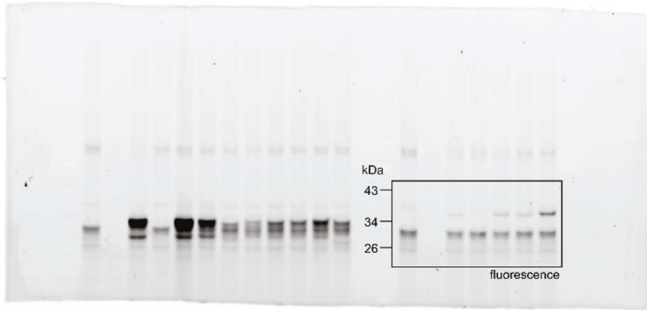


Fig. 20 A

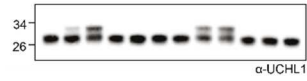
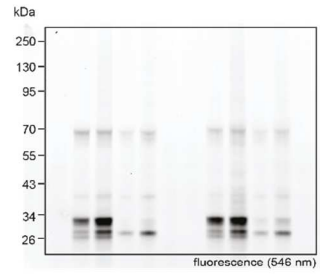


Fig. 20 C

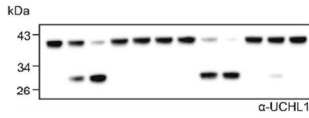


Fig. 20 D

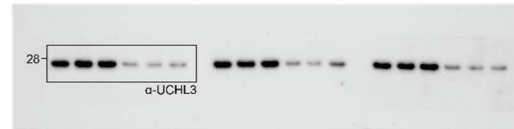
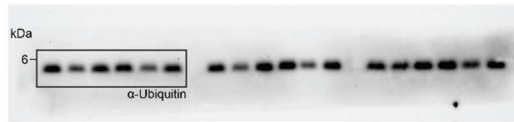


Fig. 21 A

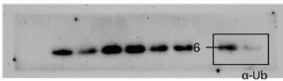
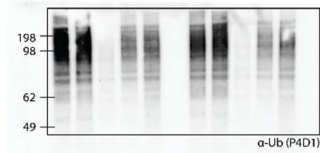


Fig. 21 C





Supplementary Data

**Fig. 22 D**

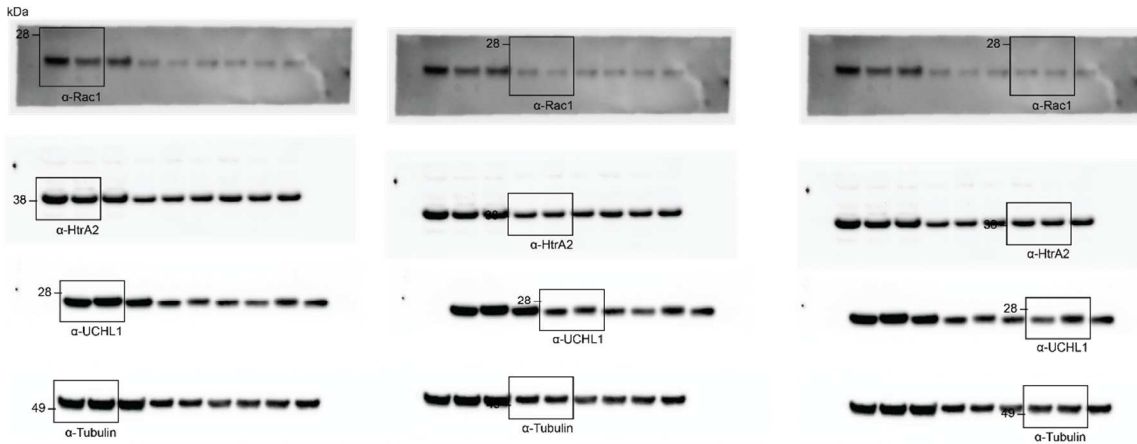


**Fig. 23 B**

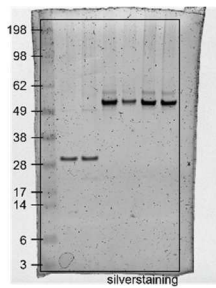


**Fig. 25 C**

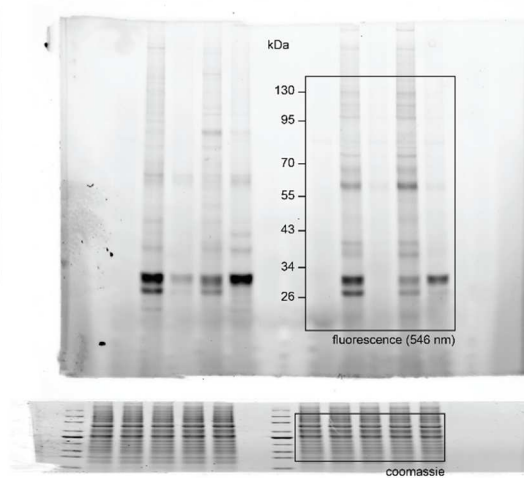


**Fig. 25 D**

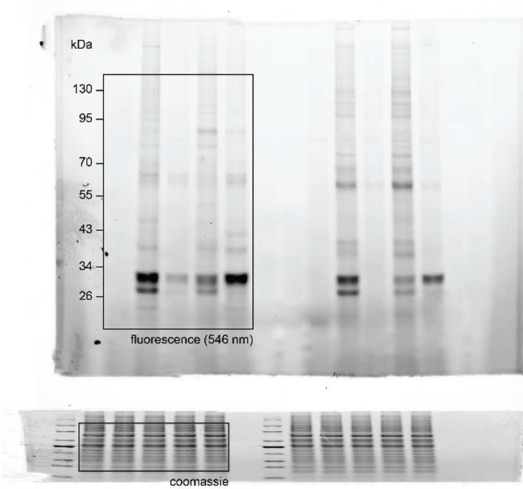


**Fig. 25 E**

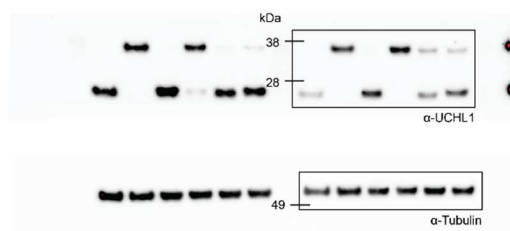
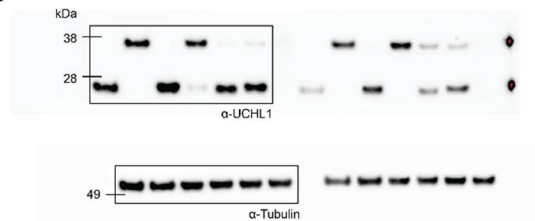


**Fig. 25 F**



Supplementary Data

Fig. 27 A

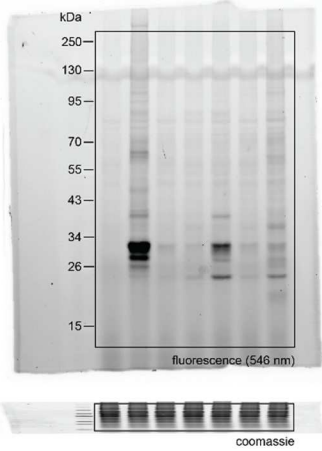


Fig. 27 B

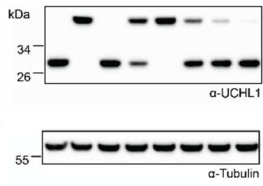


Fig. 27 C

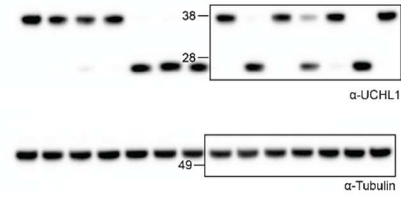


Fig. 28 B

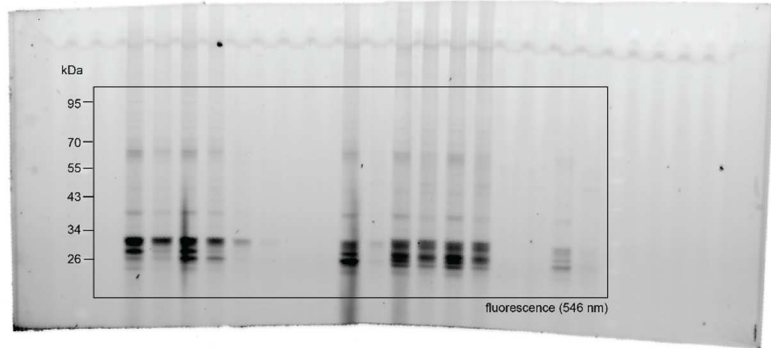


Fig. 28 A

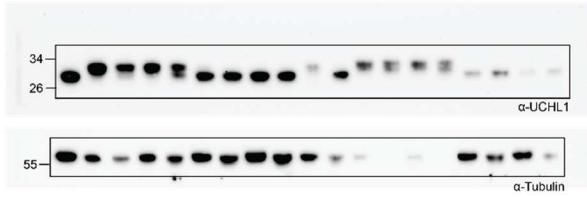
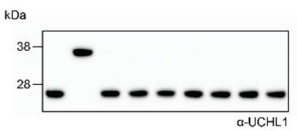
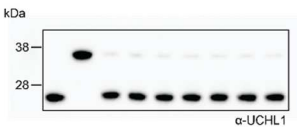
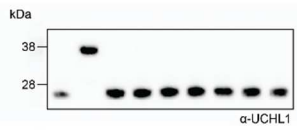
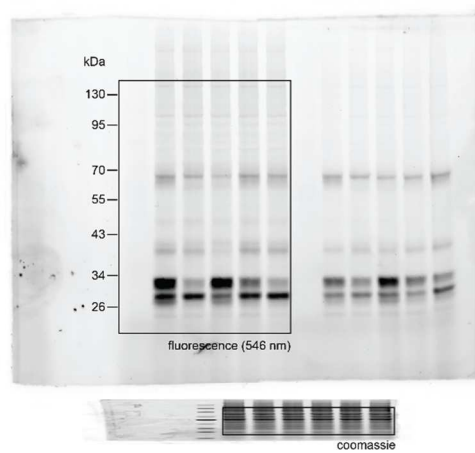


Fig. 30 B



Supplementary Data

Fig. 30 C

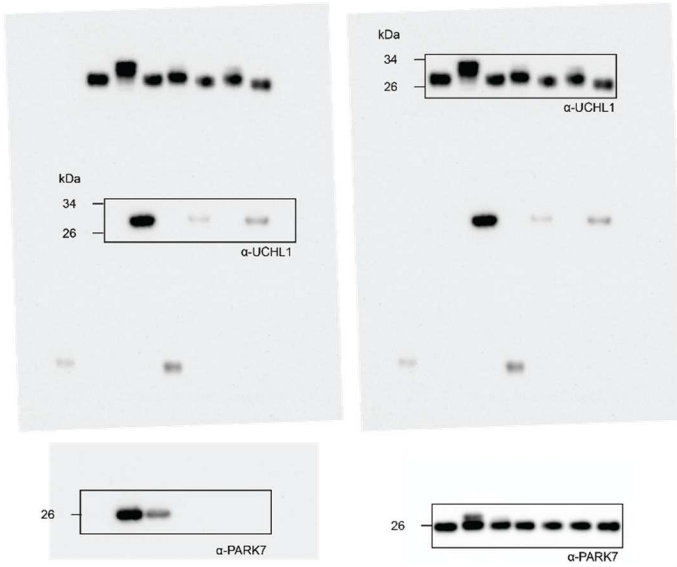


Fig. 30 E

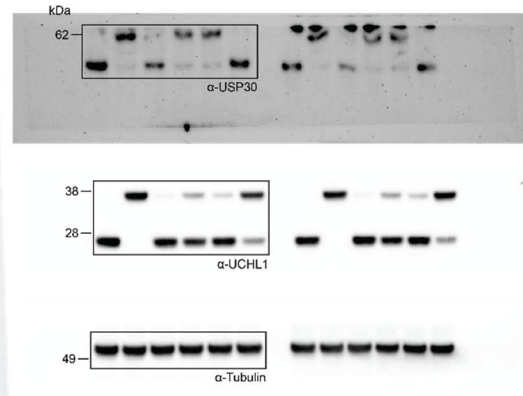


Fig. 32 D

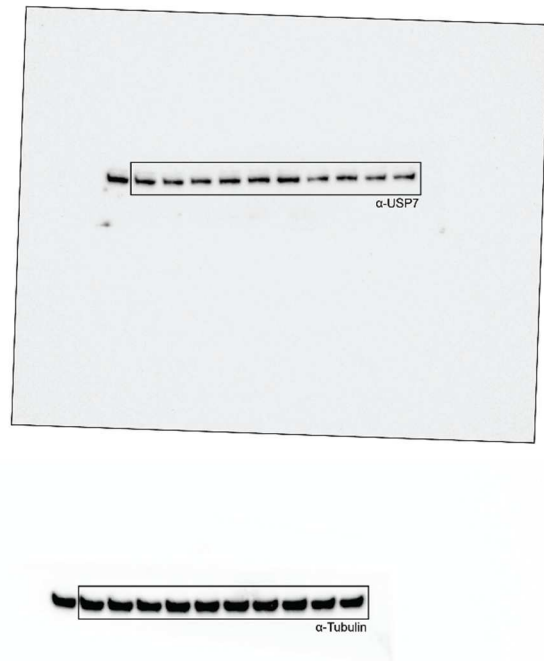
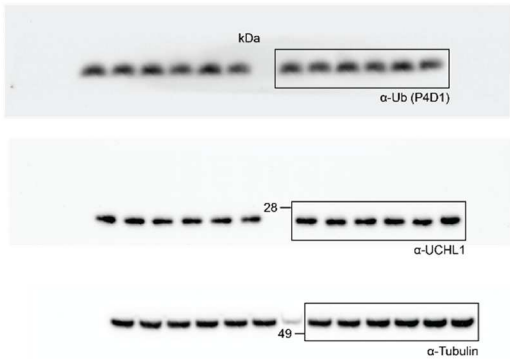
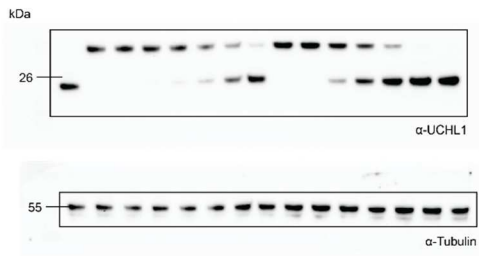


Fig. 30 F



# Supplementary Data

**Fig. 33 B**



**Fig. 33 C**

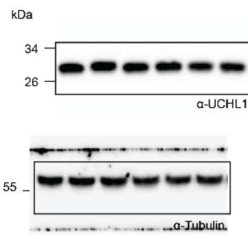


**Fig. 33 D**

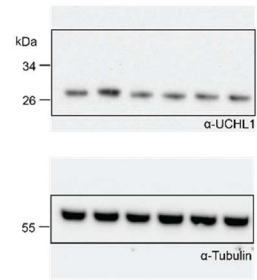
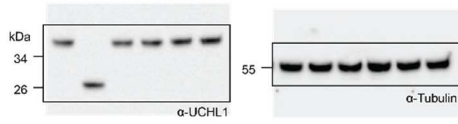
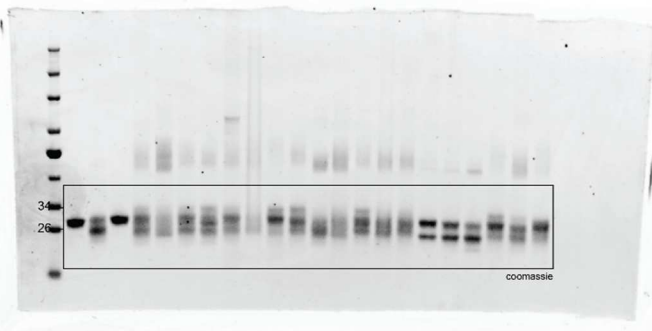
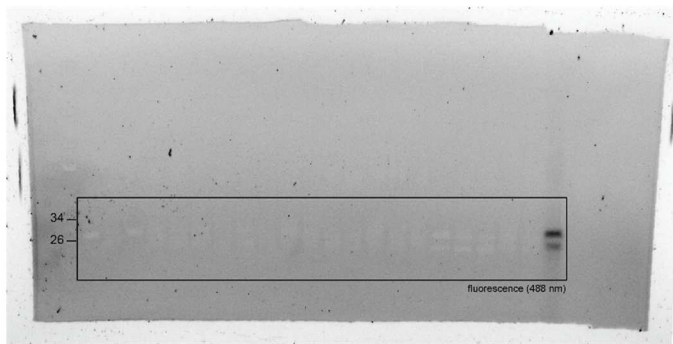
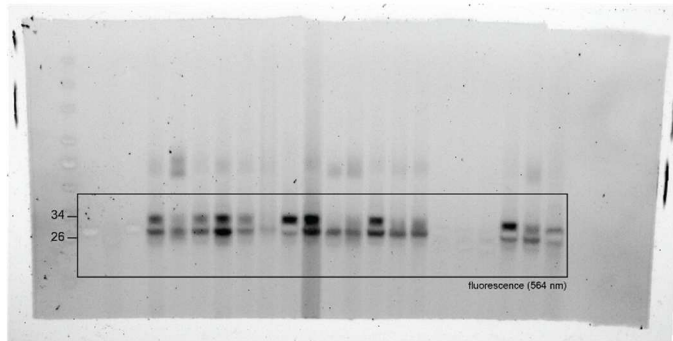


**Fig. 33 E**

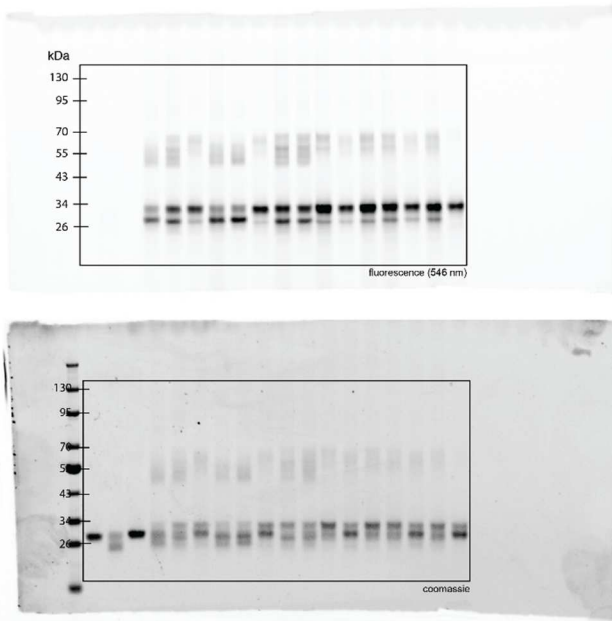


**Supp. Fig. 1 A**

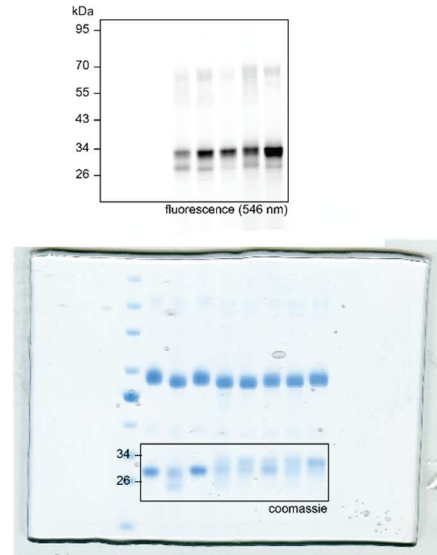


# Supplementary Data

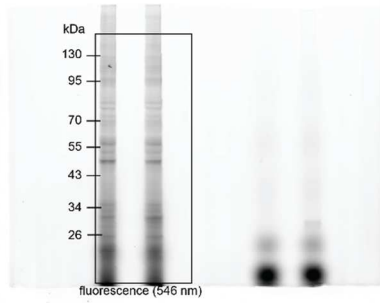
Supp. Fig. 1 B



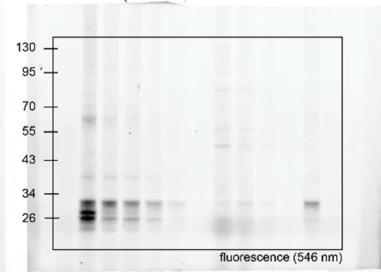
Supp. Fig. 1 C



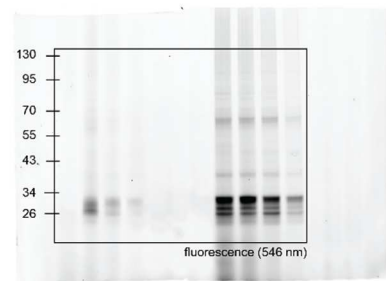
Supp. Fig. 1 D



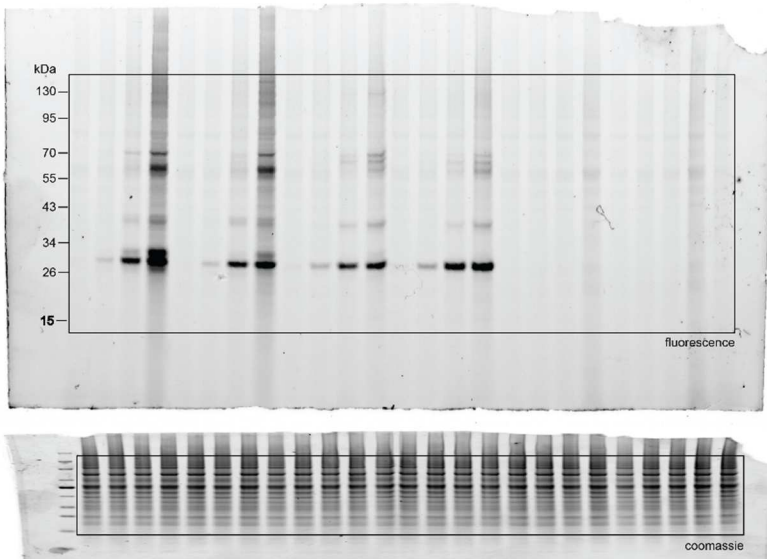
Supp. Fig. 1 E



Supp. Fig. 1 F

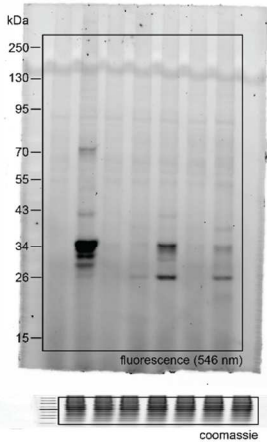


Supp. Fig. 2

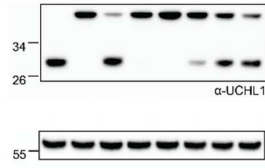


Supplementary Data

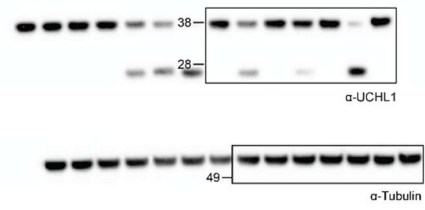
Supp. Fig. 11 A



Supp. Fig. 11 B



Supp. Fig. 11 C



## 7. References

- [1] G. Nalepa, M. Rolfe, J. W. Harper, *Nat Rev Drug Discov* **2006**, *5*, 596-613.
- [2] A. Hershko, A. Ciechanover, *Annual review of biochemistry* **1982**, *51*, 335-364.
- [3] W. Baumeister, J. Walz, F. Zühl, E. Seemüller, *Cell* **1998**, *92*, 367-380.
- [4] L. Bedford, J. Lowe, L. R. Dick, R. J. Mayer, J. E. Brownell, *Nature Reviews Drug Discovery* **2011**, *10*, 29-46.
- [5] C. Pohl, I. Dikic, *Science* **2019**, *366*, 818-822.
- [6] aT. Ravid, M. Hochstrasser, *Nat Rev Mol Cell Biol* **2008**, *9*, 679-690; bA. Hershko, A. Ciechanover, A. Varshavsky, *Nature Medicine* **2000**, *6*, 1073-1081.
- [7] aJ. Herrmann, A. Ciechanover, L. O. Lerman, A. Lerman, *Cardiovasc Res* **2004**, *61*, 11-21; bQ. Zheng, T. Huang, L. Zhang, Y. Zhou, H. Luo, H. Xu, X. Wang, *Front Aging Neurosci* **2016**, *8*, 303.
- [8] Y. T. Kwon, A. Ciechanover, *Trends Biochem Sci* **2017**, *42*, 873-886.
- [9] C. M. Pickart, *Cell* **2004**, *116*, 181-190.
- [10] D. Popovic, D. Vucic, I. Dikic, *Nature Medicine* **2014**, *20*, 1242-1253.
- [11] Y. Leestemaker, H. Ovaa, *Drug Discov Today Technol* **2017**, *26*, 25-31.
- [12] G. Asher, Y. Shaul, *Cell Cycle* **2005**, *4*, 1015-1018.
- [13] A. Ciechanover, A. Orian, A. L. Schwartz, *Bioessays* **2000**, *22*, 442-451.
- [14] S. Murata, H. Yashiroda, K. Tanaka, *Nature Reviews Molecular Cell Biology* **2009**, *10*, 104-115.
- [15] J. Myung, K. B. Kim, C. M. Crews, *Med Res Rev* **2001**, *21*, 245-273.
- [16] J. A. M. Bard, E. A. Goodall, E. R. Greene, E. Jonsson, K. C. Dong, A. Martin, *Annual Review of Biochemistry* **2018**, *87*, 697-724.
- [17] A. Y. Amerik, M. Hochstrasser, *Biochim Biophys Acta* **2004**, *1695*, 189-207.
- [18] P. D'Arcy, X. Wang, S. Linder, *Pharmacol Ther* **2015**, *147*, 32-54.
- [19] aV. M. Weake, J. L. Workman, *Mol Cell* **2008**, *29*, 653-663; bB. Suresh, J. Lee, H. Kim, S. Ramakrishna, *Cell Death Differ* **2016**, *23*, 1257-1264.
- [20] D. J. Marsh, Y. Ma, K. A. Dickson, *Cancers (Basel)* **2020**, *12*.
- [21] K. Haglund, S. Sigismund, S. Polo, I. Szymkiewicz, P. P. Di Fiore, I. Dikic, *Nat Cell Biol* **2003**, *5*, 461-466.
- [22] M. Mattern, J. Sutherland, K. Kadimisetty, R. Barrio, M. S. Rodriguez, *Trends Biochem Sci* **2019**, *44*, 599-615.
- [23] M. E. French, C. F. Koehler, T. Hunter, *Cell Discovery* **2021**, *7*, 6.
- [24] M. Akutsu, I. Dikic, A. Bremm, *Journal of Cell Science* **2016**, *129*, 875-880.
- [25] aM. L. Matsumoto, K. E. Wickliffe, K. C. Dong, C. Yu, I. Bosanac, D. Bustos, L. Phu, D. S. Kirkpatrick, S. G. Hymowitz, M. Rape, R. F. Kelley, V. M. Dixit, *Mol Cell* **2010**, *39*, 477-484; bV. Chau, J. W. Tobias, A. Bachmair, D. Marriott, D. J. Ecker, D. K. Gonda, A. Varshavsky, *Science* **1989**, *243*, 1576-1583; cL. Zhang, M. Xu, E. Scotti, Z. J. Chen, P. Tontonoz, *Journal of Lipid Research* **2013**, *54*, 1410-1420.
- [26] J. R. Morris, E. Solomon, *Hum Mol Genet* **2004**, *13*, 807-817.
- [27] M. Gatti, S. Pinato, A. Maiolica, F. Rocchio, M. G. Prato, R. Aebersold, L. Penengo, *Cell Rep* **2015**, *10*, 226-238.
- [28] aA. Ordureau, J.-M. Heo, D. M. Duda, J. A. Paulo, J. L. Olszewski, D. Yanishevski, J. Rinehart, B. A. Schulman, J. W. Harper, *Proceedings of the National Academy of Sciences* **2015**, *112*, 6637-6642; bS. Geisler, K. M. Holmström, D. Skujat, F. C. Fiesel, O. C. Rothfuss, P. J. Kahle, W. Springer, *Nature Cell Biology* **2010**, *12*, 119-131.
- [29] aY. Zhang, R.-b. Liu, Q. Cao, K.-q. Fan, L.-j. Huang, J.-s. Yu, Z.-j. Gao, T. Huang, J.-y. Zhong, X.-t. Mao, F. Wang, P. Xiao, Y. Zhao, X.-h. Feng, Y.-y. Li, J. Jin, *The Journal of Clinical Investigation*

## References

- 2019**, *129*, 2856-2871; bH. Huang, M. S. Jeon, L. Liao, C. Yang, C. Elly, J. R. Yates, 3rd, Y. C. Liu, *Immunity* **2010**, *33*, 60-70; cA. Hay-Koren, M. Caspi, A. Zilberberg, R. Rosin-Arbesfeld, *Mol Biol Cell* **2011**, *22*, 399-411.
- [30] W. C. Yuan, Y. R. Lee, S. Y. Lin, L. Y. Chang, Y. P. Tan, C. C. Hung, J. C. Kuo, C. H. Liu, M. Y. Lin, M. Xu, Z. J. Chen, R. H. Chen, *Mol Cell* **2014**, *54*, 586-600.
- [31] J. M. Boname, M. Thomas, H. R. Stagg, P. Xu, J. Peng, P. J. Lehner, *Traffic* **2010**, *11*, 210-220.
- [32] K. N. Swatek, J. L. Usher, A. F. Kueck, C. Gladkova, T. E. T. Mevissen, J. N. Pruneda, T. Skern, D. Komander, *Nature* **2019**, *572*, 533-537.
- [33] aH. J. Meyer, M. Rape, *Cell* **2014**, *157*, 910-921; bR. G. Yau, K. Doerner, E. R. Castellanos, D. L. Haakonsen, A. Werner, N. Wang, X. W. Yang, N. Martinez-Martin, M. L. Matsumoto, V. M. Dixit, M. Rape, *Cell* **2017**, *171*, 918-933.e920.
- [34] K. N. Swatek, D. Komander, *Cell Research* **2016**, *26*, 399-422.
- [35] D. A. Pérez Berrocal, K. F. Witting, H. Ovaa, M. P. C. Mulder, *Frontiers in Chemistry* **2020**, *7*.
- [36] Y. Sato, A. Yoshikawa, H. Mimura, M. Yamashita, A. Yamagata, S. Fukai, *Embo j* **2009**, *28*, 2461-2468.
- [37] R. Varadan, M. Assfalg, S. Raasi, C. Pickart, D. Fushman, *Mol Cell* **2005**, *18*, 687-698.
- [38] C. W. Park, K. Y. Ryu, *BMB Rep* **2014**, *47*, 475-482.
- [39] A. Martínez-Férriz, A. Ferrando, A. Fathinajafabadi, R. Farràs, *Seminars in Cell & Developmental Biology* **2022**, *132*, 146-154.
- [40] C. P. Grou, M. P. Pinto, A. V. Mendes, P. Domingues, J. E. Azevedo, *Scientific Reports* **2015**, *5*, 12836.
- [41] J. A. M. Bard, E. A. Goodall, E. R. Greene, E. Jonsson, K. C. Dong, A. Martin, *Annu Rev Biochem* **2018**, *87*, 697-724.
- [42] aD. Komander, M. J. Clague, S. Urbé, *Nature Reviews Molecular Cell Biology* **2009**, *10*, 550-563; bY. Kee, T. T. Huang, *Mol Cell Biol* **2016**, *36*, 524-544.
- [43] M. J. Clague, S. Urbé, D. Komander, *Nature Reviews Molecular Cell Biology* **2019**, *20*, 338-352.
- [44] N. J. Schauer, R. S. Magin, X. Liu, L. M. Doherty, S. J. Buhrlage, *J Med Chem* **2020**, *63*, 2731-2750.
- [45] N. A. Snyder, G. M. Silva, *J Biol Chem* **2021**, *297*, 101077.
- [46] J. Heideker, I. E. Wertz, *Biochem J* **2015**, *465*, 1-26.
- [47] aM. J. Clague, I. Barsukov, J. M. Coulson, H. Liu, D. J. Rigden, S. Urbé, *Physiol Rev* **2013**, *93*, 1289-1315; bC. K. Chou, Y. T. Chang, M. Korinek, Y. T. Chen, Y. T. Yang, S. Leu, I. L. Lin, C. J. Tang, C. C. Chiu, *Int J Mol Sci* **2017**, *18*.
- [48] L. Simón, J. M. Goodman, *The Journal of Organic Chemistry* **2010**, *75*, 1831-1840.
- [49] M. Walden, S. K. Masandi, K. Pawłowski, E. Zeqiraj, *Biochem Soc Trans* **2018**, *46*, 453-466.
- [50] J. A. Ronau, J. F. Beckmann, M. Hochstrasser, *Cell Research* **2016**, *26*, 441-456.
- [51] T. E. T. Mevissen, D. Komander, *Annu Rev Biochem* **2017**, *86*, 159-192.
- [52] K. Keusekotten, P. R. Elliott, L. Glockner, B. K. Fiil, R. B. Damgaard, Y. Kulathu, T. Wauer, M. K. Hospenthal, M. Gyrd-Hansen, D. Krappmann, K. Hofmann, D. Komander, *Cell* **2013**, *153*, 1312-1326.
- [53] B. J. Winborn, S. M. Travis, S. V. Todi, K. M. Scaglione, P. Xu, A. J. Williams, R. E. Cohen, J. Peng, H. L. Paulson, *J Biol Chem* **2008**, *283*, 26436-26443.
- [54] aP. Paudel, Q. Zhang, C. Leung, H. C. Greenberg, Y. Guo, Y. H. Chern, A. Dong, Y. Li, M. Vedadi, Z. Zhuang, Y. Tong, *Proc Natl Acad Sci U S A* **2019**, *116*, 7288-7297; bY. Ye, M. Akutsu, F. Reyes-Turcu, R. I. Enchev, K. D. Wilkinson, D. Komander, *EMBO Rep* **2011**, *12*, 350-357.
- [55] T. Das, S. C. Shin, E. J. Song, E. E. Kim, *Int J Mol Sci* **2020**, *21*.
- [56] aS. V. Todi, B. J. Winborn, K. M. Scaglione, J. R. Blount, S. M. Travis, H. L. Paulson, *Embo j* **2009**, *28*, 372-382; bE. Meulmeester, M. Kunze, H. H. Hsiao, H. Urlaub, F. Melchior, *Mol Cell* **2008**, *30*, 610-619.



## References

- [57] N. Mashtalir, S. Daou, H. Barbour, N. N. Sen, J. Gagnon, I. Hammond-Martel, H. H. Dar, M. Therrien, B. Affar el, *Mol Cell* **2014**, *54*, 392-406.
- [58] K. H. Ventii, K. D. Wilkinson, *Biochem J* **2008**, *414*, 161-175.
- [59] aJ. McCullough, P. E. Row, O. Lorenzo, M. Doherty, R. Beynon, M. J. Clague, S. Urbé, *Curr Biol* **2006**, *16*, 160-165; bI. Berlin, H. Schwartz, P. D. Nash, *J Biol Chem* **2010**, *285*, 34909-34921.
- [60] M. K. Mann, I. Franzoni, R. F. de Freitas, W. Tempel, S. Houlston, L. Smith, M. Vedadi, C. H. Arrowsmith, R. J. Harding, M. Schapira, *J Med Chem* **2019**, *62*, 10144-10155.
- [61] L. Arpalahti, J. Hagström, H. Mustonen, M. Lundin, C. Haglund, C. I. Holmberg, *Tumour Biol* **2017**, *39*, 1010428317716078.
- [62] M. Gersch, C. Gladkova, A. F. Schubert, M. A. Michel, S. Maslen, D. Komander, *Nature Structural & Molecular Biology* **2017**, *24*, 920-930.
- [63] S. Urbé, H. Liu, S. D. Hayes, C. Heride, D. J. Rigden, M. J. Clague, *Mol Biol Cell* **2012**, *23*, 1095-1103.
- [64] K. Velasco, B. Zhao, S. Callegari, M. Altun, H. Liu, G. Hassink, M. G. Masucci, K. Lindsten, *Biochem Biophys Res Commun* **2013**, *433*, 390-395.
- [65] M. J. Clague, C. Heride, S. Urbé, *Trends Cell Biol* **2015**, *25*, 417-426.
- [66] R. Setsuie, K. Wada, *Neurochemistry International* **2007**, *51*, 105-111.
- [67] Z. R. Zhou, Y. H. Zhang, S. Liu, A. X. Song, H. Y. Hu, *Biochem J* **2012**, *441*, 143-149.
- [68] P. Virnau, L. A. Mirny, M. Kardar, *PLoS Comput Biol* **2006**, *2*, e122.
- [69] C. Das, Q. Q. Hoang, C. A. Kreinbring, S. J. Luchansky, R. K. Meray, S. S. Ray, P. T. Lansbury, D. Ringe, G. A. Petsko, *Proc Natl Acad Sci U S A* **2006**, *103*, 4675-4680.
- [70] Y. Liu, L. Fallon, H. A. Lashuel, Z. Liu, P. T. Lansbury, Jr., *Cell* **2002**, *111*, 209-218.
- [71] M. Mondal, D. Conole, J. Nautiyal, E. W. Tate, *British Journal of Cancer* **2022**, *126*, 24-33.
- [72] J. S. Bett, M. S. Ritorto, R. Ewan, E. G. Jaffray, S. Virdee, J. W. Chin, A. Knebel, T. Kurz, M. Trost, M. H. Tatham, R. T. Hay, *Biochem J* **2015**, *466*, 489-498.
- [73] C. N. Larsen, B. A. Krantz, K. D. Wilkinson, *Biochemistry* **1998**, *37*, 3358-3368.
- [74] K. Bilguvar, N. K. Tyagi, C. Ozkara, B. Tuysuz, M. Bakircioglu, M. Choi, S. Delil, A. O. Caglayan, J. F. Baranoski, O. Erturk, C. Yalcinkaya, M. Karacorlu, A. Dincer, M. H. Johnson, S. Mane, S. S. Chandra, A. Louvi, T. J. Boggon, R. P. Lifton, A. L. Horwich, M. Gunel, *Proc Natl Acad Sci U S A* **2013**, *110*, 3489-3494.
- [75] P. Bishop, D. Rocca, J. M. Henley, *Biochem J* **2016**, *473*, 2453-2462.
- [76] aE. Tezel, K. Hibi, T. Nagasaka, A. Nakao, *Clinical Cancer Research* **2000**, *6*, 4764-4767; bT. Yamazaki, K. Hibi, T. Takase, E. Tezel, H. Nakayama, Y. Kasai, K. Ito, S. Akiyama, T. Nagasaka, A. Nakao, *Clin Cancer Res* **2002**, *8*, 192-195; cY. Miyoshi, S. Nakayama, Y. Torikoshi, S. Tanaka, H. Ishihara, T. Taguchi, Y. Tamaki, S. Noguchi, *Cancer Sci* **2006**, *97*, 523-529.
- [77] H. J. Kim, Y. M. Kim, S. Lim, Y. K. Nam, J. Jeong, H. J. Kim, K. J. Lee, *Oncogene* **2009**, *28*, 117-127.
- [78] R. Ummanni, E. Jost, M. Braig, F. Lohmann, F. Mundt, C. Barrett, T. Schlomm, G. Sauter, T. Senff, C. Bokemeyer, H. Sultmann, C. Meyer-Schwesinger, T. H. Brümmendorf, S. Balabanov, *Molecular Cancer* **2011**, *10*, 129.
- [79] A. Bheda, W. Yue, A. Gullapalli, C. Whitehurst, R. Liu, J. S. Pagano, J. Shackelford, *PLOS ONE* **2009**, *4*, e5955.
- [80] aX. S. Chen, K. S. Wang, W. Guo, L. Y. Li, P. Yu, X. Y. Sun, H. Y. Wang, Y. D. Guan, Y. G. Tao, B. N. Ding, M. Z. Yin, X. C. Ren, Y. Zhang, C. S. Chen, Y. C. Ye, J. M. Yang, Y. Cheng, *Theranostics* **2020**, *10*, 1833-1848; bY. Jin, W. Zhang, J. Xu, H. Wang, Z. Zhang, C. Chu, X. Liu, Q. Zou, *Int J Clin Exp Pathol* **2015**, *8*, 12500-12508.
- [81] aY. Goto, L. Zeng, C. J. Yeom, Y. Zhu, A. Morinibu, K. Shinomiya, M. Kobayashi, K. Hirota, S. Itasaka, M. Yoshimura, K. Tanimoto, M. Torii, T. Sowa, T. Menju, M. Sonobe, H. Kakeya, M. Toi,

## References

- H. Date, E. M. Hammond, M. Hiraoka, H. Harada, *Nat Commun* **2015**, *6*, 6153; bX. Li, A. Hattori, S. Takahashi, Y. Goto, H. Harada, H. Kakeya, *Cancer Sci* **2020**, *111*, 239-252.
- [82] aH. Liu, N. Povysheva, M. E. Rose, Z. Mi, J. S. Banton, W. Li, F. Chen, D. P. Reay, G. Barrionuevo, F. Zhang, S. H. Graham, *Proceedings of the National Academy of Sciences* **2019**, *116*, 4643-4650; bZ. Mi, H. Liu, M. E. Rose, J. Ma, D. P. Reay, X. Ma, J. J. Henchir, C. E. Dixon, S. H. Graham, *Neuroscience* **2021**, *475*, 127-136; cA. Tramutola, F. Di Domenico, E. Barone, M. Perluigi, D. A. Butterfield, *Oxidative Medicine and Cellular Longevity* **2016**, *2016*, 2756068.
- [83] W. P. Esler, M. S. Wolfe, *Science* **2001**, *293*, 1449-1454.
- [84] M. Zhang, Y. Deng, Y. Luo, S. Zhang, H. Zou, F. Cai, K. Wada, W. Song, *J Neurochem* **2012**, *120*, 1129-1138.
- [85] R. Kumar, D. K. Jangir, G. Verma, S. Shekhar, P. Hanpude, S. Kumar, R. Kumari, N. Singh, N. Sarovar Bhavesh, N. Ranjan Jana, T. Kanti Maiti, *Scientific Reports* **2017**, *7*, 44558.
- [86] R. Setsuie, Y. L. Wang, H. Mochizuki, H. Osaka, H. Hayakawa, N. Ichihara, H. Li, A. Furuta, Y. Sano, Y. J. Sun, J. Kwon, T. Kabuta, K. Yoshimi, S. Aoki, Y. Mizuno, M. Noda, K. Wada, *Neurochem Int* **2007**, *50*, 119-129.
- [87] H. Osaka, Y. L. Wang, K. Takada, S. Takizawa, R. Setsuie, H. Li, Y. Sato, K. Nishikawa, Y. J. Sun, M. Sakurai, T. Harada, Y. Hara, I. Kimura, S. Chiba, K. Namikawa, H. Kiyama, M. Noda, S. Aoki, K. Wada, *Hum Mol Genet* **2003**, *12*, 1945-1958.
- [88] P. Bishop, P. Rubin, A. R. Thomson, D. Rocca, J. M. Henley, *J Biol Chem* **2014**, *289*, 36140-36149.
- [89] Z. Mi, S. H. Graham, *Ageing Res Rev* **2023**, *86*, 101856.
- [90] P. Nielsen, J. Okarmus, M. Meyer, *Cells* **2023**, *12*.
- [91] J. Chakraborty, E. Ziviani, *Frontiers in Physiology* **2020**, *11*.
- [92] N. Townsend, D. Kazakiewicz, F. Lucy Wright, A. Timmis, R. Huculeci, A. Torbica, C. P. Gale, S. Achenbach, F. Weidinger, P. Vardas, *Nature Reviews Cardiology* **2022**, *19*, 133-143.
- [93] B. Wang, W. Cai, D. Ai, X. Zhang, L. Yao, *Journal of Cardiovascular Translational Research* **2020**, *13*, 131-141.
- [94] P. G. Richardson, T. Hideshima, K. C. Anderson, *Cancer Control* **2003**, *10*, 361-369.
- [95] R. Wei, X. Liu, W. Yu, T. Yang, W. Cai, J. Liu, X. Huang, G. T. Xu, S. Zhao, J. Yang, S. Liu, *Oncotarget* **2015**, *6*, 12872-12889.
- [96] A. M. Antao, A. Tyagi, K. S. Kim, S. Ramakrishna, *Cancers (Basel)* **2020**, *12*.
- [97] S. K. Kwon, M. Saindane, K. H. Baek, *Biochim Biophys Acta Rev Cancer* **2017**, *1868*, 404-411.
- [98] G. Sanz, M. Singh, S. Peugot, G. Selivanova, *J Mol Cell Biol* **2019**, *11*, 586-599.
- [99] S. M. Qi, G. Cheng, X. D. Cheng, Z. Xu, B. Xu, W. D. Zhang, J. J. Qin, *Front Cell Dev Biol* **2020**, *8*, 233.
- [100] O. World Health, World Health Organization, Geneva, **2020**.
- [101] Z. Fu, B. Huang, J. Tang, S. Liu, M. Liu, Y. Ye, Z. Liu, Y. Xiong, W. Zhu, D. Cao, J. Li, X. Niu, H. Zhou, Y. J. Zhao, G. Zhang, H. Huang, *Nat Commun* **2021**, *12*, 488.
- [102] C. B. McClain, N. Vabret, *Signal Transduct Target Ther* **2020**, *5*, 223.
- [103] I. Lamberto, X. Liu, H.-S. Seo, N. J. Schauer, R. E. Iacob, W. Hu, D. Das, T. Mikhailova, E. L. Weisberg, J. R. Engen, K. C. Anderson, D. Chauhan, S. Dhe-Paganon, S. J. Buhrlage, *Cell Chemical Biology* **2017**, *24*, 1490-1500.e1411.
- [104] A. P. Turnbull, S. Ioannidis, W. W. Krajewski, A. Pinto-Fernandez, C. Heride, A. C. L. Martin, L. M. Tonkin, E. C. Townsend, S. M. Buker, D. R. Lancia, J. A. Caravella, A. V. Toms, T. M. Charlton, J. Lahdenranta, E. Wilker, B. C. Follows, N. J. Evans, L. Stead, C. Alli, V. V. Zarayskiy, A. C. Talbot, A. J. Buckmelter, M. Wang, C. L. McKinnon, F. Saab, J. F. McGouran, H. Century, M. Gersch, M. S. Pittman, C. G. Marshall, T. M. Raynham, M. Simcox, L. M. D. Stewart, S. B. McLoughlin, J. A. Escobedo, K. W. Bair, C. J. Dinsmore, T. R. Hammonds, S. Kim, S. Urbé, M. J. Clague, B. M. Kessler, D. Komander, *Nature* **2017**, *550*, 481-486.

## References

- [105] G. Gavory, C. R. O'Dowd, M. D. Helm, J. Flasz, E. Arkoudis, A. Dossang, C. Hughes, E. Cassidy, K. McClelland, E. Odrzywol, N. Page, O. Barker, H. Miel, T. Harrison, *Nature Chemical Biology* **2018**, *14*, 118-125.
- [106] P. R. Leger, D. X. Hu, B. Biannic, M. Bui, X. Han, E. Karbarz, J. Maung, A. Okano, M. Osipov, G. M. Shibuya, K. Young, C. Higgs, B. Abraham, D. Bradford, C. Cho, C. Colas, S. Jacobson, Y. M. Ohol, D. Pookot, P. Rana, J. Sanchez, N. Shah, M. Sun, S. Wong, D. G. Brockstedt, P. D. Kassner, J. B. Schwarz, D. J. Wustrow, *J Med Chem* **2020**, *63*, 5398-5420.
- [107] A. Clancy, C. Heride, A. Pinto-Fernández, H. Elcocks, A. Kallinos, K. J. Kayser-Bricker, W. Wang, V. Smith, S. Davis, S. Fessler, C. McKinnon, M. Katz, T. Hammonds, N. P. Jones, J. O'Connell, B. Follows, S. Mischke, J. A. Caravella, S. Ioannidis, C. Dinsmore, S. Kim, A. Behrens, D. Komander, B. M. Kessler, S. Urbé, M. J. Clague, *J Cell Biol* **2021**, *220*.
- [108] J. D. Wrigley, G. Gavory, I. Simpson, M. Preston, H. Plant, J. Bradley, A. U. Goeppert, E. Rozycka, G. Davies, J. Walsh, A. Valentine, K. McClelland, K. E. Odrzywol, J. Renshaw, J. Boros, J. Tart, L. Leach, T. Nowak, R. A. Ward, T. Harrison, D. M. Andrews, *ACS Chem Biol* **2017**, *12*, 3113-3125.
- [109] aP. Di Lello, R. Pastor, J. M. Murray, R. A. Blake, F. Cohen, T. D. Crawford, J. Drobnick, J. Drummond, L. Kategaya, T. Kleinheinz, T. Maurer, L. Rougé, X. Zhao, I. Wertz, C. Ndubaku, V. Tsui, *Journal of Medicinal Chemistry* **2017**, *60*, 10056-10070; bA. F. Kluge, B. R. Lagu, P. Maiti, M. Jaleel, M. Webb, J. Malhotra, A. Mallat, P. A. Srinivas, J. E. Thompson, *Bioorg Med Chem Lett* **2018**, *28*, 2655-2659.
- [110] aF. Colland, E. Formstecher, X. Jacq, C. Reverdy, C. Planquette, S. Conrath, V. Trouplin, J. Bianchi, V. N. Aushev, J. Camonis, A. Calabrese, C. Borg-Capra, W. Sippl, V. Collura, G. Boissy, J.-C. Rain, P. Guedat, R. Delansorne, L. Daviet, *Molecular Cancer Therapeutics* **2009**, *8*, 2286-2295; bJ. Weinstock, J. Wu, P. Cao, W. D. Kingsbury, J. L. McDermott, M. P. Kodrasov, D. M. McKelvey, K. G. Suresh Kumar, S. J. Goldenberg, M. R. Mattern, B. Nicholson, *ACS Medicinal Chemistry Letters* **2012**, *3*, 789-792.
- [111] M. S. Ritorto, R. Ewan, A. B. Perez-Oliva, A. Knebel, S. J. Buhrlage, M. Wightman, S. M. Kelly, N. T. Wood, S. Virdee, N. S. Gray, N. A. Morrice, D. R. Alessi, M. Trost, *Nat Commun* **2014**, *5*, 4763.
- [112] J. A. Harrigan, X. Jacq, N. M. Martin, S. P. Jackson, *Nature Reviews Drug Discovery* **2018**, *17*, 57-78.
- [113] W. C. Chan, X. Liu, R. S. Magin, N. M. Girardi, S. B. Ficarro, W. Hu, M. I. Tarazona Guzman, C. A. Starnbach, A. Felix, G. Adelmant, A. C. Varca, B. Hu, A. S. Bratt, E. DaSilva, N. J. Schauer, I. Jaen Maisonet, E. K. Dolen, A. X. Ayala, J. A. Marto, S. J. Buhrlage, *Nature Communications* **2023**, *14*, 686.
- [114] D. S. Hewings, J. A. Flygare, M. Bogyo, I. E. Wertz, *Febs j* **2017**, *284*, 1555-1576.
- [115] M. G. Paulick, M. Bogyo, *Curr Opin Genet Dev* **2008**, *18*, 97-106.
- [116] W. P. Heal, T. H. Dang, E. W. Tate, *Chem Soc Rev* **2011**, *40*, 246-257.
- [117] D. S. Hameed, A. Sapmaz, L. Burggraaff, A. Amore, C. J. Slingerland, G. J. P. van Westen, H. Ovaa, *Angewandte Chemie International Edition* **2019**, *58*, 14477-14482.
- [118] M. Gorka, H. M. Magnussen, Y. Kulathu, *Seminars in Cell & Developmental Biology* **2022**, *132*, 86-96.
- [119] L. E. Sanman, M. Bogyo, *Annu Rev Biochem* **2014**, *83*, 249-273.
- [120] A. Borodovsky, H. Ovaa, N. Kolli, T. Gan-Erdene, K. D. Wilkinson, H. L. Ploegh, B. M. Kessler, *Chem Biol* **2002**, *9*, 1149-1159.
- [121] Y. A. Lam, W. Xu, G. N. DeMartino, R. E. Cohen, *Nature* **1997**, *385*, 737-740.
- [122] S. C. Johnston, S. M. Riddle, R. E. Cohen, C. P. Hill, *Embo j* **1999**, *18*, 3877-3887.
- [123] X. Sui, Y. Wang, Y.-X. Du, L.-J. Liang, Q. Zheng, Y.-M. Li, L. Liu, *Chemical Science* **2020**, *11*, 12633-12646.

## References

- [124] A. Borodovsky, B. M. Kessler, R. Casagrande, H. S. Overkleeft, K. D. Wilkinson, H. L. Ploegh, *Embo j* **2001**, *20*, 5187-5196.
- [125] D. Flierman, G. J. van der Heden van Noort, R. Ekkebus, P. P. Geurink, T. E. Mevissen, M. K. Hospenthal, D. Komander, H. Ovaa, *Cell Chem Biol* **2016**, *23*, 472-482.
- [126] F. El Oualid, R. Merkx, R. Ekkebus, D. S. Hameed, J. J. Smit, A. de Jong, H. Hilkmann, T. K. Sixma, H. Ovaa, *Angewandte Chemie International Edition* **2010**, *49*, 10149-10153.
- [127] W. Gui, C. A. Ott, K. Yang, J. S. Chung, S. Shen, Z. Zhuang, *Journal of the American Chemical Society* **2018**, *140*, 12424-12433.
- [128] D. Conole, M. Mondal, J. D. Majmudar, E. W. Tate, *Front Chem* **2019**, *7*, 876.
- [129] aR. Kooij, S. Liu, A. Sapmaz, B.-T. Xin, G. M. C. Janssen, P. A. van Veelen, H. Ovaa, P. t. Dijke, P. P. Geurink, *Journal of the American Chemical Society* **2020**, *142*, 16825-16841; bN. Panyain, A. Godinat, T. Lanyon-Hogg, S. Lachiondo-Ortega, E. J. Will, C. Soudy, M. Mondal, K. Mason, S. Elkhalfifa, L. M. Smith, J. A. Harrigan, E. W. Tate, *Journal of the American Chemical Society* **2020**, *142*, 12020-12026; cA. D. Krabill, H. Chen, S. Hussain, C. Feng, A. Abdullah, C. Das, U. K. Aryal, C. B. Post, M. K. Wendt, P. J. Galardy, D. P. Flaherty, *Chembiochem* **2020**, *21*, 712-722.
- [130] B. F. Cravatt, A. T. Wright, J. W. Kozarich, *Annu Rev Biochem* **2008**, *77*, 383-414.
- [131] L. I. Willems, H. S. Overkleeft, S. I. van Kasteren, *Bioconjug Chem* **2014**, *25*, 1181-1191.
- [132] M. J. Niphakis, B. F. Cravatt, *Annu Rev Biochem* **2014**, *83*, 341-377.
- [133] J. A. Ward, L. McLellan, M. Stockley, K. R. Gibson, G. A. Whitlock, C. Knights, J. A. Harrigan, X. Jacq, E. W. Tate, *ACS Chemical Biology* **2016**, *11*, 3268-3272.
- [134] C. J. Gerry, S. L. Schreiber, *Nature Chemical Biology* **2020**, *16*, 369-378.
- [135] Y. Che, A. M. Gilbert, V. Shanmugasundaram, M. C. Noe, *Bioorg Med Chem Lett* **2018**, *28*, 2585-2592.
- [136] G. Dong, Y. Ding, S. He, C. Sheng, *Journal of Medicinal Chemistry* **2021**, *64*, 10606-10620.
- [137] K. Baek, B. A. Schulman, *Nature Chemical Biology* **2020**, *16*, 2-3.
- [138] aC. Galdeano, M. S. Gadd, P. Soares, S. Scaffidi, I. Van Molle, I. Birced, S. Hewitt, D. M. Dias, A. Ciulli, *J Med Chem* **2014**, *57*, 8657-8663; bD. L. Buckley, J. L. Gustafson, I. Van Molle, A. G. Roth, H. S. Tae, P. C. Gareiss, W. L. Jorgensen, A. Ciulli, C. M. Crews, *Angew Chem Int Ed Engl* **2012**, *51*, 11463-11467.
- [139] T. Mori, T. Ito, S. Liu, H. Ando, S. Sakamoto, Y. Yamaguchi, E. Tokunaga, N. Shibata, H. Handa, T. Hakoshima, *Scientific Reports* **2018**, *8*, 1294.
- [140] A. R. Schneekloth, M. Pucheault, H. S. Tae, C. M. Crews, *Bioorg Med Chem Lett* **2008**, *18*, 5904-5908.
- [141] T. Ishida, A. Ciulli, *SLAS Discov* **2021**, *26*, 484-502.
- [142] D. Weerakoon, R. J. Carbajo, L. De Maria, C. Tyrchan, H. Zhao, *Journal of Chemical Information and Modeling* **2022**, *62*, 340-349.
- [143] A. Zagidullin, V. Milyukov, A. Rizvanov, E. Bulatov, *Explor Target Antitumor Ther* **2020**, *1*, 381-390.
- [144] A. Mullard, *Nat Rev Drug Discov* **2019**.
- [145] L. M. Luh, U. Scheib, K. Juenemann, L. Wortmann, M. Brands, P. M. Cromm, *Angew Chem Int Ed Engl* **2020**, *59*, 15448-15466.
- [146] S. J. Hughes, A. Testa, N. Thompson, I. Churcher, *Drug Discov Today* **2021**, *26*, 2889-2897.
- [147] aA. Murgai, I. Sosič, M. Gobec, P. Lemnitzer, M. Proj, S. Wittenburg, R. Voget, M. Gütschow, J. Krönke, C. Steinebach, *Chemical Communications* **2022**, *58*, 8858-8861; bY. Pei, J. Fu, Y. Shi, M. Zhang, G. Luo, X. Luo, N. Song, T. Mi, Y. Yang, J. Li, Y. Zhou, B. Zhou, *Angew Chem Int Ed Engl* **2022**, *61*, e202204395.
- [148] N. J. Henning, L. Boike, J. N. Spradlin, C. C. Ward, G. Liu, E. Zhang, B. P. Belcher, S. M. Brittain, M. J. Hesse, D. Dovala, L. M. McGregor, R. Valdez Misiolek, L. W. Plasschaert, D. J. Rowlands, F.

## References

- Wang, A. O. Frank, D. Fuller, A. R. Estes, K. L. Randal, A. Panidapu, J. M. McKenna, J. A. Tallarico, M. Schirle, D. K. Nomura, *Nature Chemical Biology* **2022**, *18*, 412-421.
- [149] S. Flohr, P. Furet, P. Imbach, U. Hommel, H.-U. Litscher, S. G. Parrado, U. Hassiepen, J. Zimmermann, in *US7700605*, **2010**.
- [150] M. Biju, D. Su, K. Fisher, J. Yang, K. Robell, M. Bobko, in *Ubiquitin Drug Discovery and Diagnostics Conference, Philadelphia*, **2012**.
- [151] M. L. Stockley, M. I. Kemp, A. Madin, M. D. Woodrow, in *US0172518*, **2019**.
- [152] V. Kapuria, A. Levitzki, W. G. Bornmann, D. Maxwell, W. Priebe, R. J. Sorenson, H. D. Showalter, M. Talpaz, N. J. Donato, *Cell Signal* **2011**, *23*, 2076-2085.
- [153] M. Colombo, S. Vallese, I. Peretto, X. Jacq, J. C. Rain, F. Colland, P. Guedat, *ChemMedChem* **2010**, *5*, 552-558.
- [154] C. Grethe, Doctoral Thesis thesis, TU Dortmund (unpublished), **2023**.
- [155] L. Li, Z. Zhang, *Molecules* **2016**, *21*.
- [156] M. Karlsson, C. Zhang, L. Méar, W. Zhong, A. Digre, B. Katona, E. Sjöstedt, L. Butler, J. Odeberg, P. Dusart, F. Edfors, P. Oksvold, K. von Feilitzen, M. Zwahlen, M. Arif, O. Altay, X. Li, M. Ozcan, A. Mardinoglu, L. Fagerberg, J. Mulder, Y. Luo, F. Ponten, M. Uhlén, C. Lindskog, *Science Advances* **2021**, *7*, eabh2169.
- [157] Y. Goto, L. Zeng, C. J. Yeom, Y. Zhu, A. Morinibu, K. Shinomiya, M. Kobayashi, K. Hirota, S. Itasaka, M. Yoshimura, K. Tanimoto, M. Torii, T. Sowa, T. Menju, M. Sonobe, H. Takeya, M. Toi, H. Date, E. M. Hammond, M. Hiraoka, H. Harada, *Nature Communications* **2015**, *6*, 6153.
- [158] A. Pinto-Fernández, S. Davis, A. B. Schofield, H. C. Scott, P. Zhang, E. Salah, S. Mathea, P. D. Charles, A. Damianou, G. Bond, R. Fischer, B. M. Kessler, *Frontiers in Chemistry* **2019**, *7*.
- [159] L. H. Jones, M. E. Bunnage, *Nature Reviews Drug Discovery* **2017**, *16*, 285-296.
- [160] C. M. Clements, R. S. McNally, B. J. Conti, T. W. Mak, J. P. Ting, *Proc Natl Acad Sci U S A* **2006**, *103*, 15091-15096.
- [161] F. Lind-Holm Mogensen, A. Scafidi, A. Poli, A. Michelucci, *Journal of Neuroinflammation* **2023**, *20*, 95.
- [162] aJ. Y. Lee, J. Song, K. Kwon, S. Jang, C. Kim, K. Baek, J. Kim, C. Park, *Hum Mol Genet* **2012**, *21*, 3215-3225; bI. Maksimovic, E. Finkin-Groner, Y. Fukase, Q. Zheng, S. Sun, M. Michino, D. J. Huggins, R. W. Myers, Y. David, *RSC Medicinal Chemistry* **2021**, *12*, 1232-1238.
- [163] N. Smith, M. A. Wilson, in *DJ-1/PARK7 Protein: Parkinson's Disease, Cancer and Oxidative Stress-Induced Diseases* (Eds.: H. Ariga, S. M. M. Iguchi-Ariga), Springer Singapore, Singapore, **2017**, pp. 5-24.
- [164] S. Puri, S.-T. D. Hsu, *Journal of Molecular Biology* **2021**, *433*, 166879.
- [165] U. Hassiepen, U. Eidhoff, G. Meder, J.-F. Bulber, A. Hein, U. Bodendorf, E. Lorthiois, B. Martoglio, *Analytical Biochemistry* **2007**, *371*, 201-207.
- [166] S. J. Ham, D. Lee, W. J. Xu, E. Cho, S. Choi, S. Min, S. Park, J. Chung, *Science Advances* **2021**, *7*, 4574.
- [167] P. Bishop, D. Rocca, Jeremy M. Henley, *Biochemical Journal* **2016**, *473*, 2453-2462.
- [168] Y. Liu, H. A. Lashuel, S. Choi, X. Xing, A. Case, J. Ni, L. A. Yeh, G. D. Cuny, R. L. Stein, P. T. Lansbury, Jr., *Chem Biol* **2003**, *10*, 837-846.
- [169] K. Saigoh, Y.-L. Wang, J.-G. Suh, T. Yamanishi, Y. Sakai, H. Kiyosawa, T. Harada, N. Ichihara, S. Wakana, T. Kikuchi, K. Wada, *Nature Genetics* **1999**, *23*, 47-51.
- [170] A. T. Reinicke, K. Laban, M. Sachs, V. Kraus, M. Walden, M. Damme, W. Sachs, J. Reichelt, M. Schweizer, P. C. Janiesch, K. E. Duncan, P. Saftig, M. M. Rinschen, F. Morellini, C. Meyer-Schwesinger, *Proceedings of the National Academy of Sciences* **2019**, *116*, 7963-7972.
- [171] R. K. Meray, P. T. Lansbury, *Journal of Biological Chemistry* **2007**, *282*, 10567-10575.
- [172] Y. Fang, X. Shen, *Cancer and Metastasis Reviews* **2017**, *36*, 669-682.

## References

- [173] aY. Sato, A. Yoshikawa, A. Yamagata, H. Mimura, M. Yamashita, K. Ookata, O. Nureki, K. Iwai, M. Komada, S. Fukai, *Nature* **2008**, *455*, 358-362; bY. Wang, X. Zhou, M. Xu, W. Weng, Q. Zhang, Y. Yang, P. Wei, X. Du, *Oncotarget* **2016**, *7*, 36681-36697.
- [174] P. D. Thomas, D. Ebert, A. Muruganujan, T. Mushayahama, L. P. Albou, H. Mi, *Protein Sci* **2022**, *31*, 8-22.
- [175] M. Itoh-Satoh, T. Hayashi, H. Nishi, Y. Koga, T. Arimura, T. Koyanagi, M. Takahashi, S. Hohda, K. Ueda, T. Nouchi, M. Hiroe, F. Marumo, T. Imaizumi, M. Yasunami, A. Kimura, *Biochemical and Biophysical Research Communications* **2002**, *291*, 385-393.
- [176] W. J. Jockusch, D. Speidel, A. Sigler, J. B. Sørensen, F. Varoqueaux, J.-S. Rhee, N. Brose, *Cell* **2007**, *131*, 796-808.
- [177] D.-W. Park, M.-K. Nam, H. Rhim, *Biochemical and Biophysical Research Communications* **2011**, *415*, 24-29.
- [178] P. Saini, U. Rudakou, E. Yu, J. A. Ruskey, F. Asayesh, S. B. Laurent, D. Spiegelman, S. Fahn, C. Waters, O. Monchi, Y. Dauvilliers, N. Dupré, L. Greenbaum, S. Hassin-Baer, A. J. Espay, G. A. Rouleau, R. N. Alcalay, E. A. Fon, R. B. Postuma, Z. Gan-Or, *Neurobiology of Aging* **2021**, *100*, 119.e117-119.e113.
- [179] aE. E. Bosco, J. C. Mulloy, Y. Zheng, *Cellular and Molecular Life Sciences* **2008**, *66*, 370; bS. Etienne-Manneville, A. Hall, *Nature* **2002**, *420*, 629-635.
- [180] H. Marei, A. Malliri, *Small GTPases* **2017**, *8*, 139-163.
- [181] aM. Westerlund, H. Behbahani, S. Gellhaar, C. Forsell, A. C. Belin, A. Anvret, A. Zettergren, H. Nissbrandt, C. Lind, O. Sydow, C. Graff, L. Olson, M. Ankarcrona, D. Galter, *FASEB J* **2011**, *25*, 1345-1352; bJ. Senn, V. Csizmadia, P. Hales, L. Dick, V. J. Kadambi, *Blood* **2012**, *120*, 5023-5023.
- [182] M. E. Morrow, M. T. Morgan, M. Clerici, K. Growkova, M. Yan, D. Komander, T. K. Sixma, M. Simicek, C. Wolberger, *EMBO Rep* **2018**, *19*.
- [183] R. K. Meray, P. T. Lansbury, *Journal of Biological Chemistry* **2007**, *282*, 10567-10575.
- [184] V. De Cesare, J. Moran, R. Traynor, A. Knebel, M. S. Ritorto, M. Trost, H. McLauchlan, C. J. Hastie, P. Davies, *Nature Protocols* **2020**, *15*, 4034-4057.
- [185] T. Hansen, P. Vermeeren, A. Haim, M. J. H. van Dorp, J. D. C. Codée, F. M. Bickelhaupt, T. A. Hamlin, *European Journal of Organic Chemistry* **2020**, *2020*, 3822-3828.
- [186] P. Hubbard, W. J. Brittain, *The Journal of Organic Chemistry* **1998**, *63*, 677-683.
- [187] A. L. Ruchelman, H.-W. Man, W. Zhang, R. Chen, L. Capone, J. Kang, A. Parton, L. Corral, P. H. Schafer, D. Babusis, M. F. Moghaddam, Y. Tang, M. A. Shirley, G. W. Muller, *Bioorganic & Medicinal Chemistry Letters* **2013**, *23*, 360-365.
- [188] J. Krieger, F. J. Sorrell, A. A. Wegener, B. Leuthner, F. Machrouhi-Porcher, M. Hecht, E. M. Leibrock, J. E. Müller, J. Eisert, I. V. Hartung, S. Schlesiger, *ChemMedChem* **2023**, *18*, e202200615.
- [189] D. K. Brownsey, B. C. Rowley, E. Gorobets, B. S. Gelfand, D. J. Derksen, *Chemical Science* **2021**, *12*, 4519-4525.
- [190] I. A. Dain, S. A. Zolotov, G. K. Sazonov, E. S. Ponomarev, A. S. Zolotova, N. B. Demina, *Pharmaceutical Chemistry Journal* **2022**, *56*, 1290-1296.
- [191] J. Madan, V. K. Ahuja, K. Dua, S. Samajdar, M. Ramchandra, S. Giri, *BioDrugs* **2022**, *36*, 609-623.
- [192] B. T. Worrell, J. A. Malik, V. V. Fokin, *Science* **2013**, *340*, 457-460.
- [193] V. G. Klein, C. E. Townsend, A. Testa, M. Zengerle, C. Maniaci, S. J. Hughes, K.-H. Chan, A. Ciulli, R. S. Lokey, *ACS Medicinal Chemistry Letters* **2020**, *11*, 1732-1738.
- [194] A. M. Antao, A. Tyagi, K.-S. Kim, S. Ramakrishna, *Cancers* **2020**, *12*, 1579.
- [195] A. de Jong, K. Witting, R. Kooij, D. Flierman, H. Ovaas, *Angewandte Chemie International Edition* **2017**, *56*, 12967-12970.
- [196] S. M. Lange, L. A. Armstrong, Y. Kulathu, *Molecular Cell* **2022**, *82*, 15-29.

## References

- [197] N. Panyain, A. Godinat, A. R. Thawani, S. Lachiondo-Ortega, K. Mason, S. Elkhalfa, L. M. Smith, J. A. Harrigan, E. W. Tate, *RSC Medicinal Chemistry* **2021**, *12*, 1935-1943.
- [198] R. Pfoh, I. K. Lacdao, V. Saridakis, *Endocr Relat Cancer* **2015**, *22*, T35-54.
- [199] aY. J. Kim, I. H. Jeong, Y. S. Kim, S. Sung, D. H. Lee, J. H. Jang, Y.-H. Choung, Research Square, **2022**; bP. Yuan, L. Zhou, X. Zhang, L. Yao, J. Ning, X. Han, C. Ming, Y. Zhao, L. Zhang, *Bioscience Reports* **2020**, *40*.
- [200] Z. Mi, S. H. Graham, *Ageing Research Reviews* **2023**, *86*, 101856.
- [201] J. Liang, L. Oyang, S. Rao, Y. Han, X. Luo, P. Yi, J. Lin, L. Xia, J. Hu, S. Tan, L. Tang, Q. Pan, Y. Tang, Y. Zhou, Q. Liao, *Frontiers in Oncology* **2021**, *11*.
- [202] N. J. Agard, J. A. Prescher, C. R. Bertozzi, *Journal of the American Chemical Society* **2004**, *126*, 15046-15047.
- [203] C. Grethe, M. Schmidt, G.-M. Kipka, R. O'Dea, K. Gallant, P. Janning, M. Gersch, *Nature Communications* **2022**, *13*, 5950.
- [204] J. Cox, M. Mann, *Nat Biotechnol* **2008**, *26*, 1367-1372.
- [205] S. Tyanova, T. Temu, P. Sinitcyn, A. Carlson, M. Y. Hein, T. Geiger, M. Mann, J. Cox, *Nat Methods* **2016**, *13*, 731-740.
- [206] C. S. Hughes, S. Moggridge, T. Müller, P. H. Sorensen, G. B. Morin, J. Krijgsveld, *Nature Protocols* **2019**, *14*, 68-85.
- [207] J. Rappsilber, M. Mann, Y. Ishihama, *Nature Protocols* **2007**, *2*, 1896-1906.
- [208] J. Cox, N. Neuhauser, A. Michalski, R. A. Scheltema, J. V. Olsen, M. Mann, *J Proteome Res* **2011**, *10*, 1794-1805.
- [209] S. Tyanova, T. Temu, P. Sinitcyn, A. Carlson, M. Y. Hein, T. Geiger, M. Mann, J. Cox, *Nature Methods* **2016**, *13*, 731-740.

## 8. List of Abbreviations

### A

AA	amino acids
ABP	activity-based probe
ABPP	activity-based protein profiling
ACN	acetonitrile
AD	Alzheimer's disease
AMP	adenosine monophosphate
A <sub>N</sub>	nucleophilic addition
Asn	asparagine
Arg	arginine
Asp	aspartic acid
ATG12	autophagy-related protein
ATP	adenosine triphosphate

### B

BARD1	BRCA-associated RING domain protein 1
BF	bright-field
Boc <sub>2</sub> O	di- <i>tert</i> butyl dicarbonate
BRCA1	breast cancer 1
BTTAA	2-(4-((Bis((1-( <i>tert</i> -butyl)-1 <i>H</i> -1,2,3-triazol-4-yl)methyl)amino)methyl)-1 <i>H</i> -1,2,3-triazol-1-yl)acetic acid

### C

CAA	chloroacetamide
CFTR	cystic fibrosis transmembrane conductance regulator
CH	cyclohexane
CRBN	cereblon
CuAAC	copper-catalyzed azide-alkyne cycloaddition



## List of Abbreviations

CuSO<sub>4</sub> x 5 H<sub>2</sub>O copper(II) sulfate pentahydrate

Cys cysteine

### D

DAMN 2,3-diaminosuccinonitrile

DCM dichloromethane

DIAD diisopropyl azodicarboxylate

DMF dimethylformamide

DMSO dimethyl sulfoxide

DUB deubiquitinase

DUBTAC deubiquitinase-targeting chimera

### E

E1 ubiquitin activating enzyme

E2 ubiquitin conjugating enzyme

E3 ubiquitin ligase

EA ethylacetate

EGFR epidermal growth factor receptor

ER estrogen receptor

EtOH ethanol

### F

FAT10 human leukocyte antigen F-associated transcript 10

FUBI *fau* and its ubiquitin-like domain

### G

gad gracile axonal dystrophy

Glu glutamine

### H

H<sub>2</sub>O water

## List of Abbreviations

HATU	[O-(7-Azabenzotriazol-1-yl)- <i>N,N,N,N</i> -tetramethyluronium-hexafluorophosphat]
HECT	homologous to E6AP C-terminus
HIF1	hypoxia-inducible factor 1
His	histidine
HOAt	1-hydroxy-7-azabenzotriazole
HPV	human papilloma virus
HTS	high-throughput screening

### I

Ile	isoleucine
IPTG	isopropyl-1-thio- $\beta$ -D-galactopyranoside
ISG15	interferon-stimulated gene 15

### J

JAMM	Jab1/Mov34/MPN+ protease
JAK2	Janus kinase 2

### K

kd	knockdown
kDa	kilodalton

### L

Leu	leucine
Lys	lysine

### M

MeOH	methanol
Met	methionine
MINDY	motif interacting with Ub-containing novel DUB family
MJD	Machado-Josephin domain protease
MW	molecular weight

## List of Abbreviations

### N

NEDD8	neural precursor cell-expressed developmentally down-regulated protein 8
NGS	next generation sequencing
ns	not significant

### O

OEx	overexpression
oN	over night
OUT	ovarian tumor protease

### P

Pd	palladium
PD	Parkinson's disease
PE	petroleum ether
PEG	polyethylene glycol
PI	propidium iodide
Phe	phenylalanine
POI	protein of interest
PPI	protein-protein interaction
PROTAC	proteolysis-targeting chimera
PANTHER	protein analysis through evolutionary relationships
PTM	post-translational-modification

### R

rt	room temperature
RBR	ring between ring
RING	really interesting gene
ROS	reactive oxygen species

### S

## List of Abbreviations

SAR	structure-activity relationship
scr	scrambled
Ser	serine
S <sub>N</sub> Ar	nucleophilic aromatic substitution
STAM2	signal transducing adaptor molecule 2
STS	staurosporin
SUMO	small ubiquitin like modifier

## T

TBTA	Tris((1-benzyl-4-triazolyl)methyl)amine
TGF- $\beta$	transforming growth factor $\beta$
THF	tetrahydrofuran
THPTA	Tris((1-hydroxy-propyl-1H-1,2,3-triazol-4-yl)methyl)amine
<i>T<sub>m</sub></i>	melting temperature
TMSOI	trimethylsulfoxonium iodide
TNBC	triple negative breast cancer
TSA	thermal shift assay
Tyr	tyrosine

## U

Ub	ubiquitin
Ub-Al	ubiquitin-aldehyde
Ub-CN	ubiquitin-nitrile
Ub-Mesna	ubiquitin-2-mercaptoethane sulfonate sodium
Ub-PA	ubiquitin-propargyl amide
Ub-VME	ubiquitin-vinyl methyl ester
Ub-VS	ubiquitin-vinyl methyl sulfone
Ubl	ubiquitin like modifiers
Ub-Rh	ubiquitin rhodamine
UCH	ubiquitin C-terminal hydrolase
UFM1	ubiquitin-fold modifier 1
UIM	ubiquitin-interacting motif
UPS	ubiquitin proteasome system

## List of Abbreviations

URM1                    ubiquitin-related modifier 1

USP                     ubiquitin specific protease

### **V**

Val                     valine

VHL                    von-hippel-lindau

### **Z**

ZUP1                    zinc-finger-containing Ub peptidase

# Eidesstattliche Versicherung (Affidavit)

Name, Vorname  
(Surname, first name)

Matrikel-Nr.  
(Enrolment number)

**Belehrung:**

Wer vorsätzlich gegen eine die Täuschung über Prüfungsleistungen betreffende Regelung einer Hochschulprüfungsordnung verstößt, handelt ordnungswidrig. Die Ordnungswidrigkeit kann mit einer Geldbuße von bis zu 50.000,00 € geahndet werden. Zuständige Verwaltungsbehörde für die Verfolgung und Ahndung von Ordnungswidrigkeiten ist der Kanzler/die Kanzlerin der Technischen Universität Dortmund. Im Falle eines mehrfachen oder sonstigen schwerwiegenden Täuschungsversuches kann der Prüfling zudem exmatrikuliert werden, § 63 Abs. 5 Hochschulgesetz NRW.

Die Abgabe einer falschen Versicherung an Eides statt ist strafbar.

Wer vorsätzlich eine falsche Versicherung an Eides statt abgibt, kann mit einer Freiheitsstrafe bis zu drei Jahren oder mit Geldstrafe bestraft werden, § 156 StGB. Die fahrlässige Abgabe einer falschen Versicherung an Eides statt kann mit einer Freiheitsstrafe bis zu einem Jahr oder Geldstrafe bestraft werden, § 161 StGB.

Die oben stehende Belehrung habe ich zur Kenntnis genommen:

**Official notification:**

Any person who intentionally breaches any regulation of university examination regulations relating to deception in examination performance is acting improperly. This offence can be punished with a fine of up to EUR 50,000.00. The competent administrative authority for the pursuit and prosecution of offences of this type is the chancellor of the TU Dortmund University. In the case of multiple or other serious attempts at deception, the candidate can also be unenrolled, Section 63, paragraph 5 of the Universities Act of North Rhine-Westphalia.

The submission of a false affidavit is punishable.

Any person who intentionally submits a false affidavit can be punished with a prison sentence of up to three years or a fine, Section 156 of the Criminal Code. The negligent submission of a false affidavit can be punished with a prison sentence of up to one year or a fine, Section 161 of the Criminal Code.

I have taken note of the above official notification.

Ort, Datum  
(Place, date)

Unterschrift  
(Signature)

Titel der Dissertation:  
(Title of the thesis):

---

---

---

Ich versichere hiermit an Eides statt, dass ich die vorliegende Dissertation mit dem Titel selbstständig und ohne unzulässige fremde Hilfe angefertigt habe. Ich habe keine anderen als die angegebenen Quellen und Hilfsmittel benutzt sowie wörtliche und sinngemäße Zitate kenntlich gemacht.

Die Arbeit hat in gegenwärtiger oder in einer anderen Fassung weder der TU Dortmund noch einer anderen Hochschule im Zusammenhang mit einer staatlichen oder akademischen Prüfung vorgelegen.

I hereby swear that I have completed the present dissertation independently and without inadmissible external support. I have not used any sources or tools other than those indicated and have identified literal and analogous quotations.

The thesis in its current version or another version has not been presented to the TU Dortmund University or another university in connection with a state or academic examination.\*

**\*Please be aware that solely the German version of the affidavit ("Eidesstattliche Versicherung") for the PhD thesis is the official and legally binding version.**

Ort, Datum  
(Place, date)

Unterschrift  
(Signature)